

Indonesian Throughflow Variability on Sub-Orbital Timescales during Marine Isotope Stage 3: Geochemical Aspects

Dissertation

zur Erlangung des Doktorgrades
der Mathematisch-Naturwissenschaftlichen Fakultät
der Christian-Albrechts-Universität zu Kiel

vorgelegt
von
Rina Zuraida
Kiel, 2009

Referent/in :

Koreferent/in :

Tag der mündlichen Prüfung :

Zum Druck genehmigt, Kiel, den:

der Dekan :

Abstract

This thesis examines variability of the Indonesian Throughflow (ITF) and factors controlling its variability during Marine Isotope Stage 3 (~24–62 ka B.P.). Proxy records from Cores MD01-2378 (mixing zone between ITF and Indian Ocean waters) and 185 SO185-18460 (ITF) are developed and examined. The main objectives of this study are (1) to detect the amplitude and frequency of changes in surface and thermocline temperature and $\delta^{18}\text{O}$ within the main ITF outflow during MIS 3, (2) to test the hypothesis that a slow down in thermohaline circulation during stadials reduces the cool and fresh ITF thermocline flow, (3) to test modeling predictions that a reduction in ITF thermocline flow during stadials alters hydrographic profiles in the eastern Indian Ocean and leads to a warmer and saltier tropical Indian Ocean, and (4) to assess linkages between high latitude and tropical climate evolution.

The stratigraphy was established by tuning high-resolution benthic oxygen isotope data to the isotope record of the EPICA Dronning Maud Land ice core which was synchronized to the North Greenland Ice Core Project ice core following the new Greenland Ice Core Chronology (GICC05) timescale. The age model is additionally constrained by AMS ^{14}C dates, measured on *Globigerinoides ruber* (white). The evaluation of ITF variability in both surface and upper thermocline water masses is conducted by comparing stable isotope records combined with Mg/Ca-derived temperature records from shallow- and upper thermocline-dwelling planktonic foraminifers (*G. ruber* white and *Pulleniatina obliquiloculata*), indicative of temperature, salinity and productivity changes.

Spatial variation in upper thermocline temperature during Northern Hemisphere stadials, Heinrich Events 3 to 6, indicated repeated incursions of warmer and saltier Indian Ocean thermocline water into the mixing zone. The incursions are the results of weakening of the relatively cool and fresh thermocline flow and reduced export of less saline water from the North Pacific and Indonesian Seas to the tropical Indian Ocean related to slow-down of global thermohaline circulation.

Carbon isotope records from the Timor Strait revealed convergence of surface and upper thermocline $\delta^{13}\text{C}$ preceding and/or subsequent to Heinrich Events suggesting increasing nutrient input into the Timor Strait. The nutrient input implied increased precipitation during stadials that is indicative of southward displacement of austral summer intertropical convergence zone.

Kurzfassung

In dieser Arbeit werden die Variabilität des Indonesischen Durchstroms (IDS) und die Faktoren, die seine Variabilität im der Sauerstoff-Isotopenstufe 3 (~24–62 ka B.P.) kontrollierten, untersucht. Proxydatensätze werden aus den Kernen MD01-2378 (Vermischungszone zwischen IDS und Indischem Ozean Wasser) und 185 SO185-18460 (IDS) entwickelt und untersucht. Die Hauptziele dieser Studie sind (1) die Ermittlung der Amplitude und Frequenz von Änderungen der Temperatur und des der Oberflächen und des $\delta^{18}\text{O}$ an der Oberfläche und in der Thermokline während des starken IDS im MIS 3, (2) der Test der Hypothese, dass eine Verlangsamung der thermohalines Zirkulation während der Stadiale den kalten und salzarmen IDS in der Thermokline reduziert hat, (3) die Überprüfung von Modellvorhersagen, dass eine Verringerung des IDS in der Thermokline während der Stadiale die hydrographischen Profile im östlichen Indischen Ozean verändert und zu einem wärmeren und salzigerem tropischen Indischen Ozean führt, sowie (4) eine Abschätzung, wie stark die Entwicklung des Klimas in den höheren Breiten und in den Tropen zusammenhängt.

Die Stratigraphie wurde erstellt, indem hoch aufgelöste, benthische Sauerstoffisotopen-Daten mit dem Isotopendatensatz des EPICA Dronning Maud Land Eiskerns abgeglichen wurden, der entsprechend der neuen Greenland Ice Core Chronology (GICC05) Zeitskala mit dem North Greenland Ice Core Project Eiskern synchronisiert wurde. Das Altersmodell außerdem im Einklang mit AMS ^{14}C Daten, die auf *Globigerinoides ruber* (weiß) gemessen wurden. Die Auswertung der IDS Variabilität in den Oberflächen- und oberen thermoklinen Wassermassen erfolgt durch den Vergleich von Datensätzen stabiler Isotopen, die mit Temperaturzeitreihen aus dem Mg/Ca-

Verhältnis von planktonischen Foraminiferen (*G. ruber* weiß and *Pulleniatina obliquiloculata*) im flachen und oberen thermoklinen Auftrieb kombiniert wurden, die Temperatur-, Salzgehalts- und Produktivitätsänderungen anzeigen.

Räumliche Variation der Temperatur in der oberen Thermokline während der Stadiale auf der Nordhalbkugel, Heinrich-Ereignisse 3 bis 6, implizieren wiederholtes Eindringen von warmem und salzhaltigem thermoklinen Indischen Ozean Wasser in die Vermischungszone. Das Eindringen ist eine Folge der Abschwächung der relativ kalten und salzarmen thermoklinen Strömung und des verringerten Exports von salzärmeren Wassers aus dem Nordpazifik und der Indonesischen See in den tropischen Indischen Ozean, der mit der Verlangsamung der globalen thermohalinen Zirkulation verbunden ist.

Kohlenstoffisotopaufzeichnungen aus der Timor Straße zeigten, dass $\delta^{13}\text{C}$ an der Oberfläche und in der oberen Thermokline vor und/oder nach einem Heinrich-Ereignis konvergierten, was für einen steigenden Nährstoffeintrag in die Timor Straße spricht. Der Nährstoffeintrag implizierte erhöhten Niederschlag während der Stadiale, was bezeichnend für eine südwärtsige Verschiebung der intertropischen Konvergenzzone während des südlichen Sommers ist.

Acknowledgment

The completion of this thesis would not have been possible without continued support of many people, and I would like to thank them all.

I would like to thank Prof. Dr. Wolfgang Kuhnt, Dr. Dirk Nürnberg, P.D., and Prof. Dr. Martin Frank for initiating this project and giving me the opportunity to carry out this research. I am furthermore indebted to them for supervising this thesis, and their continuous help throughout the writing of this thesis.

I would like to give special thanks to Dr. Ann Holbourn for her unfailing support and her invaluable inputs for the thesis. I am grateful to Dr. Brian Haley who introduced and taught me the intricacies of neodymium analyses.

I received a lot of help and inputs from Dr. Jian Xu who is always patient in answering my questions, particularly about sample preparation and data interpretation and also provided me with additional data. I am grateful to Dr. Marcus Regenberg for his help in data processing and interpreting. I am indebted to Anke Dürkop for her help and her inputs and data exchange.

Dieter Garbe-Schönberg, Nadine Gehre, Karin Kissling, and Lulzim Haxhiaj provided analytical expertise and technical assistance.

Thanks to the participants of Sonne 185 cruise and the crew of RV Sonne for their support during the successful cruise in 2005.

I gratefully acknowledge the Deutsche Forschungsgemeinschaft for funding this research (grant Ku 649/25) and the German Ministry for Education, Science and Technology (BMBF grant 03GO185B) for funding the Sonne 185 cruise.

I am grateful for the Institut für Geowissenschaften Christian Albrechts Universität zu Kiel who fund the last three months of my research.

I also acknowledge Marine Geological Institute of Indonesia for giving me leave of absence so I can pursue my study in Kiel.

Finally, I can't thank enough my family for their unfailing support: Mother, my sisters Hanie and Athia, my brother Gani, and my late Father.

Table of Contents

Abstract	i
Acknowledgment	v
Table of Content	vii
Table of Figures	x
List of Table	xi
1. Introduction	1-1
1.1. Regional Setting	1-2
1.1.2. Climate	1-2
1.1.3. Hydrography	1-5
1.4. Marine Isotope Stage 3	1-6
1.4. Objectives	1-8
2. Materials and Methods	2-1
2.1. Sampling Strategy	2-1
2.2. Core Description.....	2-3
2.2.1. Core MD01-2378	2-3
2.2.2. Core SO185-18460	2-4
2.3. Laboratory Analyses.....	2-4
2.3.1. Mg/Ca.....	2-4
2.3.1.1. Selection of Cleaning Method	2-4
2.3.1.2. Mg/Ca-calibration equation and evaluation of dissolution	2-9
2.3.1.3. Analytical error and replicability.....	2-11
2.3.2. Stable isotope.....	2-12
3. Evidence for Indonesian Throughflow slow-down during Heinrich Events 3-5	3-1
3.1. Introduction	3-2
3.2. Methods	3-6
3.2.1. Mg/Ca Analysis.....	3-7
3.2.2. Stable Isotope Analysis	3-11

3.2.3. Paleosalinity Reconstruction from $\delta^{18}\text{O}_{\text{seawater}}$	3-11
3.2.4. Age Model	3-13
3.3. Results	3-14
3.3.1. Oxygen Isotopes	3-14
3.3.2. Mg/Ca Temperature Reconstructions	3-15
3.3.3. Sea Surface and Upper Thermocline Salinity Estimates ($\delta^{18}\text{O}_{\text{sw}}$)	3-19
3.3.4. Carbon Isotopes	3-20
3.4. Discussion	3-21
3.4.1. Timor Sea Hydrography and Planktonic Foraminiferal Habitats	3-21
3.4.2. Decrease in ITF Intensity During Heinrich Events	3-25
3.4.3. Main Controls of ITF Variability During MIS 3	3-29
3.5. Conclusion	3-31
4. Intertropical convergence zone migration during Marine Isotope Stage 3: evidence from the Timor Sea	4-1
4.1. Introduction	4-2
4.2. Materials and Methods	4-5
4.2.1. Mg/Ca analysis	4-6
4.2.2. Stable isotope analyses	4-8
4.2.3. $\delta^{18}\text{O}_{\text{seawater}}$	4-9
4.3. Results	4-10
4.3.1. Oxygen Isotopes	4-10
4.3.2. Carbon Isotope	4-12
4.3.3. Mg/Ca temperature reconstructions	4-13
4.3.4. Surface – Thermocline Temperature Gradient	4-16
4.3.5. Regional Temperature Gradient	4-16
4.3.6. Sea surface salinity estimates ($\delta^{18}\text{O}_{\text{sw}}$)	4-18
4.4. Discussion	4-19
4.4.1. Southward migration of ITCZ during Heinrich Events	4-19
4.4.2. ITF variability during Heinrich Events	4-23
4.5. Conclusion	4-26
5. Centennial-scale climate variability in the Timor Sea during Marine Isotope Stage 3 ..	5-1
5.1. Introduction	5-1

5.2. Material and method.....	5-5
5.2.1. Paleoceanographic setting.....	5-5
5.2.2. Stable isotopes.....	5-7
5.2.3. Accelerator mass spectrometry.....	5-9
5.2.4. Benthic foraminiferal census counts.....	5-10
5.3. Results.....	5-12
5.3.1. Age model.....	5-12
5.3.2. Stable isotopes.....	5-13
5.3.3. Benthic foraminiferal census counts.....	5-15
5.4. Discussion.....	5-18
5.4.1. Northern and Southern Hemisphere climate control.....	5-18
5.4.2. Paleoproductivity variations in the Timor Sea during MIS 3.....	5-21
5.5. Conclusion.....	5-24
6. Conclusions.....	6-1
6.1. Slow down of the Indonesian Throughflow (Chapter 3).....	6-2
6.2. Migration of the Intertropical Zone (Chapter 4).....	6-2
6.3. Centennial climate variability (Chapter 5).....	6-3
7. References.....	7-1
Appendix A. Report on cleaning efficacy.....	A-1
Appendix B. MD01-2378 stable isotope and Mg/Ca of <i>Globigerinoides ruber</i>	D-1
Appendix C. MD01-2378 stable isotope and Mg/Ca of <i>Pulleniatina obliquiloculata</i>	E-1
Appendix D. SO185-18460 stable isotope and Mg/Ca of <i>Globigerinoides ruber</i>	D-1
Appendix E. SO185-18460 stable isotope and Mg/Ca of <i>Pulleniatina obliquiloculata</i>	E-1
Appendix F. Temperature gradients of SO185-18460 and MD01-2378.....	F-1

Table of Figures

Figure 1.1. Present day Indonesian Throughflow.	1-3
Figure 1.2. Modern global precipitation.	1-4
Figure 2.1. Core locations with respect to the Indonesian Throughflow.	2-3
Figure 2.2. Comparison between various calibration methods	2-10
Figure 2.3. Comparison between measured and corrected Mg/Ca values.....	2-11
Figure 3.1. Annual temperature and salinity distribution	3-6
Figure 3.2. (a) Benthic $\delta^{18}\text{O}$ (<i>P. wuellerstorfi</i>) spanning MIS 3.....	3-16
Figure 3.3. (a) Benthic $\delta^{18}\text{O}$ (<i>P. wuellerstorfi</i>) spanning MIS 3.....	3-18
Figure 3.4. (a) Benthic $\delta^{13}\text{C}$ (<i>P. wuellerstorfi</i>) spanning MIS 3.....	3-22
Figure 3.5. (a) Timor Sea temperature profiles.....	3-24
Figure 3.6. Comparison of sea level reconstructions, benthic $\delta^{18}\text{O}_{\text{sw}}$, temperatures and insolation during MIS 3.....	3-27
Figure 4.1. Annual temperature distribution in the Indo-Pacific region, based on World Ocean Atlas 2005 data [Locarnini et al., 2006].....	4-4
Figure 4.2. Comparison between Core SO-18460 (red) and Core MD01-2378 (pink) records.....	4-11
Figure 4.3. Comparison between Core SO-18460 (blue) and Core MD01-2378 (purple) records.....	4-15
Figure 4.4. $\delta^{13}\text{C}$ of <i>G. ruber</i> (red) and <i>P. obliquiloculata</i> (blue) of Timor Strait (B) and Timor Sea (C)	4-17
Figure 4.5. Temperature gradient between surface and thermocline water masses (B and C) of Cores SO185-18460 and MD01-2378.	4-20
Figure 4.6. Modern global precipitation in January when the ITCZ is over Australia and on July when the ITCZ is over Asia.....	4-24
Figure 5.1. Location of Core MD01-2378	5-6
Figure 5.2. Scanning electron micrographs of two morphotypes of the epibenthic foraminifera <i>P. wuellerstorfi</i>	5-8
Figure 5.3. a) Benthic foraminiferal oxygen isotope data versus depth spanning MIS 1-12 from Holbourn et al. [2005].....	5-11
Figure 5.4. Age/depth plot showing tie points (diamonds) between EDML ice core and MD01-2378 benthic foraminiferal $\delta^{18}\text{O}$	5-13
Figure 5.5. a) Benthic foraminiferal $\delta^{18}\text{O}$ (<i>P. wuellerstorfi</i>) in Core MD01-2378 and $\delta^{18}\text{O}$ in EDML ice core versus age.	5-15
Figure 5.6. a) Benthic and planktonic $\delta^{18}\text{O}$	5-17

List of Table

Table 2.1. Comparison between reductive and non-reductive cleaning methods.....	2-7
Table 2.2. List of cleaning reagents for reductive and non-reductive treatment.	2-8
Table 3.1. Comparison of average water temperatures at sea surface and 100 m water depth at 33 stations in the Timor Sea	3-10
Table 3.2. Tie points between MD01-2378 benthic foraminiferal $\delta^{18}\text{O}$ and EDML ice core $\delta^{18}\text{O}$ (Dürkop et al., 2008).....	3-14
Table 5.1. Tie points between benthic foraminiferal $\delta^{18}\text{O}$ and EDML ice core $\delta^{18}\text{O}$ versus depth and age.	5-9
Table 5.2. AMS ^{14}C dates measured on <i>G. ruber</i> (white) in Core MD01-2378.	5-10

Chapter 1

Introduction

1. Introduction

This thesis comprises of Mg/Ca and stable isotope studies on two planktonic foraminifer species, *Globigerinoides ruber* and *Pulleniatina obliquiloculata*, carried out in two cores from the Timor Sea. The first core is Core MD01-2378 (13°4.95'S and 121°47.27'E; 1783 m water depth) situated in the hydrographic front between Indian Ocean and Timor Sea (Chapter 3 and 5). The second core is Core SO185-18460 (128° 38.485' E and 8° 47.386' S; 1875 m water depth) located in the northeast Timor Sea (Chapter 4). For the ease of discussion, the term Timor Sea would be used as general description of both study area, but during detail discussion between two cores, the location of Core MD01-2378 would be referred as Timor Sea, and Core SO185-18460 as Timor Trough.

The general theme of this thesis is to investigate the impact of reduced global thermohaline circulation to the Indonesian Throughflow (ITF) and to assess linkages between high latitude and tropical climate evolution. The temperature and isotope records from Timor Sea reveal that changes in global thermohaline circulation, sea level and Asia-Australia monsoonal system during Marine Isotope Stage 3 leave unique imprints on surface and vertical structure of the ITF water mass.

1.1. Regional Setting

The Timor Sea is a sea bounded to the north by the island of Timor, to the east by the Arafura Sea, to the south by Australia and to the west by the Indian Ocean. The Timor Sea is adjacent to two substantial inlets on the north Australian coast, the Joseph Bonaparte Gulf and the Van Diemen Gulf. The Australian city of Darwin is the only large city to adjoin the sea.

The sea is about 480 km wide, covering an area of about 610000 km². Its deepest point is the Timor Trough, located in the northern part of the sea, which reaches a depth of 3300 m (Figure 1.1). The remainder of the sea is much shallower, much of it averaging less than 200 m deep, as it overlies the Sahul Shelf, part of the Australian continental shelf. The complicated submarine topography of this sea, and adjacent seas, is the result of collision between the northwestern edge of the Australian continent and a former oceanic subduction zone producing very deep basins with very limited interconnections due to shallow sill depth. Timor Trough, within the Timor Sea, forms one of the connections allowing the Pacific water to enter the Indian Ocean after being mixed with the Indonesian Seas.

1.1.2. Climate

The Timor Sea climate is strongly influenced by the wind regime of the Asian-Australian monsoon and associated seasonal precipitation patterns. The

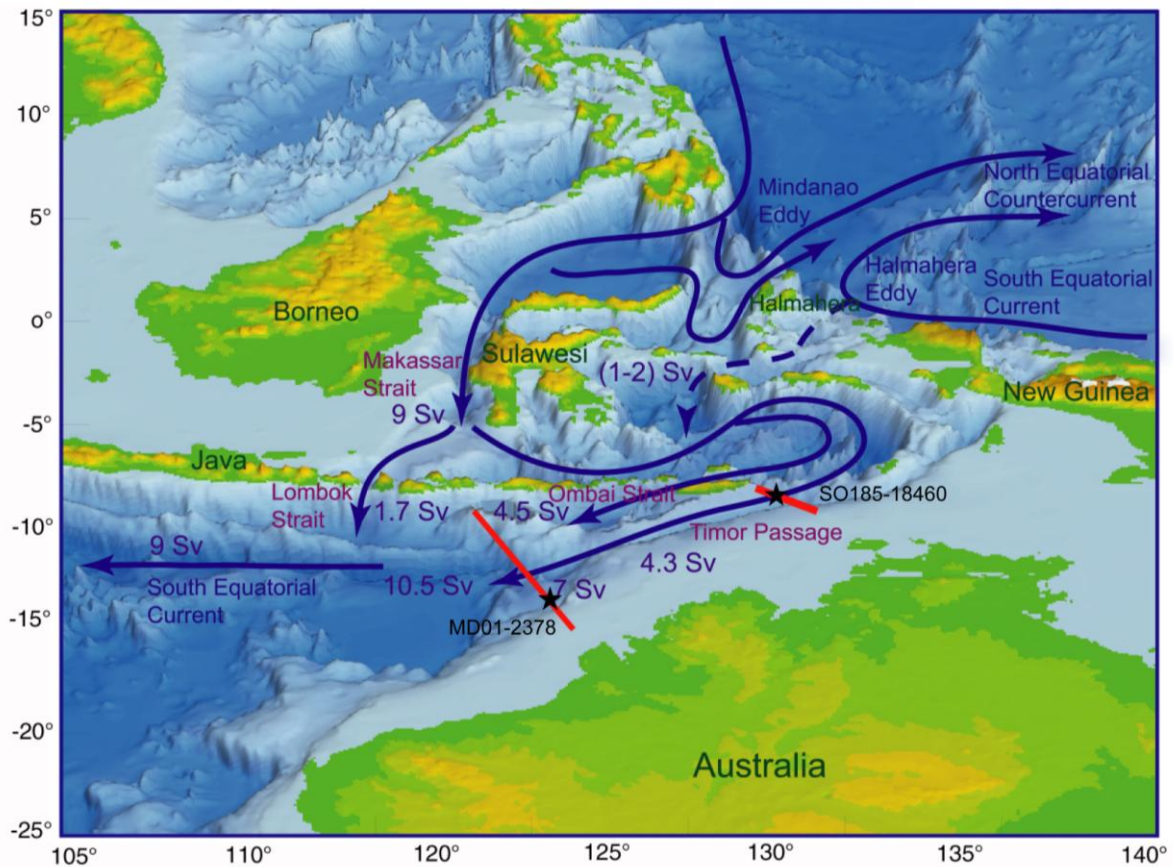


Figure 1.1. Present day Indonesian Throughflow. ITF pathways modified from Gordon [2001] and Gordon et al. [2003] are drawn on a topographic basemap derived from the ETOPO-5 bathymetric data set (Data Announcement 88-MGG-02, Digital relief of the Surface of the Earth. NOAA, National Geophysical Data Center, Boulder, Colorado, 1988). Red lines indicate schematic position of the two sampling transects during Sonne 185 cruise SO-185 in 2005, black stars indicate core locations.

Asian-Australian monsoon is a huge thermal circulation system driven by seasonal surface temperature differences between broadly central Asia and Australia [Tapper, 2002]. The Australian austral summer (northwest) monsoon, is characterized by cold, dry air flowing southward across the South China Sea. In contrast, a moist northwest monsoonal flow becomes established over northern Australia during austral summer. The winds are relatively light in the monsoon transition periods of March–April and October–November, as the Intertropical

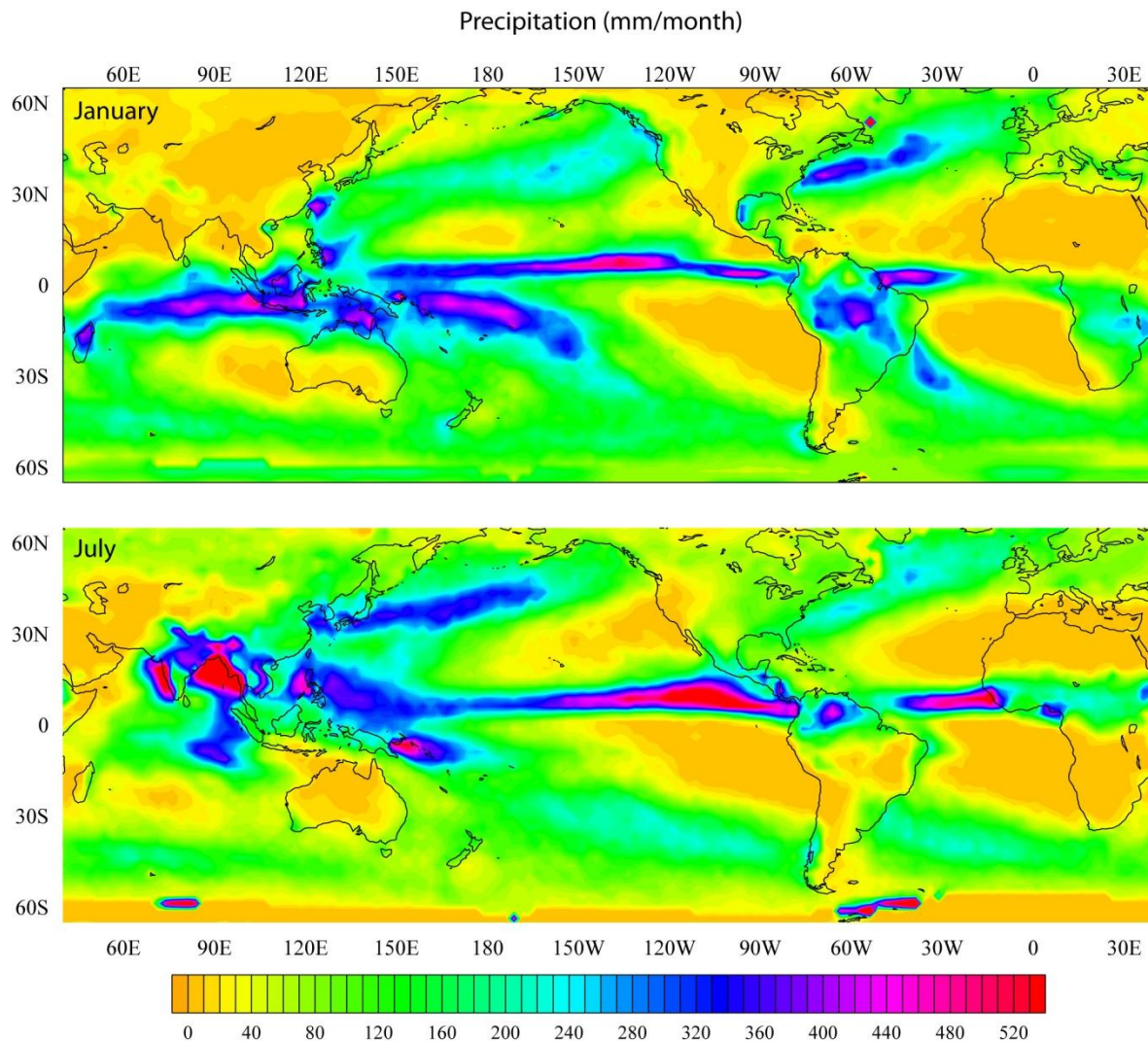


Figure 1.2. Modern global precipitation in January when the ITCZ is over Australia and on July when the ITCZ is over Asia. Data is based on Legates et al. [1990] and was downloaded from jisao.washington.edu/legates_msu/.

Convergence Zone (ITCZ) moves alternatively north and south across the region [Tapper, 2002].

The ITCZ is an equatorial region where trade winds of the Northern and Southern Hemispheres converge [Wells, 1997] and it is nearly always located near ridges of high sea surface temperature (SST), with temperatures of 28°C and above [Tomczak, 2002]. Intense humidity is responsible for almost perpetual

thunderstorms within this zone and convection associated with the ITCZ is the primary supplier of precipitation to equatorial regions. Shift in the ITCZ location has substantial impact on the seasonal precipitation for intertropical landmasses [Broccoli et al., 2006].

1.1.3. Hydrography

The Timor Sea (sill depth: 1890 m) is one of the three main exits of the Indonesian Throughflow (ITF) that connects the upper water masses of the Pacific and Indian Oceans and substantially influences the salinity and heat exchange between these oceans [Gordon and Fine, 1996]. The ITF transports an annual average ~ 16 Sv ($1 \text{ Sv} = 10^6 \text{ m}^3 \text{ s}^{-1}$) of warm, low-salinity water from the WPWP and Indonesian archipelago into the eastern Indian Ocean [Gordon and Fine, 1996].

Today, the ITF is dominated by low-salinity, well ventilated upper thermocline North Pacific water. North Pacific water mainly flows southward through the Sulawesi Sea into the Makassar Strait, and then follows two ways: one branch enters the Indian Ocean via the Lombok Strait (sill depth: 350 m) while the other branch mixes into the Flores Sea. Besides the Lombok Strait, there are two other main exit passages: the Ombai Strait (sill depth: 3250 m) and Timor Sea (sill depth: 1890 m).

The ITF that outflows through these two passages has been modified by mixing [e.g. Field and Gordon, 1992] and Ekman pumping [Gordon and Susanto, 2001] and ocean-atmosphere heat exchange [Gordon et al., 2008], resulting in a

strong thermocline with unique stratification. The Timor outflow shows more subdued interseasonal and interannual variation in comparison to the rest of exit passages: Lombok Strait and Ombai Strait that show seasonal reverse flow. The speed of surface flow (upper 50 m) at Timor Passage reduces to only near zero, during the northwest monsoon/NWM (boreal winter), with maximum speed is reached during southeast monsoon/SEM (boreal summer); the thermocline water (upper 150 m) shows more subdued intraseasonal fluctuations than the surface layer [Gordon et al., 2008].

The annual sea surface temperature in both Timor Strait and Timor Sea is ~28°C, while the upper thermocline water temperature in Timor Strait is 22.6°C and Timor Sea is 23.8°C (World Ocean Atlas 2005 data [Locarnini et al., 2006]). The 1°C thermocline temperature gradient between Timor Strait and Timor Sea implies shallower thermocline in Timor Strait (see Figure 4.1).

1.4. Marine Isotope Stage 3

Marine isotope stages (MIS) are alternating warm (interglacial) and cool (glacial) periods in the Earth's paleoclimate, deduced from oxygen isotope data reflecting temperature curves derived from data from deep sea core samples. One of the cool periods occurred during MIS 2, 3, and 4.

The MIS 3 – a period between 60 and 27 ka ago during the last glacial cycle – is characterized by high-amplitude millennial-scale climate variability, consisting of abrupt episodes of warming of 8–16°C revealed in Greenland ice core and North

Atlantic records [Huber et al., 2006] followed by more gradual returns to colder (stadial) conditions. These climatic oscillations with a typical duration of 1 to 3 ka have become known as Dansgaard-Oeschger (D-O) events. Layers of ice rafted debris, subsequently named Heinrich layers, have been identified from Northern Hemisphere climate records and linked to episodic, massive discharges of icebergs released from the Laurentide ice sheet into the North Atlantic during extreme stadials or known as Heinrich Events (HEs). These D-O events and HEs are correlated with rapid climatic change in the circum-North Atlantic region [Bond et al., 1993; Hemming, 2004]. This high-amplitude millennial-scale climate variability has been generally associated with shifts in ice sheet mass balance and changing modes of Atlantic meridional overturning circulation (AMOC) (see Clark et al. [2007] for detailed review).

Slowed down or even collapsed of AMOC during HEs has been linked to millennial-scale climate variability such as major cooling at mid latitudes in the North Atlantic and southward displacement of the intertropical convergence zone (ITCZ) [Sarnthein et al., 1994, 2001; Alley and Clark, 1999; Ganopolski and Rahmstorf, 2001; Broecker, 2003; Piotrowski et al., 2004]. The widespread climatic impact of HEs was documented well beyond the North Atlantic in a variety of continental and marine settings including the Alboran Sea [Cacho et al., 1999], Santa Barbara Basin [Hendy and Kennett, 2000], China [Wang et al., 2001], Brazil [Wang et al., 2004], Australia [Muller et al., 2008], Borneo [Partin et al., 2007] and the Indo Pacific region [Dannenmann et al., 2003; Levi et al., 2007]. The prevalence of a Northern Hemisphere climate signal at locations far away from the

North Atlantic was previously attributed to a tight coupling between regional climate systems through vigorous atmospheric teleconnections. In particular, changes in surface salinity within the Indo-Pacific region were interpreted as fundamental alterations in monsoonal regime related to southward shifts of the ITCZ during HEs.

In contrast to rapid temperature oscillations in the Northern Hemisphere, the Southern Hemisphere temperature record from Antarctica appear to have been more subdued (1–3°C) [EPICA Community Members, 2006] and showing out of phase relationship to Northern Hemisphere variations during this interval [Blunier et al., 1998; Blunier and Brook, 2001; EPICA Community Members, 2006]. In particular, episodes of greatest warming in Antarctica during MIS 3 (the so-called A1–A4 events) coincided with prolonged stadials or Heinrich events (HEs). However, the repercussion of this bipolar seesaw on Southern Hemisphere climate evolution is still unclear, in particular in the low latitudes to midlatitudes, since high resolution climate proxy records are almost exclusively available from the Northern Hemisphere and southern high latitudes [Lynch-Stieglitz, 2004].

1.4. Objectives

The Timor Sea is ideally located to monitor changes in ITF intensity and vertical structure and to resolve the impact of millennial-scale climate events on the ITF outflow and related effects on the tropical Indian Ocean. The main objectives of this work are (1) to detect the amplitude and frequency of changes in

surface and thermocline temperature and $\delta^{18}\text{O}$ within the main ITF outflow during MIS 3, (2) to test the hypothesis that a slowdown in thermohaline circulation during HEs reduces the cool and fresh ITF thermocline flow, (3) to test modeling predictions that a reduction in ITF thermocline flow during HEs alters hydrographic profiles in the eastern Indian Ocean and leads to a warmer and saltier tropical Indian Ocean, and (4) to assess linkages between high latitude and tropical climate evolution.

Chapter 2

Materials and Methods

2. Materials and Methods

The core samples and data used in this thesis were collected during two field campaigns in the Timor Sea that focused on Quaternary sediments: (1) the IMAGES 'WEPAMA' Cruise with RV "Marion Dufresne" in 2001 and (2) the SO-185 'VITAL' Cruise with RV "Sonne" in September – October 2005. During the "WEPAMA" cruise, four long Calypso cores and multicores were retrieved from different locations and water depths in the Timor Sea. During the SO-185 VITAL cruise, a total of 54 sets of multicores (MUC), 18 gravity cores, 21 piston cores, 3 kastenlot cores, and 54 CTD profiles were recovered across two depth transects in the eastern and western Timor Sea. Detailed core locations and results of initial shipboard analyses (lithology, MST, colour reflectance, CTD profiles) are provided in the relevant cruise reports (Bassinot et al., 2001 and Kuhnt et al., 2005).

2.1. Sampling Strategy

The Timor Sea (sill depth: 1890 m) is chosen for site location considering it is one of the three main exits of the ITF with an estimated transport of 4.3 Sv [Gordon, 2005]. The ITF that outflows through this passage has been modified by mixing [e.g. Field and Gordon, 1992] and Ekman pumping [Gordon and Susanto, 2001] and ocean-atmosphere heat exchange [Gordon et al., 2008], resulting in a strong thermocline with unique stratification. The Timor outflow shows more

subdued interseasonal and interannual variation in comparison to the rest of exit passages: Lombok Strait and Ombai Strait that show seasonal reverse flow. The speed of surface flow (upper 50 m) at Timor Passage reduces to only near zero, during the northwest monsoon/NWM (boreal winter), with maximum speed is reached during southeast monsoon/SEM (boreal summer); the thermocline water (upper 150 m) shows more subdued intraseasonal fluctuations than the surface layer [Gordon et al., 2008].

Under glacial boundary conditions when sea level was lower than at present, southward shift of the ITCZ during boreal winter, drier austral summer monsoon due to cooler Indian Ocean water-masses, would have different effects on the ITF. To compare the upper water column signatures of the glacial ITF from within the pathway of the ITF with a location where ITF is mixing with the Indian Ocean water, we chose two site locations (Figure 2.1) that represent each situation: Core SO185-18460 ($128^{\circ} 38.485' E$ and $8^{\circ} 47.386' S$; 1875 m water depth) and MD01-2378 ($13^{\circ}4.95'S$ and $121^{\circ}47.27'E$; 1783 m water depth). Core SO185-18460 is situated on a basinal height within the pathway of ITF outflow from the Banda Sea and represents a pure ITF signal. In contrast, Core MD01-2378 is situated at the interface between ITF derived and subtropical-tropical Indian Ocean water masses. This site is located on the passive Australian margin, far from disturbances by recent tectonic activity and turbidite emplacement. The islands to the north and west of Timor Sea, Nusa Tenggara and Lesser Sunda Islands, are formed by subduction of Indo-Australian Plate under Eurasian Plate. The subduction activity instigate seismic activity in Nusa Tenggara and Lesser

Sunda Islands causing instability in the northern slope of the Timor Sea that may trigger turbidity current, and rendering this area less suitable for coring undisturbed (climate archives in) marine sediments.

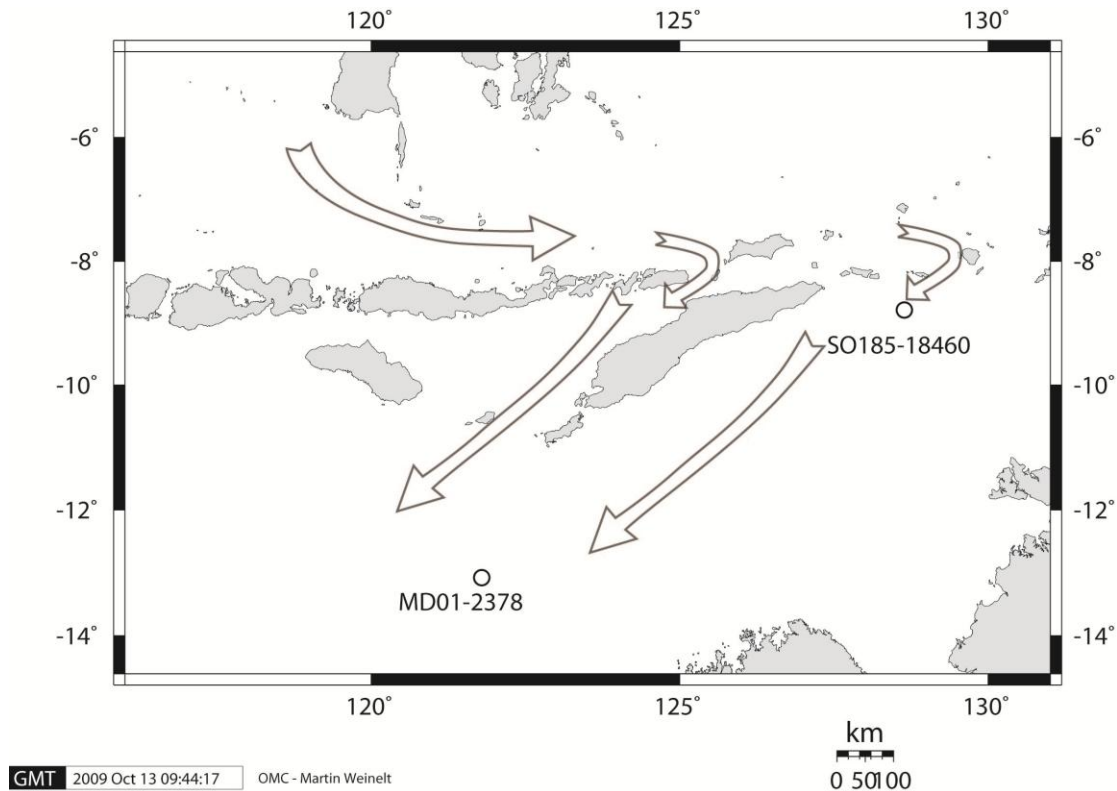


Figure 2.1. Core locations with respect to the Indonesian Throughflow.

2.2. Core Description

2.2.1. Core MD01-2378

Core MD01-2378 was acquired with the Calypso piston core during WEPAMA cruise MD122 [Bassinot et al., 2001] The total length of Core MD01-2378 is 40.73 m (461.54 ka, Holbourn et al., 2005) and composed of homogenous

clay, dominated by foram-bearing nannoplankton-oozes, slightly to heavily bioturbated [Bassinot et al., 2002]. Ash layer was found between 26.22 – 26.24 m and sandy pods rich in foraminifers are common from 15 to 27 m [Bassinot et al., 2002]. A multicore was taken at the same location during the WEPAMA cruise to ensure complete recovery of the top of the sedimentary record. A detailed age model for MIS3 was published by Dürkop et al. [2008].

2.2.2. Core SO185-18460

Core SO185-18460 was taken from a rise to the southeast of the deepest part of the eastern part of Timor Passage to avoid disturbance of the continuous record by turbidites. The core was acquired with a wide diameter piston corer, and has a total length of 15.81 m. This core mainly consists of olive green hemipelagic foraminifer-ooze, and shows medium to high bioturbation [Kuhnt et al., 2005].

2.3. Laboratory Analyses

2.3.1. Mg/Ca

2.3.1.1. Selection of Cleaning Method

The Mg/Ca analysis was carried out for a total of 911 *G. ruber* (white) samples and 910 *P. obliquiloculata* with the ICP-OES Spectro Ciros CCD SOP at the Institute of Geosciences, Christian-Albrechts-University, Kiel. Before the

analysis, samples were treated to remove contaminants that may affect the Mg/Ca values. The choice of cleaning protocol for this study was based on the following reason: 1) there is no large source of sediments near site location; 2) relatively low terrigenous content found in Core MD01-2378 by Holbourn et al. [2005]; and 3) the result of comparison between reductively-cleaned and non-reductively cleaned carried out on samples from MD01-2378. The cleaning protocol is discussed in the following paragraph along with detail comparison between the reductive and non-reductive treatment.

The cleaning procedure for Mg/Ca analysis is based on the cleaning protocol proposed by Boyle and Keigwin [1985] that was initially intended for trace element analysis. Since then, the method is developed rapidly for Mg/Ca pre-treatment purpose [e.g. Martin and Lea, 2002; Barker et al., 2003]. In general, sample treatment for Mg/Ca analysis comprises of removal of contaminants (silicate, organic matter, and/or Mn-oxides) that is followed by removal of adsorbed contaminants and leaching.

The silicate contamination removal step results in the expulsion of inorganic Mg and Fe from the samples. Removal of inorganic Mg from the samples causes a huge loss of Mg and reduces Mg/Ca values into only one-third of its original value [Barker et al., 2003].

The next step following clay removal differs between Martin and Lea [2002] and Barker et al. [2003]. Martin and Lea [2002] included a reductive step before the oxidation step and they observed that the application of this step lowered the

Mg/Ca value. They explained the decrease as the result of reduction of Mn-Fe coatings. Further study by Barker et al. [2003] showed that the Mg/Ca ratios of the reductively cleaned samples are systematically lower than untreated samples by about 10-15% indicating that this step causes partial dissolution of samples.

In order to decide which cleaning method to be used in this study, a comparison between the reductive and non-reductive step was conducted for low-resolution downcore record from Core MD01-2378. The preparation of reductively treated samples was carried out at the Institute of Geosciences, Christian-Albrechts-University, Kiel, by Xu in 2005 [Xu et al., 2006] and cleaning without reductive step was conducted at the IFM-GEOMAR in 2006/2007. The result of the comparison is listed in Table 2.1.

The study indicates that the reductive step causes a relatively large shift by 27% in the Mg/Ca ratio of *G. ruber* (white), while its effect on *P. obliquiloculata* is quite limited (4%). A possible explanation for this large disparity is the different shell structure and chemistry of each species.

G. ruber (white) shell consists of 2 or 3 layer of low- and high-Mg/Ca value (each layer is 1-6 μm thick) [Sadekov et al., 2009], which is thinner than *P. obliquiloculata*. The latter has a smooth microperforate surface calcite layer, or cortex, that has 3 to 10 times lower Mg/Ca ratio than the inner part of test wall [Sadekov et al., 2009] which may be more resistant to reduction.

The effect of reductive treatment on *G. ruber* (white) and *P. obliquiloculata* Mg/Ca values are different. However, when the Mg/Ca values are calibrated in

temperature, the average temperature differences between those steps are 0.8°C for *G. ruber* (white) and 0.2°C for *P. obliquiloculata*. Those temperature differences

Table 2.1. Comparison between reductive and non-reductive cleaning methods employed on *G. ruber* (white) and *P. obliquiloculata*

No	Depth (cm)	Age (ka)	Mg/Ca (mmol/mol) without reductive step		Mg/Ca (mmol/mol) with reductive step		Difference	
			<i>G. ruber</i>	<i>P. obliquiloculata</i>	<i>G. ruber</i>	<i>P. obliquiloculata</i>	<i>G. ruber</i>	<i>P. obliquiloculata</i>
1	451	23.07	3.74	2.26	3.80	2.26	0.06	0.01
2	461	23.70	3.70	2.40	3.66	2.17	-0.04	-0.23
3	471	24.33	3.90	2.53	3.77	2.19	-0.13	-0.34
4	481	24.95	4.09	2.16	3.61	1.95	-0.49	-0.21
5	491	25.57	3.77	2.16	3.62	2.35	-0.15	0.19
6	501	26.18	4.04	2.23	3.44	2.23	-0.61	0.01
7	511	26.78	3.67	2.38	3.42	2.27	-0.24	-0.10
8	521	27.37	4.07	2.36	3.66	2.14	-0.40	-0.22
9	531	27.96	3.67	2.21	3.79	1.88	0.11	-0.32
10	541	28.75	4.20	2.14	4.12	2.01	-0.08	-0.13
11	551	29.65	3.61	2.08	3.97	1.90	0.36	-0.18
12	561	30.57	4.03	2.10	3.76	1.88	-0.26	-0.23
13	571	31.49	3.83	2.16	3.69	2.08	-0.14	-0.08
15	591	33.33	3.81	1.99	3.63	2.34	-0.18	0.35
16	601	34.25	3.75	2.08	3.44	2.00	-0.31	-0.08
17	611	35.19	4.22	2.04	3.68	2.31	-0.54	0.27
18	621	36.13	3.94	2.04	3.57	2.30	-0.37	0.26
19	631	37.08	4.33	2.07	3.45	2.28	-0.88	0.21
20	641	38.03	3.87	2.34	3.72	2.44	-0.15	0.10
21	651	38.83	3.95	2.26	3.56	2.13	-0.39	-0.13
22	661	39.44	3.92	1.84	3.61	2.39	-0.31	0.55
23	671	40.01	3.71	2.14	3.36	2.18	-0.35	0.04
24	681	40.65	4.02	2.04	3.49	1.87	-0.53	-0.16
25	691	41.45		1.92	3.67	2.13		0.21
26	701	42.33	3.79	2.10	3.63	2.11	-0.16	0.02
27	711	43.22	3.79	2.08	3.58	2.06	-0.20	-0.02
28	721	44.10	3.51	2.15	3.54	1.94	0.03	-0.22
29	731	44.97	3.78	2.09	3.94	2.29	0.17	0.19
30	741	45.83	3.83	2.42	3.66	1.90	-0.17	-0.53
31	751	46.68	3.82	2.02	3.38	1.83	-0.43	-0.19
32	761	47.52	3.81	2.16	3.50	1.92	-0.31	-0.24
33	771	48.35	3.75	2.14	3.51	1.86	-0.24	-0.28
35	791	50.00	3.87	2.08	3.52	2.02	-0.35	-0.06
36	801	50.82	3.94	1.98	3.76	2.32	-0.19	0.34
37	811	51.76	4.03	2.17	3.83	2.22	-0.19	0.04
38	821	52.87	3.94	2.09	3.63	2.48	-0.32	0.40
39	831	54.03	3.73	2.32	3.45	2.34	-0.28	0.03
41	851	56.83	3.96	2.19	3.80	2.21	-0.16	0.03
42	861	58.61	4.29	2.50	3.89	2.08	-0.40	-0.42
43	871	60.60	4.09	2.79	3.76	2.47	-0.33	-0.33
44	881	62.78	4.44	2.37	3.58	2.27	-0.86	-0.10
45	891	65.03	3.82	2.43	3.35	2.10	-0.47	-0.33
Average			3.90	2.19	3.64	2.15	-0.27	-0.04

are actually within the error range for both species in this study, which are 0.5 – 0.6°C for *G. ruber* (white) and 0.3 – 1°C for *P. obliquiloculata*.

The oxidation of organic matter treatment is used in both cleaning methods. Barker et al. [2003] observed that this step takes away about 10% of Mg/Ca ratio that is equal to 1°C.

In order to take off barium contaminant, Martin and Lea [2002] applied alkaline chelation with DTPA, which was first proposed by Lea and Boyle [1993]. Flow through analysis shows that this step also leaches REE and is quite corrosive to the calcite [Haley and Klinkhammer, 2002]. The cleaning method employed in the Institute of Geosciences, Christian-Albrechts-University, Kiel, is a modification of the Martin and Lea [2002] cleaning method that excludes this chelation step.

The last step before dissolution is dilute-acid leaching. This step is needed to remove contaminants that may be adsorbed to the shell surfaces during the rigorous cleaning [Boyle and Keigwin, 1985]. The reagents used in Mg/Ca cleaning are presented in Table 2.2.

Table 2.2. List of cleaning reagents for reductive and non-reductive treatment.

Steps	Reagents	
	Modified Martin and Lea [2002]	Barker et al. [2003]
Clay removal	N-pure water	500 μ L UHQ H ₂ O
	Methanol	250 μ L Aristar methanol
Reduction	100 μ L buffered hydrazine made of 750 μ L anhydrous hydrazine + 10 mL ~0.5 N ammonium citrate (0.25 M) + 10 mL concentrated (~30%) ammonium hydroxide	N/A
Removal of organic matter	250 μ L buffered H ₂ O ₂ made of 50 μ L 30% H ₂ O ₂ + 15mL 0.1 N ultrapure NaOH	250 μ L 1% buffered H ₂ O ₂ made of 100 μ L 30% H ₂ O ₂ + 10 ml 0.1 M NaOH
Dilute acid leach	0.001N HNO ₃	250 μ L 0.001M HNO ₃

2.3.1.2. Mg/Ca-calibration equation and evaluation of dissolution

Estimates of SST and thermocline temperature from Mg/Ca values calculated by applying the general and species specific equations of Anand et al. [2003] for *G. ruber* (white) and *P. obliquiloculata*:

$$\text{Mg/Ca} = 0.38 (\pm 0.02) \exp 0.090 (\pm 0.003)T \text{ (general equation)}$$

$$\text{Mg/Ca} = 0.328 (\pm 0.007) \exp 0.090 (\pm 0.003)T \text{ (species specific equation)}$$

The selection of Anand et al. [2003] equations is based on comparison of 33 core top samples from the Timor Sea [Erichsen, 2008] using different calibration methods [e.g. Elderfield and Ganssen, 2000; Dekens et al., 2002; Anand et al., 2003; Regenberg et al., 2006]. The calculated Mg/Ca-temperatures from core top samples are compared to modern mean SST and thermocline temperature in the Timor Sea derived from WOA 05 [Locarnini et al., 2005] and from 19 CTD measurements during Sonne 185 cruise. Figure 2.2 shows the result of the comparisons for both species and detailed discussion of these results is presented in Chapter 3.

An additional problem encountered in Mg/Ca paleothermometry is the dissolution of carbonate tests. Regenberg et al. [2006] noted that dissolution starts as soon as calcite saturation level is below critical level in critical depth. The critical depth where $[\text{CO}_3^{2-}]$ reaches critical level vary between ocean basins, e.g. in the Caribbean Sea partial dissolution starts when the calcite saturation state reaches $\sim 18 - 26 \mu\text{mol/kg}$ at depths between $\sim 2500 - 3000 \text{ m}$ [Regenberg et al., 2006], while in some areas of the Timor Sea partial dissolution may start at depth less than 1000 m [Erichsen, 2008]. Regenberg et al. [2006] proposed the following

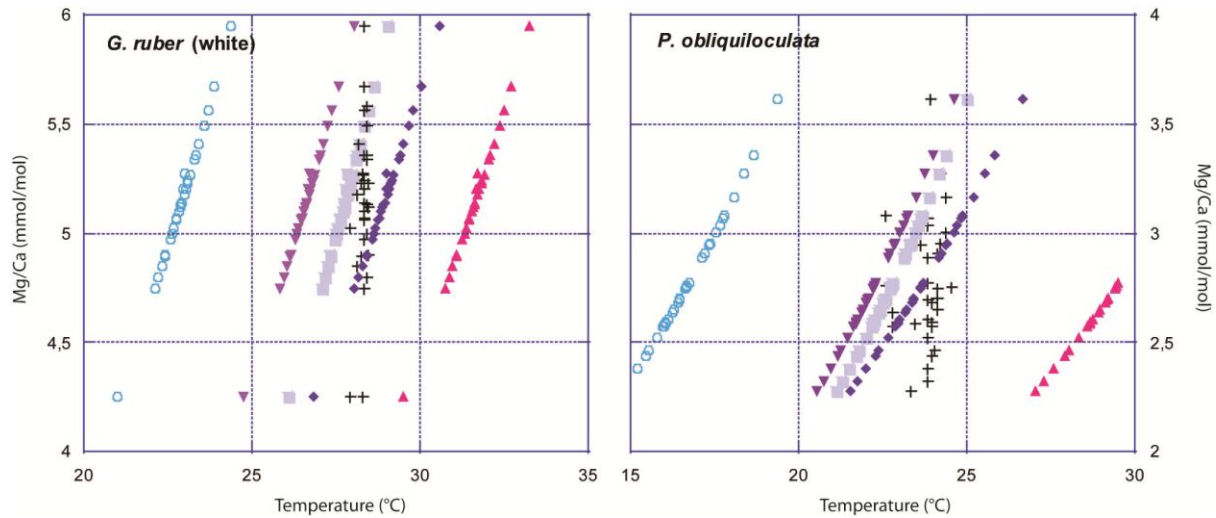


Figure 2.2. Comparison between various calibration methods for surface-dwelling *G. ruber* (white) and thermocline-dwelling *P. obliquiloculata*. Black cross represents WOA05 annual SST [Locarnini et al., 2005]; blue diamonds and purple inverse triangle are general and species specific equations for *G. ruber* (white), and species specific equation from plankton net and from sediment trap for *P. obliquiloculata* [Anand et al., 2003]; pink triangle is equation from Dekens et al. [2002]; grey square represents equation from Regenberget al. [2009]; and light blue open circle represents the equation of Elderfield and Ganssen [2000].

equation to calculate initial Mg/Ca values based on measured Mg/Ca and calcite saturation:

$$\text{Mg/Ca}_{\text{initial}} (\Delta\text{-corrected}) = \text{Mg/Ca}_{\text{measured}} (\Delta - \Delta_{\text{critical}})/b$$

where Δ is the average $\Delta[\text{CO}_3^{2-}]$ in $\mu\text{mol/kg}$ at the seafloor (with $\Delta < \Delta_{\text{critical}}$), Δ_{critical} is critical calcite saturation state ($\mu\text{mol/kg}$) where Mg^{2+} -removal due to dissolution starts, and b is the slope of regression line (12.61 for *G. ruber* (white) and 11.65 for *Neogloboquadrina dutertrei* that is used in place of *P. obliquiloculata*). The application of this correction on Timor Sea core top samples obtained from depth deeper than 500 m increases Mg/Ca values by 32% (equals to 0.6°C) and 14% (equals to 0.3°C) for *G. ruber* (white) and *P. obliquiloculata*, respectively, which is within the error range (Figure 2.3). Thus, it was decided that no dissolution correction was needed in this study.

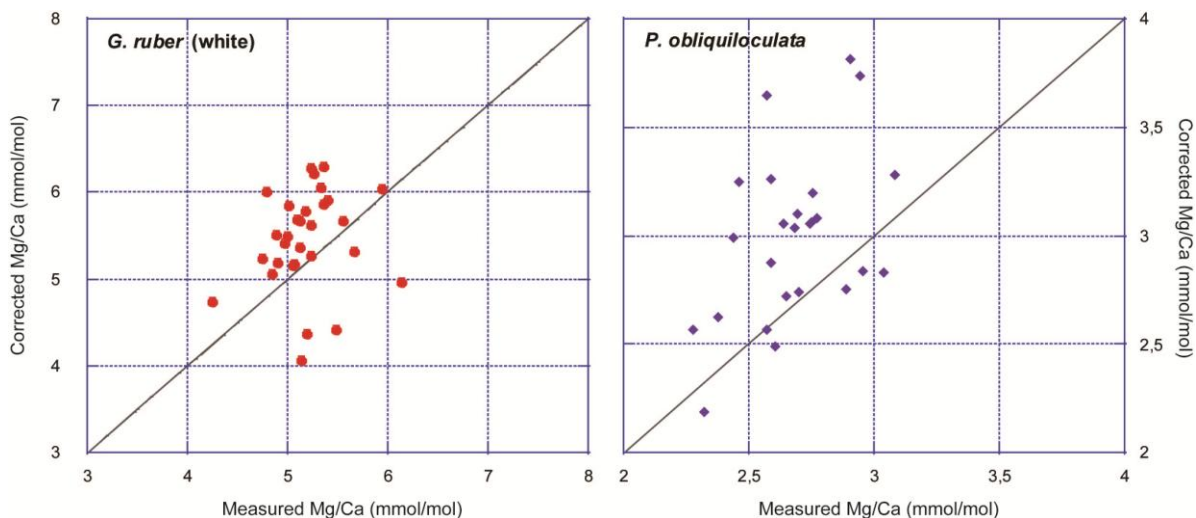


Figure 2.3. Comparison between measured and corrected Mg/Ca values of 33 core top data from Timor Sea. Core top Mg/Ca values for both species are from Erichsen (2008). The average differences between measured and corrected-Mg/Ca for *G. ruber* (white) and *P. obliquiloculata* are 32% and 14%, which is within the error range of each species, which is 0.56 and 0.61 mmol/mol, respectively.

This strategy is supported by the shell weight records of both cores. No significant effect of dissolution was detected even during the LGM and MIS 6 in Core MD01-2378, when dissolution would be most likely in the Timor Sea because of higher organic export flux [Holbourn et al., 2005], and during MIS 3 in Core SO185-18460.

2.3.1.3. Analytical error and replicability

The analytical error of the ICP-OES Spectro Ciros CCD SOP is ~0.1%, while the replicability is 0.2 mmol/mol (corresponding to 0.5°C) for *G. ruber* (white) and 0.05 mmol/mol (corresponding to 0.3°C) for *P. obliquiloculata*. Cleaning efficacy is checked by evaluating the Ca contents and Fe/Mg values of the samples using the limit of 0.1 mol/mol for the latter suggested by Barker et al. [2003]. As a result, a total of 11 samples of *G. ruber* and 10 samples of *P.*

obliquiloculata were rejected, within our data set of 911 *G. ruber* (white) and 910 *P. obliquiloculata* samples.

2.3.2. Stable isotopes

Stable isotope analyses ($\delta^{18}\text{O}$ and $\delta^{13}\text{C}$) were carried out on *P. obliquiloculata*. Stable isotope data for *G. ruber* (white) was provided by Dürkop [2009]. For stable isotope analyses, we selected 20 tests of *P. obliquiloculata* from the 250 – 315 μm size fractions. All tests were checked for cement encrustations and infillings before being gently crushed between two glass plates and cleaned with methanol in an ultrasonic bath, then dried at 40°C. Stable isotope analyses was performed at the Leibnitz Laboratory, University of Kiel, and at IFM-GEOMAR, on a Finnigan MAT 251 Mass Spectrometer with an automated Kiel carbonate preparation device. Samples were reacted by individual acid addition. The mean external error and reproducibility of carbonate standards is <0.07‰ for $\delta^{18}\text{O}$ and 0.07‰ for $\delta^{13}\text{C}$. The values are reported relative to the Peedee Belemnite (PDB) scale, based on calibration to the National Bureau of Standards (NBS) 19.

Oxygen isotop core top data are from Erichsen [2009] and carbon isotope core top data are from Xu [2009, pers. comm]. Xu [2009, pers. comm] used similar size fraction (250~315 μm) with this dissertation, while Erichsen [2009] used larger size fraction (350~500 μm).

Chapter 3

Evidence for Indonesian Throughflow slow-down during Heinrich Events 3-5

(Published in *Paleoceanography* , 24, PA2205, doi: 10.1029/2008

PA001653)

3. Evidence for Indonesian Throughflow slow-down during Heinrich Events 3-5

Rina Zuraida^{1,2}, Ann Holbourn¹, Dirk Nürnberg², Wolfgang Kuhnt¹, Anke Dürkop¹,
A. Erichsen¹

¹Institute of Geosciences, Christian-Albrechts-University, Ludewig-Meyn-Str. 10-14, D-24118 Kiel, Germany

²Leibniz-Institute of Marine Sciences, IFM-GEOMAR, Wischhofstr. 1-3, D-24148 Kiel, Germany

(Published in *Paleoceanography*, 24, PA2205, doi: 10.1029/2008PA001653)

Abstract

We present sea surface and upper thermocline temperature records (60–100 year temporal resolution) spanning marine isotope stage 3 (~24–62 ka B.P.) from International Marine Global Change Study core MD01-2378 (121°47.27'E and 13°04.95'S; 1783 m water depth) located in the outflow area of the Indonesian Throughflow within the Timor Sea. Stable isotopes and Mg/Ca of the near-surface-dwelling planktonic foraminifer *Globigerinoides ruber* (white) and the upper thermocline-dwelling *Pulleniatina obliquiloculata* reveal rapid changes in the thermal structure of the upper ocean during Heinrich events. Thermocline warming and increased $\delta^{18}\text{O}_{\text{seawater}}$ (*P. obliquiloculata* record) during Heinrich events 3, 4, and 5 reflect weakening of the relatively cool and fresh thermocline flow and reduced export of less saline water from the North Pacific and Indonesian Seas to the tropical Indian Ocean. Three main factors influenced Indonesian Throughflow

variability during marine isotope stage 3: (1) global slowdown in thermohaline circulation during Heinrich events triggered by Northern Hemisphere cooling, (2) increased freshwater export from the Java Sea into the Indonesian Throughflow controlled by rising sea level from ~60 to 47 ka, and (3) insolation-related changes in the Australasian monsoon with associated migration of hydrological fronts between Indian Ocean– and Indonesian Throughflow–derived water masses at ~46–40 ka.

3.1. Introduction

Marine isotope stage 3 (MIS 3) is characterized by high-amplitude millennial-scale climate variability, which has been generally associated with shifts in ice sheet mass balance and changing modes of Atlantic meridional overturning circulation (AMOC) (see Clark et al. [2007] for detailed review). Greenland ice core and North Atlantic records revealed that abrupt episodes of warming of 8–16°C [Huber et al., 2006] were followed by more gradual returns to colder (stadial) conditions. These climatic oscillations with a typical duration of 1 to 3 ka have become known as Dansgaard-Oeschger (D-O) events. Northern Hemisphere climate records also unmasked the occurrence of unusual layers of ice rafted debris, subsequently named Heinrich layers, which have been linked to episodic, massive discharges of icebergs released from the Laurentide ice sheet into the North Atlantic during extreme stadials.

In contrast to Northern Hemisphere signals, climate variations appear to have been more subdued in the Southern Hemisphere with temperature changes of 1–3°C recorded in Antarctica during MIS 3 [EPICA Community Members, 2006]. Synchronization of Greenland and Antarctic ice cores using methane [Blunier et al., 1998; Blunier and Brook, 2001; EPICA Community Members, 2006] additionally revealed that Southern Hemisphere climate fluctuations were clearly out of phase with Northern Hemisphere variations during this interval. In particular, episodes of greatest warming in Antarctica during MIS 3 (the so-called A1–A4 events) coincided with prolonged stadials or Heinrich events (HEs). However, the repercussion of this bipolar seesaw on Southern Hemisphere climate evolution is still unclear, in particular in the low latitudes to midlatitudes, since high resolution climate proxy records are almost exclusively available from the Northern Hemisphere and southern high latitudes [Lynch-Stieglitz, 2004].

Proxy data and ocean modeling results both indicated that millennial-scale climate variability was closely linked to changes in the rate of the AMOC. In particular, the AMOC is inferred to have considerably slowed down or even collapsed during HEs [Sarnthein et al., 1994, 2001; Alley and Clark, 1999; Ganopolski and Rahmstorf, 2001; Broecker, 2003; Piotrowski et al., 2004] resulting in major cooling at mid latitudes in the North Atlantic and southward displacement of the intertropical convergence zone (ITCZ). The widespread climatic impact of HEs was documented well beyond the North Atlantic in a variety of continental and marine settings including the Alboran Sea [Cacho et al., 1999], Santa Barbara Basin [Hendy and Kennett, 2000], China [Wang et al., 2001], Brazil [Wang et al.,

2004], Australia [Muller et al., 2008], Borneo [Partin et al., 2007] and the Indo Pacific region [Dannenmann et al., 2003; Levi et al., 2007]. The prevalence of a Northern Hemisphere climate signal at locations far away from the North Atlantic was previously attributed to a tight coupling between regional climate systems through vigorous atmospheric teleconnections. In particular, changes in surface salinity within the Indo-Pacific region were interpreted as fundamental alterations in monsoonal regime related to southward shifts of the ITCZ during HEs.

In contrast to the wealth of information concerning AMOC slowdown and related regional climatic impacts during HEs, relatively little is known about the effect of a reduction in North Atlantic deep water formation on the thermohaline circulation in the Pacific and Indian Oceans. The main return branch of the global thermohaline circulation consists of a westward flow from the Pacific Ocean through the Indonesian Archipelago where this flow is “transformed” to produce the Indonesian Throughflow (ITF). Changes in ITF volume and/or hydrographic properties significantly influence the temperature, salinity and nutrient distribution in the upper water column of the Indian Ocean with major repercussions for Australasian and African climate. The conversion of inflowing relatively cool and fresh North Pacific water through mixing and addition of freshwater within the archipelago into the ITF is modulated by seasonality and regional climate patterns [Ilahude and Gordon, 1996; Sprintall et al., 2003]. The resulting ITF flows out of the Indonesian archipelago into the Indian Ocean through three eastern passages (Lombok, Ombai and Timor Straits). Among the three outflow passages, the Timor

Strait plays the most significant role, in particular during times of lowered sea level, as it is substantially deeper and wider than the other two passages.

We generated centennial resolution records of surface and upper thermocline $\delta^{18}\text{O}$ and Mg/Ca temperatures spanning MIS 3 (24–62 ka) in core MD01-2378 (13°4.95'S and 121°47.27'E; 1783 m water depth), situated within the main ITF outflow from the Timor Strait into the eastern Indian Ocean (Figure 3.1). Thus, this core is ideally located to monitor changes in ITF intensity and vertical structure and to resolve the impact of millennial-scale climate events on the ITF outflow and related effects on the tropical Indian Ocean. This work extends previous investigations of glacial interglacial ITF variability in the same core [Holbourn et al., 2005; Xu et al., 2006, 2008] and in other cores located within the ITF outflow path [Spooner et al., 2005; Murgese and De Deckker, 2007]. Our main objectives are (1) to detect the amplitude and frequency of changes in surface and thermocline temperature and $\delta^{18}\text{O}$ within the main ITF outflow during MIS 3, (2) to test the hypothesis that a slowdown in thermohaline circulation during HEs reduces the cool and fresh ITF thermocline flow, and (3) to test modeling predictions that a reduction in ITF thermocline flow during HEs alters hydrographic profiles in the eastern Indian Ocean and leads to a warmer and saltier tropical Indian Ocean.

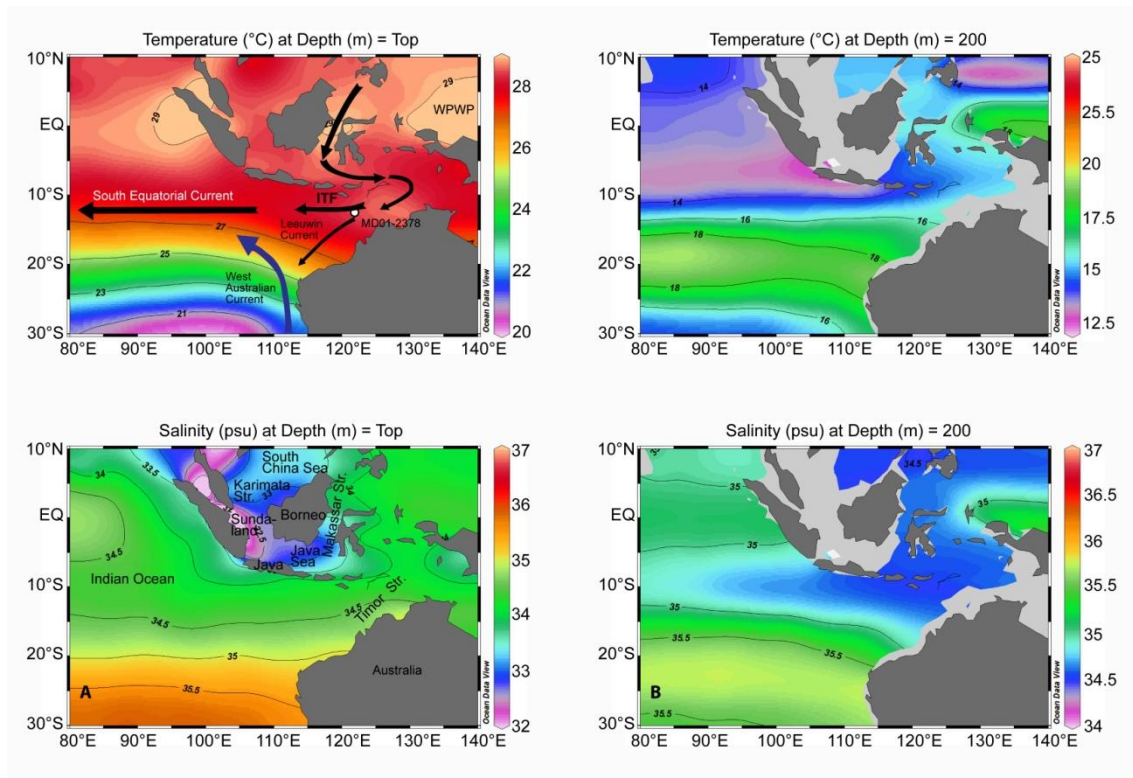


Figure 3.1. Annual temperature and salinity distribution in the Indo-Pacific region, based on World Ocean Atlas 2005 data (Locarnini et al., 2006; Antonov et al., 2006): (a) close to surface: habitat depth of *G. ruber* (white); (b) within upper thermocline: habitat depth of *P. obliquiloculata*. Arrows indicate modern current paths: ITF (black), South Equatorial Current (black), Leeuwin Current (black), and West Australian Current (dark blue). Core MD01-2378 is located within the main ITF outflow (white circle).

3.2. Methods

This study is based on sediment samples (30–40 cc from 1 cm thick slices) taken at 1 cm interval (approximating 60–100 years) between 448 and 895 cm in International Marine Global Change Study core MD01-2378. Samples were initially dried and weighed, then washed over a 63 μm sieve. Residues were dried on a sheet of filter paper and weighed, then sieved into 63–150 μm , 150–250 μm , 250–315 μm , and >315 μm fractions. Coupled Mg/Ca and $\delta^{18}\text{O}$ analyses were performed on two species of planktonic foraminifer (*Globigerinoides ruber* (white

sensu stricto) and *Pulleniatina obliquiloculata*) from the 250–315 μm size fraction to reconstruct surface and subsurface water masses conditions during MIS 3.

3.2.1. Mg/Ca Analysis

Thirty well-preserved tests of the near-surface dweller *G. ruber* (white) and 20 tests of the thermocline dweller *P. obliquiloculata* were selected under a binocular microscope, then gently crushed between two glass plates and cleaned following the protocol outlined by Barker et al. [2003]. The choice of cleaning protocol was based on the relatively low terrigenous clay content in core MD01-2378 (carbonate content >70% [Holbourn et al., 2005]). The first step (clay removal) involves rinsing foraminiferal fragments five times with ultrapure water, then twice with Aristar methanol, with ultrasonic treatment after each rinse. The next step is the removal of organic material using 250 μL of hot (97°C) oxidizing 1% NaOH/H₂O₂ reagent (10 mL 0.1 N analytical grade NaOH and 100 μL 30% suprapure H₂O₂) for 10 min. This process would produce gaseous buildup within sample tubes, therefore samples have to be agitated every 2.5 minutes to release bubbles. To maintain the chemical reaction, the samples were placed in an ultrasonic bath for a few seconds. The oxidizing solution was then removed by rinsing the samples three times with ultrapure water. The samples were then transferred into clean tubes and leached with 250 μL 0.001M HNO₃ (subboiled distilled) during a 30 seconds ultrasonic treatment, followed by two rinses with ultrapure water, in order to remove any adsorbed contaminant. The final step

involves the dissolution of samples in 500 μL 0.075 M HNO_3 (subboiled distilled). The solution has to be diluted with ultrapure water to achieve Ca concentrations of 30–70 ppm.

A total of 543 samples of *G. ruber* (white) and 596 of *P. obliquiloculata* were analyzed with the ICP-OES Spectro Ciros CCD SOP at the Institute of Geosciences, Christian-Albrechts-University, Kiel. The analytical error of the instrument is $\sim 0.1\%$. The replicability of our measurements, based on 72 *G. ruber* (white) and 77 *P. obliquiloculata* replicate samples, is 0.2 mmol/mol (corresponding to 0.6°C) for *G. ruber* (white) and 0.2 mmol/mol (corresponding to 1°C) for *P. obliquiloculata*. We checked the validity of Mg/Ca values by evaluating the Fe/Mg contents of the samples using the limit of 0.1 mol/mol suggested by Barker et al. [2003]. As a result, one sample of *G. ruber* and one sample of *P. obliquiloculata* were rejected. The effect of dissolution on Mg/Ca in the interval 1–460 ka in core MD01-2378 was evaluated by Xu et al. [2006] using shell weights and a foraminiferal test fragmentation index. No significant effect of dissolution was detected even during the LGM and MIS 6, when dissolution would be most likely in the Timor Sea because of higher organic export flux [Holbourn et al., 2005].

Sea surface temperature (SST) and upper thermocline temperature were reconstructed from *G. ruber* (white) and *P. obliquiloculata* Mg/Ca values, respectively. Conversion of Mg/Ca values into temperature was performed using the general equation $\text{Mg/Ca} = 0.38 (\pm 0.02) \exp 0.090 (\pm 0.003)T$ for *G. ruber* (white) and the species specific $\text{Mg/Ca} = 0.328 (\pm 0.007) \exp 0.090 (\pm 0.003)T$ for *P. obliquiloculata* [Anand et al., 2003]. The choice of equations was based on a study

of 33 core tops [Erichsen, 2008] and 19 conductivity temperature-depth (CTD) profiles taken during the Sonne 185 in October 2005 [Kuhnt et al., 2006] and comparison to World Ocean Atlas (WOA) data [Locarnini et al., 2006]. Mean *G. ruber* temperature (26.8°C with 0.82 standard deviation), estimated from the species specific equation of Anand et al. [2003], is significantly cooler than WOA annual average (28.3°C with 0.13 standard deviation) and CTD measurements at 10m (27.6°C, with 0.42 standard deviation) from the Sonne 185 cruise. Mean SST (29.2°C with 0.93 standard deviation), based on the general equation of Anand et al. [2003], slightly overestimates WOA annual average by ~0.9°C, and agrees with mean WOA summer (January–March) SST (29.2°C with 0.25 standard deviation). Mean *P. obliquiloculata* temperature (23.7°C with 1.21 standard deviation), estimated from the species-specific equation, closely matches WOA annual average temperature at 100 m water depth (23.8°C with 0.49 standard deviation), and is only slightly warmer than CTD measurements at 100 m water depth (22.9°C with 1.44 standard deviation) from the Sonne 185 cruise. The choice of equations is additionally supported by calculation of calcification temperatures, based on $\delta^{18}\text{O}_{\text{carbonate}}$ and $\delta^{18}\text{O}_{\text{seawater}}$ measurements at five CTD stations. Mean calcification temperatures (28.6°C for *G. ruber* and 23.9°C for *P. obliquiloculata*) are close to WOA annual average values for sea surface (28.3°C) and 100 m water depth (23.8°C) and to our Mg/Ca-based estimates (29.2°C for *G. ruber* and 23.7°C for *P. obliquiloculata*). Core top Mg/Ca data and temperatures are provided in Table 3.1. Marine isotope stage 3 stable isotope, Mg/Ca and estimated temperature at MD01-2378 are archived at <http://www.pangaea.de> (doi:10.1594/pangaea.712515).

Table 3.1. Comparison of average water temperatures at sea surface and 100 m water depth at 33 stations in the Timor Sea (CDT data from Sonne-185 cruise) with Mg/Ca derived temperature estimates from equations of Anand et al. (2003) and with $\delta^{18}\text{O}$ derived temperature estimates.

	Minimum	Maximum	Stations	Mean	Median	Std Deviation	Variance	Std Error
WOA05 annual mean SST	27.90	28.50	33	28.31	28.30	0.13	0.02	0.02
WOA05 Austral Summer (Jan-Mar) SST	28.80	29.50	33	29.16	29.20	0.25	0.06	0.04
WOA05 Austral Winter (Jul-Sep) SST	26.00	26.80	33	26.63	26.70	0.18	0.03	0.03
October 2005 SST from SO-185 CTD (at 10 m water depth)	26.80	28.40	19	27.65	27.60	0.42	0.18	0.10
Mg/Ca <i>G. ruber</i> white sensu stricto	4.25	6.62	33	5.27	5.20	0.45	0.20	0.08
Mg/Ca-SST from general equation of Anand et al. (2003)	26.80	31.80	33	29.19	29.10	0.93	0.87	0.16
Mg/Ca-SST from <i>G. ruber</i> (white) equation of Anand et al. (2003)	24.80	29.10	33	26.83	26.70	0.82	0.67	0.14
$\delta^{18}\text{O}$ <i>G. ruber</i>	-3.20	-2.30	32	-2.95	-3.00	0.19	0.04	0.03
<i>G. ruber</i> calcification temperature from $\delta^{18}\text{O}$	25.90	29.70	32	28.60	28.80	0.79	0.62	0.14
WOA05 annual mean temperature at 100 m water depth	22.60	24.50	32	23.80	23.85	0.49	0.24	0.09
WOA05 Austral Summer (Jan-Mar) temperature at 100 m water depth	22.60	24.20	32	23.41	23.30	0.36	0.13	0.06
WOA05 Austral Winter (Jul-Sep) temperature at 100 m water depth	22.40	25.10	32	23.94	23.70	0.80	0.64	0.14
October 2005 temperature from CTD SO-185 CTD (at 100 m water depth)	18.40	24.60	18	22.94	23.35	1.44	2.07	0.34
Mg/Ca <i>P. obliquiloculata</i>	2.28	3.61	32	2.78	2.72	0.31	0.10	0.05
Mg/Ca <i>P. obliquiloculata</i> temperature from species specific equation of Anand et al. (2003)	21.50	26.70	32	23.69	23.50	1.21	1.46	0.21
Mg/Ca <i>P. obliquiloculata</i> temperature from <i>G. ruber</i> (white) equation of (Anand et al. (2003)	18.60	23.20	32	20.55	20.40	1.07	1.15	0.19
$\delta^{18}\text{O}$ <i>P. obliquiloculata</i>	-2.10	-1.40	32	-1.83	-1.90	0.15	0.02	0.03
<i>P. obliquiloculata</i> calcification temperature from $\delta^{18}\text{O}$	21.90	24.90	32	23.90	24.00	0.64	0.41	0.11

3.2.2. Stable Isotope Analysis

For stable isotope analysis, we selected 20 tests of *P. obliquiloculata* from the 250–315 μm size fractions. All tests were checked for cement encrustations and infillings before being gently crushed between two glass plates and cleaned with methanol in an ultrasonic bath, then dried at 40°C. Measurements of 45 replicate samples indicate that the mean reproducibility is $\pm 0.20\%$ for $\delta^{18}\text{O}$ and $\pm 0.12\%$ for $\delta^{13}\text{C}$. Stable isotope analysis was performed at IFMGEOMAR on a Finnigan MAT 252 Mass Spectrometer with an automated Kiel carbonate preparation device. Samples were reacted by individual acid addition. The mean external error and reproducibility of carbonate standards is $< 0.07\%$ for $\delta^{18}\text{O}$ and 0.07% for $\delta^{13}\text{C}$. The values are reported relative to the Peedee Belemnite (PDB) scale, based on calibration to the National Bureau of Standards (NBS) 19. Stable isotope data for *G. ruber* (white) are from Dürkop et al. [2008].

3.2.3. Paleosalinity Reconstruction From $\delta^{18}\text{O}_{\text{seawater}}$

Although reconstruction of paleosalinity from $\delta^{18}\text{O}_{\text{seawater}}$ ($\delta^{18}\text{O}_{\text{sw}}$) may have large error propagation, estimation from paired $\delta^{18}\text{O}$ and Mg/Ca analyses allows to narrow down the uncertainty limit [Rohling, 2007]. We calculated $\delta^{18}\text{O}_{\text{sw}}$ using the following equation $\delta^{18}\text{O}_{\text{sw}} = 0.27 + (T - 16.5 + 4.8 * \delta^{18}\text{O}) / 4.8$ [Bemis et al., 1998] for both *G. ruber* (white) and *P. obliquiloculata*. We used the *Orbulina universa* LL equation for both *G. ruber* and *P. obliquiloculata*, as the equation for the

nonspinose *Globigerina bulloides* is only applicable for that species [Bemis et al., 1998]. We additionally experimented with other equations (*O. universa* HL and *G. bulloides*), but found no significant differences in our results. Since the equation extracts the effect of temperature on oxygen isotope fractionation, the calculated $\delta^{18}\text{O}_{\text{sw}}$ is mainly influenced by $\delta^{18}\text{O}_{\text{sw}}$ variability related to continental ice volume and local $\delta^{18}\text{O}_{\text{sw}}$ fluctuations related to surface and upper thermocline salinities. In order to remove the ice volume effect and to test the robustness of our $\delta^{18}\text{O}_{\text{sw}}$ reconstructions, we used two different methods.

1. We applied one ice volume correction by subtracting benthic $\delta^{18}\text{O}_{\text{sw}}$ (five-point smoothed) from planktonic $\delta^{18}\text{O}_{\text{sw}}$ within the same samples. To calculate benthic $\delta^{18}\text{O}_{\text{sw}}$, we used the Bemis et al. [1998] equation, assuming bottom water temperature of 2°C and minimal fluctuations during MIS 3 [Labeyrie et al., 1987]. The 2°C bottom water temperature assumption for MIS 3 is inferred from recent measurements of bottom temperature (2.8°C) at the location of core MD01-2378 during the Sonne 185 cruise [Kuhnt et al., 2006]. This temperature difference is approximately half of that estimated between the Holocene and LGM [Shackleton, 1987].

2. We also applied an alternative ice volume correction based on the reconstructed MIS 3 sea level curve for the central Red Sea [Siddall et al., 2003]. In order to ensure chronological compatibility, we tuned the Red Sea record to the MD01-2378 record. Then, we converted the sea level record into $\delta^{18}\text{O}$ units by assuming that a 1.1‰ change in $\delta^{18}\text{O}_{\text{sw}}$ is equivalent to 130 m sea level change. Because of

resolution difference (200 years in core KL11 and 60–100 years in core MD01-2378), we interpolated the rest of Red Sea $\delta^{18}\text{O}$ sea level values to fit the MD01-2378 age scale. Comparison between the two curves shows no significant differences in shape and absolute values, and supports that thermocline anomalies during MIS 3 are independent of the choice of ice volume correction.

3.2.4. Age Model

The original age model for the MIS 3 interval in core MD01-2378 was derived from correlation of high-resolution benthic oxygen isotope data to the isotope record of the EPICA Dronning Maud Land (EDML) ice core [EPICA Community Members, 2004], which was synchronized to the North Greenland Ice Core Project (NGRIP) ice core following the new Greenland Ice Core Chronology (GICC05) timescale [EPICA Community Members, 2006; Andersen et al., 2006; Svensson et al., 2006]. The MD01-2378 age model for this time interval is additionally constrained by 11 AMS ^{14}C dates, measured on *G. ruber* (white). Details of the original age model over the MIS 3 interval are provided by Dürkop et al. [2008, section 3.1, Figure 4]. In this study, we further constrained the MIS 3 interval between 742 and 895 cm with an additional tie point between the NGRIP oxygen isotope data on the GICC05 timescale [Svensson et al., 2008] and our high-resolution planktonic $\delta^{18}\text{O}$ record. An interpolated curve was fitted through the tie points using a Stineman function, and it was used to determine the age of each sample. The lower part of our age model from 817 to 895 cm (corresponding

to 54.5–62.5 ka) is based on linear extrapolation. Table 3.2 provides all tie points used in the revised age model for the MIS 3 interval in core MD01-2378.

Table 3.2. Tie points between MD01-2378 benthic foraminiferal $\delta^{18}\text{O}$ and EDML ice core $\delta^{18}\text{O}$ (Dürkop et al., 2008) and between planktonic foraminifera $\delta^{18}\text{O}$ and NGRIP ice core $\delta^{18}\text{O}$.

Depth [cm] (Core MD01-2378)	$\delta^{18}\text{O}$ [‰ vs. PDB] (Core MD01-2378)	GICC05 age [ka BP] (EDML ice core)	$\delta^{18}\text{O}$ [‰ SMOW] (EDML ice core)	Event
342	3.92	18.15	-51.89	$\delta^{18}\text{O}$ maximum prior to deglaciation
506	3.92	27.45	-52.53	$\delta^{18}\text{O}$ maximum after AIM 4 event
554	3.72	30.65	-51.04	$\delta^{18}\text{O}$ maximum before AIM 4 event
642	3.31	38.15	-48.68	Last $\delta^{18}\text{O}$ minimum of A1 event
664	3.65	39.85	-50.91	$\delta^{18}\text{O}$ maximum before A1 event
742	3.28	47.25	-47.44	$\delta^{18}\text{O}$ minimum in center of A2 event
additional tie point	<i>G. ruber</i>	(NGRIP ice core)	(NGRIP ice core)	
817	-1.58	54.49	-42.90	$\delta^{18}\text{O}$ maximum preceding D-O/14

3.3. Results

3.3.1. Oxygen Isotopes

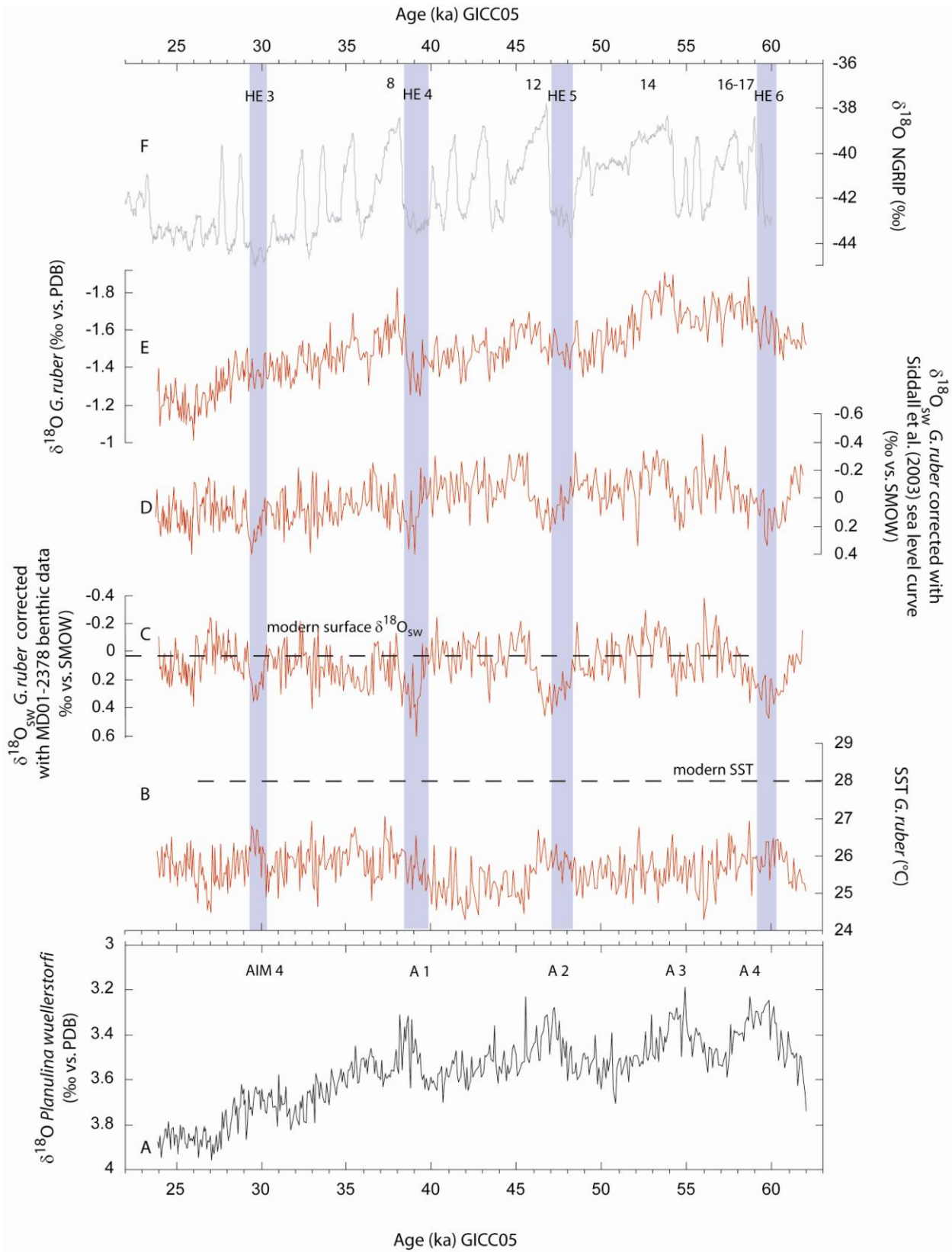
Planktonic foraminiferal $\delta^{18}\text{O}$ *G. ruber* (white) values vary between $\sim -1.1\text{‰}$ and -1.9‰ over the entire MIS 3 record (Figure 3.2). Three long-term trends are observed: (1) in the older part of the record before 55 ka, $\delta^{18}\text{O}$ values decrease from -1.5‰ to -1.9‰ ; (2) between 55 and 39 ka, planktonic $\delta^{18}\text{O}$ increases to -1.3‰ ; and (3) after a rapid decrease in planktonic $\delta^{18}\text{O}$ to -1.7‰ at 37.5 ka, a continuous increase of -0.6‰ occurs until 26 ka, followed by a slight decrease in values. Superimposed on this long-term variability are high-frequency variations, which show close affinity to fluctuations characteristic of northern high-latitude

planktonic and ice core records. However, only the longer lasting D-O warm events 8, 12, 14 and 16–17 are clearly expressed by decreases of -0.2‰ in the MD01-2378 record, whereas HEs 3–6 are marked by increases of $-0.1\text{--}0.2\text{‰}$ (Figure 3.2).

The $\delta^{18}\text{O}$ *P. obliquiloculata* varies between 0.1 and -0.8‰ , showing somewhat higher-amplitude variations than $\delta^{18}\text{O}$ *G. ruber* (white) (Figure 3.3). Three long-term trends are evident over the MIS 3 interval: (1) prior to 53.5 ka, $\delta^{18}\text{O}$ *P. obliquiloculata* values decrease from -0.2‰ to -0.7‰ ; (2) between 53 and 39 ka there is an overall increase from -0.7 to 0.0‰ ; and (3) following an initial decline to -0.3‰ at 39–38 ka, a long-term increase from -0.3 to 0.1‰ occurs between 38 and 24 ka. The $\delta^{18}\text{O}$ *P. obliquiloculata* curve is also characterized by high-frequency variations and the most pronounced D-O warm events 8, 12, 14 and 16–17 and the HEs 3–6 are detected by respective distinct increases and decreases of $-0.1\text{--}0.2\text{‰}$ (Figure 3.3).

3.3.2. Mg/Ca Temperature Reconstructions

Average surface (25.6°C) and upper thermocline (21.0°C) Mg/Ca temperature estimates over MIS 3 in core MD01-2378 are cooler by nearly 3°C , compared to present day mean annual SST of 28.3°C and upper thermocline temperature of 23.8°C (World Ocean Atlas 2005 data [Locarnini et al., 2006]). Figures 3.2 and 3.3 show that temperature oscillations are more pronounced within the thermocline

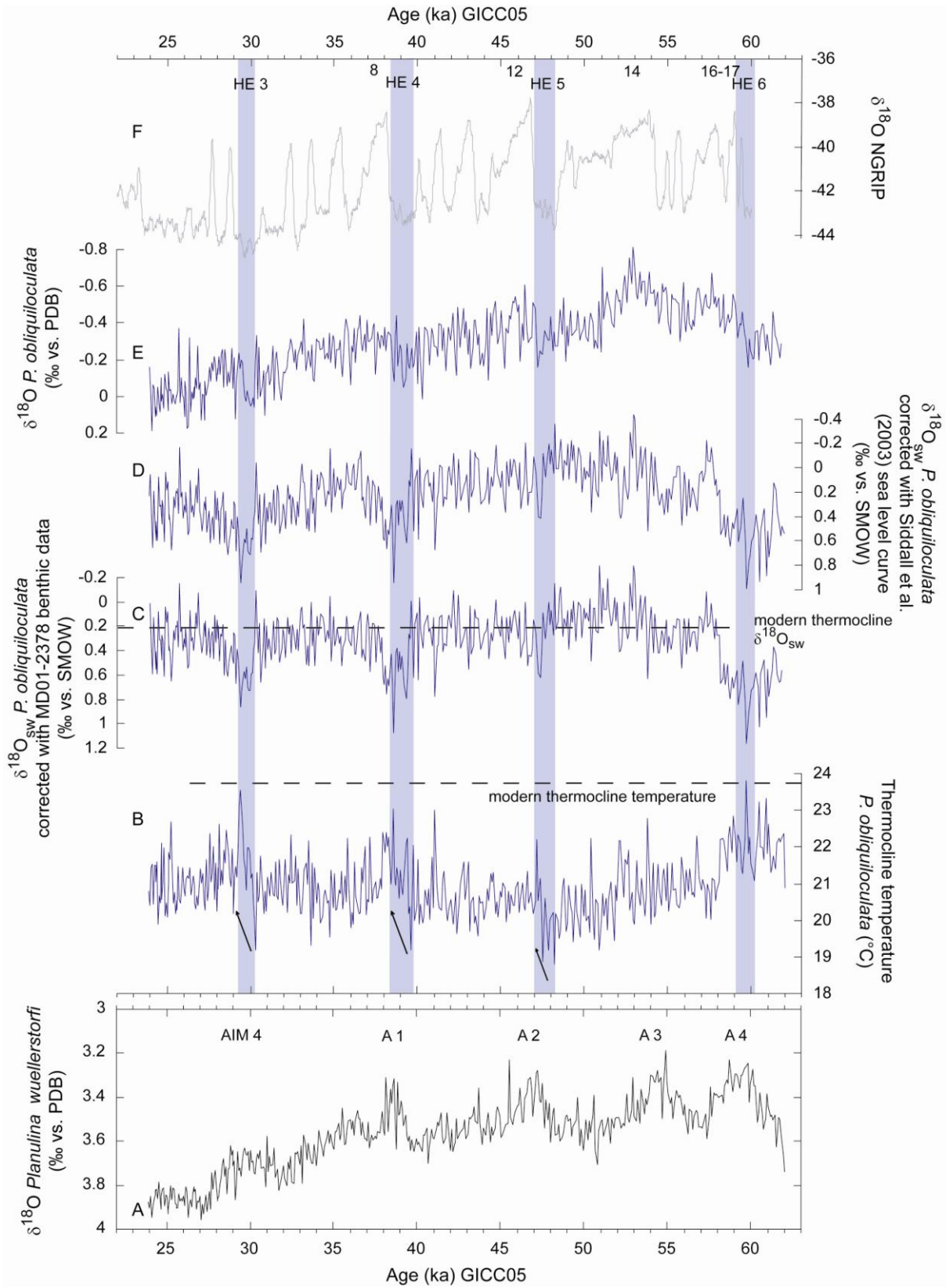


water mass than at the surface: SST varies between 24.3°C and 27.0°C, whereas upper thermocline temperature varies between 18.8°C and 23.8°C.

From 63 to 45 ka, SST values oscillate between 25 and 26°C. At 45–40 ka, the SST record is marked by a prominent cooling event, which corresponds to the interval between HE 4 and HE 5 and Antarctic warm events A1 and A2 (Figure 3.2). This major cooling event starts with a rather abrupt decrease of 1.5°C at the end of A 2 (46–45 ka), after which values oscillate around 25°C for a further ~5 ka. The end of the cooling event is marked by a gradual warming of 1.5°C from ~40 to 37 ka, after which SST are maintained around 25–26°C. In contrast to the thermocline temperature estimates, SST shows no clear imprint of HEs.

Relatively high temperature values (centering around 22°C) are registered in the upper thermocline during HE 6 (Figure 3.3). From the end of HE 6, the upper thermocline record shows an overall cooling trend: from 22°C at 60 ka to 19.5°C at 48 ka, in contrast to the more consistent SST values. From 48 to 24 ka, temperatures fluctuate between 22°C and 20°C. However, a salient feature of the upper thermocline record within this interval is the occurrence of prominent increases in temperature during HEs 3–5, with lowest temperatures of ~19.5°C at the beginning of each HE and peak temperatures in excess of 22–24°C at the end of each HE.

Figure 3.2. (a) Benthic $\delta^{18}\text{O}$ (*P. wuellerstorfi*) spanning MIS 3 in Core MD01-2378 from Dürkop et al. (2008). AIM 4 and A 1-4 refer to Antarctic warm events; (b) *G. ruber* (white) Mg/Ca derived SST, average SST over MIS 3 is 25.6°C in contrast to present day annual SST of 28.3°C (Locarnini et al., 2006); (c) Surface $\delta^{18}\text{O}_{\text{sw}}$; note: dashed line indicates modern surface $\delta^{18}\text{O}_{\text{sw}}$ measured in water samples from SO-185 cruise (0.05‰); (d) Surface $\delta^{18}\text{O}_{\text{sw}}$ corrected with Red Sea ice volume curve of Siddall et al. (2003); (e) planktonic $\delta^{18}\text{O}$ of *G. ruber* (white) from Dürkop et al. (2008); (f) NGRIP ice core $\delta^{18}\text{O}$ plotted on common GICC05 time scale (Svensson et al., 2006; 2008). Numbers refer to longer-lasting D-O events. Shaded bars indicate Heinrich events (HEs 3-6).



3.3.3. Sea Surface and Upper Thermocline Salinity Estimates

($\delta^{18}\text{O}_{\text{sw}}$)

The MD01-2378 surface $\delta^{18}\text{O}_{\text{sw}}$ record (corrected for ice volume, see Methods) fluctuates between -0.3‰ and 0.4‰ SMOW with an average of 0.1‰ over MIS 3. Northern Hemisphere stadial events HEs 3–6 are marked by prominent increases of $\sim 0.2\text{--}0.3\text{‰}$ in surface $\delta^{18}\text{O}_{\text{sw}}$ (Figure 3.2). HE 5 differs somewhat from other HEs, because high values ($\sim 0.6\text{--}0.4\text{‰}$) are maintained for ~ 1 ka during the early part of this interstadial.

Thermocline $\delta^{18}\text{O}_{\text{sw}}$ oscillates between -0.2‰ and 1.2‰ with an average of 0.4‰ over MIS 3. Values increase markedly by $\sim 0.2\text{--}0.4\text{‰}$ (Figure 3.3) during HEs 3–6. The increase in thermocline $\delta^{18}\text{O}_{\text{sw}}$ during HE 5 is more gradual and less pronounced than during HEs 3–4. As for surface $\delta^{18}\text{O}_{\text{sw}}$, interstadials are generally characterized by values close to modern $\delta^{18}\text{O}_{\text{sw}}$.

On the basis of measurements of water samples obtained during Sonne cruise 185, the modern values of surface $\delta^{18}\text{O}_{\text{sw}}$ and thermocline $\delta^{18}\text{O}_{\text{sw}}$ close to the position of our core are 0.05‰ and 0.20‰ , respectively, which gives a difference of -0.15‰ between surface and thermocline. During MIS 3, the

Figure 3.3. (a) Benthic $\delta^{18}\text{O}$ (*P. wuellerstorfi*) spanning MIS 3 in Core MD01-2378 from Dürkop et al. (2008). AIM 4 and A 1-4 refer to Antarctic warm events; (b) *P. obliquiloculata* Mg/Ca derived upper thermocline temperature (100 m water depth), average value over MIS 3 is 21°C in contrast to present day annual value of 23.8°C (Locarnini et al., 2006); (c) upper thermocline $\delta^{18}\text{O}_{\text{sw}}$; note: dashed line indicates modern upper thermocline $\delta^{18}\text{O}_{\text{sw}}$ measured in water samples from SO-185 cruise (0.20‰); (d) Thermocline $\delta^{18}\text{O}_{\text{sw}}$ corrected with Red Sea ice volume curve of Siddall et al. (2003); (e) planktonic $\delta^{18}\text{O}$ of *P. obliquiloculata*; (f) NGRIP ice core $\delta^{18}\text{O}$ plotted on common GICC05 time scale (Svensson et al., 2006; 2008). Numbers refer to longer lasting D-O events. Shaded bars indicate Heinrich events (HEs 3-6). Arrows highlight temperature changes during HEs.

average difference between $\delta^{18}\text{O}_{\text{sw}}$ surface and thermocline water masses was -0.3‰, indicating a somewhat more stratified upper water column during MIS 3.

3.3.4. Carbon Isotopes

Planktonic $\delta^{13}\text{C}$ of *G. ruber* (white) decreases between 64 and 60 ka during HE 6, reaching minimum value of $\sim -0.95\text{‰}$ at 61 ka (Figure 3.4). From the end of HE 6, values show a two stepped, long-term increase: (1) from ~ -1.2 to 1.5‰ between 60 and 52 ka and (2) from ~ -1.4 to 1.6‰ between 52 and 31 ka. After 31 ka, values exhibit an overall decrease, reaching $\sim -1.3\text{‰}$ at 23 ka. The $\delta^{13}\text{C}$ record of *P. obliquiloculata* also shows a decrease during HE 6: from ~ -0.9 at 64 ka to $\sim -0.6\text{‰}$ at 61 ka, after which values increase until ~ 50 ka, when a maximum of $\sim -1.1\text{‰}$ is attained. From 50 to 31 ka, values generally oscillate between ~ -1.1 and 0.9‰ . Between 31 and 23 ka, values show an overall decreasing trend from ~ -1.1 to 0.9‰ . As for the present day, the gradient between the *G. ruber* (white) and *P. obliquiloculata* $\delta^{13}\text{C}$ does not deviate markedly from 0.5‰ over the whole interval studied (Figure 3.4).

Figure 3.4 shows that the *G. ruber* (white) and *P. obliquiloculata* $\delta^{13}\text{C}$ records exhibit overall similar trends as the epibenthic $\delta^{13}\text{C}$ in core MD01-2378. Comparison of surface, thermocline and bottom water $\delta^{13}\text{C}$ profiles in core MD01-2378 reveals an increasing trend from ~ 60 to 50 ka, followed by a plateau until ~ 30 ka and a final decrease until ~ 23 ka. Comparison with Atlantic and Pacific records [Pahnke and Zahn, 2005; Piotrowski et al., 2005] suggests that the increase at ~ 60

to 50 ka is a global feature. Values ranging between ~ 0.0 and 0.3‰ for benthic $\delta^{13}\text{C}$ are significantly lower than for planktonic $\delta^{13}\text{C}$, and are in agreement with present-day values at this location in the Timor Sea (Figure 3.5).

3.4. Discussion

3.4.1. *Timor Sea Hydrography and Planktonic Foraminiferal Habitats*

The present-day upper thermal structure in the Timor Sea, close to the location of core MD01-2378, is characterized by a near-surface water mass (0–50 m water depth) with a relatively stable temperature averaging $\sim 28^\circ\text{C}$ and a thermocline water mass (50–250 m water depth) exhibiting a steep temperature gradient from ~ 28 to 12°C (Figure 3.5). Along with this marked temperature change, a sharp contrast in $\delta^{13}\text{C}$ also occurs within the upper water column (Figure 3.5) with values $>1.2\text{‰}$ in the upper 50 m declining to $<1\text{‰}$ at ~ 100 m and reaching $\sim 0.4\text{--}0.1\text{‰}$ below 250 m. The temperature difference between surface and upper thermocline (~ 100 m water depth) water masses is $\sim 5^\circ\text{C}$ today, which compares well with the range of values registered during MIS 3 (Figures 3.2 and 3.3), suggesting that our temperature reconstructions provide realistic estimates, although thermocline temperature appears to have fluctuated more than SST during MIS 3. The planktonic and benthic $\delta^{13}\text{C}$ profiles over MIS 3 also show broad agreement with modern $\delta^{13}\text{C}$ values for surface, thermocline and bottom

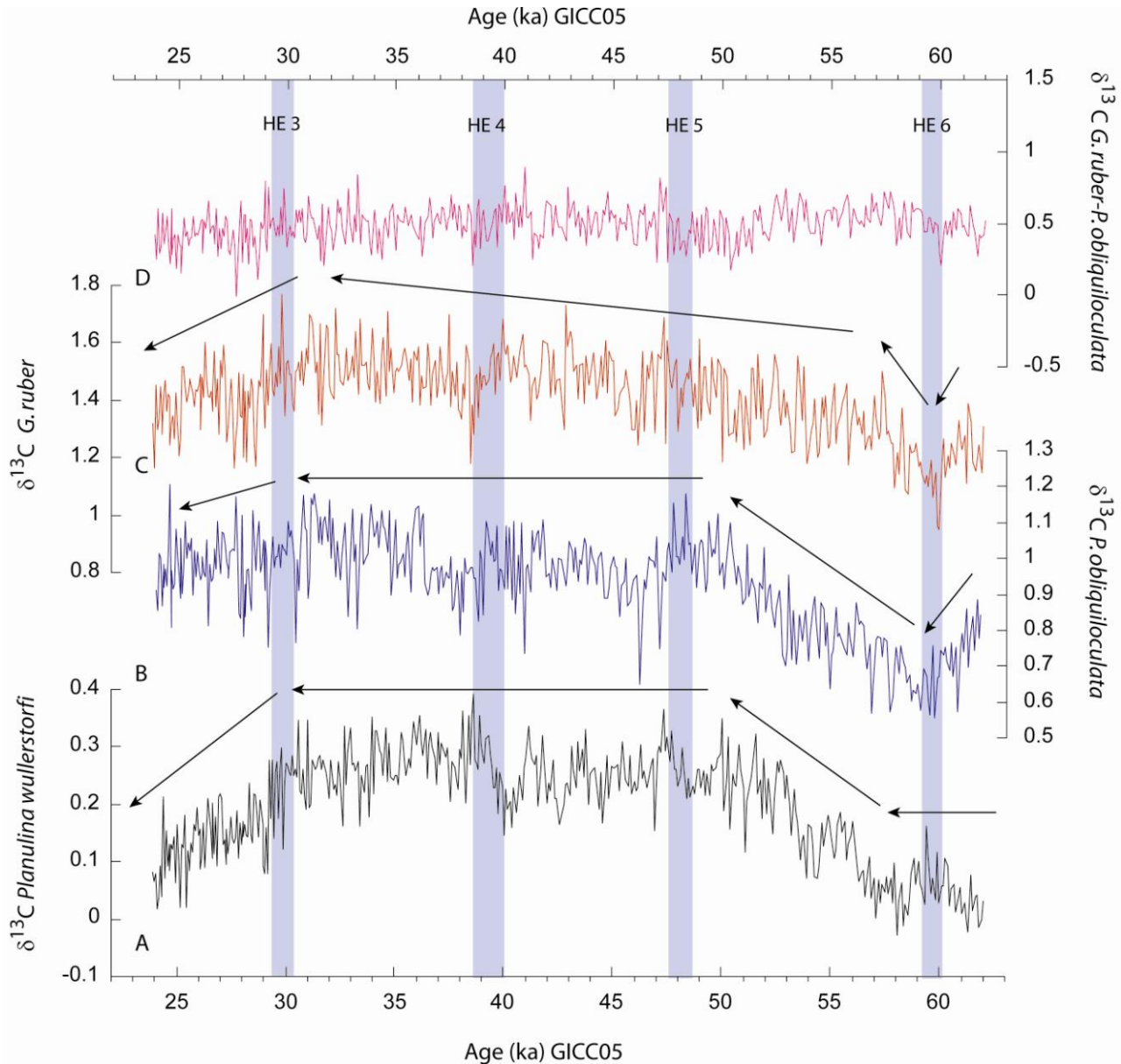


Figure 3.4. (a) Benthic $\delta^{13}\text{C}$ (*P. wuellerstorfi*) spanning MIS 3 in Core MD01-2378 from Dürkop et al. (2008); (b) planktonic $\delta^{13}\text{C}$ of upper thermocline dweller *P. obliquiloculata*; (c) planktonic $\delta^{13}\text{C}$ of near surface dweller *G. ruber* from Dürkop et al. (2008); (d) Consistent $\delta^{13}\text{C}$ gradient between *G. ruber* and *P. obliquiloculata* supports that respective depth habitats of these two species did not change significantly during MIS 3. Arrows highlight main trends during MIS 3.

water masses, even though long- and short-term temporal variations are detected within the three records (Figure 3.4).

One of the limitations in the application of multispecies Mg/Ca thermometry is that interspecies differences may reflect the migration of some species within the water column during their life cycle and/or changes in habitat depth rather than real temperature changes at a constant depth. The near-surface dweller *G. ruber* (white) exhibits relatively consistent Mg/Ca values [Eggins et al., 2003] indicating that the effect due to vertical migration is negligible and calculated SST accurately reflect the assigned habitat depth of upper 50m for this species [Anand et al., 2003]. In terms of seasonality, *G. ruber* (white) Mg/Ca commonly reflects average annual hydrographic conditions because of the almost uniform occurrence of this species throughout the year [Hemleben et al., 1989; Lin et al., 1997; Tedesco and Thunell, 2003]. However, in the Timor Sea, core top values of *G. ruber* fall into the range of average summer SST (29°C) [Xu et al., 2006, Table 1]. Although the deeper dweller *P. obliquiloculata* exhibits high mobility in the water column and seasonality [Prell and Damuth, 1978], sediment trap studies indicate that this species mainly calcifies below the mixed layer [Bé, 1977; Ravelo et al., 1990; Pflaumann and Jian, 1999] or between 50 and 100 m [Anand et al., 2003]. Ravelo and Fairbanks [1992] and Cléroux et al. [2007] also inferred *P. obliquiloculata* living within the seasonal thermocline, which in the Timor Sea is between 50 and 250 m (CTD data from SO-185 cruise).

Several lines of evidence also support that temperature estimates derived from *P. obliquiloculata* in core MD01-2378 do not relate to changes in habitat depth but to temperature variations occurring within the upper thermocline. First, a comparison of CTD temperature profiles from the Timor Sea with temperature

estimates of *P. obliquiloculata* from 33 Timor Sea core tops confirms that an estimated habitat depth below 100m for *P. obliquiloculata* is reasonable for the present day in this area (Table 3.1). Second, the overall $\delta^{13}\text{C}$ gradient between *G. ruber* (white) and *P. obliquiloculata* does not deviate substantially from $\sim 0.5\text{‰}$ throughout MIS 3 (Figure 3.4), supporting that the respective habitat depths of *P. obliquiloculata* and *G. ruber* (white) remained overall quite consistent over this extended interval. Finally, $\delta^{13}\text{C}$ and temperature do not covary during MIS 3, which would be expected if *P. obliquiloculata* migrated through the upper water column and thus reflected ambient temperature and $\delta^{13}\text{C}$ gradients. For instance, temperature increases during HEs coincide with no significant change or even with slight decreases in $\delta^{13}\text{C}$ (Figures 3.3 and 3.4).

3.4.2. Decrease in ITF Intensity During Heinrich Events

A striking feature of the Timor Sea record over MIS 3 is the contrast between the benthic and planktonic oxygen isotope signals (Figures 3.2 and 3.3). Whereas benthic $\delta^{18}\text{O}$ captures Antarctic warming and cooling trends including the AIM 4 and A1 to A4 warm events, planktonic $\delta^{18}\text{O}$ shows closer similarity to Northern Hemisphere records [Dürkop et al., 2008]. For instance, increases in $\delta^{18}\text{O}$ *G. ruber* (white) of $\sim 0.1\text{--}0.2\text{‰}$ are registered during stadials HEs 3–6, which also correspond to the early phases of warming in Southern Hemisphere A1–A4 events. This distinct out of phase relationship between benthic and planktonic $\delta^{18}\text{O}$ events was previously interpreted as a bipolar

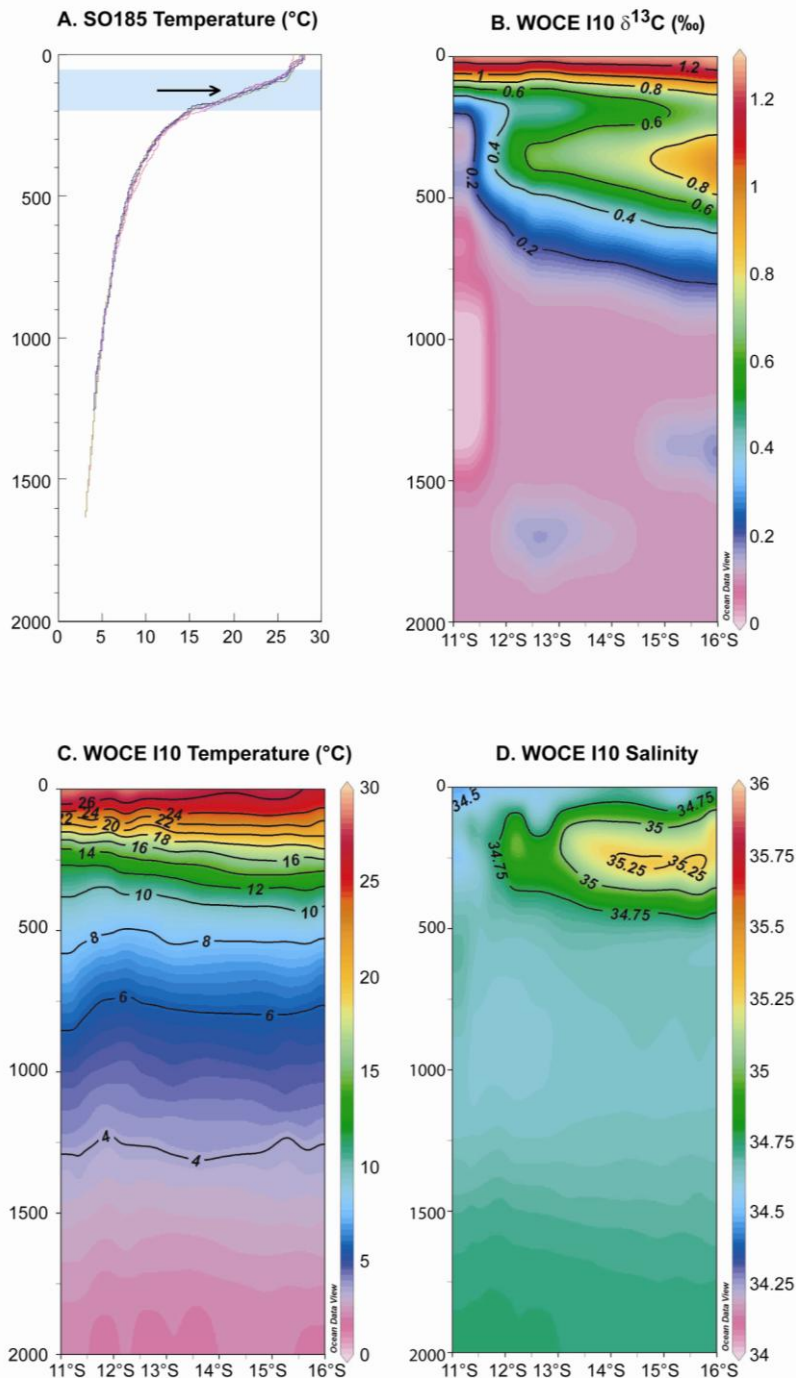


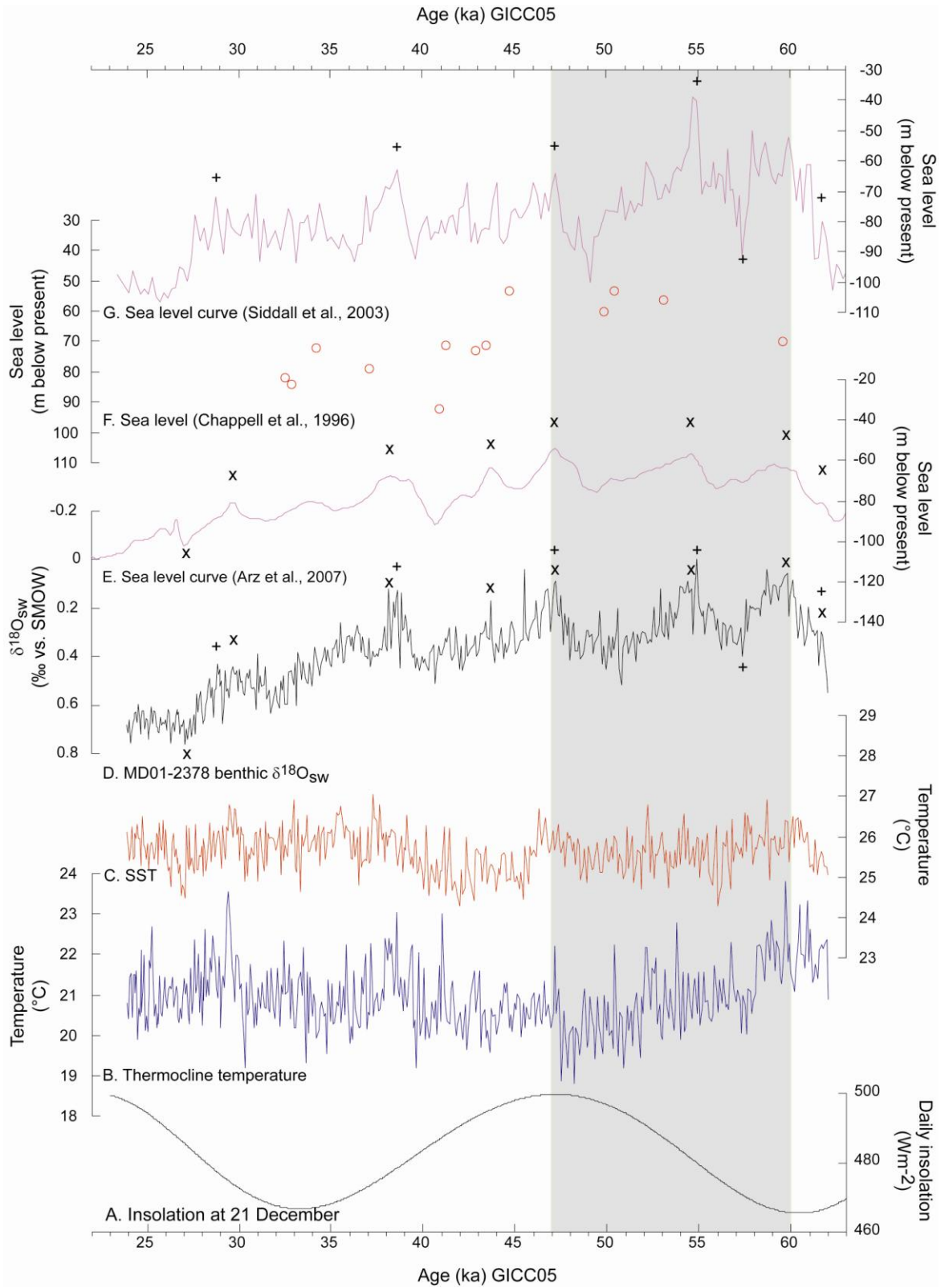
Figure 3.5. (a) Timor Sea temperature profiles obtained in September 2005 during SO-185 cruise (Kuhnt et al., 2005) indicates temperature difference of $\sim 5^\circ\text{C}$ between surface and upper thermocline. Shaded bar indicates extent of thermocline with arrow at base of upper thermocline. Shaded bar indicates extent of thermocline with arrow at base of upper thermocline, where *P. obliquiloculata* calcifies (Ravelo and Fairbanks, 1993; Cléroux et al., 2007); (b) Temperature profile along WOCE Line i10 (plotted section starts from South Java); (c) $\delta^{13}\text{C}$ profile along WOCE Line i10; (d) Salinity profile along WOCE Line i10. WOCE data are available at <http://doi.pangaea.de/10.1594/PANGAEA.277652>.

climate seesaw, as Northern Hemisphere cooling/warming is balanced by Southern Hemisphere warming/cooling [Broecker, 1998; Shackleton et al., 2000].

However, our SST record indicates little change during stadials and interstadials, implying that $\delta^{18}\text{O}$ *G. ruber* (white) maxima during HEs 3–6 are mainly due to $\delta^{18}\text{O}_{\text{sw}}$ increases, as shown in Figure 3.2. Tropical records from the West Pacific Warm Pool region also revealed that stadials

were characterized by heavier $\delta^{18}\text{O}_{\text{sw}}$ in surface-dwelling foraminifers. These $\delta^{18}\text{O}_{\text{sw}}$ increases were interpreted as a shift toward cooler and drier (El Niño-like) conditions during stadials [Stott et al., 2002; Dannenmann et al., 2003; Rosenthal et al., 2003; Levi et al., 2007]. However, the Timor Sea record from core MD01-2378 additionally displays prominent increases in thermocline temperature and $\delta^{18}\text{O}_{\text{sw}}$ during HEs 3–6 (Figures 3.2 and 3.3). We attribute these changes to an increased influence of warmer, saltier thermocline water from the tropical Indian Ocean and a concurrent decrease in cool, fresh ITF thermocline flow, due to an overall slowdown in the global thermohaline circulation during HEs. The decreased freshwater export from the North Pacific would additionally contribute to higher salinity ($\delta^{18}\text{O}_{\text{sw}}$) in the tropical eastern Indian Ocean.

Proxy data and ocean model simulations indicate a near collapse of the MOC during HEs [Sarnthein et al., 1994, 2001; Alley and Clark, 1999; Ganopolski and Rahmstorf, 2001; Broecker, 2003; Piotrowski et al., 2004]. Model experiments also predict that a slowdown in the global thermohaline circulation (for instance during the LGM) would result in a weaker ITF, which in turn would diminish the southward flowing Leeuwin Current and the fresh and cool thermocline flow feeding the South Equatorial Current [De Deckker et al., 2003; Gordon, 2005]. Today, the southern front of the cool and fresh thermocline water mass, which is



injected into the eastern equatorial Indian Ocean by the ITF, is located at approximately 13– 14°S [Gordon, 2005; Locarnini et al., 2006; Antonov et al., 2006], close to the position of core MD01-2378. During periods of reduced thermohaline circulation and weakened ITF flow, this front might have moved northward. Thus, the location of core MD01-2378 became increasingly influenced by relatively warm, salty thermocline water from the Indian Ocean rather than by cooler, fresher thermocline water flowing out of the Indonesian seas into the Timor Sea.

The pace and amplitude of thermocline warming and $\delta^{18}\text{O}_{\text{sw}}$ changes differed significantly during successive HEs. The most sustained episode of ITF weakening and thermohaline slowdown occurred at the end of MIS 4 and through HE 6, as indicated by highest temperature and $\delta^{18}\text{O}_{\text{sw}}$ values persisting over ~3 ka (Figure 3.3). Sharp drops in thermocline temperature and $\delta^{18}\text{O}_{\text{sw}}$ occurred only at ~58.5 ka, which is ~1 ka later than the end of HE 6. The early part of HE 5 was characterized by minimum thermocline temperature values and low $\delta^{18}\text{O}_{\text{sw}}$, marking the end of a long-term increase in ITF intensity from ~60 to 47 ka before a sharp decrease in ITF flow toward the end of HE 5. HEs 3–4 also coincided with

Figure 3.6. Comparison of sea level reconstructions, benthic $\delta^{18}\text{O}_{\text{sw}}$, temperatures and insolation during MIS 3. (a) December 21 maximum insolation at 25°S; (b) *P. obliquiloculata* Mg/Ca derived upper thermocline temperature; (c) *G. ruber* (white) Mg/Ca derived SST; (d) benthic $\delta^{18}\text{O}_{\text{sw}}$, + indicates tie points to sea level curve from central Red Sea (Siddall et al., 2003), x indicates tie points to sea level curve from northern Red Sea (Arz et al., 2007); (e) Sea level curve from northern Red Sea (Arz et al., 2007) tuned to MD01-2378 to maintain chronological consistency; (f) coral-based sea level data from Huon Peninsula plotted on independent age scale (Chappell et al., 1996); (g) sea level curve from central Red Sea (Siddall et al., 2003) tuned to MD01-2378 to maintain consistency. Thermocline cooling coincident with rising sea level (~60 m below present) and increasing insolation over Australia in the early part of MIS 3 (60 - 47 ka) is indicated by grey bar.

prominent decreases in ITF flow, however the declines in ITF intensity occurred more gradually over these stadial events. For HE 4, the decrease in ITF flow was maintained for a few hundred years after the end of the stadial, which is not surprising, as HE 4 is considered the most intense of the six Heinrich layers in the North Atlantic [Hemming, 2004].

3.4.3. Main Controls of ITF Variability During MIS 3

Global changes in thermohaline circulation evidently exert a major control on ITF variability, as demonstrated by the prominent decreases in outflow intensity registered during HEs 3–6. However, the different expression of HEs as well as the longer trends of ITF variability detected in our Timor Sea record suggest that the strength of the thermohaline circulation is not the sole control on ITF intensity and that additional factors may also play a significant role. Today, links between wind surges from the South China Sea prior to and during the onset of the Australian monsoon provide evidence for cross-equatorial atmospheric connections between the Asian winter monsoon and Australian summer monsoon [Suppiah and Wu, 1998]. During MIS 3, such cross equatorial connections would have effectively linked ITF outflow intensity to rapid, large-amplitude climate events in the Northern Hemisphere high latitudes. Intensification of the Australian monsoon triggered by episodes of Northern Hemisphere cooling would have piled up water masses in the eastern Indian Ocean, thus decreasing further the ITF outflow into the Timor Sea during HEs.

A unique feature of the ITF is the en route alteration of inflowing Pacific water into a strongly stratified thermocline dominated flow at the southern end of the Makassar Strait [Gordon, 2005]. This change in ITF vertical structure is dependent on sea level and the strength of the SE Asian boreal winter monsoon. Today, thermocline flow of relatively cool water dominates during boreal winter, as the warm surface flow becomes blocked by the development of a fresh water plug at the southern tip of the Makassar Strait, driven by monsoonal winds from the South China Sea through the Java Sea [Gordon et al., 2003]. As a result, the ITF becomes cooler, fresher, and dominated by thermocline rather than surface flow [Gordon et al., 2003]. However, this mechanism requires an open marine connection between the South China and Java Seas over a flooded Sunda shelf, which relates to a sea level position of at least 80 m above the LGM sea level, equivalent to the present-day sill depth of the Karimata Strait (~40 m).

Comparison of sea level reconstructions for MIS 3 indicates that this threshold was not reached during MIS 4, most of MIS 3 and the LGM (Figure 3.6). However, significant freshwater input may have occurred from Java, Borneo and Sundaland into the Java Sea, which increasingly became submerged at times of rising sea level during MIS 3. The most recent sea level curves [Siddall et al., 2003; Arz et al., 2007] indicate that the shelf of the Java Sea became flooded in the early part of MIS 3 (after ~60 ka), as sea level reached 60–70 m below present-day level. The long term increasing trend of thermocline cooling from 60 to 47 ka (Figure 3.3) may have been driven by the establishment of the Java Sea freshwater export, as sea level rose following the MIS 4 lowstand. Intensified SE

Asian winter monsoon linked to increasing insolation during this interval [Wang et al., 2001] would have additionally enhanced the thermocline cooling trend (Figure 3.6). This effect even continued in the early part of HE 5, as the onset of ITF slowdown appears delayed during this HE.

However, thermocline cooling stopped rather abruptly at the end of HE 5, and the intensity of the thermocline outflow remained overall decreased after HE 5 (Figure 3.3). After 47 ka, peak insolation over the neighboring Australian continent appears to have strongly influenced the hydrography of the Timor Sea (Figure 3.6). The sharp decrease in ITF intensity at the end of HE 5, which interrupts the long-term thermocline cooling trend from ~60 to 47 ka occurs ~1 ka before a prominent surface cooling at 46 ka, lasting until 40 ka. Dürkop et al. [2008] interpreted this event as the intrusion of a cold surface water tongue with increased influence of cooler, more nutrient rich waters from the West Australian Current and overall weakening of the ITF. The maximum in austral summer (21 December, 25°S) insolation at 47 ka would have favored the intensification of monsoonal winds over northern Australia, and in turn influenced the migration of hydrological fronts between Indian Ocean– and ITF-derived water masses, thus altering ITF flow and intensity.

3.5. Conclusion

Our high-resolution stable isotope and Mg/Ca records of surface and thermocline dwelling planktonic foraminifers in core MD01-2378 from the Timor

Sea indicate substantial temperature and salinity ($\delta^{18}\text{O}_{\text{sw}}$) changes in ITF outflow water masses during HEs 3–6. We interpret thermocline warming during HEs 3–6 as evidence for the increased influence of warmer, saltier thermocline water from the tropical Indian Ocean and attendant decrease in cool, fresh ITF thermocline flow, due to an overall slowdown in the global thermohaline circulation during HEs 3–6. These changes in the ITF structure and intensity during HEs must have had far-reaching repercussions on the hydrography of the tropical Indian Ocean as well as regional and global climate evolution. The resulting warmer and saltier eastern tropical Indian Ocean would have in turn strongly influenced the Asian Monsoon system and significantly altered the heat and energy budget within the “warm” return branch of the global thermohaline circulation.

Three main factors appear to have influenced ITF variability during MIS 3: (1) global slowdown in thermohaline circulation during HEs, triggered by Northern Hemisphere cooling and restricted deep water formation in the North Atlantic; (2) increased freshwater export from the Java Sea into the ITF during the early part of MIS 3, principally controlled by sea level and (3) insolation-related changes in Australasian monsoonal intensity leading to the migration of hydrological fronts between Indian Ocean– and ITF-derived water masses at 46–40 ka. The complex interplay between these factors resulted in a unique pattern of ITF variability during MIS 3, which differs from changes recorded on glacial-interglacial timescales. Previous work focusing on Terminations I and II indicated that an overriding control of ITF thermocline flow intensity during terminations was the establishment of an open connection through the Java Sea to the South China Sea, when sea level

reached ~40 m below present, in conjunction with a fully developed Australasian monsoonal system [Xu et al., 2008]. Such conditions were only reached at peak interglacials during MIS 5e and the late Holocene.

Chapter 4
Intertropical Convergence
Zone migration during
Marine Isotope Stage 3:
evidence from the Timor
Sea

4. Intertropical convergence zone migration during Marine Isotope Stage 3: evidence from the Timor Sea

Abstract

We present high resolution sea surface and upper thermocline temperature and stable isotope records spanning Marine Isotope Stage 3 (~24-62 kyr BP) from SO185-18460 (128° 38.485' E and 8° 47.386' S; 1875 m water depth) located within the Indonesian Throughflow passage in the Timor Strait. Comparison between stable isotopes and Mg/Ca of the near surface dwelling planktonic foraminifer *Globigerinoides ruber* (white) and the upper thermocline dwelling *Pulleniatina obliquiloculata* between Core SO185-18460 and existing data from Core MD01-2378 (situated in the southwest Timor Sea) indicate repeated incursions of warmer and saltier Indian Ocean thermocline water into the Western Timor Sea. These incursions occurred during Northern Hemisphere stadials, Heinrich Events 3 to 6 and are reflected by maximum thermocline temperature gradient between NE (Indonesian Throughflow) and SW (mixing zone) Timor Sea. We relate these events of thermocline warming in the SW Timor Sea to a slow-down of global thermohaline circulation. Increased precipitation inferred from $\delta^{13}\text{C}$ during stadials was observed in Timor Strait reflecting southward migration of the Intertropical Convergence Zone.

4.1. Introduction

Semi-periodic instability of ice sheets during the last glacial period (Marine Isotope Stages, MIS 2 and 3) result in abrupt and massive iceberg discharges to the North Atlantic, periods that have been termed Heinrich Events (HEs) [Bond et al., 1993; Dansgaard et al., 1993; Broecker, 1994] and were recorded as cooling events (stadials) in Greenland ice core records. The freshwater influx into the North Atlantic decrease water salinity and disrupt the Atlantic Meridional Overturning Circulation (AMOC) that drives the global thermohaline circulation. Proxy data and ocean modeling results both indicated that the AMOC is considerably slowed down or even collapsed during HEs [Sarthein et al., 1994, 2001; Alley and Clark, 1999; Ganopolski and Rahmstorf, 2001; Broecker, 2003; Piotrowski et al., 2004] resulting in major cooling at mid latitudes in the North Atlantic, reduced precipitation in East Asia and low-latitude Northern Hemisphere, and increased precipitation south of the equator related to southward displacement of the Intertropical Convergence Zone (ITCZ) [Arz et al., 1998; Wang et al., 1999, 2001 and 2004; Behling et al., 2000; Peterson et al., 2000; Kienast et al., 2001; Stott et al., 2002; Koutavas et al., 2002; Partin et al., 2007; Müller et al., 2008; Griffiths et al., 2009].

The Indonesian Throughflow (ITF) forms the main return branch of the global thermohaline circulation consisting of a westward flow from the Pacific Ocean through the Indonesian Archipelago where this flow is “transformed” to produce the Indonesian Throughflow (ITF). Present day ITF transports an annual

average ~ 16 Sv ($1 \text{ Sv} = 10^6 \text{ m}^3 \text{ s}^{-1}$) of low salinity waters into the eastern Indian Ocean [Gordon and Fine, 1996; Gordon et al., 2003]. The primary pathway of the inflowing North Pacific thermocline water is via Makassar Strait, where the transport of the ITF at the southern tip of the Strait is modulated by seasonal build up of fresh water plug. The fresh water plug is driven from the Java Sea by westerly winds during boreal winter monsoon and inhibits the warm surface water from the Pacific Ocean from flowing southward into the Indian Ocean, leading to a cooler Indian Ocean sea surface, which in turn may weaken the Asian monsoon [Gordon et al., 2003].

Previous study from adjacent core in the Timor Sea revealed variability in the ITF intensity during Terminations I and II [Xu et al, 2006; 2008] and last glacial [Zuraida et al., 2009] that directly influences the temperature, salinity and nutrient distribution in the upper water column of the Indian Ocean [Gordon et al., 2003]. Variability in ITF intensity during MIS 3 is the result of interactions between three factors: slow-down on global thermohaline circulation during HEs, increased freshwater export from the Java Sea related to rising sea-level and insolation-related changes in the Australasian monsoon [Dürkop et al., 2008; Zuraida et al., 2009]. Reduced global thermohaline circulation may lead to a progressive southward displacement of the austral-summer ITCZ and increased precipitation in southern Indonesia [Griffiths et al., 2009].

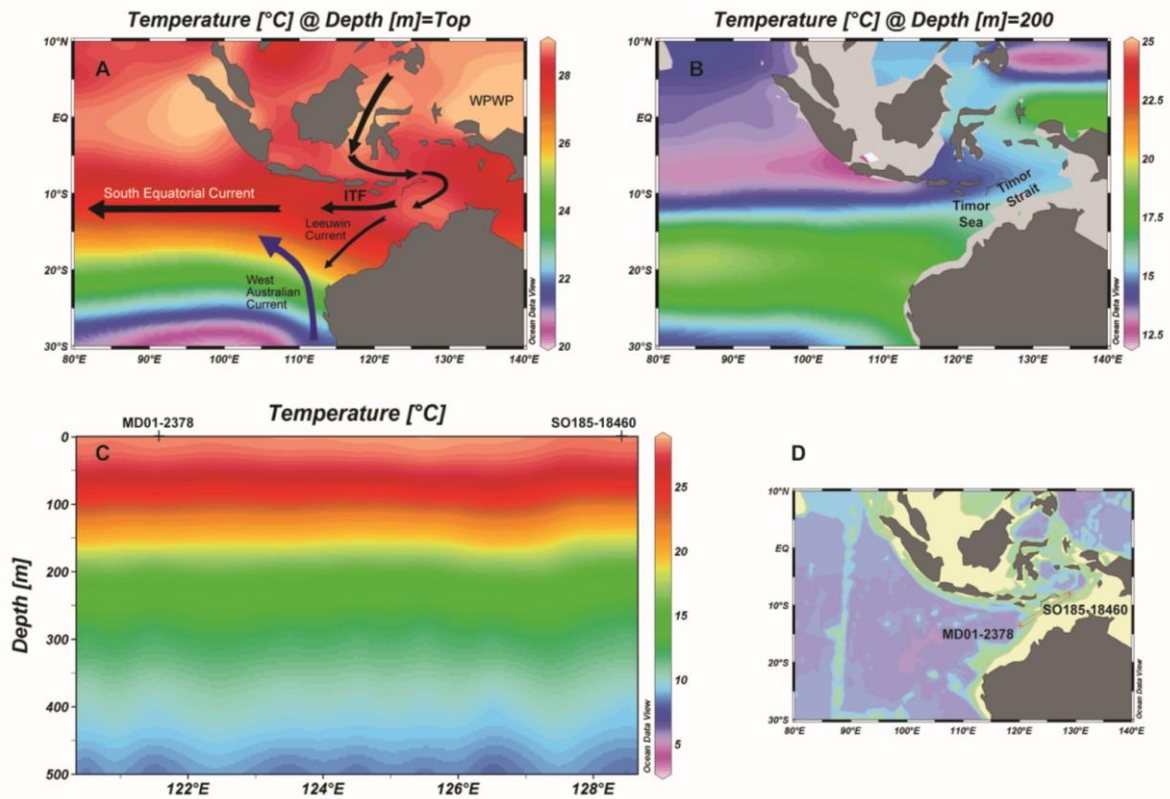


Figure 4.1. Annual temperature distribution in the Indo-Pacific region, based on World Ocean Atlas 2005 data [Locarnini et al., 2006]: a) close to the surface which is the habitat depth of *G. ruber* (white); b) within upper thermocline water mass which is the habitat depth of *P. obliquiloculata*; c) annual mean temperature vs. water depth profile between Timor Strait (Core SO185-18460) and Timor Sea (Core MD01-2378); d) bathymetric chart and core locations.

Core SO185-18460 (128° 38.485' E and 8° 47.386' S; 1875 m water depth) is located in the Timor Strait, close to the Lesser Sunda Islands, where one of the main ITF exits is located (Figure 4.1). Relatively high sedimentation rates during MIS 3 offer an exceptional opportunity to study climatic and paleoceanographic change during stadials in high-resolution. The combination of new isotope and Mg/Ca data from this core and existing data from Core MD01-2378 (121°47.27' E and 13°4.95' S; 1783 m water depth), situated in a more distal location within the outflow pathway of the ITF in the mixing zone of ITF pathway with subtropical

Indian Ocean waters (Figure 4.1), allows detailed investigation of the interaction between the ITF and the ITCZ during an interval of rapid global climate change.

4.2. Materials and Methods

Sediment samples (30–40 cc from 1 cm thick slices) were taken every 3 cm during interstadials and every 1 cm during stadials between 356 and 835 cm in Core SO185-18460 (128° 38.485' E and 8° 47.386' S; 1875 m water depth). The selection of stadal and interstadial intervals was based on the age of stadials observed in Core MD01-2378 (121°47.27'E and 13°4.95'S; 1783 m water depth) that is located in the west Timor Sea in the easternmost Indian Ocean (Figure 4.1). The paleotemperature record of Core MD01-2378 was published by Zuraida et al. [2009].

Sample preparation involved drying and weighing, and washing over a 63 μm sieve to dispose of the mud fraction within the samples. Then, the residues were dried on a sheet of filter paper and weighed. Afterward, the residues were sieved into 63–150 μm , 150–250 μm , 250–315 μm , and >315 μm fractions. This study used coupled Mg/Ca and $\delta^{18}\text{O}$ analyses on two species of planktonic foraminifer (*Globigerinoides ruber* (white sensu stricto) and *Pulleniatina obliquiloculata*) from the 250-315 μm size fraction to reconstruct surface and subsurface water masses conditions during MIS 3.

4.2.1. Mg/Ca analysis

We used Mg/Ca-temperature of *G. ruber* and *P. obliquiloculata* as indicators of SST and thermocline temperature, respectively. *G. ruber* is a well-known surface dweller, whereas *P. obliquiloculata* has a preferred depth habitat within the seasonal thermocline [Mohtadi et al., 2009; Xu et al., 2006 and references therein; Cléroux et al., 2007; Farmer et al., 2007]. Approximately 30 tests of *G. ruber* and ~20 tests of *P. obliquiloculata* (250~315 μm size fraction), weighing ~0.3–0.5 mg/sample, were measured for Mg/Ca. Tests were gently crushed and cleaned following the standard procedure outlined in Barker et al. [2003].

The choice of cleaning protocol was based on the following reason: 1) there is no large source of sediments near the site location; 2) relatively low terrigenous content found in Core MD01-2378 by Holbourn et al. [2005]; and 3) the result of a comparison between reductively-cleaned and non-reductively cleaned carried out on samples from MD01-2378 (see Chapter 2 Section 2.3.1.1 for detail). The reductive cleaning was conducted at the Institute of Geosciences, Christian-Albrechts University of Kiel, by Xu [2006] while the non-reductive cleaning was carried out at the IfM-GEOMAR, Kiel. Results show that in general the reductive step would reduce the Mg/Ca of *G. ruber* by an average of 0.27mmol/mol, while it has no effect on Mg/Ca of *P. obliquiloculata*. The negligible difference in Mg/Ca of treated and non-treated samples of *P. obliquiloculata* suggests that the Mg-content related to Mn-contaminant is very small. The huge difference in the Mg/Ca of treated and non-treated samples of *G. ruber* is speculated as the loss of Mg from the tests during the reductive cleaning.

A total of 368 samples of *G. ruber* (white) and 314 of *P. obliquiloculata* were analyzed with the ICP-OES Spectro Ciros CCD SOP at the Institute of Geosciences, Christian-Albrechts-University, Kiel. The analytical error of the instrument is ~0.1%. The replicability of our measurements, based on 28 *G. ruber* (white) and 28 *P. obliquiloculata* replicate samples, is 0.2 mmol/mol (corresponding to 0.5°C) for *G. ruber* (white) and 0.05 mmol/mol (corresponding to 0.3°C) for *P. obliquiloculata*. We checked the validity of Mg/Ca values by evaluating the Ca contents and Fe/Mg values of the samples using the limit of 0.1 mol/mol for the latter suggested by Barker et al. [2003]. As a result, 10 samples of *G. ruber* and 9 samples of *P. obliquiloculata* were rejected. Shell weight of both *G. ruber* (white) and *P. obliquiloculata* show no significant changes during MIS 3 (Table 4.1) indicating no significant dissolution occur in site location.

Sea surface temperature (SST) and upper thermocline temperature were reconstructed from *G. ruber* (white) and *P. obliquiloculata* Mg/Ca values, respectively. Conversion of Mg/Ca values into temperature was performed using the general equation $Mg/Ca = 0.38 (\pm 0.02) \exp 0.090 (\pm 0.003)T$ for *G. ruber* (white) and the species specific $Mg/Ca = 0.328 (\pm 0.007) \exp 0.090 (\pm 0.003)T$ for *P. obliquiloculata* [Anand et al., 2003]. The choice of equations was describe in detail in Zuraida et al. [2009].

Xu et al. [2006] employed the temperature gradient (ΔT) between sea surface and thermocline water masses as indicator of ITF intensity. Temperature gradient was calculated by subtracting Mg/Ca-temperature of *P. obliquiloculata* from Mg/Ca-temperature of *G. ruber*. At present, ΔT changes seasonally as a

result of freshwater influx from the Java Sea during the boreal winter monsoon [Gordon et al., 2003] resulting in maximum throughflow in June/July during boreal summer monsoon and minimum in February during boreal winter monsoon [Schott and McCreary, 2001].

We also calculate temperature gradients between the Timor Strait and Timor Sea by point to point subtraction of MD01-2378 temperature from SO185-18460 temperature. Before the subtraction, we resample the temperature data of both sites into equivalent age interval (every 100 years). Due to negligible differences in age model, no age tuning for Core MD01-2378 was performed in this operation.

4.2.2. Stable isotope analyses

For stable isotope ($\delta^{18}\text{O}$ and $\delta^{13}\text{C}$) analyses, we selected 20 tests of *P. obliquiloculata* from the 250 – 315 μm size fractions. All tests were checked for cement encrustations and infillings before being gently crushed between two glass plates and cleaned with methanol in an ultrasonic bath, then dried at 40°C. Stable isotope analyses were performed at Leibnitz Institute, University of Kiel, on a Finnigan MAT 251 Mass Spectrometer with an automated Kiel carbonate preparation device. Samples were reacted by individual acid addition. The mean external error and reproducibility of carbonate standards is <0.07‰ for $\delta^{18}\text{O}$ and 0.07‰ for $\delta^{13}\text{C}$. The values are reported relative to the Peedee Belemnite (PDB) scale, based on calibration to the National Bureau of Standards (NBS) 19. Stable

isotope data for *G. ruber* (white) are from Dürkop [2009], using the same methods and instruments. Oxygen isotope core top data are from Erichsen [2009] and carbon isotope core top data are from Xu [2009, pers. comm]. Xu [2009, pers. comm] used similar size fraction (250~315 μm) with this dissertation, while Erichsen [2009] used larger size fraction (350~500 μm).

4.2.3. $\delta^{18}\text{O}_{\text{seawater}}$

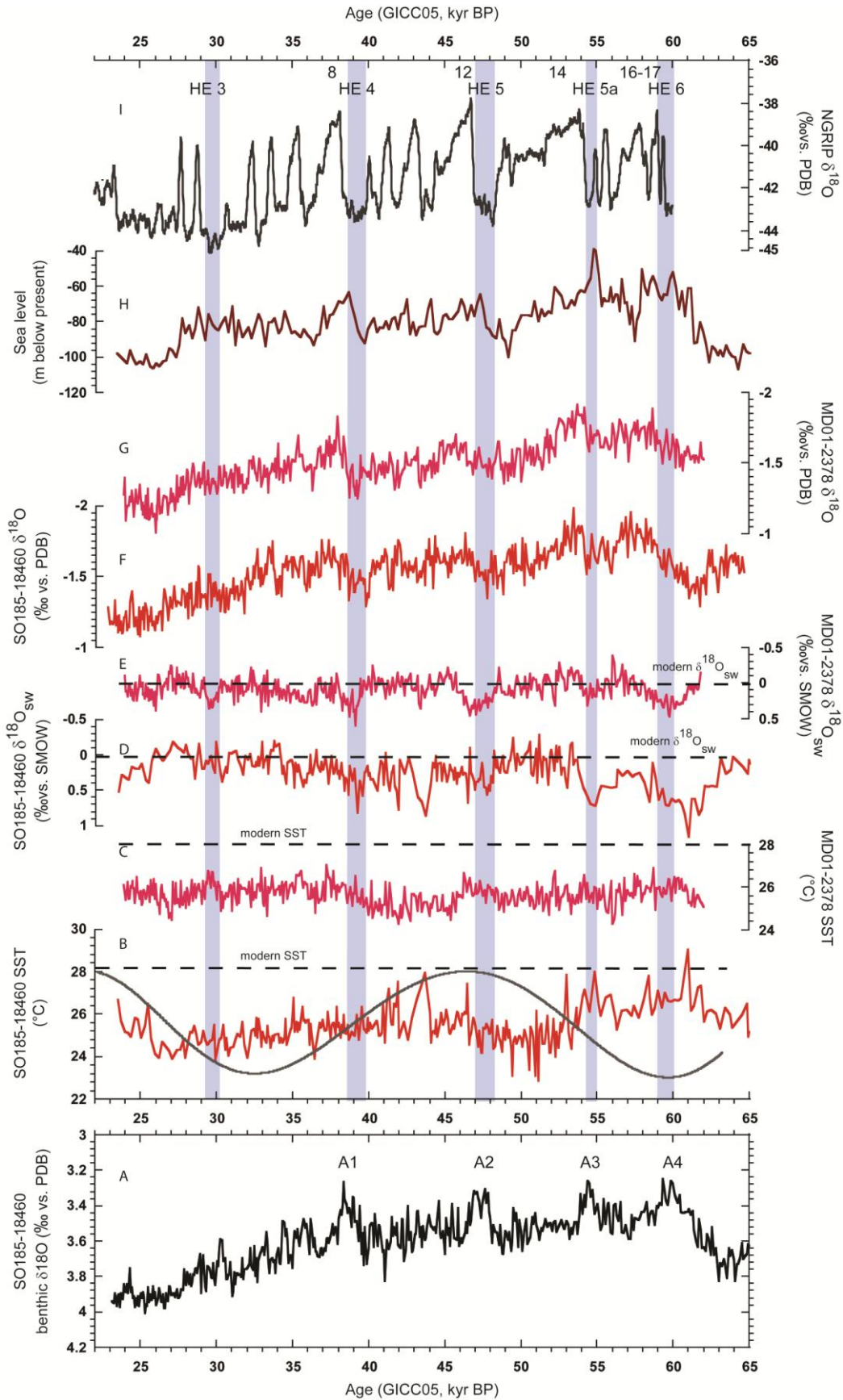
The equation applied to reconstruct paleo-salinity from $\delta^{18}\text{O}_{\text{seawater}}$ ($\delta^{18}\text{O}_{\text{sw}}$) for both species is the *Orbulina universa* LL equation of Bemis et al. (1998): $\delta^{18}\text{O}_{\text{sw}} = 0.27 + (T - 16.5 + 4.8 * \delta^{18}\text{O}) / 4.8$. The reasoning why we used the same equation for both *G. ruber* and *P. obliquiloculata* is described in detail in Zuraida et al. [2009]. Because the equation extracts the effect of temperature on oxygen isotope fractionation, the calculated $\delta^{18}\text{O}_{\text{sw}}$ is mainly influenced by $\delta^{18}\text{O}_{\text{sw}}$ variability related to continental ice volume and local $\delta^{18}\text{O}_{\text{sw}}$ fluctuations related to surface and upper thermocline salinities. Ice volume correction was conducted by subtracting benthic $\delta^{18}\text{O}_{\text{sw}}$ (five-point smoothed) from planktonic $\delta^{18}\text{O}_{\text{sw}}$ within the same samples, following the method described in Zuraida et al. [2009].

4.3. Results

4.3.1. Oxygen Isotopes

The *G. ruber* (white) $\delta^{18}\text{O}$ values of Core SO-18460 vary between $\sim -1.1\text{‰}$ and $\sim -2\text{‰}$ over the entire MIS 3 record (Figure 4.2), with an average of -1.5‰ , which is $\sim -1.3\text{‰}$ heavier than present day value from the core top data [Erichsen, 2008]. The oxygen isotope of *G. ruber* (white) exhibits long-term trends similar to the record from Core MD01-2378 with exception of the older part, between 65 and 63 ka, that is marked by increased $\delta^{18}\text{O}$ from $\sim -1.6\text{‰}$ to $\sim -1.4\text{‰}$. From 63 ka to ~ 53 ka, the oxygen isotope decreases from -1.4‰ to $\sim -2.0\text{‰}$. Between ~ 53 ka and ~ 40 ka, the $\delta^{18}\text{O}$ values decrease to reach its minimum value of $\sim -1.3\text{‰}$. After a rapid decrease to $\sim -1.8\text{‰}$ at ~ 37 ka, $\delta^{18}\text{O}$ *G. ruber* continues rising to reach maximum value of $\sim -1.1\text{‰}$ at ~ 23 ka. The rapid decrease at ~ 37 ka shows strong similarity to the benthic $\delta^{18}\text{O}$ record and probably represent ice volume component. Superimposed on this long-term variability are high frequency variations, which show similarities to fluctuations characteristic of northern high latitude planktonic and ice core records. However, as was observed in Core MD01-2378, only longer lasting D-O warm events 8, 12, 14 and 16-17. The associated stadials HEs are marked by increases of $\sim 0.3\text{‰}$ - 0.4‰ (Figure 4.2).

The $\delta^{18}\text{O}$ values of *P. obliquiloculata* vary between 0.9‰ and -0.7‰ with an average of 0‰ which is 1.7‰ heavier than modern value [Erichsen, 2008]. The $\delta^{18}\text{O}$ *P. obliquiloculata* of Timor Strait are significantly heavier than the $\delta^{18}\text{O}$ of the



same species from Core MD01-2378 (Figure 4.3), reflecting the difference in position between the two cores with regard to the ITF. Due to its position within the flow of ITF, $\delta^{18}\text{O}$ of *P. obliquiloculata* of Core SO185-18460 points to cooler thermocline water mass in site location, which is also indicated by modern thermocline temperature difference between both sites (see the following section). The $\delta^{18}\text{O}$ of *P. obliquiloculata* also exhibits higher-amplitude variations than *G. ruber* (white) of the same core and *P. obliquiloculata* of Core MD01-2378. The $\delta^{18}\text{O}$ *P. obliquiloculata* broadly trace the $\delta^{18}\text{O}$ *G. ruber* and show similar long term trend of increasing $\delta^{18}\text{O}$ between 65 and ~63 ka from ~-0.5‰ to ~-0.2‰. Between 63 ka to ~53 ka, $\delta^{18}\text{O}$ decreases from -0.1‰ to ~-0.5‰. The $\delta^{18}\text{O}$ values increase to reach ~-0.2‰ at ~40 ka followed by rapid decrease to reach the minimum value of ~-0.7‰ at ~37 ka. From ~37 ka to ~23 ka, $\delta^{18}\text{O}$ *P. obliquiloculata* continues rising to reach maximum value of ~-0.3‰ at ~24 ka. Unlike MD01-2378, $\delta^{18}\text{O}$ *P. obliquiloculata* of SO185-18460 shows no clear high-frequency variations that are attributable to D-O warm events but shows increased values during HEs 3 and 5.

4.3.2. Carbon Isotope

Carbon isotope records from Timor Strait show a significantly lower gradient between $\delta^{13}\text{C}$ of *G. ruber* and *P. obliquiloculata* than during Core MD01-2378 from

Figure 4.2. Comparison between Core SO-18460 (red) and Core MD01-2378 (pink) records of SST (B and C), $\delta^{18}\text{O}_{\text{sw}}$ (D and E), $\delta^{18}\text{O}$ (F and G), Central Red Sea MIS 3 sea level (H) from Siddall et al. (2003), and NGRIP $\delta^{18}\text{O}$ record (I), and SO-18460 *Planulina wuellerstorfi* $\delta^{18}\text{O}$ (A). Blue bars depicted Heinrich events. The timing for each HEs follows Svensson et al.[2008], except for HE5a. The timing for HE5a is inferred from Rashid et al. [2003].

the Timor Sea (Figure 4.4). The $\delta^{13}\text{C}$ of *G. ruber* from the Timor Sea is almost always heavier (average MIS 3 $\delta^{13}\text{C}$ is $\sim 1.4\text{‰}$) than in the Timor Strait (average $\delta^{13}\text{C}$ is $\sim 1.2\text{‰}$), while average MIS 3 $\delta^{13}\text{C}$ *P. obliquiloculata* from both cores is $\sim 0.9\text{‰}$. This low gradient is mostly caused by lower $\delta^{13}\text{C}$ values of *G. ruber* rather than higher $\delta^{13}\text{C}$ of *P. obliquiloculata*.

A comparison of the vertical $\delta^{13}\text{C}$ gradient of two cores shows that the average $\delta^{13}\text{C}$ difference in the Timor Sea is 0.5‰ , while in the Timor Strait it is only 0.3‰ . Four events of low $\delta^{13}\text{C}$ gradient were observed in Core SO185-18460, which occurred during stadial HEs 3 – 5a (Figure 4.4C): $\delta^{13}\text{C}$ gradients during HEs 3 - 5 are $\sim 0.1\text{‰}$ and during HE 5a is 0.2‰ . Clear trend of decreased $\delta^{13}\text{C}$ *G. ruber* is exposed during HE 4 and HE 5.

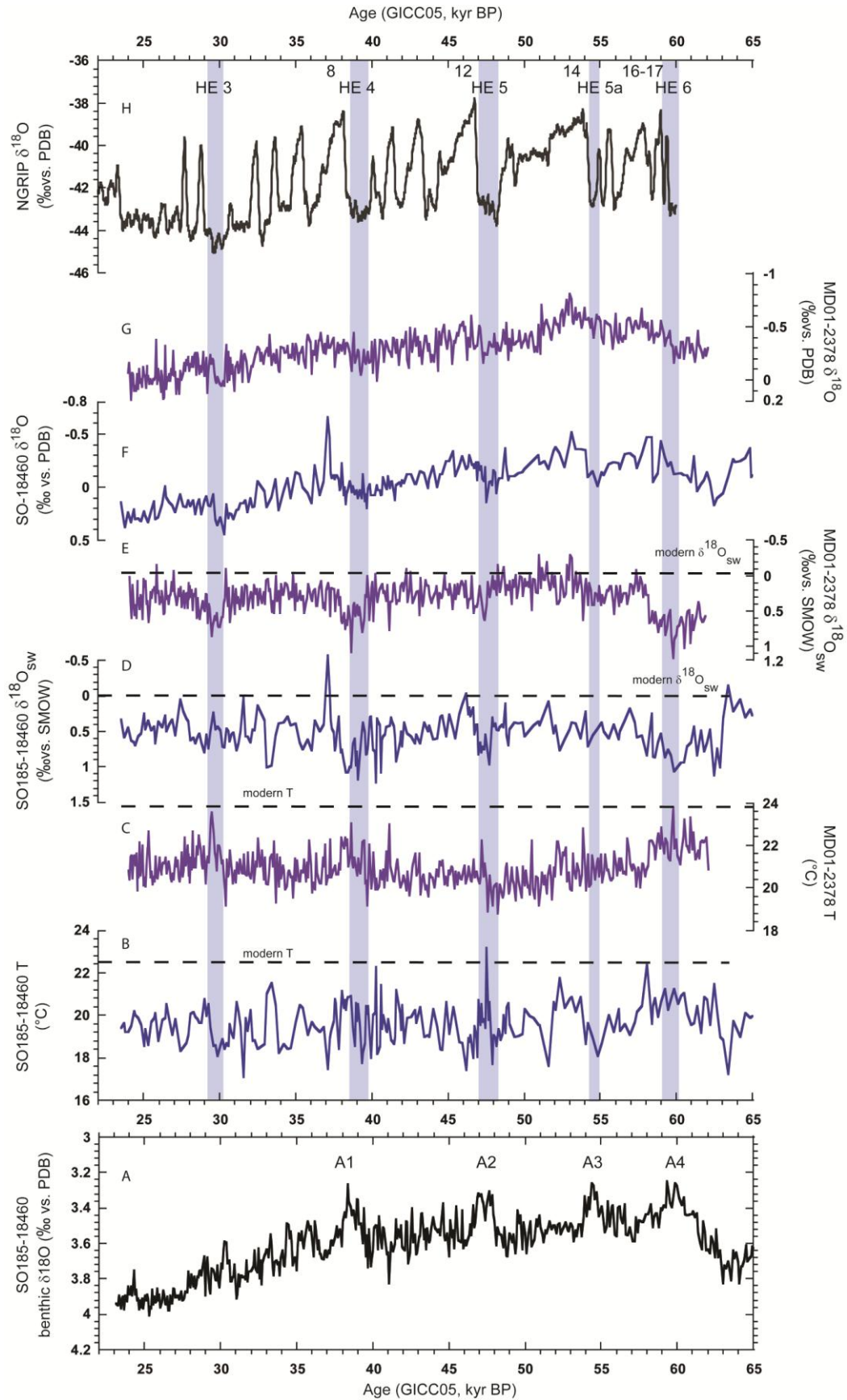
4.3.3. Mg/Ca temperature reconstructions

The average Mg/Ca-sea surface temperature (SST) estimates of Core SO-18460 over MIS 3 is 25.5°C , which is similar to the average MIS 3 SST in Core MD01-2378. This average SST is 3°C cooler than present day annual SST of 28.2°C [World Ocean Atlas 2005 data; Locarnini et al., 2006], but close to present day Southeast Monsoon (SEM) SST range ($26.1 - 27.4^{\circ}\text{C}$) in the West Banda Sea [Ilahude and Gordon, 1996]. Over MIS 3, the average thermocline temperature of Core SO-18460 is 19.6°C , which is 1°C lower than the average temperature in Core MD01-2378. The MIS 3 thermocline temperature of Core SO-18460 is 3°C

lower than the present day annual thermocline temperature of 22.6°C near the site location [World Ocean Atlas 2005 data; Locarnini et al., 2006]. The 1°C temperature gradient within thermocline water mass persists until today suggesting no considerable change in the water structure of the Timor Sea. Figures 4.2 and 4.3 show that temperature oscillations in surface and thermocline water masses in Core SO-18460 are twice as large as those in Core MD01-2378: SST varies between 22.8°C and 29.0°C (MD01-2378: 24.3 - 27.0°C), whereas upper thermocline temperature varies between 17.1°C and 23.2°C (MD01-2378: 18.8 - 23.8°C).

The SST values between 63 and 53 ka oscillate between 25 and 27°C and forms a warm temperature plateau above the SST average (25.2°C) during MIS 3 (Figure 4.2). This trend is similar to the thermocline temperature trend of Core MD01-2378 but the warm SST record of Core SO-18460 lasted longer by 5 ka. After 53 ka, SST cooled with values mainly below the MIS 3 average. The cooling event between HE 4 and HE 5 or Antarctic warm events A 1 and A 2 that was observed at 45-40 ka in Core MD01-2378 [Zuraida et al., 2009] is absent, but a slight cooling occurred between 54 and 47 ka. SST continued to cool until 23 ka before it started to increase toward MIS 2.

The structure of the upper thermocline temperature record evolution in Core SO-18460 over MIS 3 is different from Core MD01-2378 (Figure 4.3). The SO185-18460 record shows no warming trend during Heinrich Events as was observed in Core MD01-2378, with the exception of HE 5, where thermocline warming of ~5°C is observed at the end of the stadial.



4.3.4. Surface - Thermocline Temperature Gradient

The Marine Isotope Stage 3 surface – thermocline temperature gradient (ΔT) of Core SO185-18460 fluctuated around the value of 5.8°C (Figure 4.5). The average temperature gradient during MIS 3 is similar to present day value of 5.6°C, based on CTD measurement in site location during Sonne 185 VITAL Cruise [Kuhnt et al., 2006]. The temperature gradient curve exhibits high ΔT , above present day average, between 63 and 55 ka, follows by low ΔT , mostly below present day average, between 55 and 45 ka. From 45 to 23 ka, ΔT fluctuated around the MIS 3 average.

4.3.5. Regional Temperature Gradient

The average SST gradient between SO185-18460 and MD01-2378 over MIS 3 is -0.1°C , which is in the range of modern SST gradient between the two sites. However, Figure 4.5 shows that this gradient underwent strong variability during MIS 3 with prominent positive gradients related to warmer SST in the Timor Strait between 63 and 54 ka and SST cooling event in the Timor Sea between 46 and 40 ka.

The average of thermocline temperature gradient between SO185-18460 and MD01-2378 over MIS 3 is -1.2°C , which is also within range of modern

Figure 4.3. Comparison between Core SO-18460 (blue) and Core MD01-2378 (purple) records of thermocline temperature (B and C), $\delta^{18}\text{O}_{\text{sw}}$ (D and E), $\delta^{18}\text{O}$ (F and G), Central Red Sea MIS 3 sea level (H) from Siddall et al. (2003), and NGRIP $\delta^{18}\text{O}$ record (I), and SO-18460 *Planulina wuellerstorfi* $\delta^{18}\text{O}$ (A). Blue shades denote Heinrich Events 3 - 6.

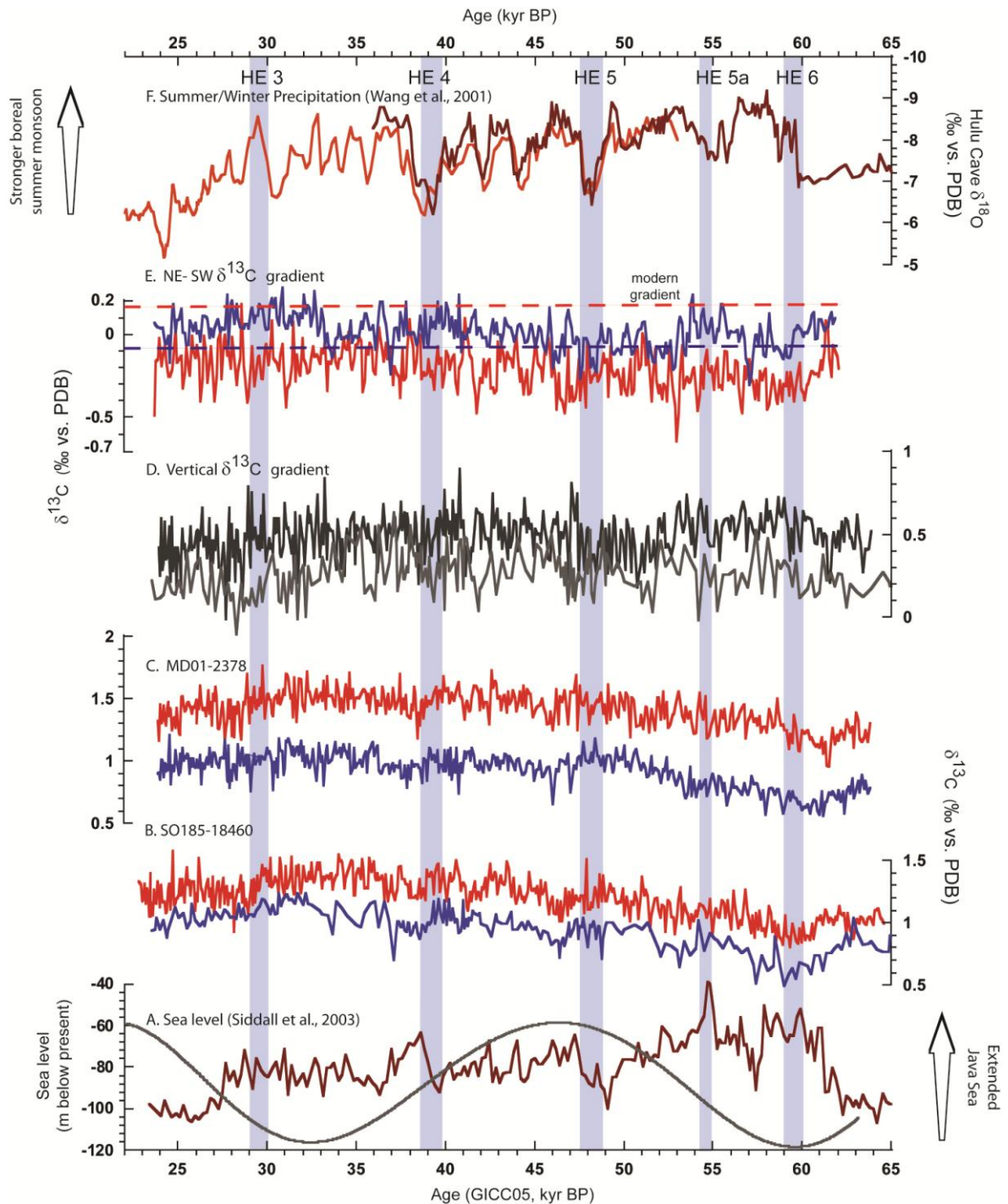


Figure 4.4. $\delta^{13}\text{C}$ of *G. ruber* (red) and *P. obliquiloculata* (blue) of Timor Strait (B) and Timor Sea (C), vertical gradient of $\delta^{13}\text{C}$ in Cores MD01-2378 and SO185-18460 (D) and regional/spatial gradient of $\delta^{13}\text{C}$ (E) compared to MIS 3 sea level indicating periods of extended Java Sea (A) and intensity of East Asian Monsoon (D). Black curve is maximum austral summer insolation over 25°S at 21 December. Black line in (D) represents Core SO185-18460 and grey MD01-2378. Red line in (E) is regional $\delta^{13}\text{C}$ gradient of *G. ruber* and blue is for *P. obliquiloculata*. Dashed line is modern value of $\delta^{13}\text{C}$ gradient for each species [Xu, 2009, pers.comm]. Blue bars indicate Heinrich Events.

thermocline temperature gradient indicating shallower thermocline in Timor Strait compared to Timor Sea (Figure 4.1C). The gradient reaches its maximum values during HEs 3, 4, 5a and 6 (Figure 4.5) when Timor Strait upper thermocline water was 4°C cooler than Timor Sea.

4.3.6. Sea surface salinity estimates ($\delta^{18}O_{sw}$)

The SO-18460 surface $\delta^{18}O_{sw}$ record (corrected for ice volume, following Zuraida et al., 2009) fluctuates between -0.3‰ and 1.2‰ SMOW with an average of 0.2‰ over MIS 3 (Figure 4.2). The average surface $\delta^{18}O_{sw}$ value of Core MD01-2378 is 0.1‰, while present day surface $\delta^{18}O_{sw}$ close to the position of our core is 0.02‰. In contrast to MD01-2378, no prominent increase in surface $\delta^{18}O_{sw}$ was observed during Northern Hemisphere stadial events HEs 3-6, except for HE 5.

Thermocline $\delta^{18}O_{sw}$ varies between 0 and 0.8‰ with an average of 0.4‰, which is similar to the value from Core MD01-2378 (Figure 4.3). The thermocline $\delta^{18}O_{sw}$ of Timor Strait broadly traces the record from Timor Sea, with the conspicuous absence of increasing $\delta^{18}O_{sw}$ during HEs.

4.4. Discussion

4.4.1. *Southward migration of ITCZ during Heinrich Events*

Heinrich Events have been recognized from Indo-Pacific equatorial region as either warming of upper thermocline water [Zuraida et al., 2009]; warmer and more saline surface water [Levi et al., 2007]; increase surface salinity [Dannenmann et al., 2003]; colder SST in Eastern Pacific [Kienast et al., 2006]; dry condition in northern Borneo and northern Australia [Partin et al., 2007, Turney et al., 2004]; relatively warm and saline surface water [Stott et al., 2002]; and warmer SST in mid-latitude Southern Indian Ocean [Sicre et al., 2005]. Warm and saltier surface water was reported from the tropical Atlantic Ocean [Schmidt et al., 2006], while strong mixing of surface and near-surface water in high latitude based on $\delta^{18}\text{O}$ was observed in Labrador Sea [Rashid and Boyle, 2007]. In the southwest Timor Sea, Heinrich Events 3, 4 and 5 were characterized by increasing thermocline temperature, and increasing $\delta^{18}\text{O}_{\text{sw}}$ of both surface and thermocline water [Zuraida et al., 2009]. Despite changes within surface and thermocline water masses, the vertical structure of the SW Timor Sea is relatively stable over MIS 3 [Zuraida et al., 2009]. Temperature fluctuations during that period are mainly caused by slowing down of global thermohaline circulation, enhanced by changes in freshwater input from the Indonesian Seas which is controlled by sea level, and insolation-related monsoon intensity.

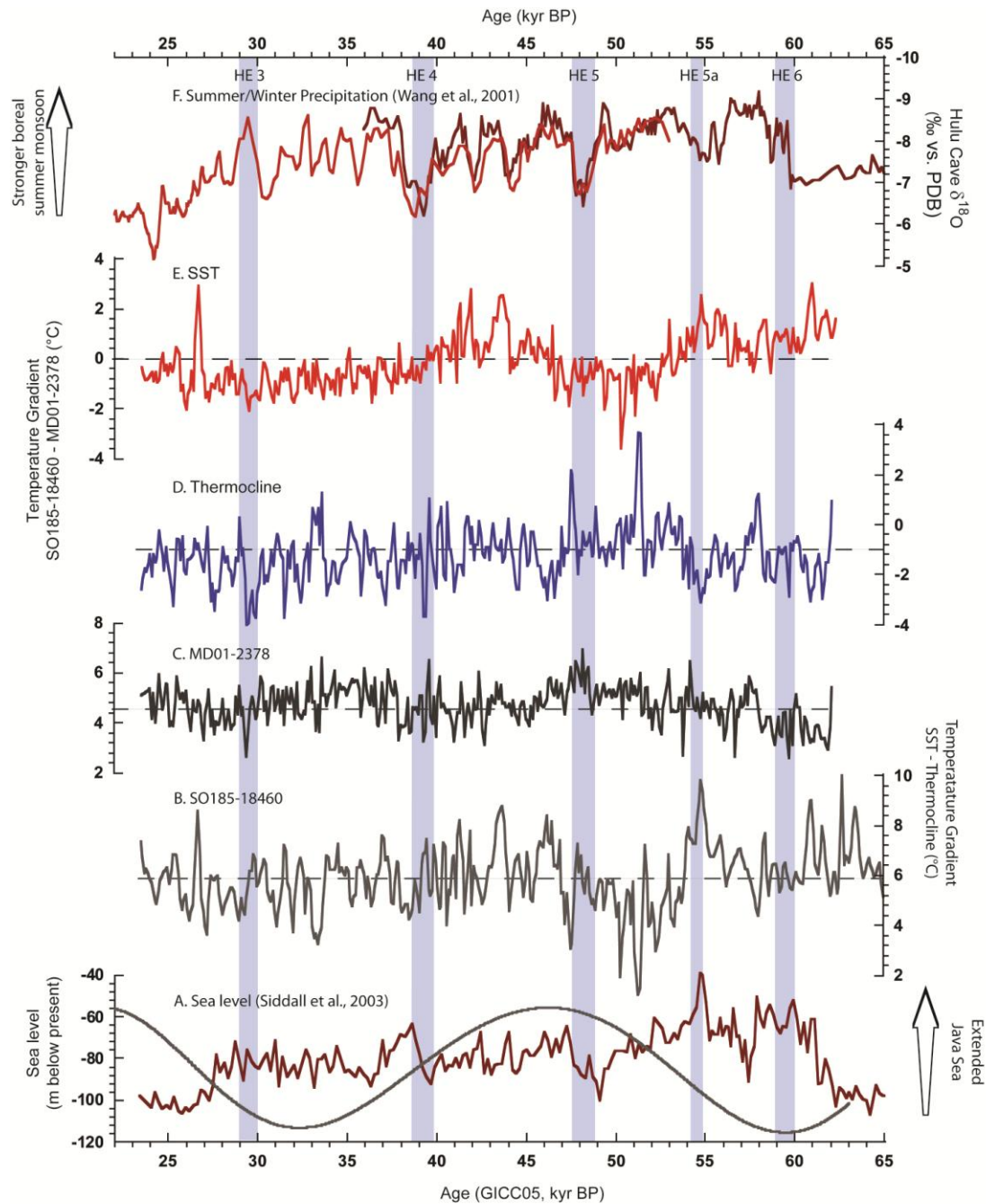


Figure 4.5. Temperature gradient between surface and thermocline water masses (B and C) of Cores SO185-18460 and MD01-2378; Thermocline temperature and SST gradients of Timor Strait (SO185-18460) and Timor Sea (MD01-2378) (D and E); compared to MIS 3 sea level indicating periods of extended Java Sea (A) and intensity of East Asian Monsoon (F). Solid black line is austral summer insolation over 25°S at 21 December. Dashed lines are modern values. Blue bars indicate Heinrich Events.

A different signal was observed in Timor Strait where HEs are not clearly detected in temperature, $\delta^{18}\text{O}$ and $\delta^{18}\text{O}_{\text{sw}}$ records of both surface and upper thermocline water masses (Figure 4.3), although quite obvious in the $\delta^{13}\text{C}$ signal. The carbon isotope records of surface- and thermocline-dwelling planktonic foraminifers from Core SO185-18460 reveal $\delta^{13}\text{C}$ convergence during HEs 3 to 6 (Figure 4.4). This is in contrast to the clear divergence between $\delta^{13}\text{C}$ of *G. ruber* and *P. obliquiloculata* over MIS 3 in Core MD01-2378.

There are several possibilities for this discrepancy in the $\delta^{13}\text{C}$ records: this may be due to 1) changes in the organic carbon biological pump, or 2) increasing surficial nutrient influx into the Timor Sea. The biological pump is driven by the amount of depleted organic carbon that is produced by phytoplankton in the photic zone and sinks down into deeper part of the water column, when it is remineralized, resulting in lower $\delta^{13}\text{C}$ values. However, this explanation implies decreased $\delta^{13}\text{C}$ values in the deeper water column.

The smaller $\delta^{13}\text{C}$ difference between *G. ruber* and *P. obliquiloculata* in Core SO185-18460 compared to Core MD01-2378 might be explained as thinner mixed layer, as was suggested by Spooner et al. [2005] from their study in the Banda Sea. However, temperature and $\delta^{18}\text{O}$ records from the same core suggest that a vertical structure persisted over MIS 3, which is approximately similar to present day. Another possible explanation is intensified mixing and deepening of the mixed layer during HEs related to increasing storminess, as was observed in the

Labrador Sea by Rashid and Boyle [2007]. However, it requires convergence in both stable isotope records, which is absent in Core SO185-18460.

Increasing nutrient influx into the Timor Strait is one mechanism remaining to explain the convergence in upper water column $\delta^{13}\text{C}$. During glacial, Sahul Shelf, the primary source for nutrients in this area, was also above sea level. The Sahul Shelf is a broad shallow platform to the north of the Australian coasts (water depth: 50 - 120 m) featuring a shallow depression in the middle (Bonaparte Depression) before dropping sharply into the Timor Sea. The Bonaparte Depression formed an estuarine embayment or a shallow lake with depths of 18 to 28 m [Lavering, 1993, from <http://www.aims.gov.au>] during the LGM. Nutrients from this depression could be transported by extensive paleo-river channels, some up to 150 km long and 5 km wide and up to 240 m deep, that connected the Bonaparte Depression to the Timor Sea. Increasing riverine nutrient flux leading to lighter $\delta^{13}\text{C}$ during low sea level was also observed in South China Sea and in the Eastern Mediterranean [Jian et al., 1999; Fontugne and Calvert, 1992].

Increased flux of terrigenous nutrient into the Timor Sea requires precipitation increases over Australia during HEs. Increased monsoon precipitation and riverine nutrient flux during glacial was observed in South China Sea [Jian et al., 1999; Kuhnt et al., 1999]. Proxies for precipitation/wetness from the Lynch Crater, NE Australia, and speleothem records from Liang Luar Cave, southern Indonesia, indicate enhanced rainfall in the region during Heinrich events (HEs 1–3) and Younger Dryas [Muller et al., 2008; Griffiths et al., 2009], while speleothem

records from Northern Borneo revealed drier conditions during HE 1 [Partin et al., 2007], suggesting that during stadials ITCZ shifted southward of present day position (Figure 4.6). Wetter conditions related to ITCZ migration during HEs over MIS 3 were also reported from the equatorial Atlantic region [Wang et al., 2004; Behling et al., 2000; Arz et al., 1998]. Southward migration of the ITCZ would increase monsoonal wind patterns offshore NW Australia that would push terrigenous nutrients into Timor Strait. Simulations of past ITCZ positions [Broccoli et al., 2006] indicate that increased temperature gradients between the Northern and Southern Hemispheres are the driving mechanism for the southern displacement of the ITCZ and that the sea ice extent in the North Atlantic was a major factor influencing the ITCZ position in the Atlantic [e.g. Kienast et al., 2006].

4.4.2. ITF variability during Heinrich Events

The ITF as part of global thermohaline circulation is influenced by global slowdown in thermohaline circulation during HEs triggered by Northern Hemisphere cooling. Climate proxies from Core MD01-2378 revealed thermocline warming and increased $\delta^{18}\text{O}_{\text{sw}}$ during HEs 3, 4, and 5 reflect weakening of the relatively cool and fresh ITF thermocline flow and reduced export of less saline water from the North Pacific and Indonesian Seas to the tropical Indian Ocean [Zuraida et al., 2009]. However, Core SO185-18460, which is located closer to the Indonesian Archipelago and in the path of the Throughflow, records the ITF outflow, regardless of its intensity. This implies that ITF slow-down would result in

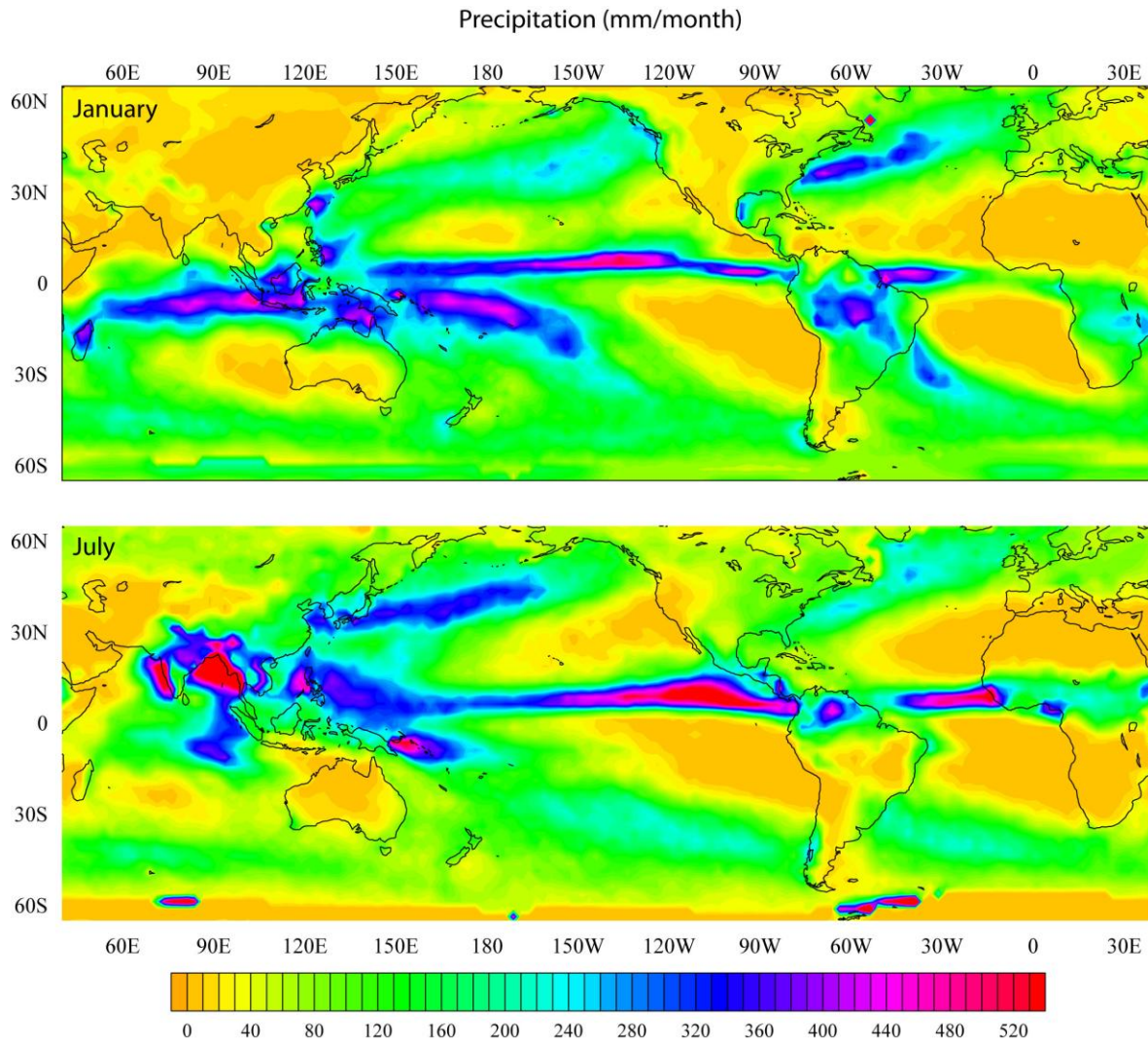


Figure 4.6. Modern global precipitation in January when the ITCZ is over Australia and on July when the ITCZ is over Asia. Data is based on Legates et al. [1990] and was downloaded from jsao.washington.edu/legates_msu/.

the intrusion of Indian Ocean thermocline water mass into SW Timor Sea. This intrusion would be reflected as increase in regional or spatial thermocline temperature gradient of the Timor Sea that can be detected when comparing data from Cores MD01-2378 and SO185-18460.

The duration and amplitude of the NE – SW temperature gradient changes differed significantly during successive HEs. Two prominent negative excursions were observed during HE 3 and HE 5a and indicated by minimum temperature gradient of $\sim -3^{\circ}\text{C}$ (Figure 4.5). Another major temperature gradient increase was observed at the end of HE 5, while HEs 4 and 6 were characterized by sharp drops of temperature gradients within short time.

Previous studies suggested that intensification of the Australian monsoon triggered by episodes of northern hemisphere cooling would have piled up water masses in the eastern Indian Ocean, thus decreasing further the already reduced-ITF outflow into the SW Timor Sea during HEs [e.g. Zuraida et al., 2009, Xu et al., 2008 and 2006]. Regional thermocline temperature gradient from the Timor Sea revealed repeated incursions of Indian Ocean thermocline water mass during HEs coincided with southward migration of the ITCZ. The maximum insolation over Australia also played a major role in the hydrography of the Timor Sea [Dürkop et al., 2008; Zuraida et al., 2009], which may also be responsible for the delay in the thermocline temperature gradient change during HE 5 (Figure 4.5).

Today, thermocline flow of relatively cool water dominates during boreal winter, as the warm surface flow becomes blocked by the development of a fresh water plug at the southern tip of the Makassar Strait, driven by monsoonal winds from the South China Sea through the Java Sea [Gordon et al., 2003]. As a result, the ITF becomes cooler, fresher, and dominated by thermocline rather than surface flow [Gordon et al., 2003]. This mechanism could only affect MIS 3 ITF intensity if there were an open marine connection between the South China and

Java Seas over a flooded Sunda shelf, which relates to a sea level position of at least 80 m above the LGM sea level, equivalent to the present day sill depth of the Karimata Strait (~40 m), as was observed by Xu et al. [2008]. However, regional thermocline temperature gradient showed negligible effect of high-sea level on ITF slow-down during HEs 3, 5a and 6 when the sea level was ~-80 m during HE 3 and ~-40 m during HEs 5a and 6 (Figure 4.5).

4.5. Conclusion

Comparison between high-resolution stable isotope and Mg/Ca records of surface and thermocline dwelling planktonic foraminifers in Cores MD01-2378 and SO185-18460 from the Timor Sea indicate significant variability in the vertical structure and intensity of the Indonesia Throughflow during HEs 3–6. We interpret convergence of carbon isotope data between *G. ruber* white and *P. obliquiloculata* during HEs in Core SO185-18460 as evidence of increased precipitation related to southward migration of the ITCZ. Prominent decreases in regional thermocline temperature gradient during HEs 3–6 are interpreted as evidence for an increased influence of warmer, saltier thermocline water from the tropical Indian Ocean in the Timor Sea and a corresponding decrease in the cool, fresh ITF thermocline flow, due to an overall slowdown in the global thermohaline circulation during HEs 3–6.

Chapter 5

Centennial-scale climate variability in the Timor Sea during Marine Isotope Stage 3

(Dürkop, A., A. Holbourn, W. Kuhnt, R. Zuraida, N. Andersen, and P.M. Grootes (2008), Centennial-scale climate variability in the Timor Sea during Marine Isotope Stage 3, *Mar. Micropal.*, 66 (3), 208-221, doi: 10.1016/j.marmicro.2007.10.002.)

5. Centennial-scale climate variability in the Timor Sea during Marine Isotope Stage 3

Anke Dürkop¹, Ann Holbourn¹, Wolfgang Kuhnt¹, Rina Zuraida^{1,2}, Nils Andersen³,
Pieter M. Grootes³

¹ Institute of Geosciences, Christian-Albrechts-University, Ludewig-Meyn-Str. 10-14, D-24118 Kiel, Germany

² Leibniz-Institute of Marine Sciences, IFM-GEOMAR, Wischhofstr. 1-3, D-24148 Kiel, Germany

³ Leibniz-Laboratory for Radiometric Dating and Stable Isotope Research, Christian-Albrechts-University, Max-Eyth-Str. 11 - 13, D-24118 Kiel, Germany

(Dürkop, A., A. Holbourn, W. Kuhnt, R. Zuraida, N. Andersen, and P.M. Grootes (2008), Centennial-scale climate variability in the Timor Sea during Marine Isotope Stage 3, *Mar. Micropal.*, 66 (3), 208-221, doi: 10.1016/j.marmicro.2007.10.002.)

Abstract

We present a high-resolution (~60–110 yr) multi-proxy record spanning Marine Isotope Stage 3 from IMAGES Core MD01-2378 (13°04.95' S and 121°47.27' E, 1783 m water depth), located in the Timor Sea, off NW Australia. Today, this area is influenced by the Intertropical Convergence Zone, which drives monsoonal winds during austral summer and by the main outflow of the Indonesian Throughflow, which represents a key component of the global thermohaline circulation system. Thus, this core is ideally situated to monitor the linkages between tropical and high latitude climate variability. Benthic $\delta^{18}\text{O}$ data (*Planulina wuellerstorfi*) clearly reflect Antarctic warm events (A1–A4) as recorded

by the EPICA Byrd and Dronning Maud Land ice cores. This southern high latitude signal is transferred by deep and intermediate water masses flowing northward from the Southern Ocean into the Indian Ocean. Planktonic $\delta^{18}\text{O}$ shows closer affinity to northern high latitudes planktonic and ice core records, although only the longer-lasting Dansgaard–Oeschger warm events, 8, 12, 14, and 16–17 are clearly expressed in our record. This northern high latitude signal in the surface water is probably transmitted through atmospheric teleconnections and coupling of the Asian–Australian monsoon systems. Benthic foraminiferal census counts suggest a coupling of Antarctic cooling with carbon flux patterns in the Timor Sea. We relate increasing abundances of carbon-flux sensitive species at 38–45 ka to the northeastward migration of the West Australian Current frontal area. This water mass reorganization is also supported by concurrent decreases in Mg/Ca and planktonic $\delta^{18}\text{O}$ values (*Globigerinoides ruber white*).

5.1. Introduction

One of the most fascinating and enigmatic findings of paleoclimate research is the succession of extremely rapid and large-amplitude climate fluctuations during the last glacial period: the so called Dansgaard–Oeschger (D–O) events. These dramatic climate events are most clearly seen in Greenland ice cores [Johnsen et al., 1992; Dansgaard et al., 1993; Grootes et al., 1993] and in sediment cores from the adjacent North Atlantic, but were also recorded in many other localities of the Northern Hemisphere [Voelker, 2002]. The most rapid shifts

occurred during Marine Isotope Stage 3 (MIS 3) from cool stadial to warm interstadial conditions in the North Atlantic region (D–O warm events) with temperatures rising by 8–16°C [Landais et al., 2004; Huber et al., 2006] within a few decades followed by a gradual temperature decrease back to stadial conditions within approximately 1500 yr. In contrast, the Southern Hemisphere experienced slower millennial changes with moderate temperature fluctuations of approximately 1–3°C [Watanabe et al., 2003; EPICA Community members, 2004]. Climate models and paleoceanographic records suggest that when Greenland warmed during D–O events the North Atlantic sea surface warmed, trade winds strengthened and the Asian monsoon intensified [Voelker, 2002; Ruth et al., 2007].

In the tropics climate variability during MIS 3 is still poorly understood due to the scarcity of high-resolution marine archives. Distinct, sub-orbital scale $\delta^{18}\text{O}$ changes during MIS 3 in the northern part of the West Pacific Warm Pool (WPWP) were detected in high-resolution records from the Mindanao Eddy and Sulu Sea [Stott et al., 2002; Dannenmann et al., 2003]. These changes were related to increased South East Asian summer monsoon rainfall and warmer and fresher surface conditions in the WPWP during Northern Hemisphere interstadials. It remains an open question, whether such changes also affected the Southern Hemisphere part of the SE Asian tropics, in particular northern Australia and the northeastern Indian Ocean, where high-resolution records of glacial climate variability are still missing or contradictory during MIS 3. There is, for instance, considerable debate concerning the transhemispheric coupling between the South East Asian and Australian monsoon systems and their relation to high latitude

climate change [Wyrwoll and Miller, 2001; Wyrwoll and Valdes, 2003; Miller et al., 2005].

A further major influence on the climate of the Indonesian–Australian region is the intensity of surface water flow from the Pacific into the Indian Ocean (=Indonesian Throughflow, ITF). At the onset of Greenland-Interstadials D–O 5, 8, 12, 14 and 17, substantial sea-level highstands (+9 to 26 m) were recorded in coral terraces at Huon Peninsula in Papua New Guinea [Chappell, 2002]. Similar magnitudes of sealevel fluctuations during MIS 3 were reported from the Red Sea [Siddall et al., 2003], where the magnitude of sea-level fluctuations during MIS 3 reached 35 ± 12 m, which is comparable to the maximum values of 26 m estimated by Chappell [2002] from coral reef data. Proxy records on glacial–interglacial timescales in the ITF outflow area and circulation models indicated reduced flow during cold intervals [Müller and Opdyke, 2000; Kuhnt et al., 2004; Holbourn et al., 2005]. These authors related this reduced throughflow to lowered sealevel and changed local paleoceanographic and climatic boundary conditions (i.e. reduced precipitation and higher salinity in the central part of the WPWP or differing monsoonal wind patterns). Planktonic foraminiferal oxygen isotope and paleoproductivity studies in the outflow region of the ITF already indicated high variability during MIS 3 [Holbourn et al., 2005]. However, the time resolution of these studies did not allow detection of individual D–O events nor detailed correlation to high latitude climate records during this interval of rapid climate change.

Here, we present a centennial-scale resolution multiproxy record spanning MIS 3 from IMAGES Core MD01-2378, located in the tropical eastern Indian Ocean between Indonesia and Australia. This core is situated close to the main outflow of the ITF, and is also influenced by the Asian–Australian monsoon system, which induces strong seasonal changes in atmospheric deep convection and local wind and precipitation patterns. Thus, this core is ideally placed to investigate regional climate variability in relation to thermohaline circulation changes and to assess linkages between high latitude and tropical climate evolution.

5.2. Material and method

5.2.1. Paleoceanographic setting

IMAGES Core MD01-2378 (13°04.950' S, 121°47.270' E, water depth: 1783 m) was recovered in May 2001 at the northwestern margin of the Scott Plateau in the Timor Sea (Figure 5.1). Core MD01-2378 is located close to the oceanographic front between relatively cool, saline water carried northward by the West Australian Current (WAC) and warm, fresh water from the ITF partly feeding the South Equatorial Current (SEC) and the Leeuwin Current (LC), which continues southward along the West Australian coast and is mainly active during austral autumn and winter [Godfrey and Weaver, 1991; Tomczak and Godfrey, 2003; Peter et al., 2005]. Today, tropical water masses clearly dominate at the coring site

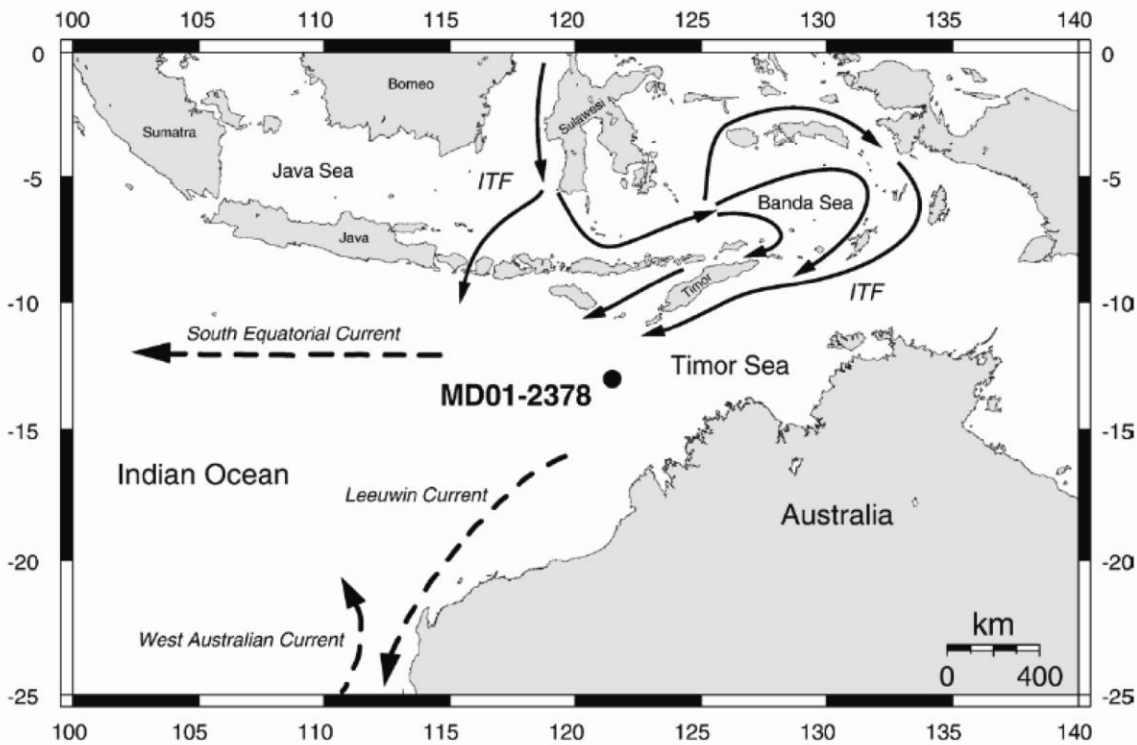


Figure 5.1. Location of Core MD01-2378 (13°04.950' S, 121°47.270' E, water depth: 1783 m) in the Timor Sea. Solid arrows indicate main pathways of the Indonesian Throughflow (=ITF, after Gordon, 2005). Dashed arrows indicate the South Equatorial Current, Leeuwin Current and West Australian Current.

resulting in warm ($\sim 29.5^{\circ}\text{C}$ and $\sim 27.5^{\circ}\text{C}$), low-saline (~ 34.1 psu and ~ 34.4 psu) surface water, and a deep thermocline ($=18^{\circ}\text{C}$ isotherm, 170 m) [May 2001 and September 2005 CTD data given by Bassinot et al., 2002 and Kuhnt et al., 2005] with low nutrient levels and a deep chlorophyll maximum [Longhurst, 1998]. However, this situation may have been fundamentally changed towards stronger influence of the WAC during glacial times, when the NW Australian shelf was exposed, the ITF reduced, and the LC weakened [Wells and Wells, 1994; Kuhnt et al., 2004; Holbourn et al., 2005].

5.2.2. Stable isotopes

Samples (30–40 cm³ from 1 cm thick sediment slices) were taken at 1 cm interval between 448 and 895 cm in Core MD01-2378. Samples were dried and weighed, then washed over a 63 µm sieve. Residues were dried on a sheet of filter paper and weighed, then sieved into 63–150 µm, 150–250 µm, 250–315 µm, and >315 µm fractions. For stable isotope analysis, we selected 3 to 8 tests (>250 µm) of the epibenthic foraminifera *Planulina wuellerstorfi* and 20 tests (250–315 µm) of the planktonic foraminifera *Globigerinoides ruber* (white). In a few samples, where benthic foraminiferal density was low, a smaller number (1–2) of specimens were analyzed. Tests were checked for cement encrustations and infillings before being broken into large fragments, then cleaned in ethanol in an ultrasonic bath and dried at 40°C. Stable carbon and oxygen isotope measurements were made with the Finnigan MAT 251 mass spectrometer at the Leibniz Laboratory, University of Kiel. The instrument is coupled online to a Carbo-Kiel Device (Type I) for automated CO₂ preparation from carbonate samples for isotopic analysis. Samples were reacted by individual acid addition. The mean external error and reproducibility of carbonate standards is better than ±0.07‰ and ±0.05‰ for δ¹⁸O and δ¹³C, respectively. Results were calibrated using the National Institute of Standards and Technology (Gaithersburg, Maryland) carbonate isotope standard NBS 20 and in addition NBS 19 and 18, and are reported on the PeeDee belemnite (PDB) scale.

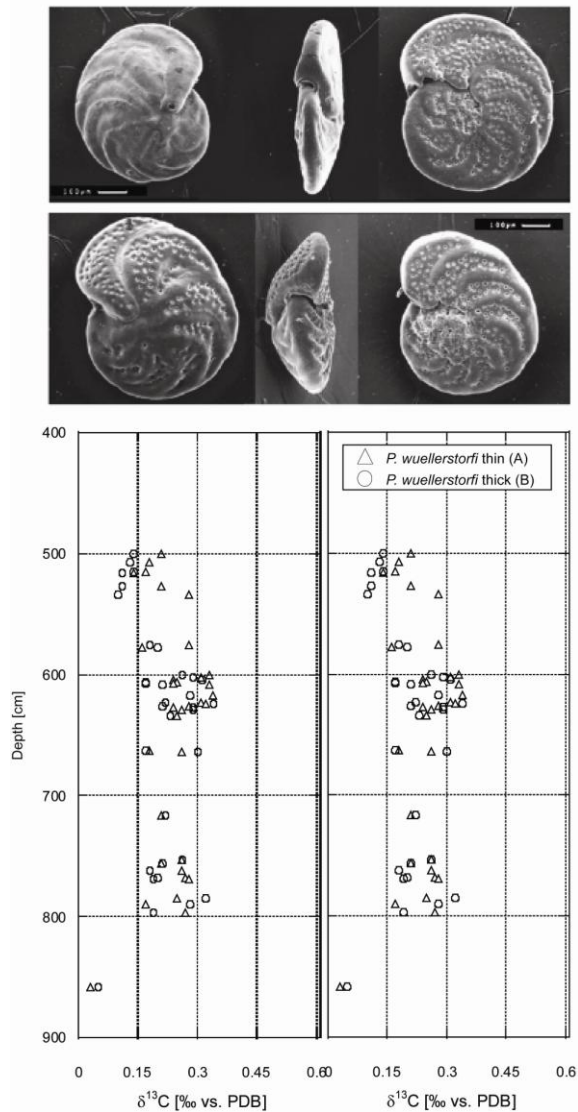


Figure 5.2. Scanning electron micrographs of two morphotypes of the epibenthic foraminifera *P. wuellerstorfi*. a) Morphotype A: flat in cross-section with thinner wall; b) morphotype B: plano-convex in cross-section with thicker wall. Umbilical, apertural and spiral views of morphotypes A and B are from different specimens; c) Paired stable isotope measurements on morphotypes A (triangles) and B (circles) in Core MD01-2378. Reproducibility between the two morphotypes is better than $\pm 0.06\text{‰}$ and $\pm 0.05\text{‰}$ for $\delta^{18}\text{O}$ and $\delta^{13}\text{C}$, respectively.

We recognized two different morphotypes of *P. wuellerstorfi*: morphotype A is generally flatter in cross-section and has a thinner wall, whereas morphotype B has a more plano-convex cross-section and thicker wall (Figure 5.2). Most of our measurements were performed on *P. wuellerstorfi* A, except in ten samples, where this morphotype was rare, and *P. wuellerstorfi* B was measured. We determined from 33 paired samples that there is no statistically significant difference between morphotypes A and B of *P. wuellerstorfi* (reproducibility is better than $\pm 0.06\text{‰}$ and $\pm 0.05\text{‰}$ for

$\delta^{18}\text{O}$ and $\delta^{13}\text{C}$, respectively). Replicate measurements on 51 paired samples of *P. wuellerstorfi* A indicated that the mean reproducibility is better than

$\pm 0.06\text{‰}$ and $\pm 0.04\text{‰}$ for $\delta^{18}\text{O}$ and $\delta^{13}\text{C}$, respectively. For the planktonic foraminifera *G. ruber* (white), the reproducibility is better than $\pm 0.08\text{‰}$ for $\delta^{18}\text{O}$ and $\delta^{13}\text{C}$ in 49 paired measurements.

The difference in $\delta^{13}\text{C}$ between planktonic and benthic foraminifera ($\Delta\delta^{13}\text{CPF-BF}$) has been used for qualitative estimates of export productivity in tropical and subtropical oceans [Sarnthein and Winn, 1990; Jian et al., 2001; Holbourn et al., 2005], even though additional complex factors are influencing the $\delta^{13}\text{C}$ profiles in the ocean, including mixing rates and exposure time of surface waters to the atmosphere. However, in the extended, low-resolution MD01-2378 time series [Holbourn et al., 2005], the $\Delta\delta^{13}\text{CPF-BF}$ curve exhibits striking similarities to other productivity proxy records and thus, probably reflects productivity changes in near-surface waters at this site.

Table 5.1. Tie points between benthic foraminiferal $\delta^{18}\text{O}$ and EDML ice core $\delta^{18}\text{O}$ versus depth and age.

Depth [cm] (Core MD01-2378)	$\delta^{18}\text{O}$ [‰ vs. PDB] (Core MD01-2378)	GICC05 age [ka BP] (EDML ice core)	$\delta^{18}\text{O}$ [‰ SMOW] (EDML ice core)	Event
342	3.92	18.15	-51.89	$\delta^{18}\text{O}$ maximum prior to deglaciation
506	3.92	27.45	-52.53	$\delta^{18}\text{O}$ maximum after AIM 4 event
554	3.72	30.65	-51.04	$\delta^{18}\text{O}$ maximum before AIM 4 event
642	3.31	38.15	-48.68	Last $\delta^{18}\text{O}$ minimum of A1 event
664	3.65	39.85	-50.91	$\delta^{18}\text{O}$ maximum before A1 event
742	3.28	47.25	-47.44	$\delta^{18}\text{O}$ minimum in center of A2 event

5.2.3. Accelerator mass spectrometry

For accelerator mass spectrometry (AMS) ^{14}C dating, approximately 1500 well preserved tests of the planktonic foraminifera *G. ruber* (white) were picked from the $>250\ \mu\text{m}$ fraction at levels, where *G. ruber* showed maximum abundance, to minimize the proportion of tests displaced by bioturbation. AMS conventional ^{14}C

ages (Table 1) were determined at the Leibniz Laboratory, University of Kiel using standard methods described by Nadeau et al. [1997] and Schleicher et al. [1998].

Table 5.2. AMS ^{14}C dates measured on *G. ruber* (white) in Core MD01-2378.

Lab code	Sample (Core MD01-2378)	^{14}C -Conventional age (BP)	CAL-age (BP)
KIA 19611	316.5 cm, 1.0 mg C	14260±70	16280±150
KIA 19612	338.5 cm, 1.2 mg C	15410±70	18310±160
KIA 19613	364.5 cm, 1.0 mg C	16340±80	19170±110
KIA 19614	390.5 cm, 1.0 mg C	17440±90	20320±100
KIA 19615	424.5 cm, 1.1 mg C	18990±100	22300±100
KIA 19616	440.5 cm, 1.0 mg C	19960±110	23490±170
KIA 31094	500.0 cm, 1.2 mg C	23210±170	27510±240
KIA 31095	534.0 cm, 1.1 mg C	24970±210	29530±320
KIA 19617	591.5 cm, 1.1 mg C	29920+330 / - 310	35040±350
KIA 31096	642.0 cm, 1.1 mg C	34560+650 / - 600	39630±650
KIA 31785	683.0 cm, 1.4 mg C	35660+750 / - 690	40670±720

Calendar ages obtained with the radiocarbon calibration program from Fairbanks et al. [2005] (<http://www.radiocarbon.ldeo.columbia.edu/research/radiocarbon.htm>), after applying a reservoir age correction of 300 yr [Butzin et al., 2005].

5.2.4. Benthic foraminiferal census counts

An average of 150 benthic foraminifera were picked and counted in size fractions >250 μm following the approach of Holbourn et al. [2005]. In samples, where benthic foraminiferal abundance was high, a quantitative split of the >250 μm size fractions was picked, and census counts were then reconverted to whole samples. Counts of globocassidulinids include *Globocassidulina subglobosa* and *Globocassidulina elegans*. Buliminids counts include *Globobulimina* spp., *Bulimina aculeata*, *Bulimina marginata* and *Bulimina mexicana*. Low-resolution counts from Holbourn et al. [2005] were integrated with our high-resolution counts. Benthic foraminiferal accumulation rates (BFAR: number of specimens >250 μm cm^{-2} kyr^{-1}) were calculated as the product of the number of benthic foraminifera per

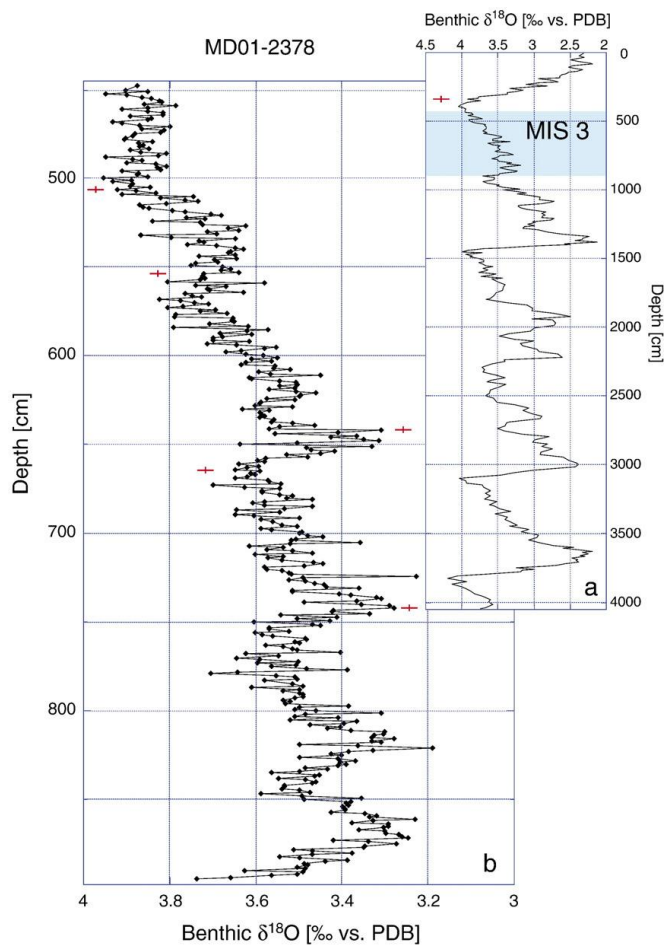


Figure 5.3. a) Benthic foraminiferal oxygen isotope data versus depth spanning MIS 1-12 from Holbourn et al. [2005]; b) and centennial-scale resolution record spanning MIS 3 (this study) Crosses indicate tie points between Core MD01-2378 and the EDML ice core used record spanning MIS 3 (this study) Crosses indicate tie points between Core MD01-2378 and the EDML ice core used as basis for MIS 3 age model.

gram dry sediment and the sediment accumulation rate (in $\text{g cm}^{-2} \text{ kyr}^{-1}$). Accumulation rates (AR) of buliminids and globocassidulinids were calculated in the same fashion. We calculated sediment accumulation rates based on sedimentation rates derived from the age model and dry bulk density values (g cm^{-3}) [van Andel et al., 1975]. Dry bulk density values were determined every 20 cm of the core from discrete samples taken with a metal tube of 10 cm^3 inner volume and a 9 pt running

average smooth was used to avoid artificial fluctuations in mass accumulation rates [Holbourn et al., 2005]. The resulting values show only a small scatter between 0.6 and 0.7 g cm^{-3} for the studied interval.

5.3. Results

5.3.1. Age model

Our age model is based on the correlation of high resolution benthic oxygen isotope data to the new EDML ice core recovered from the interior of Dronning Maud Land within the European Project for Ice Coring in Antarctica [EPICA Community members, 2004]. This ice core has been synchronized to the layer counted NGRIP ice core following the new Greenland Ice Core Chronology (GICC05) timescale [EPICA Community members, 2006; Andersen et al., 2006]. Between 15 and 48 ka six tie points were used to correlate MD01-2378 and EDML (Figure 5.3–5.5; Table 5.1). An interpolated curve was fitted through the tie points using a Stineman function in Kaleidagraph Version 4, and the curve was then sampled. A change in sedimentation rates from ~ 11 to ~ 16 cm kyr⁻¹ is evident at a depth of about 554 cm (~ 30 ka). This change is most probably caused by sediment oversampling in the upper part of the core during the piston coring process [Széreméta et al., 2004; Holbourn et al., 2005]. As no isotopic data are published beyond 50 ka for the EDML ice core, the lower part of our age model (740–895 cm corresponding to 47–64 ka) is based on linear extrapolation. Comparison of MD01-2378 planktonic $\delta^{18}\text{O}$ with NGRIP (Figure 5.5) fully supports this linear extrapolation.

Eleven AMS dates including 7 dates from Holbourn et al. [2005] provide additional constraint for our age model (Figure 5.4, Table 5.2). However, within this interval the earth magnetic field showed several episodes of weakness leading to

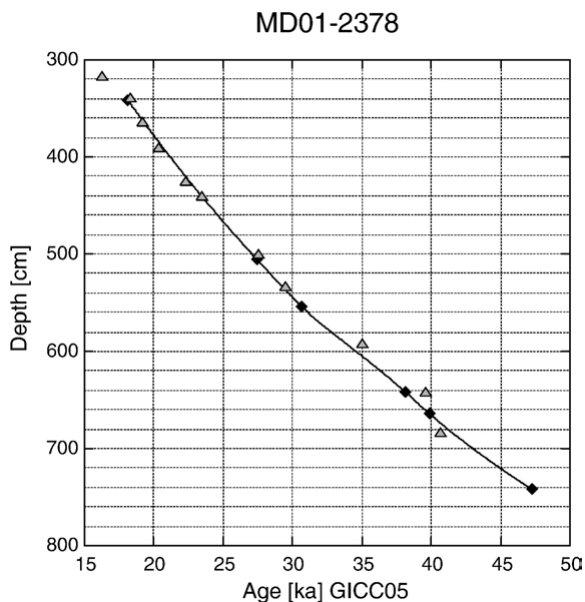


Figure 5.4. Age/depth plot showing tie points (diamonds) between EDML ice core and MD01-2378 benthic foraminiferal $\delta^{18}\text{O}$. Our age model is further constrained by 11 AMS ^{14}C dates (triangles).

increased production of cosmogenic isotopes and resulting in occurrence of ^{14}C -plateaux, such as the Laschamp Event at around 41 ka [Voelker et al., 2000; Hughen et al., 2004]. Significant changes in thermohaline circulation intensity occurred during this time interval, in particular during Heinrich events [NGRIP members, 2004].

Hence, most of the conditions for constant marine reservoir ages do not

hold [Grootes and Sarnthein, 2006; Sarnthein et al., 2007], and the calibration of AMS ^{14}C dates and the estimation of reservoir ages for MIS 3 are not straightforward. The AMS ^{14}C dates show relatively good correlation to the EDML tie points between 18 and 47 ka (Figure 5.4). However, converted calendar ages show more pronounced deviations between 27 and 40 ka, due to increasing uncertainty in the Fairbanks calibration curve prior to 29 ka [Svensson et al., 2006]. This problem is additionally compounded by the occurrence of the Mono Lake event at 34 ka [Hughen et al., 2004].

5.3.2. Stable isotopes

Benthic and planktonic foraminiferal $\delta^{18}\text{O}$ records indicate complete

recovery of a continuous hemipelagic sedimentary succession between 22 and 64 ka, spanning the entire MIS 3 with a time resolution of ~60–110 yr (Figure 5.5). The benthic $\delta^{18}\text{O}$ record varies between ~3.9–3.2‰ exhibiting a maximum amplitude fluctuation of 0.7‰. Most prominent features in the older part of the record are the four distinct excursions to lower $\delta^{18}\text{O}$ with an amplitude fluctuation of 0.3‰ at ~62 ka, ~55 ka, ~46 ka and ~38 ka, which we correlate to Antarctic warm events A1–A4 (Figure 5.5a). The upper part of the time series is characterized by two gradual increases in $\delta^{18}\text{O}$ values: Step 1 occurs between 38.0–31.0 ka with an increase from 3.5‰ to 3.8‰. After a minor decrease of about 0.2‰, step 2 takes place between 31.0–26.5 ka with an increase from 3.7‰ to 3.9‰. The benthic $\delta^{13}\text{C}$ record (Supplementary figure) exhibits an overall variability of 0.4‰. $\delta^{13}\text{C}$ values show an increase of about 0.2‰ between 59–51 ka, then vary between 0.2‰ and 0.3‰ until 29 ka. The younger record (29–24 ka) shows an increasing trend from 0.2‰ and 0.1‰.

Planktonic foraminiferal $\delta^{18}\text{O}$ values vary between ~-1.0‰ and -1.9‰ over the entire record (Figure 5.5b). In general, three main trends are observed. In the lower part before 55 ka, $\delta^{18}\text{O}$ values decrease from -1.5‰ to -1.9‰. Between 55 and 39 ka, planktonic $\delta^{18}\text{O}$ increases to -1.3‰. After a rapid decrease in planktonic $\delta^{18}\text{O}$ to -1.8‰ at 38.0 ka, an overall increase of 0.6‰ occurs until 26 ka, followed by a slight decrease in values. The planktonic $\delta^{13}\text{C}$ record shows a maximum amplitude fluctuation of 0.6‰ (Supplementary figure). The lower part

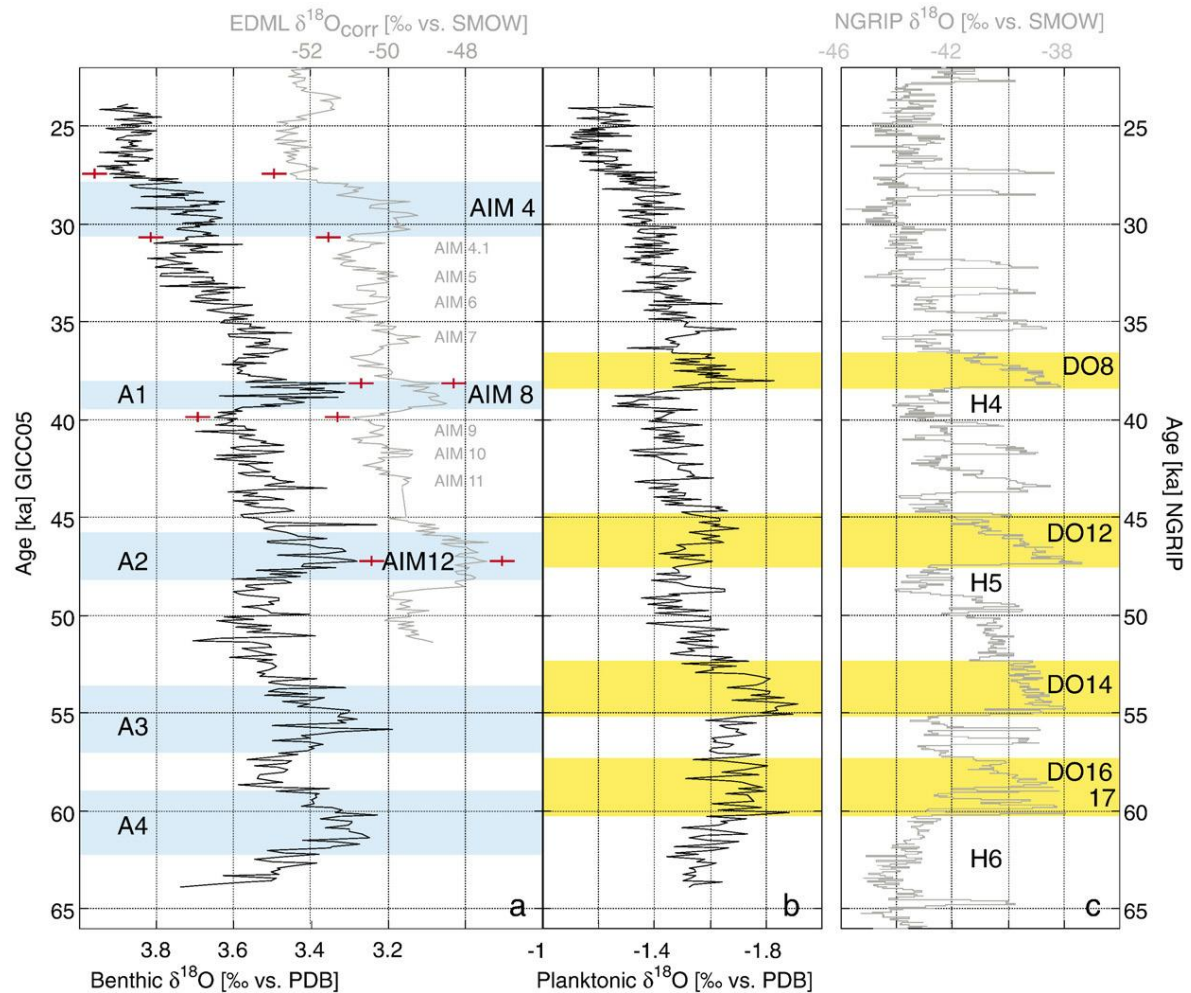


Figure 5.5. a) Benthic foraminiferal $\delta^{18}\text{O}$ (*P. wuellerstorfi*) in Core MD01-2378 and $\delta^{18}\text{O}$ in EDML ice core versus age. Crosses indicate tie points between $\delta^{18}\text{O}$ records. Antarctic warm events (A1-A4) and Antarctic Isotope Maxima (AIM4, AIM8 and AIM12) indicated by shaded bars; b) Benthic (*P. wuellerstorfi*) and planktonic (*G. ruber*) foraminiferal $\delta^{13}\text{C}$ versus age; c) and d) Comparison of MD01-2378 planktonic foraminiferal $\delta^{18}\text{O}$ with Greenland ice core $\delta^{18}\text{O}$; only longer-lasting D-O warm events (shaded grey) are clearly expressed in the MD01-2378 planktonic record.

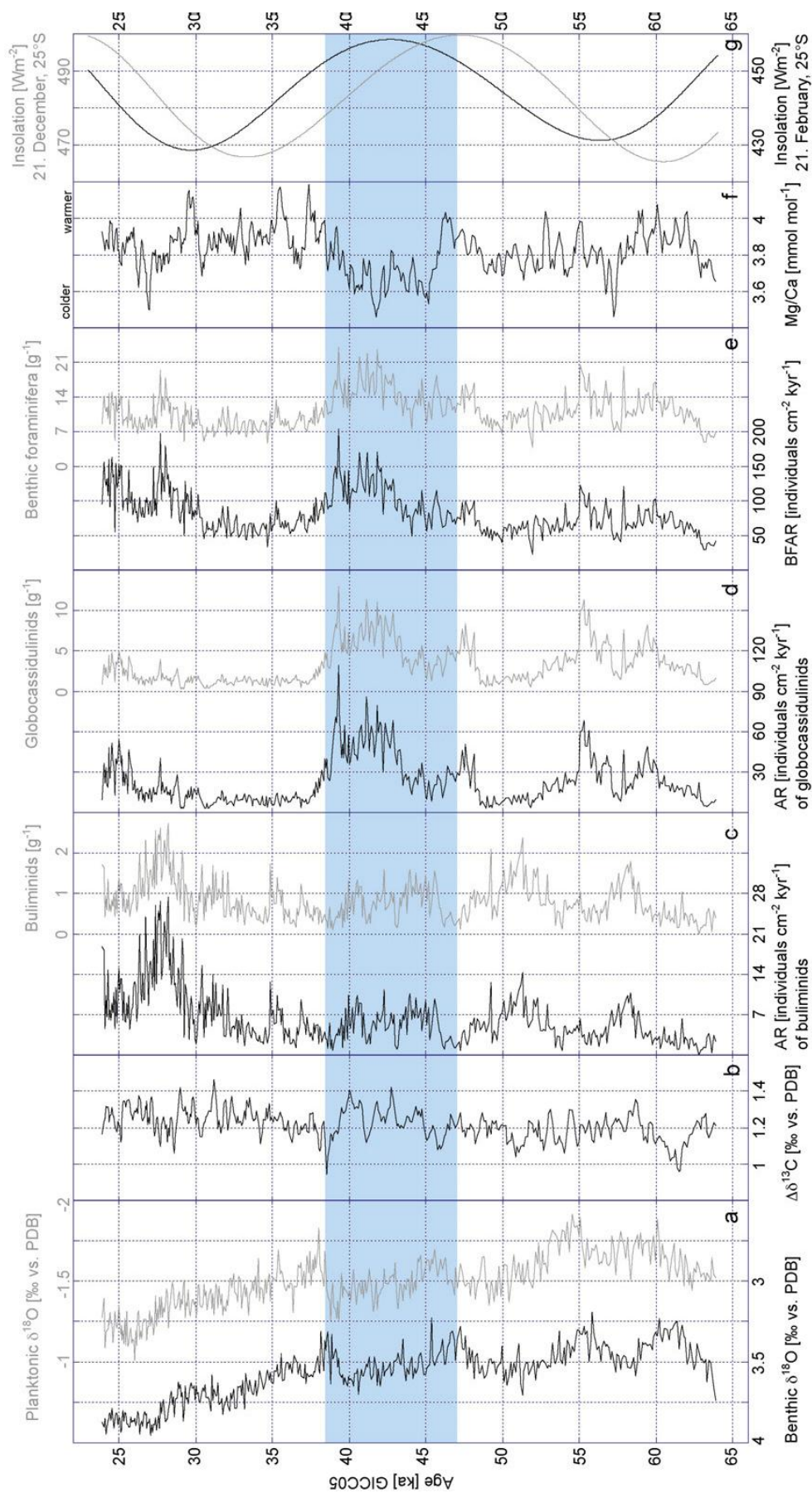
(64–59 ka) is characterized by the lowest $\delta^{13}\text{C}$ values around 1.2‰ increasing after 59 ka to an almost constant level of about 1.5‰.

5.3.3. Benthic foraminiferal census counts

Robust methods to estimate carbon flux and paleoproductivity using benthic

foraminifera include BFAR [Herguera and Berger, 1991; Herguera, 2000] and the accumulation rates and relative abundances of organic flux indicator species such as buliminids [Lutze and Coulbourn, 1984; Altenbach and Sarnthein, 1989; Thomas and Gooday, 1996; Jian et al., 1999; Holbourn et al., 2005]. Figure 5.6 documents BFAR variations and the distribution of organic flux indicator taxa (buliminids and globocassidulinids) in relation to benthic and planktonic $\delta^{18}\text{O}$. The number of buliminids per gram shows a clear positive correlation to benthic $\delta^{18}\text{O}$. Such co-variance was already evident in the low-resolution benthic foraminiferal and $\delta^{18}\text{O}$ records from the same core spanning the last 460 ka, published by Holbourn et al. [2005]. In our high-resolution records, the number of buliminids increases to ~ 2.5 specimens per gram (or an accumulation rate of ~ 26 individuals $\text{cm}^{-2} \text{ kyr}^{-1}$) during stadials and decreases to ~ 0.5 specimens per gram (or an accumulation rate of ~ 5 individuals $\text{cm}^{-2} \text{ kyr}^{-1}$) during interstadials. Globocassidulinids show marked variations in number (from ~ 1 to 12 specimens per gram or an accumulation rate of $\sim 10\text{--}110$ individuals $\text{cm}^{-2} \text{ kyr}^{-1}$) and represent up to half of the total benthic foraminiferal assemblage. The distribution of globocassidulinids exhibits four prominent increases between 60 and 39 ka. Three of the peaks coincide with A4–A2 event, whereas the last and most sustained increase at 43–39 ka is not directly correlated to the A1 event.

The total number of benthic foraminifera per gram varies from 4 to 24 (or an accumulation rate of $\sim 50\text{--}200$ individuals $\text{cm}^{-2} \text{ kyr}^{-1}$). Although globocassidulinids provide the stronger imprint on benthic foraminiferal distribution, the number of buliminids per gram also significantly affects total abundances (see for instance, at



27–28 ka). However, the main increases in the number of specimens between ~60 and 39 ka generally reflect marked rises in the numbers of globocassidulinids.

5.4. Discussion

5.4.1. Northern and Southern Hemisphere climate control

A striking feature in the Core MD01-2378 records from the Timor Sea is the contrast between the benthic and planktonic oxygen isotope signals (Figure 5.5). The benthic $\delta^{18}\text{O}$ record captures Antarctic cooling and warming trends, including warm events A1 to A4 in the Byrd ice core following the nomenclature of Blunier and Brook [2001] and Antarctic Isotope Maximum 4 (AIM4) in the EDML ice core following the nomenclature of the EPICA Community members [2006]. However, during times of gradual warming in the Southern Hemisphere as shown by the MD01-2378 benthic $\delta^{18}\text{O}$, the planktonic isotope data indicate cooling. Thus, planktonic $\delta^{18}\text{O}$ shows closer affinity to northern high latitudes planktonic and ice core records, although only the longer-lasting D–O warm events 8, 12, 14, and 16–17 are clearly expressed in the MD01-2378 core (Figure 5.5). This phase relationship between warming and cooling events in the Southern and Northern Hemispheres, previously detected in ice cores and Northern Hemisphere sediment

Figure 5.6. a) Benthic and planktonic $\delta^{18}\text{O}$; b) $\Delta\delta^{13}\text{C}$ obtained by subtracting $\delta^{13}\text{C}_{\text{benthic}}$ from $\delta^{13}\text{C}_{\text{planktonic}}$; c–e) Accumulation rates (black) and census counts (grey) of buliminids, globocassidulinids and total benthic specimens; f) Mg/Ca measured on *G. ruber* (white) [Zuraida et al. 2009]; g) December (grey) and February (black) insolation at 25°S, February maximum insolation at 25°S is shaded.

cores, was interpreted as a bipolar climate seesaw, as Northern Hemisphere cooling is balanced by Southern Hemisphere warming [Broecker, 1998].

Shackleton and Hall [2000] and Martrat et al. [2007] described a clear out-of-phase relationship for Cores MD95-2042, MD01-2444 and MD01-2443 from the Iberian Margin, where the onsets of warm events in benthic $\delta^{18}\text{O}$ lead rapid cold-to-warm transitions in planktonic $\delta^{18}\text{O}$. Benthic $\delta^{18}\text{O}$ values from the Iberian Margin display an Antarctic temperature signal, whereas planktonic $\delta^{18}\text{O}$ values reflect Greenland temperature variations. Martrat et al. [2007] suggested, that benthic $\delta^{13}\text{C}$ values reflected the mixing of southern and northern sourced deep-water masses. In particular, depleted benthic $\delta^{13}\text{C}$ values coinciding with high planktonic $\delta^{18}\text{O}$ document dominance of Antarctic Bottom Water in the North Atlantic.

An interesting hypothesis to explain rapid climate changes during MIS 3 was proposed by Adkins et al. [2005]. These authors suggested that during slowdowns of the Meridional Overturning Circulation (MOC) bottom water is increasingly warmed by geothermal heat in a more stratified deep ocean, eventually leading to instability in stratification and re-start of northern deep-water formation. During MOC re-acceleration heat would be released to the atmosphere in the Southern Ocean, driving the ice core record. According to Adkins et al.'s hypothesis, the warming should be confined to bottom water, whereas warming in much of the water column should occur with the ingression of warmer southern sourced intermediate and deep waters ("bipolar seesaw" hypothesis). Our benthic $\delta^{18}\text{O}$ data from Core MD01-2378 at 1783 m water depth show warming during

slowdowns of the MOC associated with Heinrich events 4–6 (Figure 5.5), which implies that warming extended to much of the water column in accordance with the bipolar seesaw hypothesis.

The Southern Hemisphere signal in the MD01-2378 benthic oxygen isotope record is probably transmitted through the transfer of deep and intermediate water masses towards the Timor Sea. Data analysis and numerical models suggest that today the major formation region for Antarctic Intermediate Water is in the southeastern Pacific [McCartney, 1977; England, 1992] and that these waters flow eastward through the Drake Passage along the Antarctic Circumpolar Current towards the Indian Ocean. The deep water enters the Indian Ocean through the South-Australian-Basin, flows further north into the West-Australian-Basin into the Central-Indian-Basin [McCorkle et al., 1998]. Radiocarbon ages of deep water indicate that the transfer between the Antarctic Circumpolar Current and Timor Sea is relatively rapid, in the order of 300 yr [Matsumoto and Key, 2004].

However, a different transfer mechanism must be invoked to explain the occurrence of prolonged D–O events 8, 12, 14 and 16–17 in the Timor Sea planktonic $\delta^{18}\text{O}$ record, far away from the source of northern climate variability. D–O events are widely detected in Northern Hemisphere records, and model studies by Knutti et al. [2004] suggested that atmospheric processes largely transmit these climatic signals. Furthermore, oxygen isotope studies of stalagmites show evidence of atmospheric teleconnections between North Atlantic climate and the East Asian monsoonal convection [Wang et al., 2001; Burns et al., 2003; Ruth et al., 2007]. Modeling experiments also support that North Atlantic cooling can be

transmitted through atmospheric teleconnections leading to cooling of the Asian continent and thereby weakening of the Asian summer monsoon [Timmermann et al., 2005]. Fluctuations in Asian monsoon intensity may have far reaching repercussions in the tropics through the coupling of Asian and Australian monsoon systems [Hung et al., 2004]. The migration of the Intertropical Convergence Zone (ITCZ) over the Indonesian archipelago represents a crucial link between the two monsoon systems. For instance, reconstructions of thermocline variability during Terminations I and II suggested that the displacement of the ITCZ largely controlled Australian monsoon intensity and ITF variability [Xu, et al., 2006; Xu, pers. comm., 2007]. A similar mechanism may have operated on shorter timescales during MIS 3 and played a crucial role in controlling climate and oceanography in the Timor Sea.

5.4.2. Paleoproductivity variations in the Timor Sea during MIS 3

Benthic foraminiferal abundance and distribution patterns are closely related to the availability of food at the sea floor, which is almost exclusively derived from the export flux of primary production in the photic zone [e.g. Loubere, 1991; Altenbach, 1992; Loubere, 1994, 1996]. Holbourn et al. [2005] suggested that variations in the intensity of NW monsoonal winds over northern Australia were closely related to productivity fluctuations in the Timor Sea on a precessional scale. These authors interpreted increases in the numbers of buliminids and benthic foraminifera per gram as reflecting increased export flux due to more

intense mixing within the upper water column, leading to nutrient enrichment and enhanced primary production. In our high-resolution record spanning MIS 3, buliminids exhibit maximum abundance during stadials whereas numbers decrease significantly during interstadials (Figure 5.6), suggesting that the intensity of the Australian monsoon may have also varied significantly on much shorter timescales. For instance, the intensity of monsoonal winds and frequency of related cyclones are related to the intensity of low-pressure systems over NW Australia [Tapper, 2002]. The strength of these low-pressure systems is not only controlled by insolation but also by changes in albedo, related to vegetation cover and cloudiness over the Pilbara region over relatively short timescales. Tropical cyclones, which form mostly between 10° and 20° S [Suppiah, 1992], can additionally contribute to strong vertical mixing of the upper water column [Sriver and Huber, 2007], leading to increasing primary production [Lin et al., 2003].

Buliminids show their highest abundance at 25–30 ka (Figure 5.6), close to the Last Glacial Maximum, when sea surface temperature (SST) was at a minimum [Xu, pers. comm., 2007] and productivity at a maximum [Holbourn et al., 2005]. In contrast, the abundance of globocassidulinids increases markedly from 2 to 11 g⁻¹, during an interval (38–45 ka), which corresponds to the 25°S February insolation maximum (Figure 5.6) and to more intense heating of the NW Australian landmass, triggering peak monsoon conditions and tropical cyclones. This is also the period, when the ITCZ reaches its most southerly position. The globocassidulinid maximum also coincides with somewhat higher $\Delta \delta^{13}\text{C}$ values during a sustained interval of low Mg/Ca (*G. ruber* white) and low planktonic $\delta^{18}\text{O}$,

indicating lower SST and increased sea surface salinity. Core top data from the Timor Sea indicate that globocassidulinid maxima occur at intermediate carbon flux rates to the seafloor ($4^{-10} \text{ g m}^{-2} \text{ yr}^{-1}$), whereas buliminds are associated with higher flux rates [Holbourn, unpublished data]. It is also known that globocassidulinids increase in abundance following seasonal pulses of fresh phytodetritus [Gooday, 1988, 1993] and appear to selectively favour diatoms as food [Suhr et al., 2003]. Therefore, a change in regional oceanography must have been responsible for the increase in globocassidulinids: for instance a stronger influence of cool, silicate-rich surface-water providing a different food source.

The ITF transports low-salinity tropical waters from the western Pacific through the Indonesian Archipelago into the Eastern Indian Ocean, thereby feeding the SEC and LC. The low-salinity LC flows along the Western Australian coast into the Great Australian Bight [Pearce and Cresswell, 1985], whereas relatively cool, high salinity water is transported northward by the undercurrent [Cresswell, 1991], which is linked to the eastern component of the Southern Hemisphere subtropical gyre forming the WAC. Isotopic data from the Exmouth Plateau [Core RS53-GC06, McCorkle et al., 1998] document that the distribution of water masses during the Last Glacial Maximum (LGM) was different from the present day. Large zones of cool surface-water occurred during glacial times, probably reflecting the increased influence of the WAC on surface-water circulation [Wells and Wells, 1994]. These authors suggested that a large-scale reorganization of regional circulation patterns occurred with the development of a hydrological front between 15° – 19° S, as the LC and WAC respectively decreased

and increased in intensity. Thus during the LGM, the WAC acted as a dominant eastern boundary current locally associated with upwelling of cool nutrient-rich water. A similar but less pronounced shift in water masses may have also taken place during cooler intervals of MIS 3 and explain the distribution of carbon-flux sensitive benthic foraminifera. Rapid and short-lived increases in globocassidulinids also occurred during Antarctic warm events A2–A4, which approximately corresponded to Heinrich events in the Northern Hemisphere. Shutdown of the thermohaline circulation during these events may have reduced the ITF, weakened the intensity of the LC and favoured transient migrations of the hydrological front, thus altering the food export flux to the seafloor.

5.5. Conclusion

The benthic oxygen isotope record from Core MD01-2378 exhibits a Southern Hemisphere signal with Antarctic warm events A1–A4 distinctly expressed, whereas the planktonic oxygen isotope record reflects Northern Hemisphere climate with a strong imprint of longer-lasting D–O events 8, 12, 14 and 16–17. The Southern Hemisphere signal in the benthic $\delta^{18}\text{O}$ is probably transmitted through the transport of deep and intermediate water masses from the Southern Ocean into the eastern Indian Ocean and Timor Sea. In contrast, the Northern Hemisphere signal in the planktonic $\delta^{18}\text{O}$ may be transferred through atmospheric teleconnections due to the tight coupling between Asian and Australian monsoon systems.

High-resolution stable isotope data and benthic foraminiferal census counts from Core MD01-2378 provide new insights into centennial climate variability in the Timor Sea during MIS 3. Increasing abundance of high productivity indicators (buliminids) during stadials and decreasing abundance during interstadials point to significant changes in Australian monsoon intensity on these relatively short timescales. A sustained increase in globocassidulinids between Antarctic warm events A1 and A2 (38–45 ka), corresponding to the February insolation maximum at 25° S and an episode of intensified Australian monsoon, suggest northward migration of the hydrological front between the WAC and LC and resulting change in food export towards diatom dominated particulate organic carbon to the seafloor. This water mass shift is also supported by concurrent decreases in Mg/Ca and planktonic $\delta^{18}\text{O}$.

Chapter 6

Conclusions

6. Conclusions

The geographical setting and hydrology of the Timor Sea (Figure 6.1) not only creates the possibility to understand the variability of the Indonesian Throughflow (ITF) related to slow down of global thermohaline circulation during Marine Isotope Stage 3 (MIS 3), but also gives light to the inter-hemisphere atmospheric teleconnections and coupling of the Asian–Australian monsoon systems. The objectives of this study are to investigate the impact of reduced global thermohaline circulation to the ITF and to assess linkages between high latitude and tropical climate evolution.

Slow down of global thermohaline circulation during HEs not only changed the ITF structure and intensity but also affected the hydrography of the tropical Indian Ocean. The spatial thermocline temperature gradient of study area reached maximum value during stadials reflecting repeated incursions of the Indian Ocean waters into the Timor Sea. Increasing abundance of high productivity indicators (buliminids) during stadials and decreasing abundance during interstadials point to significant changes in Australian monsoon intensity on these relatively short timescales.

6.1. Slow down of the Indonesian Throughflow (Chapter 3)

Timor Sea is one of major outflow passages of the ITF and is sensitive to changes in the intensity and thermal structure of ITF water masses related to global thermohaline circulation. During MIS 3, Timor Sea is characterized by substantial temperature and salinity ($\delta^{18}\text{O}_{\text{sw}}$) changes in the surface and upper thermocline water masses. Increased thermocline temperature during HEs 3–6 indicated incursion of warmer, saltier thermocline water from the tropical Indian Ocean as a result of reduced cool, fresh ITF thermocline flow, related to slowdown in the global thermohaline circulation. The resulting warmer and saltier eastern tropical Indian Ocean would have in turn strongly influenced the Asian Monsoon system and significantly altered the heat and energy budget within the “warm” return branch of the global thermohaline circulation. In addition to global slowdown in thermohaline circulation during HEs, ITF variability was also influenced by sea level-controlled increase of freshwater export from the Java Sea into the ITF during the early part of MIS 3 and by insolation-related changes in Australasian monsoonal intensity leading to the migration of hydrological fronts between Indian Ocean– and ITF-derived water masses.

6.2. Migration of the Intertropical Zone (Chapter 4)

Temperature and stable isotope records from the Timor Sea revealed repeated incursions of Indian Ocean thermocline water mass during HEs 3–6

related to slowdown of global thermohaline circulation coincided with increased precipitation reflecting southward migration of the Intertropical Convergence Zone (ITCZ). Today, this region is influenced by various ocean–atmosphere interactions including the seasonal migration of the ITCZ, changing intensity of SE Asian and Australian monsoonal systems and variable occurrence of El Niño–Southern Oscillation (ENSO) events [Rosenthal et al., 2003; Stott et al., 2004; Koutavas et al., 2006]. Slowdown or even collapsed of the thermohaline circulation during HEs resulted in major cooling at mid latitudes in the North Atlantic, reduced precipitation in high-latitude East Asia and southward displacement of the ITCZ [Arz et al., 1998; Wang et al., 1999, 2001 and 2004; Behling et al., 2000; Peterson et al., 2000; Kienast et al., 2001; Stott et al., 2002; Koutavas et al., 2002; Partin et al., 2007; Müller et al., 2008]. Griffiths et al. [2009] show that the Australian-Indonesian southern hemisphere summer monsoon precipitation increased during Younger Dryas cooling event, when Atlantic meridional overturning circulation was relatively weak and the ITCZ shifted southwards.

6.3. Centennial climate variability (Chapter 5)

Planktonic foraminifer $\delta^{18}\text{O}$ from the Timor Sea is characterized by Northern Hemisphere climate signals with a strong imprint of longer-lasting D–O events 8, 12, 14 and 16–17 indicating atmospheric teleconnections due to the tight coupling between Asian and Australian monsoon systems. Benthic oxygen isotope record from Core MD01-2378 exhibits a Southern Hemisphere signal with Antarctic warm

events A1–A4 distinctly expressed. The Southern Hemisphere signal in the benthic $\delta^{18}\text{O}$ is probably transmitted through the transport of deep and intermediate water masses from the Southern Ocean into the eastern Indian Ocean and Timor Sea. Benthic foraminiferal census counts from Timor Sea shows increasing abundance of high productivity indicators (buliminids) during stadials and decreasing abundance during interstadials that also point to significant changes in Australian monsoon intensity on these relatively short timescales. A sustained increase in globocassidulinids between Antarctic warm events A1 and A2 (38–45 ka), corresponding to the February insolation maximum at 25° S and an episode of intensified Australian monsoon, suggest northward migration of the hydrological front between the Indian Ocean and the ITF and resulting change in food export towards diatom dominated particulate organic carbon to the seafloor.

Appendix A. Report on experiment on cleaning efficacy for Neodymium isotope analysis in foraminifer tests

The Indonesian Throughflow (ITF) connects the upper water masses of the Pacific and Indian Oceans and may be regarded as the 'warm' return branch of the global thermohaline circulation. The modern ITF is dominated by low-salinity, well-ventilated upper thermocline waters of North Pacific origin flowing through the Sulawesi Sea into the Makassar Strait [Gordon and Fine, 1996], while saltier lower thermocline and deeper water masses originated in the South Pacific and entering the Indonesian seas via the deeper eastern route through Lifamatola Strait [Talley and Sprintall, 2005; van Aken et al., 2009] form the rest of the ITF. As a part of the global thermohaline circulation, the ITF was affected by slowing down of the circulation due to perturbation in the production of the North Atlantic Deep Water (NADW) during glacial times. A study on Neodymium (Nd) isotopes from the South Atlantic revealed that NADW was stronger during interstadials and weaker during stadials [Piotrowski et al., 2004].

Neodymium isotopes were first applied in an oceanographic context by O'Nions et al. [1978] and have now become a widely used ocean tracer [e.g. Jeandel et al., 1998; Piotrowski et al., 2004; Haley et al., 2005]. The isotopic composition ($^{143}\text{Nd}/^{144}\text{Nd}$) is expressed as $\epsilon\text{Nd} = ((^{143}\text{Nd}/^{144}\text{Nd}_{\text{meas}}/0.512638) - 1 \times 10000)$ where 0.512638 is the present-day CHUR value [Chondritic Uniform

Reservoir taken as reference; Jacobsen and Wasserburg, 1980]. The ϵNd value varies in the rocks of the Earth as a result of the decay of ^{147}Sm ($t^{1/2} = 10^6 - 10^9$ years), whereby the Sm/Nd ratio of the rocks and their age control the ϵNd signature. In the oceans, the dissolved values reflect the age of the continental weathering sources of Nd [Goldstein and Hemming, 2003]. Therefore more positive ϵNd values are found in the Pacific Ocean (caused by weathering of volcanic arcs), while more negative values are found in Atlantic Ocean (weathering of old continental crust). The advantage of using Nd-isotope as ocean-tracer is related to its intermediate residence time, 500 – 1000 years (Tachikawa et al., 2003), compared with the global turnover rate of seawater, ca. 1000 years [Tachikawa et al., 2003]. Because of that, different water masses have distinct Nd-isotopic signatures depending on the isotopic composition of the adjacent continental landmasses in their sources areas.

To date, Nd isotope analysis within foraminifer tests is conducted after cleaning of the tests following the method developed by Boyle and Keigwin [1985] for Cd analyses. Previous studies suggest that 30% carbonate was lost during Mg/Ca cleaning, with the greatest loss occurring during physical cleaning to remove silicate contaminants [Barker et al., 2003]. Therefore, Nd analysis in foraminifer tests usually needs large amount of samples (>10 mg) [e.g. Haley and Klinkhammer, 2002]. This requirement limits the application of Nd analysis to very abundant species. The aim of this experiment is to examine the possibility of extracting seawater ϵNd values from foraminifer test using small amounts of sample by improving the cleaning efficacy in sample preparation.

The experiment was carried out in upper thermocline-dweller planktonic foraminifera *P. obliquiloculata* (see Zuraida et al., 2009) from the size fraction larger than 250 μm . A total of 11 core top samples from the Sonne 185 VITAL cruise and 10 down core samples from MD01-2378 were chosen for this experiment. The downcore samples and 7 of the core top samples were analyzed by Dr. Brian Haley, from IFM-GEOMAR before the experiment to get a first idea of the ϵNd distribution in the Timor Sea (preliminary data shown in Table A.1) without conducting any cleaning and using smaller amount of sample (<10 mg). The resulting ϵNd in planktonic foraminifera from the Timor Sea varies from -6.8 to -2.3 (samples 10 – 14 and 19 – 25), which is similar to but scatters around the present day sea water ϵNd value of Jeandel et al. [1998], which yielded a value of -4.1. The large scatter ϵNd values was interpreted as clear indication that the samples needed to be cleaned more thoroughly before column separation of Nd from other disturbing elements.

A.1. Sample Preparations

This experiment was carried out on a core top sample located closest to sea water station 33 of Jeandel et al. [1998], which is sample SO185-18507 from the Sonne 185 VITAL cruise. The cleaning efficacy experiment was conducted on *P. obliquiloculata* from SO185-18507 (120°0.008' E, 13°5.993' S, water depth: 2453 m). Three samples (F036 – F038) were crushed and underwent physical cleaning (Table A.2) using the standard batch method of Barker et al. [2003]. The physical

cleaning involved four times rinsing with MilliQ water followed by sonication and twice rinsing with methanol.

Table A.1. Preliminary results of previous Nd isotope analysis conducted at the IFM-GEOMAR. Measured $^{143}\text{Nd}/^{144}\text{Nd}$ was corrected for instrumental bias applying a $^{146}\text{Nd}/^{144}\text{Nd} = 0.7219$. All $^{143}\text{Nd}/^{144}\text{Nd}$ values were normalized to the accepted value of the La Jolla standard of 0.511858.

Sample No.	Core No	Size range (mm)	No. of ind.	Age (kyr)	Longitude (°E)	Latitude (°S)	Water depth (m)	ϵNd	error
F010	SO185-18459 MUCG	>250	60		128.167	8.500	1743	-5.3115	0.267011
F012	SO185-18507 MUCB	>250	160		120.000	13.100	2453	-5.07312	0.174181
F013	SO185-18478-2 MUCA	>250	165		120.084	11.016	1769	-2.32088	0.145181
F014	SO185-18471-1 MUCH	>250	197		129.983	9.367	485	-6.05666	0.252855
F016	Redissolution of F014	>250	90		129.983	9.367	485	-8.85474	5.26863
F017	F008+F011				128.167	8.500	1743	-5.01265	0.925021
F018	F009+F015				119.501	15.311	2410	-5.53036	0.484658
F019	SO-18460 MUC J 0-1 cm	>250		0	128.642	8.790	1876	-4.52879	0.274531
F020	SO 18473-1 MUC H 0-1 cm	>250		0	122.417	11.517	2464	-5.13477	1.447447
F021	SO-18490-1 MUC E 0-1 cm	>250		0	122.948	13.235	407	-4.44402	0.798258
F022	SO-18460-3/Section 3/99-100 cm	>315		18	128.642	8.790	1876	-2.41273	0.577761
F023	SO-18462-2 MUC F 0-1 cm	>250		0	129.237	9.089	1422	-5.70419	0.743668
F024	SO-18499-1 MUC A 0-1 cm	>250		0	120.566	14.908	1383	-4.79339	0.334023
F025	SO-18503-1 MUC F 0-1 cm	>250			121.083	15.314	354	-6.82976	1.897613
F026	MD01-2378/Section 3/136-137 cm	>315		18	121.788	13.083	1783	-4.16584	0.637851
F027	MD01-2378/Section 4/7-8 cm	>250	100	24.18	121.788	13.083	1783	-9.16458	1.463435
F028	MD01-2378/Section 4/81-82 cm	>250	100	28.813	121.788	13.083	1783	-5.1892	0.165406
F029	MD01-2378/Section 4/127-128 cm	>250	100	32.184	121.788	13.083	1783	-5.25591	0.246898
F030	MD01-2378/Section 5/51-52 cm	>250	100	38.54	121.788	13.083	1783	-4.52711	0.175108
F031	MD01-2378/Section 5/97-98 cm	>250	100	42.079	121.788	13.083	1783	-3.70604	0.189285
F032	MD01-2378/Section 5/141-142 cm	>250	102	46.711	121.788	13.083	1783	-4.81016	0.175432
F033	MD01-2378/Section 6/8-9 cm	>250	106	48.552	121.788	13.083	1783	-4.81699	0.161885
F034	MD01-2378/Section 6/67-68 cm	>315	112	54.956	121.788	13.083	1783	-4.25003	0.160529
F035	MD01-2378/Section 6/89-90 cm	>315	104	57.344	121.788	13.083	1783	-8.22375	0.426821

Table A.2. Cleaning steps conducted on sample SO185-18507.

Sample No.	No. of ind.	Weight (mg)	Cleaning Step
F036	230	10.58	Physical cleaning + Hydrazine + DTPA (diethylene triamine pentaacetic acid)
F037	281	10.53	Physical cleaning + Hydrazine
F038	170	10.03	Physical cleaning + rinsing
F042	250	9.7	Physical cleaning + rinsing

Following the physical cleaning step, the samples were dried overnight at 50°C. For the chemical cleaning experiment, the samples were then placed in a 13-mm filter. The experiment was conducted using a simplified flow-through method following Haley and Klinkhammer [2002] and the Cd-cleaning method of Boyle and Keigwin [1985]. This experiment used a flow-through pump that was connected to cleaning reagents (Table A.3) on one end and to the filter containing the foraminifer samples on the other end (Figure A.1). The fractions of cleaning solutions from each cleaning step were collected.

Table A.3. Cleaning reagents used in the experiment.

Reagents	Concentration
HNO ₃	0.5 M
	30 mM
	15 mM
Hydrazine	2.5 mL anhydrous Hydrazine + 70 mL ammonium citrate
DTPA	0.01 N DTPA solution buffered in 0.1 N NH ₄ OH

This experiment used a 1.2 mL/minute flow rate and collection of fractions was conducted every 1.5 minutes. A total of 140 fractions were collected and 100 µL of 121 fractions were diluted to 3 mL and measured via ICP-OES Spectro Ciros CCD SOP at the Institute of Geosciences, Christian-Albrechts-University, Kiel. Both cleaning steps and elemental measurements were carried out on HNO₃ based-

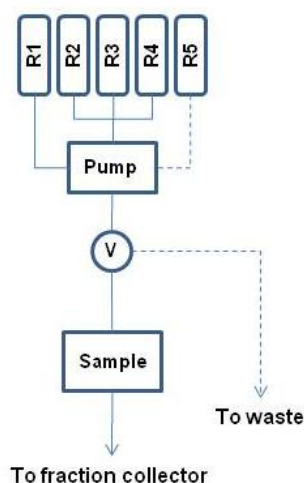


Figure A.1. Schematic of the system. Flow generally follows from top to bottom of the diagram. Reagents: R1: hydrazine, R2: DTPA, R3: weak acid (15 mM and 30 mM HNO₃), R4: ultrapure water, R5: 0.5M HNO₃ for system cleaning. V: valve.

solution. Concurrent with the cleaning experiment, the effect of cracking open foraminiferal tests was investigated applying similar cleaning steps to intact *P. obliquiloculata*. Subsequent to the chemical cleaning procedure, the samples were run through cation columns to separate the REEs followed by Nd separation from the REEs following the method of Cohen et al [1988]. After the samples had been under ultraviolet light, the Nd isotopes were measured by Thermal Ionisation Mass Spectrometry (TIMS) at IFM-GEOMAR, Kiel.

A.2. Result

A.2.1. Physical cleaning for clay removal

Cracking open foraminiferal tests before cleaning is aimed to allow any chamber fill to be removed during subsequent cleaning stages [Barker et al., 2003]. The experiment of using intact *P. obliquiloculata* tests was carried out based the following assumptions: 1) the continuous flowing of cleaning reagents in the flowthrough method would rinse any contaminant from each layer; 2) the filter would hold particulate contaminants from flowing into collection tubes.

Observation on sample F039 suggests that due to the size range being used (>250 μm) the filter was blocked and backflow of the reagents built up. The

blockage might also be related to the more resistant test of *P. obliquiloculata* that consists of intercalating low-Mg and high-Mg in the inner part and smooth microperforate surface calcite layer, or cortex, in the outer part [Sadekov et al., 2009].

Physical cleaning causes ~30 – 40% weight loss of the total sample [Haley and Klinkhammer, 2002] which explains the similarities in total carbonate of all samples (Table A.4, Figure A.2) since all samples were subjected to physical cleaning prior to chemical-cleaning steps. The efficacy and reproducibility of physical cleaning are evidenced in the nearly identical Sr/Ca value (Figure A.2).

A.2.2. Removal of oxide coating

The removal of oxide coating from the foraminiferal tests is vital in Cd/Ca and Ba/Ca determination [Boyle and Keigwin, 1985], but was found to be corrosive to carbonate and causes partial dissolution of the sample to the effect of lowering Mg/Ca ratio [Brown and Elderfield, 1996; Rosenthal et al., 2000].

Table A.4. Preliminary elemental ratio on collected fractions.

Cleaning Step	Total carbonate (mg)	% Ca dissolved	Mg:Ca	Sr:Ca	Mn:Ca	Fe:Ca	Zn:Ca	Ba:Ca	Li:Ca	Ti:Ca
Phys + Hydrazine + DTPA	1.60	49.41	2.60	1.35	9.33	0.00	0.00	10.35	0.00	0.00
Phys + Hydrazine	1.23	60.88	2.53	1.38	0.00	219.80	10.75	0.00	0.00	55.34
Phys + rinsing	1.63	49.74	2.55	1.35	31.74	0.00	33.76	3.82	0.00	119.41
Phys + rinsing	1.69	62.15	2.62	1.37	35.04	0.00	55.32	25.16	0.00	0.00

Removal of oxide coating was accomplished by basic hydrazine solution. Samples that were subjected to this step show a decrease in carbonate content by

Table A.5. Preliminary result of ϵ Nd measurement on various types of samples used in column calibration. Synthetic foram solution constitutes 10 ng/mL REE SPEX + 2 mg/mL Ca + 1.9417088 ng/mL spike solution.

No	Sample ID	Sample type	ϵ Nd	error
1	1A-02	Nd 10 ng	15105	14110.9
2	2A-02	Nd 10 ng	-29.8	0.1
3	3A-02	Nd 10 ng	-30.3	0.2
4	4A-02	Nd 10 ng	-30.2	0.0
5	5A-02	Nd 10 ng	-30	0.1
6	1B-02	SPEX 10 ng Spiked	-31	0.8
7	3B-02	SPEX 10 ng Spiked	-126	52.4
8	4B-02	SPEX 10 ng Spiked	-30.6	0.4
9	5B-02	SPEX 10 ng Spiked	-31	0.6
10	1E-02	SPEX REE 10 ng	-30	0.1
11	2E-02	SPEX REE 10 ng	-30.5	0.1
12	3E-02	SPEX REE 10 ng	-28.4	1.0
13	4E-02	SPEX REE 10 ng	-30.1	0.1
14	5E-02	SPEX REE 10 ng	-30	0.2
15	1D-02	SPEX REE Spiked	-34	0.3
16	2D-02	SPEX REE Spiked	-37	0.4
17	3D-02	SPEX REE Spiked	-34	0.3
18	5D-02	SPEX REE Spiked	-35	0.3
19	200208_06F	synthetic foram spiked	-34.8	0.5
20	200208_07F	synthetic foram spiked	-36.1	0.7
21	200208_08F	synthetic foram spiked	-135.5	18.8
22	200208_09F	synthetic foram spiked	-92.6	539.7
23	200208_10F	synthetic foram spiked	-93.9	3.3
24	SF-01	synthetic foram spiked	-35.0	0.7
25	SF-02	synthetic foram spiked	-57.7	2.2
26	SF-03	synthetic foram spiked	-41.4	1.3

15% [Barker et al., 2003] and also decrease in manganese concentrations in the collected fractions (Table A.4, Figure A.2).

A.2.3. Removal of 'refractory' phase

The removal of a 'refractory' phase was first introduced by Lea and Boyle [1993] to clean barium contamination from foraminiferal calcite. This step was conducted by running a solution of 1 mM diethylene triamine pentaacetic acid (DTPA), brought up to pH 9 with

ammonium hydroxide over the sample. Haley and Klinkhammer [2002] noticed enrichment of REEs, which act in a manner similar to barium in many ways, in this

“refractory” phase. However, sample F036 that was subjected to this step showed no REEs enrichment and lower barium concentration (Table A.4, Figure A.2).

A.2.4. $^{143}\text{Nd}/^{144}\text{Nd}$ determination

Neodymium loss during column separation, most likely caused by and erroneous calibration of the columns, resulted in very small Nd concentrations of the samples and unfortunately four markedly different ϵNd values with unacceptably high uncertainties. To resolve this problem, new shorter columns were tested. A series of column calibration were conducted in order to establish a new procedure followed by column tests using a synthetic foraminifer solution (Table A.5). The resulting ϵNd values indicated that Nd concentrations were still too low and the uncertainties were still unacceptably high.

A.3. Discussion and Conclusion

The relative importance of chemical cleaning prior to neodymium determination is clearly evident in this experiment. The intensity of the cleaning procedure had no effect on the percentage of carbonate dissolved from each samples and ranged between 49.4 – 69.1% (Figure A.2). Different cleaning procedures provided no consequences in Mg/Ca and Sr/Ca, which are comparable to core top value of 2.46 mmol/mol and 1.34 mmol/mol [Erichsen, 2009], respectively.

Samples that were subjected to the hydrazine step show less manganese than samples that only received physical cleaning. The efficacy of this step is demonstrated by manganese concentration in samples F036 and F037 that are similar to manganese concentration in blank samples. However, this step was reported to remobilize metaloxide [Haley et al., 2005] who suggested careful application of this step.

The application of a DTPA step to remove REE rich 'refractory' phase is proven to be efficient in lowering barium content in this experiment. However, as was noted by Haley and Klinkhammer [2002] and Haley et al. [2005], readsorption of REE is possible to occur afterwards. An increase of barium content was observed within all dissolved fractions. Nevertheless, the barium concentration is nearly identical to barium concentration in blank samples indicating that the barium concentration measured in the samples is within the error range of the system.

Because the ϵNd measured from foraminifer samples from this region varies largely, new series of cation and Nd columns needed to be prepared. Building on the results obtained here, future experiments need to be conducted to acquire more consistent results on the extraction and cleaning of Nd and to develop a final procedure for the acquisition of past seawater Nd isotope compositions of surface waters in the Indonesian Throughflow region.

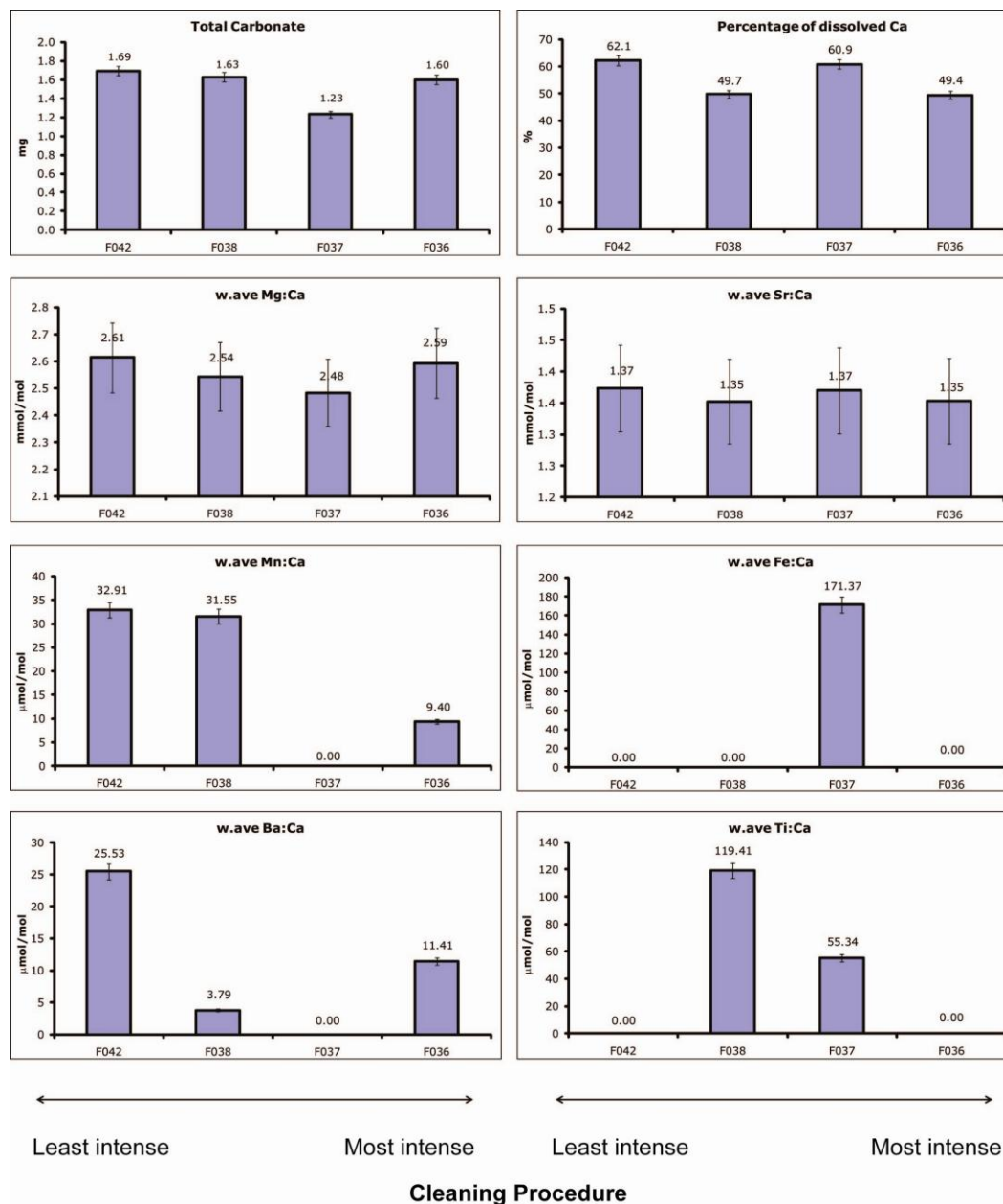


Figure A.2. Preliminary results of elemental ratio from collected fractions during experiment. Least intense cleaning procedure points to physical cleaning and rinsing before dissolution. Most intense indicates sample that experienced all cleaning steps used in this experiment.

7. References

- Adkins, J.F., A.P. Ingersoll, C. Pasquero (2005), Rapid climate change and conditional instability of the glacial deep ocean from the thermobaric effect and geothermal heating, *Quat. Sci. Rev.*, *24*, 581–594, doi: 10.1016/j.quascirev.2004.11.005.
- Alley, R.B., and P.U. Clark (1999), The Deglaciation of the Northern Hemisphere: A Global Perspective, *Ann. Rev. Earth Planet. Sci.*, *27* (1), 149-182, doi: 10.1146/annurev.earth.27.1.149.
- Altenbach, A.V. (1992), Short term processes and patterns in the foraminiferal response to organic flux rates, *Mar. Micropal.*, *19*, 119–129.
- Altenbach, A.V., and M. Sarnthein (1989), Productivity record in benthic foraminifera. In: Berger, W.H., V.S. Smetacek, G. Wefer (Eds.), *Productivity of the Ocean: Present and Past*. John Wiley and Sons, New York, pp. 255–269.
- Anand, P., H. Elderfield, and M.H. Conte (2003), Calibration of Mg/Ca thermometry in planktonic foraminifera from a sediment trap time series, *Paleoceanography*, *18* (2), 1050, doi: 10.1029/2002PA000846.
- Andersen, K.K., A. Svensson, S.J. Johnsen, S.O. Rasmussen, M. Bigler, R. Röthlisberger, U. Ruth, M.-L. Siggaard-Andersen, J. Peder Steffensen, D. Dahl-Jensen, B.M. Vinther, and H.B. Clausen (2006), The Greenland Ice Core Chronology 2005, 15-42 ka. Part 1: constructing the time scale, *Quat. Sci. Rev.*, *25* (23-24), 3246-3257.
- Antonov, J.I., R.A. Locarnini, T.P. Boyer, A.V. Mishonov, and H.E. Garcia (2006), World Ocean Atlas 2005, Volume 2: Salinity, in *NOAA Atlas NESDIS 62S*. Levitus, pp. 182, U.S. Government Printing Office, Washington, D.C.
- Arz, H.W., J. Patzold, and G. Wefer (1998), Correlated millennial-scale changes in surface hydrography and terrigenous sediment yield inferred from last glacial marine deposits off Northeastern Brazil, *Quaternary Research*, *50*, 157–166.
- Arz, H. W., F. Lamy, A. Ganopolski, N. Nowaczyk, and J. Pätzold (2007), Dominant Northern Hemisphere climate control over millennial-scale glacial sea-level variability, *Quat. Sci. Rev.*, *26* (3-4), 312-321, doi: 10.1029/2003GC000559.
- Australian Institute of Marine Science (2001), Big Bang Shoals of the Timor Sea: An environmental resource atlas, <http://www.aims.gov.au>.
- Bassinot, F., et al. (2002), Scientific report of the WEPAMA Cruise MD122/ IMAGES VII.
- Blunier, T., and E.J. Brook (2001), Timing of millennial-scale climate change in Antarctica and Greenland during the last glacial period, *Science*, *291*, 109–112, doi: 10.1126/science.291.5501.109.
- Barker, S., M. Greaves, and H. Elderfield (2003), A study of cleaning procedures used for foraminiferal Mg/Ca paleothermometry, *Geochem. Geophys. Geosyst.*, *4* (9), 8407, doi: 10.1029/2003GC000559.

- Bé, A.W.H. (1977), An ecological, zoogeographical and taxonomic review of recent planktonic foraminifera, in *Oceanic Micropaleontology*, edited by A. T. S. Ramsay, pp. 1 – 100, Elsevier, New York.
- Behling, H., H.W. Arz, J. Patzold, and G. Wefer (2000), Late Quaternary vegetational and climate dynamics in northeast Brazil, inferences from marine core GeoB 3104-1, *Quat. Sci. Rev.*, *19*, 981–994, doi: 10.1016/S0277-3791(99)00046-3.
- Bemis, B.E., H.J. Spero, J. Bijma, and D.W. Lea (1998), Reevaluation of the Oxygen Isotopic Composition of Planktonic Foraminifera: Experimental Results and Revised Paleotemperature Equations, *Paleoceanography*, *13* (2), 150–160.
- Blunier, T., J. Chappellaz, J. Schwander, A. Dallenbach, B. Stauffer, T.F. Stocker, D. Raynaud, J. Jouzel, H.B. Clausen, C.U. Hammer, and S.J. Johnsen (1998), Asynchrony of Antarctic and Greenland climate change during the last glacial period, *Nature*, *394* (6695), 739–743, doi: 10.1038/29447.
- Blunier, T., and E.J. Brook (2001), Timing of Millennial-Scale Climate Change in Antarctica and Greenland During the Last Glacial Period, *Science*, *291* (5501), 109–112, doi: 10.1126/science.291.5501.109.
- Boyle, E.A., and L.D. Keigwin (1985), Comparison of Atlantic and Pacific paleochemical records for the past 215,000 y.: changes in deep ocean circulation and chemical inventories. *Earth Planet. Sci. Lett.*, *76*, 135– 150.
- Broccoli, A.J., K.A. Dahl, R.J. Stouffer (2006), Response of the ITCZ to Northern Hemisphere cooling, *Geophys. Res. Lett.*, *33*, 1–4, doi: 10.1029/2005GL024546.
- Broecker, W.S. (1998), Paleocean Circulation during the Last Deglaciation: A Bipolar Seesaw?, *Paleoceanography*, *13* (2), 119–121.
- Broecker, W.S. (2003), Does the Trigger for Abrupt Climate Change Reside in the Ocean or in the Atmosphere?, *Science*, *300* (5625), 1519–1522, doi: 10.1126/science.1083797.
- Brown, S. J., and H. Elderfield, Variations in Mg/Ca and Sr/Ca ratios of planktonic foraminifera caused by postdepositional dissolution: Evidence of shallow Mg-dependent dissolution (1996), *Paleoceanography*, *11*, 543–551.
- Burns, S.J., D. Fleitmann, A. Matter, J. Kramers, A.A. Al-Subbary (2003), Indian Ocean climate and an absolute chronology over Dansgaard/Oeschger events 9 to 13, *Science*, *301*, 1365–1367, doi: 10.1126/science. 1086227.
- Butzin, M., M. Prange, G. Lohmann (2005), Radiocarbon simulations for the glacial ocean: the effects of wind stress, Southern Ocean sea ice and Heinrich events, *Earth Planet. Sci. Lett.*, *235*, 45–61, doi: 10.1016/j.epsl.2005.03.003.
- Cacho, I., J.O. Grimalt, C. Pelejero, M. Canals, F.J. Sierro, J.A. Flores, and N. Shackleton (1999), Dansgaard-Oeschger and Heinrich Event Imprints in Alboran Sea Paleotemperatures, *Paleoceanography*, *14* (6), 698–705.
- Clark, P. U., S.W. Hostetler, N.G. Pisias, A. Schmittner, and K.J. Meissner (2007), Mechanisms for an ~7-kyr Climate and Sea-Level Oscillation During Marine Isotope Stage 3, in *Past and Future Changes of the Ocean Meridional*

- Overturning Circulation: Mechanisms and Impacts*, AGU Monograph, edited by A. Schmittner, J.C.H. Chiang, and S.R. Hemming, pp. 209-246.
- Chappell, J. (2002), Sea level changes forced ice breakouts in the Last Glacial cycle: new results from coral terraces, *Quat. Sci. Rev.*, 21, 1229–1240, doi: 10.1016/S0277-3791(01)00141-X.
- Cléroux, C., E. Cortijo, J.-C. Duplessy, and R. Zahn (2007), Deep-dwelling foraminifera as thermocline temperature recorders, *Geochem. Geophys. Geosyst.*, 8, Q04N11, doi: 10.1029/2006GC001474.
- Cohen, A.S., R.K. O’Nions, R. Siegenthaler, and W.L. Griffin (1988), Chronology of the pressure-temperature history recorded by a granulite terrain, *Contrib. Mineral. Petrol.*, 98, 303-311.
- Cresswell, G.R. (1991), The Leeuwin Current — observations and recent models, *The Journal of the Royal Society of Western Australia*, 74, 1–14.
- Dannenmann, S., B.K. Linsley, D.W. Oppo, Y. Rosenthal, and L. Beaufort (2003), East Asian monsoon forcing of suborbital variability in the Sulu Sea during Marine Isotope Stage 3: Link to Northern Hemisphere climate, *Geochem. Geophys. Geosyst.*, 4 (1), 1001, doi: 10.1029/2002GC000390.
- Dansgaard, W., S.J. Johnsen, H.B. Clausen, D. Dahl-Jensen, N.S. Gundestrup, C.U. Hammer, C.S. Hvidberg, J.P. Steffensen, A.E. Sveinbjörnsdóttir, J. Jouzel, G. Bond (1993), Evidence for general instability of past climate from a 250-kyr ice-core record, *Nature*, 364, 218–220.
- Data Announcement 88-MGG-02 (1988), Digital relief of the Surface of the Earth. NOAA, National Geophysical Data Center, Boulder, Colorado.
- de Deckker, P., N.J. Tapper, and S. van der Kaars (2003), The status of the Indo-Pacific Warm Pool and adjacent land at the Last Glacial Maximum, *Global Planet. Change*, 35 (1-2), 25-35, doi: 10.1016/S0921-8181(02)00089-9.
- Dekens, P.S., D.W. Lea, D.K. Pak, and H.J. Spero (2002), Core top calibration of Mg/Ca in tropical foraminifera: Refining paleotemperature estimation, *Geochem. Geophys. Geosyst.*, 3(4), 1022, doi: 10.1029/2001GC000200.
- Dürkop, A., A. Holbourn, W. Kuhnt, R. Zuraida, N. Andersen, and P.M. Grootes (2008), Centennial-scale climate variability in the Timor Sea during Marine Isotope Stage 3, *Mar. Micropal.*, 66 (3), 208-221, doi: 10.1016/j.marmicro.2007.10.002.
- Dürkop, A. (2009), Climate variability in the Eastern Indian Ocean during the Marine Isotope Stage 3: high resolution proxy studies of the Timor Sea, Unpublished PhD-Thesis, Mathematisch-Naturwissenschaftliche Fakultät der Christian-Albrechts-Universität zu Kiel.
- Eggins, S., P. De Deckker, and J. Marshall (2003), Mg/Ca variation in planktonic foraminifera tests: implications for reconstructing palaeo-seawater temperature and habitat migration, *Earth Planet. Sci. Lett.*, 212 (3-4), 291-306, doi: 10.1016/S0012-821X(03)00283-8.
- Elderfield, H., and G. Ganssen (2000), Past temperature and d18O of surface ocean waters inferred from foraminiferal Mg/Ca ratios, *Nature*, 405, 442–445.

- England, M.H. (1992), On the formation of Antarctic intermediate and bottom water in ocean general circulation models, *J. of Phys. Ocean.*, 22, 918–926.
- EPICA Community Members (2004), Eight glacial cycles from an Antarctic ice core, *Nature*, 429 (6992), 623–628, doi: 10.1038/nature02599.
- EPICA Community Members (2006), One-to-one coupling of glacial climate variability in Greenland and Antarctica, *Nature*, 444 (7116), 195–198, doi: 10.1038/nature05301.
- Erichsen, A. (2008), Impact of calcite dissolution on Mg/Ca ratios of core-top planktonic foraminifers from the Timor Sea. Unpublished Diploma-Thesis, Mathematisch-Naturwissenschaftliche Fakultät der Christian-Albrechts-Universität zu Kiel. 48 pp.
- Fairbanks, R.G., R.A. Mortlock, T.-C. Chiu, L. Cao, A. Kaplan, T.P. Guilderson, T.W. Fairbanks, A.L. Bloom, P.M. Grootes, M.-J. Nadeau (2005), Radiocarbon calibration curve spanning 0 to 50000 years BP based on paired $^{230}\text{Th}/^{234}\text{U}/^{238}\text{U}$ and ^{14}C dates on pristine corals, *Quat. Sci. Rev.*, 24, 1781–1796, doi: 10.1016/j.quascirev.2005.04.007.
- Farmer, E.C., A. Kaplan, P.B. de Menocal, and J. Lynch-Stieglitz (2007), Corroborating ecological depth preferences of planktonic foraminifera in the tropical Atlantic with the stable oxygen isotope ratios of core top specimens, *Paleoceanography*, 22, PA3205, doi: 10.1029/2006PA001361.
- Ffield, A. and A.L. Gordon (1992), Vertical mixing in the Indonesian Thermocline, *J. Phys. Oceanogr.*, 22(2), 184–195.
- Fontugne, Michel R; Calvert, Stephen E (1992), Late Pleistocene variability of the carbon isotopic composition of organic matter in the eastern Mediterranean: monitor of changes in carbon sources and atmospheric CO₂ concentrations. *Paleoceanography*, 7(1), 1–20, doi:10.1029/91PA02674.
- Ganopolski, A., and S. Rahmstorf (2001), Rapid changes of glacial climate simulated in a coupled climate model, *Nature*, 409, 153–158, doi: 10.1038/35051500.
- Godfrey, J., and A. Weaver (1991), Is the Leeuwin Current driven by Pacific heating and winds? *Progress in Oceanography* 27, 225–272.
- Goldstein, S.L., and S.R. Hemming (2003), Long-lived Isotopic Tracers in Oceanography, Paleooceanography and Ice Sheet Dynamics, in H. Elderfield (Vol. Ed), H.D. Holland and K.K. Turekian (Series Ed), Treatise on Geochemistry, Vol. 6, 453–489.
- Gooday, A.J. (1988), A response by benthic foraminifera to the deposition of phytodetritus in the deep sea, *Nature*, 332, 70–73.
- Gooday, A.J. (1993), Deep-sea benthic foraminiferal species which exploit phytodetritus: characteristic features and controls on distribution, *Mar. Micropal.*, 22, 187–205.
- Gordon, A. L., and R. A. Fine (1996), Pathways of water between the Pacific and Indian oceans in the Indonesian seas, *Nature*, 379, 146–149.

- Gordon, A.L., and R.D. Susanto (2001), Banda Sea Surface Layer Divergence, *Ocean Dynamics*, 52, 2-10.
- Gordon, A.L., R.D. Susanto, and K. Vranes (2003), Cool Indonesian throughflow as a consequence of restricted surface layer flow, *Nature*, 425 (6960), 824-828, doi: 10.1038/nature02038.
- Gordon, A.L. (2005), Oceanography of the Indonesian Seas and Their Throughflow, *Oceanography*, 18 (4), 14-27.
- Gordon, A., S. Wijffels, J. Sprintall, D. Susanto, R. Molcard, H. Van Aken, A. Field, Indroyono Soesilo and Sugiarta Wirasantosa (2008), The Indonesian Throughflow, 3-year INSTANT composite view, unpublished.
- Griffiths, M. L., R. N. Drysdale, M. K. Gagan, J.-x. Zhao, L. K. Ayliffe, J. C. Hellstrom, W. S. Hantoro, S. Frisia, Y.-x. Feng, I. Cartwright, E. St. Pierre, M. J. Fischer & B. W. Suwargadi (2009), Increasing Australian–Indonesian monsoon rainfall linked to early Holocene sea-level rise, *Nature Geoscience*, 2, 636 – 639, doi: 10.1038/ngeo605.
- Grootes, P.M., and M. Sarnthein (2006), Marine ¹⁴C reservoir ages oscillate, *Pages Newsletter*, 14 (3), 18–19.
- Grootes, P.M., M. Stuiver, J.W.C. White, S.J. Johnsen, J. Jouzel (1993), Comparison of oxygen isotope records from the GISP2 and GRIP Greenland ice cores, *Nature* 366, 552–554.
- Haley, B., and G.P. Klinkhammer (2002), Development of a flow-through system for cleaning and dissolving foraminiferal tests, *Chem. Geol.*, 185, 51–69, doi: 10.1016/S0009-2541(01)00399-0.
- Haley, B., G.P. Klinkhammer, A.C. Mix (2005), Revisiting the rare earth elements in foraminiferal tests, *Earth Planet. Sci. Lett.*, 239, 79– 97, doi: 10.1016/j.epsl.2005.08.014.
- Hemleben, C., M. Spindler, and O.R. Anderson (1989), *Modern Planktonic Foraminifera*, 363 pp., Springer-Verlag, New York.
- Hemming, S.R. (2004), Heinrich events: Massive late Pleistocene detritus layers of the North Atlantic and their global climate imprint, *Rev. Geophys.*, 42, RG1005, doi:10.1029/2003RG000128.
- Hendy, I.L., and J.P. Kennett (2000), Dansgaard-Oeschger Cycles and the California Current System: Planktonic Foraminiferal Response to Rapid Climate Change in Santa Barbara Basin, Ocean Drilling Program Hole 893A, *Paleoceanography*, 15 (1), 30–42.
- Herguera, J.C. (2000), Last glacial paleoproductivity patterns in the eastern equatorial Pacific: benthic foraminifera records, *Mar. Micropal.*, 40, 259–275, doi: 10.1016/S0377-8398(00)00041-4.
- Herguera, J.C., and W.H. Berger (1991), Paleoproductivity from benthic foraminifera abundance: glacial to postglacial change in the west equatorial Pacific, *Geology*, 19, 1173–1176.

- Holbourn, A.E., W. Kuhnt, H. Kawamura, Z. Jian, P. Grootes, H. Erlenkeuser, H. and J. Xu (2005), Orbitally-paced paleoproductivity variations in the Timor Sea and Indonesian Throughflow variability during the last 460-ky. *Paleoceanography*, 20 (3), 3002, doi: 10.1029/2004PA001094.
- Hughen, K., S. Lehman, J. Southon, J. Overpeck, O. Marchal, C. Herring, J. Turnbull (2004), ^{14}C activity and global carbon cycle changes over the past 50000 years, *Science*, 303, 202–207, doi: 10.1126/science. 1090300.
- Hung, C.-W., X. Liu, M. Yanai (2004), Symmetry and asymmetry of the Asian and Australian summer monsoons, *J. of Climate*, 17, 2413–2426, doi: 10.1175/1520-0442(2004)017.
- Huber, C., M. Leuenberger, R. Spahni, J. Flückiger, J. Schwander, T.F. Stocker, S. Johnsen, A. Landais, J. Jouzel (2006), Isotope calibrated Greenland temperature record over Marine Isotope Stage 3 and its relation to CH_4 , *Earth Planet. Sci. Lett.*, 245, 504–519, doi: 10.1016/j.epsl.2006.01.002.
- Ilahude, A.G., and A.L. Gordon (1996), Thermocline stratification within the Indonesian Seas, *J. Geophys. Res.*, 101 (C5), 12,401–12,409.
- Jacobsen, S.B and G.J. Wasserburg (1980), Sm-Nd isotope evolution of chondrites, *Earth Planet. Sci. Lett.*, 50, 139-155.
- Jeandel, C., D. Thouron and M. Fieux (1998), Concentration and isotopic compositions of neodymium in the eastern Indian Ocean and Indonesian straits, *Geochim. Cosmochim. Acta* 62, 2597–2607.
- Jian, Z.M., L.J. Wang, M. Kienast, M. Sarnthein, W. Kuhnt, H.L. Lin, P.X. Wang (1999), Benthic foraminiferal paleoceanography of the South China Sea over the last 40000 years, *Mar. Geo.*, 156, 159–186.
- Jian, Z., B. Huang, W. Kuhnt, H-L. Lin, H.-L. (2001), Late Quaternary upwelling intensity and east Asian monsoon forcing in the South China Sea, *Quat. Res.*, 55, 363–370, doi: 10.1006/qres.2001.2231.
- Jones, R.W. (1994), *The Challenger Foraminifera*, Oxford University Press, New York.
- Johnsen, S.J., H.B. Clausen, W. Dansgaard, K. Fuhrer, N. Gundestrup, C.U. Hammer, P. Iversen, J. Jouzel, B. Stauffer, J.P. Steffensen, J.P. (1992), Irregular glacial interstadials recorded in a new Greenland ice core, *Nature*, 359, 311–313.
- Kienast, M., S. Kienast, S. Calvert, T. Eglinton, G. Mollenhauer, R. Francois, and A. Mix (2006), Eastern Pacific cooling and Atlantic overturning circulation during the last deglaciation, *Nature*, 443, 846–849, doi: 10.1038/nature05222.
- Knutti, R., Flückiger, J., Stocker, T.F., Timmermann, A. (2004), Strong hemispheric coupling of glacial climate through freshwater discharge and ocean circulation, *Nature*, 430, 851–856, doi: 10.1038/nature02786.
- Koutavas, A., J. Lynch-Stieglitz, T.M. Marchitto Jr., J.P. Sachs (2002), El Niño-like pattern in ice age tropical Pacific sea surface temperature, *Science*, 297, 226–230.

- Koutavas, A., P.B. deMenocal, G.C. Olive, and J. Lynch-Stieglitz (2006), Mid-Holocene El Niño Southern Oscillation (ENSO) attenuation revealed by individual foraminifera in eastern tropical Pacific sediments, *Geology*, 34 (12), 993–996, doi:10.1130/G22810A.1.
- Kuhnt, W., S. Hess, and Z. Jian (1999), Quantitative composition of benthic foraminiferal assemblages as a proxy indicator for organic carbon flux rates in the South China Sea, *Mar. Geol.*, 156, 123–158.
- Kuhnt, W., A. Holbourn, R. Hall, M. Zuvela, R. Käse (2004), Neogene history of the Indonesian Throughflow, In: Clift, P., et al. (Eds.), *Continent-Ocean Interactions Within East Asia Marginal Seas, Geophysical Monograph Series, vol. 149*. AGU, Washington D.C., pp. 299–320.
- Kuhnt, W., et al. (2006), Cruise report SONNE-185 “Variability of the Indonesian Throughflow and Australasian climate history of the last 150 000 years (VITAL)”, report, Ins. für Geowiss., Christian-Albrechts-Univ. Zu Kiel, Kiel, Germany.
- Labeyrie, L. D., J. C. Duplessy, and P. L. Blanc (1987), Variations in mode of formation and temperature of oceanic deep waters over the past 125,000 years, *Nature*, 327 (6122), 477–482, doi: 10.1038/327477a0.
- Landais, A., Caillon, N., Goujon, C., Grachev, A., Barnola, J., Chappellaz, J., Jouzel, J., Masson-Delmotte, V., Leuenberger, M. (2004), Quantification of rapid temperature change during DO event 12 and phasing with methane inferred from air isotopic measurements, *Earth Planet. Sci. Lett.*, 225, 221–232, doi:10.1016/j.epsl.2004.06.009.
- Lea, D.W., and E.A. Boyle (1993), Determination of carbonate-bound barium in foraminifera and corals by isotope dilution plasma mass spectrometry, *Chem. Geol.*, 103, 73–84.
- Legates, D.R., and C.J. Willmott (1990), Mean seasonal and spatial variability in gauge-corrected, global precipitation, *Int. J. Climatology*, 10, 111–127.
- Levi, C., L. Labeyrie, F. Bassinot, F. Guichard, E. Cortijo, C. Waelbroeck, N. Caillon, J. Duprat, T. d. Garidel-Thoron, and H. Elderfield (2007), Low-latitude hydrological cycle and rapid climate changes during the last deglaciation, *Geochem. Geophys. Geosyst.*, 8 (5), Q05N12, doi: 10.1029/2006GC001514.
- Lin, H.-L., L. C. Peterson, J. T. Overpeck, S. E. Trumbore, and D. W. Murray (1997), Late Quaternary climate change from $\delta^{18}\text{O}$ records of multiple species of planktonic foraminifera: high-resolution records from the anoxic Cariaco Basin Venezuela, *Paleoceanography*, 12 (3), 417–427.
- Lin, I., Liu, W.T., Wu, C.-C., Wong, G.T.F., Hu, C., Chen, Z., Liang, W.-D., Yang, Y., Liu, K.-K. (2003), New evidence for enhanced ocean primary production triggered by tropical cyclone, *Geophysic. Res. Lett.*, 30, doi: 10.1029/2003GL017141.
- Locarnini, R. A., A. V. Mishonov, J. I. Antonov, T. P. Boyer, and H. E. Garcia (2006), World Ocean Atlas 2005. Volume 1: Temperature, in *NOAA Atlas NESDIS 61*, edited by S. Levitus, pp. 182, U.S. Government Printing Office, Washington, D.C.

- Loeblich, A.R., Tappan, H. (1994), Foraminifera of the Sahul Shelf and Timor Sea. Cushman Foundation for Foraminiferal Research, Cambridge (U.S.A.).
- Longhurst, A.R. (1998), Ecological Geography of the Sea. Academic Press, San Diego.
- Loubere, P. (1991), Deep-sea benthic foraminiferal assemblage response to a surface ocean productivity gradient: a test, *Paleoceanography*, 6, 193–204.
- Loubere, P. (1994), Quantitative estimation of surface ocean productivity and bottom water oxygen concentration using benthic foraminifera, *Paleoceanography*, 9, 723–737.
- Loubere, P. (1996), The surface ocean productivity and bottom water oxygen signals in deep water benthic foraminiferal assemblages, *Mar. Micropal.*, 28, 247–261.
- Lutze, G.F., Coulbourn, W.T. (1984), Recent benthic foraminifera from the continental margin of northwest Africa: community structure and distribution, *Mar. Micropal.*, 8, 361–401.
- Lynch-Stieglitz, J. (2004), OCEAN SCIENCE: Hemispheric Asynchrony of Abrupt Climate Change, *Science*, 304 (5679), 1919–1920, doi: 10.1126/science.1100374.
- Martin, P. A., and D. W. Lea (2002), A simple evaluation of cleaning procedures on fossil benthic foraminiferal Mg/Ca, *Geochem. Geophys. Geosyst.*, 3(10), 8401, doi:10.1029/2001GC000280.
- Martrat, B., Grimalt, J.O., Shackleton, N.J., de Abreu, L., Hutterli, M.A., Stocker, T.F. (2007), Four climate cycles of recurring deep and surface water destabilizations on the Iberian Margin, *Science*, 317, 502–507, doi: 10.1126/science.1139994.
- Matsumoto, K., Key, R.M. (2004). Natural radiocarbon distribution in the deep ocean, In: Shiyomi, M., et al. (Eds.), Global Environmental Change in the Ocean and on Land. Terra Pub., Tokyo, pp. 45–58.
- McCartney, M.S. (1977), Subantarctic mode water, In: Angel, M.V. (Ed.), A Voyage of Discovery: George Deacon 70th Anniversary Volume. Pergamon Press, Oxford, pp. 103–119.
- McCorkle, D.C., Heggie, D.T., Veeh, H.H. (1998), Glacial and Holocene stable isotope distributions in the southeastern Indian Ocean, *Paleoceanography*, 13, 20–34.
- Miller, G., Mangan, J., Pollard, D., Thompson, S., Felzer, B., Magee, J. (2005), Sensitivity of the Australian Monsoon to insolation and vegetation: implications for human impact on continental moisture balance, *Geology*, 33, 65–68, doi: 10.1130/G21033.1
- Mohtadi, M., S. Steinke, J. Groeneveld, H. G. Fink, T. Rixen, D. Hebbeln, B. Donner, and B. Herunadi (2009), Low-latitude control on seasonal and interannual changes in planktonic foraminiferal flux and shell geochemistry off south Java: A sediment trap study, *Paleoceanography*, 24, PA1201, doi:10.1029/2008PA001636.

- Murgese, Davide S., and Patrick de Deckker (2007), The Late Quaternary evolution of water masses in the eastern Indian Ocean between Australia and Indonesia, based on benthic foraminifera faunal and carbon isotopes analyses, *Palaeogeography, Palaeoclimatology, Palaeoecology*, *247*, 382–401, doi:10.1016/j.palaeo.2006.11.002.
- Müller, A., Opdyke, B.N. (2000), Glacial–interglacial changes in nutrient utilization and paleoproductivity in the Indonesian Throughflow sensitive Timor Trough, easternmost Indian Ocean, *Paleoceanography*, *15* (1), 85–94.
- Muller, J., M. Kylander, R. A. J. Wüst, D. Weiss, A. Martinez-Cortizas, A. N. LeGrande, T. Jennerjahn, H. Behling, W. T. Anderson, and G. Jacobson (2008), Possible evidence for wet Heinrich phases in tropical NE Australia: The Lynch's Crater deposit, *Quat. Sci. Rev.*, *27*, 468-475, doi: 10.1016/j.quascirev.2007.11.006.
- Nadeau, M.-J., Schleicher, M., Grootes, P.M., Erlenkeuser, H., Gott dang, A., Mous, D.J.W., Sarnthein, M., Willkomm, H. (1997), The Leibniz-Labor AMS facility at the Christian–Albrechts Universität Kiel, Germany, *Nuclear Instruments and Methods in Physics Research Sect. B* (123), 22–30.
- NGRIP members (2004), High-resolution record of Northern Hemisphere climate extending into the last interglacial period, *Nature*, *43*, 147–151.
- O’Nions, R.K., S.R., Carter, R.S. Cohen, N.M. Evensen, N. M., and P.J. Hamilton (1978), Pb, Nd and Sr isotopes in oceanic ferromanganese deposits and ocean floor basalts. *Nature*, *273*, 435-8.
- Pahnke, K., and R. Zahn (2005), Southern Hemisphere water mass conversion linked with North Atlantic climate variability, *Science*, *307* (1741), 1741-1746, doi: 10.1126/science.1102163.
- Partin, J. W., K. M. Cobb, J. F. Adkins, B. Clark, and D. P. Fernandez (2007), Millennial-scale trends in west Pacific warm pool hydrology since the Last Glacial Maximum, *Nature*, *449* (7161), 452-455, doi: 10.1038/nature06164.
- Pearce, A.F., and G.R. Cresswell (1985), Ocean circulation off Western Australia and the Leeuwin Current. CSIRO Information Service Sheet (16–3), 1–4.
- Peter, B.N., P. Sreeraj, and K.G.V. Kumar (2005), Structure and variability of the Leeuwin Current in the south eastern Indian Ocean, *The J. of the Indian Geophysic. Union*, *9*, 107–119.
- Peterson, L.C., G.H. Haug, K.A. Hughen, U. Röhl, (2000), Rapid changes in the hydrologic cycle of the tropical Atlantic during the last glacial, *Science*, *290*, 1947–1951.
- Piotrowski, A. M., S. L. Goldstein, S. R. Hemming, and R. G. Fairbanks (2004), Intensification and variability of ocean thermohaline circulation through the last deglaciation, *Earth Planet. Sci. Lett.*, *225* (1-2), 205-220, doi:10.1016/j.epsl.2004.06.002.
- Piotrowski, A.M., S.L. Goldstein, S.R. Hemming, and R.G. Fairbanks (2005), Temporal relationships of carbon cycling and ocean circulation at glacial boundaries, *Science*, *307*, 1933-1938, doi: 10.1126/science.1104883.

- Pflaumann, U., and Z. Jian (1999), Modern distribution patterns of planktonic foraminifera in the South China Sea and western Pacific: a new transfer technique to estimate regional sea-surface temperatures, *Marine Geology*, 156 (1-4), 41-83, doi: 10.1016/S0025-3227(98)00173-X.
- Prell, W. L., and J. E. Damuth (1978), The climate-related diachronous disappearance of *Pulleniatina obliquiloculata* in late quaternary sediments of the Atlantic and Caribbean, *Mar. Micropal.*, 3 (3), 267-277.
- Rashid, H., and E.A. Boyle (2007), Mixed-Layer Deepening During Heinrich Events: A Multi-Planktonic Foraminiferal $\delta^{18}\text{O}$ Approach, *Science*, 318, 439-441, doi:10.1126/science.1146138.
- Ravelo, C. A., and R. G. Fairbanks (1992), Oxygen isotopic composition of multiple species of planktonic foraminifera: recorders of the modern photic zone temperature gradient, *Paleoceanography*, 7 (6), 815-831.
- Ravelo, A.C., R. G. Fairbanks, and G. Philander (1990), Reconstructing tropical Atlantic hydrography using planktonic foraminifera and an ocean model. *Paleoceanography*, 5, 409-431.
- Regenberg, M., D. Nürnberg, S. Steph, J. Groeneveld, D. Garbe-Schönberg, R. Tiedemann, and W.-C. Dullo (2006), Assessing the effect of dissolution on planktonic foraminiferal Mg/Ca ratios: Evidence from Caribbean core tops, *Geochem. Geophys. Geosyst.*, 7, Q07P15, doi:10.1029/2005GC001019.
- Rohling, E. J. (2007), Progress in palaeosalinity: overview and presentation of a new approach, *Paleoceanography*, 22, PA3215, doi: 10.1029/2007PA001437.
- Rosenthal, Y., G. P. Lohmann, K. C. Lohmann, and R. M. Sherrell, Incorporation and preservation of Mg in *Globigerinoides sacculifer*: Implications for reconstructing the temperature and O-18/O-16 of seawater (200), *Paleoceanography*, 15, 135-145.
- Rosenthal, Y., D. W. Oppo, and B. K. Linsley (2003), The amplitude and phasing of climate change during the last deglaciation in the Sulu Sea, western equatorial Pacific, *Geophys. Res. Lett.*, 30, 1, doi: 10.1029/2002GL016612.
- Ruth, U., Bigler, M., Röthlisberger, R., Siggaard-Andersen, M.-L., Kipfstuhl, S., Goto-Azuma, K., Hansson, M.E., Johnsen, S.J., Lu, H., Steffensen, J.P. (2007), Ice core evidence for a very tight link between North Atlantic and east Asian glacial climate, *Geophysic. Res. Lett.*, 34, doi: 10.1029/2006GL027876.
- Sadekov, A., S. M. Eggins, P. De Deckker, U. Ninnemann, W. Kuhnt, and F. Bassinot (2009), Surface and subsurface seawater temperature reconstruction using Mg/Ca microanalysis of planktonic foraminifera *Globigerinoides ruber*, *Globigerinoides sacculifer*, and *Pulleniatina obliquiloculata*, *Paleoceanography*, 24, PA3201, doi:10.1029/2008PA001664.
- Sarnthein, M., Winn, K. (1990), Reconstruction of low and middle latitude export productivity, 30000 years B.P. to present: implications for global carbon reservoirs, In: Schlesinger, M.E. (Ed.), *Climate Ocean Interaction*. Springer, New York, pp. 317-342.

- Sarnthein, M., K. Winn, S. J. A. Jung, J.-C. Duplessy, L. Labeyrie, H. Erlenkeuser, and G. Ganssen (1994), Changes in East Atlantic Deepwater Circulation Over the Last 30,000 years: Eight Time Slice Reconstructions, *Paleoceanography*, 9 (2), 209–267.
- Sarnthein, M., K. Stattegger, D. Dreger, H. Erlenkeuser, P. M. Grootes, B. Haupt, S. Jung, T. Kiefer, W. Kuhnt, U. Pflaumann, C. Schäfer-Neth, M. Schulz, D. Seidov, J. Simstich, S. van Kreveld-Alfane, E. Vogelsang, V. A., and M. Weinelt (2001), Fundamental modes and abrupt changes in North Atlantic circulation and climate over the last 60 ky - Numerical modelling and reconstruction, in P. Schäfer et al. (Eds.), *The northern North Atlantic: a changing environment*, Springer, Berlin.
- Sarnthein, M., Grootes, P.M., Kennett, J.P., Nadeau, M.-J. (2007), ^{14}C reservoir ages show deglacial changes in ocean currents and carbon cycle, In: Schmittner, A., Chiang, J.C.H., Hemming, S.R. (Eds.), *Ocean Circulation: Mechanisms and Impacts – Past and Future Changes of Meridional Overturning*. American Geophysical Union, Washington D.C., pp. 175–196.
- Schleicher, M., Grootes, P., Nadeau, M.-J., Schoon, A. (1998). The carbonate ^{14}C background and its components at the Leibniz AMS facility, *Radiocarbon*, 40, 85–93.
- Schott, F., and J. McCreary (2001), The monsoon circulation of the Indian Ocean, *Prog. Oceanogr.*, 51, 1-123, doi: 10.1016/S0079-6611(01)00083-0.
- Schmidt, M.W., M.J. Vautravers and H.J. Spero (2006), Rapid subtropical North Atlantic salinity oscillations across Dansgaard–Oeschger cycles, *Nature*, 443, 561-564, doi:10.1038/nature05121.
- Shackleton, N. J. (1987), Oxygen isotopes, ice volume and sea level, *Quat. Sci. Rev.*, 6 (3-4), 183-190.
- Shackleton, N. J., M. A. Hall, and E. Vincent (2000), Phase Relationships Between Millennial-Scale Events 64,000-24,000 Years Ago, *Paleoceanography*, 15 (6), 565–569, doi: 10.1029/2000PA000513.
- Sicre, M.A., L. Labeyrie, U. Ezat, J. Duprat, J.L. Turon, S. Schmidt, E. Michel, and A. Mazaud (2005), Mid-latitude Southern Indian Ocean response to Northern Hemisphere Heinrich events, *Earth Planet. Sci. Lett.*, 240, 724–731, doi: 10.1016/j.epsl.2005.09.032.
- Siddall, M., E. J. Rohling, A. Almogi-Labin, C. Hemleben, D. Meischner, I. Schmelzer, and D. A. Smeed (2003), Sea-level fluctuations during the last glacial cycle, *Nature*, 423 (6942), 853-858, doi: 10.1038/nature01690.
- Spooner, Michelle I., Timothy T. Barrows, Patrick De Deckker, Martine Paterne (2005), Palaeoceanography of the Banda Sea, and Late Pleistocene initiation of the Northwest Monsoon, *Global Planetary Change*, 49, 28– 46, doi:10.1016/j.gloplacha.2005.05.002.
- Sprintall, J., J. T. Potemra, S. L. Hautala, N. A. Bray, and W. W. Pandoe (2003), Temperature and salinity variability in the exit passages of the Indonesian Throughflow, *Deep Sea Res. Part II: Topical Studies in Oceanography*.

- Physical Oceanography of the Indian Ocean: from WOCE to CLIVAR*, 50 (12-13), 2183-2204, doi: 10.1016/S0967-0645(03)00052-3.
- Sriver, R.L., Huber, M. (2007), Observational evidence for an ocean heat pump induced by tropical cyclones, *Nature*, 447, 577–580, doi: 10.1038/nature05785.
- Stott, L., C. Poulsen, S. Lund, and R. Thunell (2002), Super ENSO and Global Climate Oscillations at Millennial Time Scales, *Science*, 297 (5579), 222-226, doi: 10.1126/science.1071627.
- Suhr, S.B., Pond, D.W., Gooday, A.J., Smith, C.R. (2003), Selective feeding by benthic foraminifera on phytodetritus on the western Antarctic Peninsula shelf: evidence from fatty acid biomarker analysis, *Marine Ecology Progress Series*, 262, 153–162.
- Suppiah, R., and X. Wu (1998), Surges, cross-equatorial flows and their links with the Australian summer monsoon circulation and rainfall. Australian meteorological magazine. Vol. 47, no. 2, June 1998. pp. 113-130.
- Suppiah, R. (1992), The Australian summer monsoon: a review, *Progress in Physical Geography*, 16, 283–318.
- Svensson, A., K. K. Andersen, M. Bigler, H. B. Clausen, D. Dahl-Jensen, S. M. Davies, S. J. Johnsen, R. Muscheler, S. O. Rasmussen, R. Röthlisberger, J. Peder Steffensen, and B. M. Vinther (2006), The Greenland Ice Core Chronology 2005, 15-42 ka. Part 2: comparison to other records, *Quat. Sci. Rev.*, 25 (23-24), 3258-3267, doi: 10.1016/j.quascirev.2006.08.003.
- Svensson, A., K. K. Andersen, M. Bigler, H. B. Clausen, D. Dahl-Jensen, S. M. Davies, S. J. Johnsen, R. Muscheler, F. Parrenin, S. O. Rasmussen, R. Röthlisberger, I. Seierstad, J. P. Steffensen, and B. M. Vinther (2008), A 60 000 year Greenland stratigraphic ice core chronology, *Clim. Past*, 4, 47–57.
- Széréméta, N., Bassinot, F., Balut, Y., Labeyrie, L., Pagel, M., 2004. Oversampling of sedimentary series collected by giant piston corer: Evidence and corrections based on 3.5-kHz chirp profiles. *Paleoceanography* 19. doi:10.1029/2002PA000795.
- Tachikawa, K., V. Athias, and C. Jeandel (2003), Neodymium budget in the modern ocean and paleo-oceanographic implications, *J. Geophys. Res.*, 108(C8), 3254, doi:10.1029/1999JC000285.
- Talley, L. D., and J. Sprintall (2005), Deep expression of the Indonesian Throughflow: Indonesian Intermediate Water in the South Equatorial Current, *J. Geophys. Res.*, 110, C10009, doi:10.1029/2004JC002826.
- Tapper, N. (2002), Climate, climatic variability and atmospheric circulation patterns in the Maritime Continent region, In: Kershaw, P., et al. (Eds.), *Bridging Wallace's Line: The Environmental and Cultural History and Dynamics of the Southeast Asian – Australian Region*. Catena, Reiskirchen (Germany), pp. 12–30.
- Tedesco, K. A., and R. C. Thunell (2003), Seasonal and Interannual Variations in Planktonic Foraminiferal Flux and Assemblage Composition in the Cariaco Basin, Venezuela, *J. Foram. Res.*, 33 (3), 192-210, doi: 10.2113/33.3.192.

- Thomas, E., Gooday, A.J. (1996), Deep-sea benthic foraminifera: tracers for Cenozoic changes in oceanic productivity? *Geology*, *24*, 355–358.
- Timmermann, A., Krebs, U., Justino, F., Goosse, H., Ivanochko, T. (2005), Mechanisms for millennial-scale global synchronization during the last glacial period, *Paleoceanography*, *20*, doi:10.1029/2004PA001090.
- Tomczak, M., Godfrey, J. (2002), *Regional Oceanography: An Introduction*, 2nd edition. Daya, Delhi.
- Turney, C.S.M., A.P. Kershaw, S.C. Clemens, N. Branch, P.T. Moss, and L.K. Fifield (2004), Millennial and orbital variations of El Niño/Southern Oscillation and high-latitude climate in the last glacial period, *Nature*, *428*, 306–310, doi: 10.1038/nature02386.
- van Aken, H. M, I. S. Brodjonegoro, and Indra Jaya (2009), The deep-water motion through the Lifamatola Passage and its contribution to the Indonesian Throughflow, *Deep-Sea Research I*, *56*, 1203–1216.
- van Andel, T.H., Heath, G.R., Moore, T.C. (1975), Cenozoic history and paleoceanography of the central equatorial Pacific Ocean, *Memoirs of the Geological Society of America*, *143*, 1–134.
- van der Kaars, S., X. Wang, P. Kershaw, F. Guichard, D.A. Setiabudi, D.A. (2000), A late Quaternary palaeoecological record from the Banda Sea, Indonesia: patterns of vegetation, climate and biomass burning in Indonesia and northern Australia, *Palaeogeog., Palaeoclim, Palaeoeco.*, *155*, 135– 153.
- Voelker, A.H.L., workshop participants (2002), Global distribution of centennial-scale records for marine isotope stage (MIS) 3: a database, *Quat. Sci. Rev.*, *21*, 1185–1214, doi: 10.1016/S0277-3791(01)00139-1.
- Voelker, A.H., Grootes, P.M., Nadeau, M.-J., Sarnthein, M. (2000), Radiocarbon levels in the Iceland Sea from 25–53 kyr and their link to the Earth's magnetic field intensity, *Radiocarbon*, *42* (3), 437–452.
- Wang, L., M. Sarnthein, H. Erlenkeuser, J. Grimalt, P. Grootes, S. Heilig, E. Ivanova, M. Kienast, C. Pelejero, and U. Pflaumann (1999), East Asian monsoon climate during the Late Pleistocene: high-resolution sediment records from the South China Sea, *Mar. Geo.*, *156*, 245–284.
- Wang, Y. J., H. Cheng, R. L. Edwards, Z. S. An, J. Y. Wu, C.-C. Shen, and J. A. Dorale (2001), A High-Resolution Absolute-Dated Late Pleistocene Monsoon Record from Hulu Cave, China, *Science*, *294* (5550), 2345-2348, doi: 10.1126/science.1064618.
- Wang, X., A. S. Auler, R. L. Edwards, H. Cheng, P. S. Cristalli, P. L. Smart, D. A. Richards, and C.-C. Shen (2004), Wet periods in northeastern Brazil over the past 210-kyr linked to distant climate anomalies, *Nature*, *432* (7018), 740-743, doi: 10.1038/nature03067.
- Watanabe, O., Jouzel, J., Johnsen, S., Parrenin, F., Shoji, H., Yoshida, N. (2003), Homogeneous climate variability across East Antarctica over the past three glacial cycles, *Nature*, *422*, 509–512, doi: 10.1038/nature01525.

- Wells, P.E., Wells, G.M. (1994), Large-scale reorganization of ocean currents offshore Western Australia during the Late Quaternary, *Mar. Micropal.*, *24*, 157–186.
- Wyrwoll, K.-H., Miller, G.H. (2001), Initiation of the Australian summer monsoon 14000 years ago, *Quat. Internat.*, *83–85*, 119–128, doi: 10.1016/S1040-6182(01)00034-9.
- Wyrwoll, K.-H., Valdes, P. (2003), Insolation forcing of the Australian monsoon as controls of Pleistocene mega-lake events, *Geophys. Res. Lett.*, *30*, doi:10.1029/2003GL018486.
- Xu, J., W. Kuhnt, A. Holbourn, N. Andersen, and G. Bartoli (2006), Changes in the vertical profile of the Indonesian Throughflow during Termination II: Evidence from the Timor Sea, *Paleoceanography*, *21*, PA4202, doi: 10.1029/2006PA001278.
- Xu, J., A. Holbourn, W. Kuhnt, Z. Jian, and H. Kawamura (2008), Changes in the Thermocline Structure of the Indonesian Outflow during Terminations I and II, *Earth Planet. Sci. Let.*, *273*, 152-162, doi: 10.1016/j.epsl.2008.06.029.
- Zuraida, R., A. Holbourn, D. Nürnberg, W. Kuhnt, A. Dürkop, and A. Erichsen (2009), Evidence for Indonesian Throughflow slowdown during Heinrich events 3–5, *Paleoceanography*, *24*, PA2205, doi: 10.1029/ 2008PA001653.

**Appendix B. MD01-2378 stable isotopes and Mg/Ca of
Globigerinoides ruber (white)**

Depth (cm)	Age (GICC05 kyr BP)	Mg/Ca (mmol/mol)	SST (°C) [Anand et al., 2003]	$\delta^{18}\text{O}$ (‰ PDB) [Dürkop, 2009]	$\delta^{13}\text{C}$ (‰ PDB) [Dürkop, 2009]	Surface $\delta^{18}\text{O}_{\text{sw}}$
448	23.9	4.0	26.1	-1.3	1.3	
450	24.0	3.9	25.8	-1.4	1.2	-0.1
451	24.1	3.7	25.4	-1.1	1.5	0.1
452	24.1	3.9	25.8	-1.2	1.3	0.1
453	24.2	4.0	26.2	-1.2	1.3	0.2
454	24.2	3.8	25.4	-1.2	1.4	0.0
455	24.3	3.8	25.5	-1.3	1.3	0.0
456	24.4	4.0	26.1	-1.2	1.3	0.2
457	24.4	3.9	26.0	-1.3	1.4	0.1
458	24.5	4.1	26.3	-1.2	1.5	0.2
459	24.5	3.9	25.9	-1.2	1.4	0.1
460	24.6	3.9	26.0	-1.1	1.4	0.3
461	24.7	3.7	25.3	-1.2	1.4	0.0
462	24.7	3.8	25.6	-1.3	1.2	0.0
463	24.8	4.1	26.5	-1.2	1.3	0.2
464	24.8	3.9	25.8	-1.2	1.3	0.1
465	24.9	3.8	25.7	-1.3	1.3	0.1
466	25.0	3.8	25.4	-1.3	1.4	-0.1
467	25.0	3.9	25.8	-1.3	1.3	0.1
468	25.1	3.7	25.2	-1.2	1.2	0.0
469	25.1	3.7	25.3	-1.2	1.2	0.0
470	25.2	3.9	25.7	-1.1	1.3	0.2
471	25.3	3.9	25.9	-1.2	1.5	0.2
472	25.3	3.9	25.7	-1.1	1.5	0.2
473	25.4	3.8	25.4	-1.3	1.4	0.0
474	25.4	3.8	25.6	-1.1	1.4	0.2
475	25.5	4.0	26.1	-1.3	1.4	0.1
476	25.6	3.9	25.9	-1.1	1.5	0.2
477	25.6	3.7	25.3	-1.1	1.5	0.1
478	25.7	4.1	26.3	-1.2	1.4	0.2
479	25.7	3.9	25.8	-1.2	1.4	0.1
480	25.8	3.8	25.7	-1.1	1.4	0.2

Depth (cm)	Age (GICC05 kyr BP)	Mg/Ca (mmol/mol)	SST (°C) [Anand et al., 2003]	$\delta^{18}\text{O}$ (‰ PDB) [Dürkop, 2009]	$\delta^{13}\text{C}$ (‰ PDB) [Dürkop, 2009]	Surface $\delta^{18}\text{O}_{\text{sw}}$
481	25.9	4.1	26.4	-1.1	1.4	0.3
482	25.9	3.8	25.5	-1.1	1.4	0.1
483	26.0	4.0	26.2	-1.0	1.5	0.4
484	26.1	3.8	25.5	-1.2	1.5	0.1
485	26.1	3.8	25.4	-1.1	1.3	0.2
486	26.2	3.7	25.1	-1.3	1.5	-0.1
487	26.2	3.7	25.2	-1.3	1.4	-0.1
488	26.3	3.5	24.8	-1.1	1.6	0.0
489	26.4	3.9	25.9	-1.2	1.5	0.1
490	26.4	4.0	26.1	-1.1	1.4	0.2
491	26.5	3.8	25.5	-1.2	1.4	0.0
492	26.6	3.8	25.7	-1.3	1.4	0.1
493	26.6	3.7	25.3	-1.3	1.4	0.0
494	26.7	3.8	25.5	-1.3	1.4	0.0
495	26.7	3.6	25.1	-1.2	1.6	-0.1
496	26.8	3.7	25.3	-1.1	1.4	0.1
497	26.9	3.5	24.5	-1.2	1.5	-0.2
498	26.9	3.5	24.8	-1.2	1.3	-0.1
499	27.0	3.5	24.7	-1.3	1.5	-0.2
500	27.1	3.4	24.5	-1.2	1.5	-0.2
501	27.1	4.0	26.3	-1.3	1.6	0.1
502	27.2	3.7	25.4	-1.3	1.5	-0.1
503	27.3	3.7	25.2	-1.2	1.3	0.0
504	27.3	4.0	26.2	-1.2	1.3	0.2
505	27.4	3.7	25.3	-1.4	1.3	-0.2
506	27.5	3.8	25.5	-1.2	1.4	0.0
507	27.5	3.7	25.3	-1.3	1.5	-0.1
508	27.6	3.6	25.1	-1.3	1.4	-0.1
509	27.6	4.1	26.3	-1.4	1.2	0.1
510	27.7	3.7	25.2	-1.3	1.3	0.0
511	27.8	3.7	25.2	-1.4	1.3	-0.1
512	27.8	3.8	25.6	-1.3	1.5	0.1
513	27.9	3.8	25.5	-1.3	1.3	0.0
514	28.0	3.9	25.8	-1.3	1.3	0.1
515	28.0	3.6	25.0	-1.4	1.5	-0.2
516	28.1	3.9	26.0	-1.5	1.2	-0.1
517	28.2	3.8	25.7	-1.4	1.4	-0.1

Depth (cm)	Age (GICC05 kyr BP)	Mg/Ca (mmol/mol)	SST (°C) [Anand et al., 2003]	$\delta^{18}\text{O}$ (‰ PDB) [Dürkop, 2009]	$\delta^{13}\text{C}$ (‰ PDB) [Dürkop, 2009]	Surface $\delta^{18}\text{O}_{\text{sw}}$
518	28.2	3.7	25.1	-1.2	1.2	0.0
519	28.3	3.8	25.5	-1.3	1.4	0.0
520	28.4	3.9	25.9	-1.4	1.4	0.1
521	28.4	4.1	26.3	-1.4	1.5	0.1
522	28.5	3.7	25.4	-1.5	1.4	-0.1
523	28.6	3.9	25.8	-1.5	1.3	0.0
524	28.6	4.0	26.1	-1.4	1.2	0.1
525	28.7	3.8	25.5	-1.3	1.4	0.1
526	28.7	3.9	25.8	-1.4	1.5	0.1
527	28.8	4.0	26.1	-1.4	1.5	0.2
528	28.9	4.0	26.1	-1.4	1.5	0.2
529	28.9	3.9	25.8	-1.3	1.7	0.2
530	29.0	3.9	25.8	-1.4	1.5	0.1
531	29.1	3.7	25.2	-1.4	1.3	0.0
532	29.1	4.0	26.3	-1.5	1.5	0.1
533	29.2	3.9	25.8	-1.5	1.4	-0.1
534	29.3	3.8	25.5	-1.3	1.5	0.1
535	29.3	4.0	26.2	-1.4	1.6	0.2
536	29.4	4.0	26.1	-1.3	1.4	0.2
537	29.5	4.2	26.8	-1.4	1.4	0.2
538	29.5	4.2	26.7	-1.3	1.5	0.4
539	29.6	4.0	26.3	-1.3	1.4	0.3
540	29.7	3.9	26.0	-1.3	1.6	0.2
541	29.7	4.2	26.7	-1.4	1.5	0.3
542	29.8	4.2	26.7	-1.4	1.8	0.3
543	29.9	4.0	26.0	-1.4	1.6	0.2
544	29.9	4.0	26.2	-1.4	1.3	0.2
545	30.0	3.7	25.4	-1.3	1.5	0.1
546	30.1	4.0	26.3	-1.3	1.5	0.3
547	30.2	4.0	26.0	-1.5	1.5	0.1
548	30.2	4.0	26.0	-1.5	1.5	0.1
549	30.3	3.6	24.9	-1.3	1.4	0.0
550	30.4	3.9	25.8	-1.3	1.4	0.1
551	30.4	3.6	25.0	-1.4	1.5	0.0
552	30.5	3.8	25.6	-1.5	1.5	0.0
553	30.6	3.7	25.4	-1.4	1.5	0.0
554	30.7	3.8	25.7	-1.4	1.5	0.0

Depth (cm)	Age (GICC05 kyr BP)	Mg/Ca (mmol/mol)	SST (°C) [Anand et al., 2003]	$\delta^{18}\text{O}$ (‰ PDB) [Dürkop, 2009]	$\delta^{13}\text{C}$ (‰ PDB) [Dürkop, 2009]	Surface $\delta^{18}\text{O}_{\text{sw}}$
555	30.7	3.8	25.6	-1.3	1.6	0.1
556	30.8	3.8	25.6	-1.4	1.5	0.0
557	30.9	4.0	26.1	-1.4	1.5	0.1
558	31.0	4.0	26.1	-1.5	1.6	0.1
559	31.0	3.6	24.9	-1.3	1.5	0.0
560	31.1	3.9	25.9	-1.4	1.7	0.1
561	31.2	4.0	26.2	-1.3	1.7	0.3
562	31.3	3.8	25.7	-1.5	1.7	0.0
563	31.3	3.7	25.2	-1.5	1.5	-0.1
564	31.4	4.1	26.4	-1.3	1.5	0.3
565	31.5	3.7	25.3	-1.5	1.4	-0.1
566	31.6	4.0	26.1	-1.4	1.7	0.2
567	31.7	3.9	25.9	-1.4	1.3	0.0
568	31.8	3.9	26.0	-1.3	1.5	0.2
569	31.8	3.9	26.0	-1.3	1.7	0.1
570	31.9	3.9	25.9	-1.3	1.6	0.1
571	32.0	3.8	25.7	-1.4	1.5	0.0
572	32.1	3.9	25.8	-1.4	1.4	0.1
573	32.2	4.0	26.2	-1.5	1.4	0.0
574	32.3	3.6	25.1	-1.5	1.7	-0.2
575	32.4	4.1	26.4	-1.5	1.6	0.1
576	32.4	3.7	25.4	-1.5	1.6	-0.2
577	32.5	3.9	25.8	-1.4	1.5	0.0
578	32.6	3.8	25.5	-1.4	1.5	0.0
579	32.7	4.0	26.1	-1.4	1.5	0.2
580	32.8	4.0	26.2	-1.5	1.6	0.0
581	32.9	3.9	25.8	-1.5	1.5	0.0
582	33.0	4.3	26.9	-1.3	1.5	0.4
583	33.1	3.7	25.2	-1.4	1.6	0.0
584	33.1	3.6	25.1	-1.5	1.5	-0.1
585	33.2	4.1	26.4	-1.4	1.6	0.3
586	33.3	3.5	24.6	-1.5	1.4	-0.2
587	33.4	4.0	26.0	-1.3	1.7	0.3
588	33.5	3.9	25.7	-1.4	1.5	0.1
589	33.6	4.0	26.0	-1.4	1.5	0.1
590	33.7	4.1	26.5	-1.5	1.5	0.2
591	33.8	3.8	25.6	-1.4	1.5	0.0

Depth (cm)	Age (GICC05 kyr BP)	Mg/Ca (mmol/mol)	SST (°C) [Anand et al., 2003]	$\delta^{18}\text{O}$ (‰ PDB) [Dürkop, 2009]	$\delta^{13}\text{C}$ (‰ PDB) [Dürkop, 2009]	Surface $\delta^{18}\text{O}_{\text{sw}}$
592	33.9	3.8	25.6	-1.5	1.4	0.0
593	34.0	3.9	25.9	-1.4	1.7	0.2
594	34.0	3.9	25.9	-1.6	1.5	0.0
595	34.1	4.0	26.1	-1.4	1.4	0.2
596	34.2	3.8	25.6	-1.5	1.5	0.1
597	34.3	4.0	26.3	-1.4	1.4	0.2
598	34.4	3.7	25.3	-1.4	1.6	0.1
599	34.5	4.0	26.0	-1.5	1.6	0.1
600	34.6	4.0	26.2	-1.4	1.4	0.2
601	34.7	3.7	25.4	-1.5	1.7	0.0
602	34.8	3.8	25.7	-1.5	1.5	0.0
603	34.8	4.0	26.1	-1.4	1.6	0.3
604	34.9	4.0	26.1	-1.5	1.4	0.2
605	35.0	4.0	26.2	-1.5	1.5	0.2
606	35.1	3.9	25.7	-1.5	1.5	0.1
607	35.2	3.9	25.9	-1.5	1.5	0.1
608	35.3	4.2	26.6	-1.6	1.5	0.2
609	35.4	4.1	26.5	-1.7	1.6	0.1
610	35.5	4.2	26.6	-1.5	1.6	0.3
611	35.6	4.2	26.8	-1.6	1.6	0.3
612	35.6	4.0	26.3	-1.5	1.5	0.2
613	35.7	3.9	26.0	-1.5	1.5	0.2
614	35.8	4.0	26.3	-1.5	1.4	0.3
615	35.9	4.0	26.2	-1.4	1.6	0.3
616	36.0	4.0	26.1	-1.5	1.5	0.3
617	36.1	3.8	25.5	-1.5	1.6	0.1
618	36.2	3.8	25.4	-1.5	1.4	0.1
619	36.2	4.0	26.1	-1.5	1.5	0.3
620	36.3	3.8	25.5	-1.3	1.4	0.3
621	36.4	3.9	26.0	-1.5	1.4	0.3
622	36.5	3.5	24.8	-1.5	1.6	0.0
623	36.6	4.0	26.2	-1.5	1.5	0.3
624	36.7	3.7	25.2	-1.6	1.4	-0.1
625	36.8	3.7	25.4	-1.6	1.5	0.0
626	36.8	3.8	25.4	-1.6	1.5	-0.1
627	36.9	3.7	25.4	-1.5	1.4	0.1
628	37.0	4.0	26.2	-1.6	1.5	0.1

Depth (cm)	Age (GICC05 kyr BP)	Mg/Ca (mmol/mol)	SST (°C) [Anand et al., 2003]	$\delta^{18}\text{O}$ (‰ PDB) [Dürkop, 2009]	$\delta^{13}\text{C}$ (‰ PDB) [Dürkop, 2009]	Surface $\delta^{18}\text{O}_{\text{sw}}$
629	37.1	3.7	25.3	-1.5	1.6	0.1
630	37.2	3.7	25.4	-1.5	1.5	0.0
631	37.3	4.3	27.0	-1.7	1.4	0.2
632	37.3	4.1	26.5	-1.6	1.5	0.2
633	37.4	4.1	26.4	-1.7	1.5	0.1
634	37.5	4.1	26.4	-1.5	1.7	0.3
635	37.6	3.8	25.5	-1.6	1.4	-0.1
636	37.7	4.2	26.8	-1.6	1.5	0.3
637	37.8	3.9	25.9	-1.7	1.4	0.0
638	37.8	4.0	26.1	-1.6	1.5	0.1
639	37.9	3.7	25.4	-1.7	1.4	-0.1
640	38.0	4.0	26.1	-1.8	1.4	-0.1
641	38.1	3.9	25.8	-1.6	1.3	0.1
642	38.2	4.0	26.0	-1.6	1.5	0.2
643	38.2	3.9	26.0	-1.6	1.4	0.2
644	38.3	4.0	26.2	-1.5	1.6	0.4
645	38.4	4.0	26.1	-1.7	1.5	0.1
646	38.5	4.0	26.1	-1.6	1.2	0.3
647	38.5	3.8	25.6	-1.4	1.4	0.3
648	38.6	3.7	25.3	-1.4	1.3	0.2
649	38.7	3.8	25.6	-1.4	1.5	0.3
650	38.8	3.9	25.8	-1.3	1.5	0.5
651	38.8	4.0	26.0	-1.4	1.3	0.3
652	38.9	3.6	25.1	-1.5	1.5	0.1
653	39.0	3.8	25.7	-1.3	1.4	0.4
654	39.1	3.8	25.7	-1.3	1.5	0.4
655	39.2	4.1	26.5	-1.3	1.5	0.6
656	39.2	3.9	25.9	-1.4	1.5	0.3
657	39.3	3.7	25.3	-1.2	1.5	0.3
658	39.4	3.8	25.5	-1.4	1.6	0.2
659	39.5	3.7	25.2	-1.6	1.6	-0.1
660	39.5	3.9	25.8	-1.4	1.6	0.2
661	39.6	3.9	25.9	-1.5	1.4	0.1
662	39.7	3.6	25.1	-1.5	1.5	0.0
663	39.8	3.7	25.1	-1.4	1.6	0.0
664	39.9	3.8	25.5	-1.4	1.5	0.1
665	39.9	3.7	25.1	-1.4	1.7	0.0

Depth (cm)	Age (GICC05 kyr BP)	Mg/Ca (mmol/mol)	SST (°C) [Anand et al., 2003]	$\delta^{18}\text{O}$ (‰ PDB) [Dürkop, 2009]	$\delta^{13}\text{C}$ (‰ PDB) [Dürkop, 2009]	Surface $\delta^{18}\text{O}_{\text{sw}}$
666	40.0	3.5	24.7	-1.4	1.6	-0.1
667	40.1	3.7	25.2	-1.4	1.6	0.1
668	40.2	4.0	26.3	-1.5	1.6	0.2
669	40.3	3.5	24.5	-1.6	1.5	-0.2
670	40.4	3.6	25.0	-1.5	1.5	-0.1
671	40.5	3.7	25.3	-1.4	1.6	0.1
672	40.6	3.6	25.0	-1.4	1.5	0.0
673	40.7	3.6	24.9	-1.5	1.5	-0.1
674	40.8	3.7	25.4	-1.5	1.6	0.0
675	40.9	3.5	24.7	-1.4	1.6	-0.1
676	40.9	3.7	25.2	-1.5	1.5	0.0
677	41.0	3.7	25.2	-1.4	1.5	0.1
678	41.1	4.0	26.2	-1.5	1.5	0.2
679	41.2	3.5	24.5	-1.4	1.3	0.0
680	41.3	3.6	24.9	-1.5	1.4	0.0
681	41.4	4.0	26.2	-1.6	1.5	0.2
682	41.5	3.7	25.3	-1.5	1.4	0.0
683	41.6	3.5	24.7	-1.5	1.4	-0.1
684	41.7	3.6	24.9	-1.3	1.5	0.1
685	41.8	3.5	24.8	-1.3	1.6	0.1
686	41.9	3.5	24.5	-1.5	1.6	-0.1
687	42.0	3.4	24.3	-1.3	1.6	0.0
688	42.1	3.7	25.2	-1.4	1.5	0.1
689	42.2	3.5	24.6	-1.4	1.4	-0.1
690	42.3	3.5	24.7	-1.4	1.6	-0.1
691	42.4	3.9	26.0	-1.5	1.4	0.2
692	42.5	3.7	25.3	-1.6	1.5	0.0
693	42.6	3.6	24.9	-1.5	1.5	0.0
695	42.8	3.4	24.4	-1.5	1.3	-0.1
696	42.9	3.8	25.7	-1.5	1.7	0.1
697	42.9	3.8	25.7	-1.5	1.6	0.1
698	43.0	3.8	25.6	-1.5	1.6	0.1
699	43.1	3.8	25.6	-1.5	1.6	0.1
700	43.2	3.6	24.9	-1.6	1.5	-0.1
701	43.3	3.8	25.6	-1.4	1.5	0.3
702	43.4	3.9	25.8	-1.3	1.4	0.4
703	43.5	3.6	24.8	-1.5	1.5	0.0

Depth (cm)	Age (GICC05 kyr BP)	Mg/Ca (mmol/mol)	SST (°C) [Anand et al., 2003]	$\delta^{18}\text{O}$ (‰ PDB) [Dürkop, 2009]	$\delta^{13}\text{C}$ (‰ PDB) [Dürkop, 2009]	Surface $\delta^{18}\text{O}_{\text{sw}}$
704	43.6	3.7	25.3	-1.5	1.5	0.1
705	43.7	3.7	25.3	-1.4	1.4	0.2
706	43.8	3.7	25.3	-1.5	1.6	0.1
707	43.9	3.6	25.1	-1.4	1.5	0.1
708	44.0	3.5	24.6	-1.5	1.5	-0.1
709	44.1	3.7	25.2	-1.5	1.6	0.0
710	44.2	3.6	25.0	-1.4	1.5	0.1
711	44.3	3.8	25.5	-1.6	1.4	0.0
712	44.4	3.8	25.6	-1.4	1.5	0.2
713	44.5	3.8	25.5	-1.5	1.6	0.1
714	44.6	3.6	24.9	-1.4	1.4	0.0
715	44.7	3.6	24.9	-1.6	1.6	-0.1
716	44.8	3.6	24.9	-1.6	1.4	-0.1
717	44.9	3.8	25.6	-1.7	1.6	0.0
718	45.0	3.6	24.9	-1.5	1.5	0.0
719	45.0	3.6	24.9	-1.5	1.5	-0.1
720	45.1	3.6	25.0	-1.6	1.3	-0.1
721	45.2	3.5	24.7	-1.6	1.4	-0.2
722	45.3	3.6	25.1	-1.6	1.4	-0.1
723	45.4	3.4	24.4	-1.6	1.4	-0.1
724	45.5	3.9	25.8	-1.6	1.4	0.1
725	45.6	3.8	25.4	-1.6	1.5	0.1
726	45.7	3.6	24.8	-1.7	1.4	-0.2
727	45.8	3.9	25.8	-1.6	1.4	0.1
728	45.9	3.8	25.5	-1.5	1.3	0.1
729	46.0	3.8	25.7	-1.6	1.3	0.1
730	46.1			-1.6	1.4	
731	46.2	3.8	25.5	-1.6	1.2	0.1
732	46.3	4.2	26.7	-1.6	1.4	0.3
733	46.4	4.0	26.2	-1.6	1.6	0.2
734	46.5	3.9	25.8	-1.5	1.3	0.3
735	46.6	4.0	26.2	-1.5	1.5	0.4
736	46.7	4.1	26.5	-1.5	1.5	0.5
737	46.8	3.9	25.8	-1.5	1.6	0.3
738	46.9	3.8	25.6	-1.4	1.5	0.4
739	47.0	3.8	25.7	-1.6	1.3	0.2
740	47.1	4.0	26.2	-1.5	1.6	0.5

Depth (cm)	Age (GICC05 kyr BP)	Mg/Ca (mmol/mol)	SST (°C) [Anand et al., 2003]	$\delta^{18}\text{O}$ (‰ PDB) [Dürkop, 2009]	$\delta^{13}\text{C}$ (‰ PDB) [Dürkop, 2009]	Surface $\delta^{18}\text{O}_{\text{sw}}$
741	47.2	3.8	25.7			
742	47.3	3.9	25.8	-1.6	1.5	0.2
743	47.3	4.1	26.3	-1.6	1.7	0.4
744	47.4	3.9	25.8	-1.5	1.2	0.3
745	47.5	3.8	25.6	-1.5	1.6	0.3
746	47.6	3.9	25.9	-1.5	1.5	0.3
747	47.7	3.7	25.3	-1.5	1.4	0.1
748	47.8	4.0	26.1	-1.4	1.5	0.4
749	47.9	3.9	25.9	-1.5	1.5	0.2
750	48.0	4.0	26.0	-1.5	1.3	0.2
751	48.1	3.8	25.6	-1.4	1.4	0.3
752	48.2	3.9	25.9	-1.5	1.4	0.2
753	48.3	3.7	25.3	-1.5	1.5	0.1
754	48.4	3.9	26.0	-1.5	1.5	0.1
755	48.5	3.9	25.8	-1.6	1.5	0.0
756	48.6	3.6	24.9	-1.7	1.5	-0.2
757	48.7	3.7	25.2	-1.5	1.4	0.1
758	48.8	3.8	25.7	-1.5	1.5	0.1
759	48.9	3.6	24.9	-1.4	1.3	0.1
760	49.0	3.9	25.7	-1.5	1.6	0.2
761	49.1	3.8	25.6	-1.5	1.3	0.2
762	49.2	3.7	25.2	-1.4	1.5	0.2
763	49.3	3.7	25.2	-1.5	1.5	0.0
764	49.4	3.8	25.5	-1.4	1.4	0.2
765	49.5	3.9	25.9	-1.6	1.3	0.1
766	49.6	3.8	25.5	-1.4	1.6	0.2
767	49.7	3.6	25.1	-1.5	1.5	0.1
768	49.7	3.6	25.1	-1.6	1.4	-0.1
769	49.8	3.8	25.6	-1.6	1.5	0.0
770	49.9	3.9	25.9	-1.6	1.5	0.0
771	50.0	3.8	25.4	-1.4	1.2	0.2
772	50.1	3.7	25.4	-1.5	1.5	0.1
773	50.2	3.9	25.8	-1.5	1.5	0.1
774	50.3	3.7	25.4	-1.7	1.3	-0.1
775	50.4	3.9	26.0	-1.5	1.3	0.2
776	50.5	3.9	25.8	-1.6	1.3	0.1
777	50.6	3.6	25.1	-1.6	1.4	-0.1

Depth (cm)	Age (GICC05 kyr BP)	Mg/Ca (mmol/mol)	SST (°C) [Anand et al., 2003]	$\delta^{18}\text{O}$ (‰ PDB) [Dürkop, 2009]	$\delta^{13}\text{C}$ (‰ PDB) [Dürkop, 2009]	Surface $\delta^{18}\text{O}_{\text{sw}}$
778	50.7	3.8	25.6	-1.5	1.3	0.1
779	50.8	3.7	25.4	-1.6	1.4	-0.1
780	50.9	3.6	25.0	-1.5	1.4	0.0
781	51.0	3.7	25.2	-1.5	1.2	-0.1
782	51.1	4.0	26.2	-1.6	1.4	0.1
783	51.2	3.7	25.2	-1.5	1.4	0.0
784	51.3	3.9	25.7	-1.5	1.2	0.1
785	51.4	4.0	26.0	-1.5	1.5	0.2
786	51.5	3.6	24.9	-1.5	1.5	0.0
787	51.6	3.7	25.3	-1.7	1.3	-0.1
788	51.7	3.8	25.7	-1.6	1.6	0.0
789	51.8	3.8	25.6	-1.7	1.3	-0.1
790	51.9	3.5	24.7	-1.5	1.5	0.0
791	52.0	3.9	25.8	-1.7	1.3	0.0
792	52.1	3.8	25.6	-1.6	1.3	0.0
793	52.2	4.1	26.4	-1.6	1.4	0.2
794	52.3	4.2	26.8	-1.5	1.4	0.3
795	52.4	3.6	25.1	-1.7	1.5	-0.2
796	52.5	3.9	26.0	-1.8	1.6	0.0
797	52.5	3.6	25.0	-1.8	1.5	-0.3
798	52.6	3.8	25.6	-1.8	1.4	-0.1
799	52.7	3.8	25.5	-1.8	1.3	-0.1
800	52.8	3.9	25.7	-1.8	1.4	0.0
801	52.9	3.9	26.0	-1.7	1.3	0.1
802	53.0	4.0	26.1	-1.7	1.4	0.1
803	53.1	3.7	25.3	-1.8	1.3	-0.2
804	53.2	3.8	25.7	-1.8	1.2	-0.1
805	53.3	3.5	24.7	-1.7	1.2	-0.2
806	53.4	3.8	25.6	-1.9	1.4	-0.1
807	53.5	3.7	25.3	-1.7	1.6	0.0
808	53.6	3.7	25.2	-1.8	1.4	-0.1
809	53.7	3.8	25.7	-1.9	1.3	-0.2
810	53.8	3.7	25.3	-1.8	1.5	-0.2
811	53.9	4.0	26.2	-1.8	1.2	0.1
812	54.0	3.7	25.3	-1.8	1.2	-0.1
813	54.1	4.0	26.3	-1.8	1.3	0.2
814	54.2	4.2	26.6	-1.9	1.3	0.1

Depth (cm)	Age (GICC05 kyr BP)	Mg/Ca (mmol/mol)	SST (°C) [Anand et al., 2003]	$\delta^{18}\text{O}$ (‰ PDB) [Dürkop, 2009]	$\delta^{13}\text{C}$ (‰ PDB) [Dürkop, 2009]	Surface $\delta^{18}\text{O}_{\text{sw}}$
815	54.3	3.8	25.5	-1.7	1.4	0.1
816	54.4	4.0	26.2	-1.6	1.2	0.3
817	54.5	3.7	25.3	-1.6	1.2	0.2
818	54.6	3.8	25.5	-1.8	1.4	0.0
819	54.7	3.9	25.7	-1.6	1.3	0.2
820	54.8	3.7	25.3	-1.7	1.4	0.1
821	54.9	3.9	26.0	-1.7	1.2	0.2
822	55.0	3.9	25.9	-1.7	1.3	0.2
823	55.1	3.6	25.0	-1.7	1.4	-0.1
824	55.2	3.9	25.9	-1.7	1.5	0.1
825	55.3	3.7	25.4	-1.6	1.3	0.1
826	55.4	3.8	25.6	-1.6	1.3	0.1
827	55.5	4.0	26.1	-1.6	1.4	0.2
828	55.6	3.6	25.1	-1.7	1.4	-0.1
829	55.6	3.6	24.9	-1.7	1.4	-0.1
830	55.7	3.5	24.8	-1.6	1.5	0.0
831	55.8	3.7	25.4	-1.6	1.2	0.1
832	55.9	4.0	26.3	-1.6	1.3	0.2
833	56.0	3.4	24.3	-1.8	1.4	-0.4
834	56.1	3.4	24.5	-1.7	1.4	-0.3
835	56.2	3.6	24.8	-1.5	1.3	0.0
836	56.3	3.9	25.9	-1.6	1.3	0.1
837	56.4	3.9	25.8	-1.7	1.3	-0.1
838	56.5	4.0	26.1	-1.8	1.4	0.0
839	56.6	3.7	25.4	-1.8	1.2	-0.1
840	56.7	3.5	24.7	-1.7	1.3	-0.3
841	56.8	4.1	26.4	-1.6	1.3	0.2
842	56.9	3.7	25.4	-1.8	1.2	-0.2
843	57.0	3.9	25.9	-1.7	1.4	0.0
844	57.1	3.9	25.7	-1.5	1.3	0.2
845	57.2	3.8	25.6	-1.7	1.3	-0.1
846	57.3	3.8	25.7	-1.7	1.3	-0.1
847	57.4	3.8	25.5	-1.7	1.5	-0.1
848	57.5	4.2	26.6	-1.8	1.4	0.1
849	57.6	3.8	25.6	-1.7	1.3	0.0
850	57.7	4.1	26.5	-1.8	1.3	0.1
851	57.8	4.0	26.0	-1.7	1.3	0.2

Depth (cm)	Age (GICC05 kyr BP)	Mg/Ca (mmol/mol)	SST (°C) [Anand et al., 2003]	$\delta^{18}\text{O}$ (‰ PDB) [Dürkop, 2009]	$\delta^{13}\text{C}$ (‰ PDB) [Dürkop, 2009]	Surface $\delta^{18}\text{O}_{\text{sw}}$
852	57.9	4.0	26.3	-1.7	1.2	0.1
853	58.0	3.7	25.3	-1.7	1.1	0.0
854	58.1	3.8	25.7	-1.8	1.2	0.0
855	58.2	3.8	25.7	-1.8	1.1	0.0
856	58.3	4.0	26.0	-1.6	1.4	0.2
857	58.4	3.9	26.0	-1.7	1.3	0.1
858	58.4	3.9	26.0	-1.8	1.1	0.1
859	58.5	3.9	25.8	-1.6	1.1	0.2
860	58.6	4.1	26.3	-1.9	1.2	0.1
861	58.7	4.3	26.9	-1.7	1.2	0.4
862	58.8	3.6	24.9	-1.6	1.2	0.1
863	58.9	3.9	26.0	-1.7	1.2	0.2
864	59.0	3.9	25.9	-1.6	1.2	0.3
865	59.1	3.9	26.0	-1.7	1.2	0.2
866	59.2	3.8	25.7	-1.6	1.1	0.2
867	59.3	3.8	25.5	-1.5	1.1	0.3
868	59.4	3.9	26.0	-1.6	1.1	0.3
869	59.5	3.8	25.7	-1.7	1.1	0.2
870	59.6	3.8	25.7	-1.7	1.2	0.2
871	59.7	4.1	26.4	-1.6	1.1	0.4
872	59.8	4.1	26.4	-1.5	1.1	0.5
873	59.9	3.7	25.4	-1.6	1.0	0.2
874	60.0	3.9	26.0	-1.7	1.0	0.2
875	60.1	4.1	26.5	-1.6	1.2	0.4
876	60.2	3.8	25.7	-1.5	1.3	0.3
877	60.3	4.1	26.4	-1.7	1.1	0.3
878	60.4	4.1	26.5	-1.6	1.2	0.3
879	60.5	3.9	25.9	-1.5	1.2	0.3
880	60.6	4.1	26.4	-1.6	1.2	0.3
881	60.7	3.9	25.9	-1.4	1.2	0.3
882	60.8	3.9	25.8	-1.6	1.2	0.2
883	60.9	4.0	26.1	-1.6	1.3	0.2
884	61.0	3.9	25.8	-1.6	1.3	0.1
885	61.1	3.7	25.2	-1.6	1.2	0.0
886	61.2	3.7	25.3	-1.5	1.3	0.1
887	61.2	3.6	25.1	-1.5	1.1	0.0
888	61.3	3.9	25.9	-1.5	1.4	0.1

Depth (cm)	Age (GICC05 kyr BP)	Mg/Ca (mmol/mol)	SST (°C) [Anand et al., 2003]	$\delta^{18}\text{O}$ (‰ PDB) [Dürkop, 2008]	$\delta^{13}\text{C}$ (‰ PDB) [Dürkop, 2008]	Surface $\delta^{18}\text{O}_{\text{sw}}$
889	61.4	3.6	25.1	-1.5	1.3	0.0
890	61.5	3.7	25.4	-1.5	1.2	0.0
891	61.6	3.8	25.6	-1.5	1.2	0.1
892	61.7	3.8	25.5	-1.5	1.2	0.1
893	61.8	3.7	25.3	-1.6	1.2	-0.2
894	61.9	3.7	25.2	-1.5	1.1	
895	62.0	3.6	25.1	-1.5	1.3	

**Appendix C. MD01-2378 stable isotopes and Mg/Ca of
*Pulleniatina obliquiloculata***

Depth (cm)	Age (GICC05 kyr BP)	Mg/Ca (mmol/mol)	T °C (Anand et al., 2003)	$\delta^{18}\text{O}$ (‰ PDB)	$\delta^{13}\text{C}$ (‰ PDB)	Thermocline $\delta^{18}\text{O}_{\text{sw}}$
448	23.9	2.1	20.8	-0.1	0.9	
450	24.0	2.1	20.4	-0.2	0.9	0.2
451	24.1	2.3	21.4	0.0	0.9	0.6
452	24.1	2.3	21.5	0.2	1.0	0.8
453	24.2	2.1	20.4	-0.1	1.0	0.3
454	24.2	2.3	21.5	0.0	0.9	0.6
455	24.3	2.3	21.5	0.1	1.0	0.8
456	24.4	2.2	21.0	0.1	0.9	0.6
457	24.4	2.3	21.6	0.1	1.0	0.8
458	24.5	2.0	19.9	-0.1	0.9	0.3
459	24.5	2.1	20.7	0.0	1.0	0.5
460	24.6	2.1	20.5	0.1	1.2	0.5
461	24.7	2.4	22.1	-0.1	0.8	0.7
462	24.7	2.1	20.6	0.0	1.0	0.5
463	24.8	2.2	21.1	0.0	0.9	0.5
464	24.8	2.4	22.0	0.1	0.9	0.8
465	24.9	2.0	20.1	-0.1	1.1	0.3
466	25.0	2.1	20.5	0.0	1.0	0.4
467	25.0	2.0	20.1	0.0	1.0	0.3
468	25.1	2.2	21.1	0.1	0.9	0.6
469	25.1	2.3	21.9	-0.1	1.1	0.6
470	25.2	2.3	21.7	0.0	0.9	0.6
471	25.3	2.5	22.7	0.0	1.0	0.9
472	25.3	2.3	21.5	0.0	1.1	0.7
473	25.4	2.1	20.5	0.0	1.0	0.4
474	25.4	2.1	20.8	0.0	1.0	0.5
475	25.5	2.0	20.2	0.0	1.0	0.4
476	25.6	2.1	20.5	0.0	1.1	0.4
477	25.6	2.0	20.3	0.0	1.0	0.4
478	25.7	2.3	21.5	0.0	0.9	0.6

Depth (cm)	Age (GICC05 kyr BP)	Mg/Ca (mmol/mol)	T °C (Anand et al., 2003)	$\delta^{18}\text{O}$ (‰ PDB)	$\delta^{13}\text{C}$ (‰ PDB)	Thermocline $\delta^{18}\text{O}_{\text{sw}}$
479	25.7	2.1	20.6	-0.4	1.0	0.1
480	25.8	2.1	20.5	0.0	1.0	0.5
481	25.9	2.2	20.9	-0.1	1.0	0.4
482	25.9	2.3	21.4	0.0	1.0	0.6
483	26.0	2.1	20.9	0.0	0.9	0.5
484	26.1	2.1	20.7	0.1	1.0	0.6
485	26.1	2.1	20.8	-0.1	1.0	0.4
486	26.2	2.2	21.1	0.0	1.0	0.5
487	26.2	2.2	21.2	0.2	0.9	0.7
488	26.3	2.2	21.1	0.2	1.1	0.7
489	26.4	2.3	21.4	-0.3	0.8	0.3
490	26.4	2.1	20.7	0.1	1.0	0.5
491	26.5	2.2	21.0	0.0	0.9	0.5
492	26.6	2.2	21.2	0.0	0.9	0.6
493	26.6	2.2	21.0	-0.1	1.0	0.5
494	26.7	2.1	20.5	0.0	1.0	0.5
495	26.7	2.0	20.3	-0.1	1.0	0.3
496	26.8	2.1	20.7	0.0	1.1	0.4
497	26.9	2.1	20.4	-0.3	1.0	0.1
498	26.9	2.2	21.0	0.0	1.0	0.5
499	27.0	2.3	21.4	-0.1	1.1	0.5
500	27.1	2.2	21.0	0.1	1.1	0.6
501	27.1	2.2	21.3	0.0	1.0	0.5
502	27.2	2.1	20.6	0.0	1.0	0.4
503	27.3	2.0	20.3	0.1	1.0	0.5
504	27.3	2.1	20.7	-0.1	0.9	0.4
505	27.4	2.3	21.7	0.0	1.0	0.6
506	27.5	2.1	20.5			
507	27.5	2.1	20.9	-0.1	1.0	0.4
508	27.6	2.5	22.4	-0.2	1.0	0.7
509	27.6	2.2	21.1	-0.1	1.2	0.5
510	27.7	2.2	21.3	-0.2	1.0	0.5
511	27.8	2.4	22.0	-0.1	0.8	0.7
512	27.8	2.1	20.6	-0.2	0.8	0.3
513	27.9	2.3	21.6	-0.2	1.1	0.5
514	28.0	2.0	20.3	-0.1	0.8	0.4
515	28.0	2.3	21.4	-0.2	0.9	0.5

Depth (cm)	Age (GICC05 kyr BP)	Mg/Ca (mmol/mol)	T °C (Anand et al., 2003)	$\delta^{18}\text{O}$ (‰ PDB)	$\delta^{13}\text{C}$ (‰ PDB)	Thermocline $\delta^{18}\text{O}_{\text{sw}}$
516	28.1	2.1	20.9	-0.1	0.8	0.4
517	28.2	2.5	22.6	-0.2	1.0	0.7
518	28.2	2.2	20.9	-0.1	1.0	0.5
519	28.3	2.2	21.4	-0.2	0.9	0.5
520	28.4	2.2	21.0	-0.3	0.9	0.4
521	28.4	2.4	21.9	-0.1	1.1	0.8
522	28.5	2.3	21.5	-0.3	1.0	0.5
523	28.6	2.5	22.5	-0.2	1.0	0.8
524	28.6	2.4	22.1	-0.1	1.1	0.8
525	28.7	2.3	21.8	-0.1	1.1	0.7
526	28.7	2.2	21.1	-0.1	1.0	0.6
527	28.8	2.2	20.9	-0.1	1.0	0.6
528	28.9	2.4	22.0	-0.3	1.1	0.7
529	28.9	2.2	21.1	0.0	0.9	0.7
530	29.0	2.0	20.2	0.0	1.0	0.5
531	29.1	2.2	21.2	-0.2	1.0	0.5
532	29.1	2.3	21.5	0.1	0.8	0.9
533	29.2	2.2	21.2	-0.1	0.9	0.6
534	29.3	2.4	22.0	-0.2	1.0	0.7
535	29.3	2.6	23.2	-0.2	1.1	0.9
536	29.4	2.7	23.6	-0.2	1.0	1.1
537	29.5	2.6	23.0	-0.2	1.0	0.9
538	29.5	2.5	22.5	-0.2	1.0	0.8
539	29.6	2.3	21.7	-0.1	1.0	0.8
540	29.7	2.3	21.5	0.0	1.0	0.8
541	29.7	2.1	20.8	0.0	1.0	0.7
542	29.8	2.4	22.0	0.0	1.0	0.9
543	29.9	2.4	22.0	0.0	1.0	0.9
544	29.9	2.3	21.9	0.0	1.0	0.9
545	30.0	2.2	21.1	0.1	1.1	0.8
546	30.1	2.2	21.3	0.0	1.1	0.8
547	30.2	2.1	20.5	0.0	1.1	0.6
548	30.2	2.0	20.0	0.1	1.0	0.5
549	30.3	1.8	19.2	-0.2	1.0	0.1
550	30.4	2.2	21.3	-0.3	0.8	0.4
551	30.4	2.1	20.5	0.0	1.0	0.6
552	30.5	2.1	20.7	-0.3	0.9	0.4

Depth (cm)	Age (GICC05 kyr BP)	Mg/Ca (mmol/mol)	T °C (Anand et al., 2003)	$\delta^{18}\text{O}$ (‰ PDB)	$\delta^{13}\text{C}$ (‰ PDB)	Thermocline $\delta^{18}\text{O}_{\text{sw}}$
553	30.6	2.3	21.7	0.0	1.0	0.9
554	30.7			-0.2	0.9	
555	30.7	2.1	20.8	-0.1	1.2	0.6
556	30.8	2.0	20.2	-0.1	1.1	0.3
557	30.9	2.1	20.8	0.1	1.1	0.7
558	31.0	2.0	20.3	-0.1	0.9	0.4
559	31.0	2.2	21.2	-0.1	0.9	0.6
560	31.1	2.2	20.9	-0.2	1.2	0.5
561	31.2	2.1	20.7	-0.1	1.1	0.6
562	31.3	2.2	21.3	-0.1	1.2	0.7
563	31.3	2.1	20.7	-0.3	1.1	0.4
564	31.4	2.1	20.7	0.0	1.0	0.6
565	31.5	2.3	21.6	-0.2	1.1	0.6
566	31.6	2.1	20.7	-0.2	1.0	0.3
567	31.7	2.1	20.6	-0.2	1.1	0.4
568	31.8	2.3	21.7	-0.1	1.1	0.7
569	31.8	2.1	20.7	0.0	1.0	0.6
570	31.9	2.1	20.4	-0.1	1.2	0.4
571	32.0	2.2	20.9	-0.1	1.0	0.5
572	32.1	2.3	21.7	-0.1	1.1	0.7
573	32.2	2.0	20.2	-0.2	1.0	0.3
574	32.3	2.2	21.2	-0.2	1.0	0.5
575	32.4	2.2	21.0	-0.3	1.0	0.4
576	32.4	2.5	22.3	-0.3	0.9	0.6
577	32.5	2.2	21.0	-0.3	1.0	0.4
578	32.6	2.2	21.1	-0.2	1.1	0.5
579	32.7	2.3	21.8	-0.3	1.0	0.6
580	32.8	2.1	20.4	-0.1	0.8	0.4
581	32.9	2.3	21.4	-0.2	1.0	0.6
582	33.0	2.0	20.2	-0.3	1.1	0.3
583	33.1	2.0	20.2	-0.3	1.0	0.3
584	33.1	2.1	20.6	-0.2	1.0	0.4
585	33.2	2.2	21.4	-0.4	0.8	0.4
586	33.3	2.3	21.6	-0.1	1.1	0.7
587	33.4	2.2	21.0	-0.2	1.1	0.6
588	33.5	2.4	22.2	-0.2	1.0	0.7
589	33.6	1.9	19.3	-0.2	1.0	0.2

Depth (cm)	Age (GICC05 kyr BP)	Mg/Ca (mmol/mol)	T °C (Anand et al., 2003)	$\delta^{18}\text{O}$ (‰ PDB)	$\delta^{13}\text{C}$ (‰ PDB)	Thermocline $\delta^{18}\text{O}_{\text{sw}}$
590	33.7	2.3	21.6	-0.3	1.0	0.6
591	33.8	2.0	20.0	-0.1	1.1	0.4
592	33.9	2.3	21.5	-0.1	1.1	0.7
593	34.0	2.1	20.5	-0.3	1.1	0.3
594	34.0	2.2	21.0	-0.3	1.1	0.5
595	34.1	2.1	20.8	-0.3	1.1	0.4
596	34.2	2.0	19.9	-0.3	1.0	0.3
597	34.3	2.0	20.1	-0.3	1.1	0.3
598	34.4	2.1	20.7	-0.3	1.1	0.4
599	34.5	2.1	20.8	-0.2	1.1	0.5
600	34.6	2.1	20.5	-0.2	1.0	0.4
601	34.7	2.1	20.5	-0.2	1.1	0.5
602	34.8	1.9	19.5	-0.3	0.9	0.2
603	34.8	2.2	21.4	-0.2	0.9	0.7
604	34.9	2.0	20.3	-0.3	1.1	0.3
605	35.0	2.2	21.3	-0.3	0.9	0.6
606	35.1	2.0	20.3	-0.2	1.0	0.5
607	35.2	2.0	20.3	-0.3	1.0	0.4
608	35.3	2.1	20.8	-0.3	1.0	0.6
609	35.4	2.1	20.7	-0.3	1.0	0.5
610	35.5	2.2	21.3	-0.2	1.0	0.7
611	35.6	2.0	20.3	-0.1	1.1	0.6
612	35.6	2.2	21.2	-0.4	0.9	0.5
613	35.7	2.1	20.5	-0.4	1.1	0.3
614	35.8	2.4	22.2			
615	35.9	2.2	21.1	-0.3	1.1	0.5
616	36.0	1.9	19.8	-0.1	1.1	0.6
617	36.1	2.0	20.2	-0.3	1.0	0.4
618	36.2	2.0	19.9	-0.2	1.1	0.4
619	36.2	2.3	21.6	-0.4	1.1	0.6
620	36.3	2.1	20.7	-0.2	0.9	0.6
621	36.4	2.0	20.3	-0.4	0.9	0.4
622	36.5	2.0	20.2	-0.4	0.9	0.3
623	36.6	2.0	20.2	-0.4	1.0	0.3
624	36.7	2.3	21.4	-0.3	1.0	0.7
625	36.8	2.2	21.0	-0.3	1.0	0.6
626	36.8	2.4	22.0	-0.3	1.0	0.7

Depth (cm)	Age (GICC05 kyr BP)	Mg/Ca (mmol/mol)	T °C (Anand et al., 2003)	$\delta^{18}\text{O}$ (‰ PDB)	$\delta^{13}\text{C}$ (‰ PDB)	Thermocline $\delta^{18}\text{O}_{\text{sw}}$
627	36.9	2.0	20.1	-0.2	0.9	0.4
628	37.0	2.1	20.6	-0.4	1.0	0.3
629	37.1	2.1	20.5	-0.3	1.0	0.4
630	37.2	2.4	22.3	-0.3	0.9	0.8
631	37.3	2.1	20.5	-0.3	1.0	0.4
632	37.3	2.1	20.8	-0.4	1.0	0.4
633	37.4	2.2	20.9	-0.4	0.9	0.4
634	37.5	2.2	21.1	-0.1	1.0	0.7
635	37.6	2.1	20.6	-0.2	0.9	0.5
636	37.7	2.1	20.6	-0.4	0.9	0.4
637	37.8	2.2	21.1	-0.3	1.0	0.6
638	37.8	2.1	20.9	-0.3	0.9	0.5
639	37.9	2.5	22.4	-0.3	0.8	0.8
640	38.0	2.4	22.2	-0.3	1.0	0.9
641	38.1	2.3	21.9	-0.4	0.8	0.7
642	38.2	2.5	22.4	-0.2	1.0	1.0
643	38.2	2.4	22.0	-0.3	1.0	0.8
644	38.3	2.4	22.3	-0.3	1.0	0.9
645	38.4	2.2	21.0	-0.3	1.0	0.6
646	38.5	2.3	21.5	-0.3	1.0	0.8
647	38.5	2.6	23.0	-0.1	0.9	1.3
648	38.6	2.2	21.2	-0.1	0.9	0.9
649	38.7	2.2	21.0	-0.3	0.9	0.6
650	38.8	2.3	21.4	-0.4	0.8	0.6
651	38.8	2.2	21.2	-0.2	1.0	0.8
652	38.9	2.1	20.6	-0.2	1.0	0.6
653	39.0	2.2	21.4	-0.3	0.8	0.8
654	39.1	2.2	20.9	-0.3	1.0	0.7
655	39.2	2.1	20.7	-0.1	1.1	0.8
656	39.2	2.2	21.2	-0.1	1.1	0.9
657	39.3	2.4	22.1	-0.1	1.0	1.0
658	39.4	2.4	22.2	-0.3	1.0	0.8
659	39.5	2.0	20.2	-0.2	1.0	0.5
660	39.5	2.1	20.4	-0.2	1.0	0.5
661	39.6	1.8	19.2	-0.2	1.1	0.2
662	39.7	2.1	20.6	-0.3	0.9	0.4
663	39.8	2.4	22.0	-0.2	1.0	0.8

Depth (cm)	Age (GICC05 kyr BP)	Mg/Ca (mmol/mol)	T °C (Anand et al., 2003)	$\delta^{18}\text{O}$ (‰ PDB)	$\delta^{13}\text{C}$ (‰ PDB)	Thermocline $\delta^{18}\text{O}_{\text{sw}}$
664	39.9	2.0	20.0	-0.2	1.0	0.4
665	39.9	2.1	20.4	-0.4	0.9	0.3
666	40.0	2.3	21.6	-0.1	1.1	0.9
667	40.1	2.0	19.9	-0.4	0.9	0.2
668	40.2	2.1	20.4	-0.2	1.1	0.4
669	40.3	2.0	19.9	0.0	0.9	0.6
670	40.4	2.0	20.1	-0.2	1.1	0.4
671	40.5	2.1	20.8	-0.4	0.8	0.4
672	40.6	2.1	20.4	-0.4	1.0	0.3
673	40.7	2.1	20.9	-0.3	0.9	0.5
674	40.8	2.0	20.0	-0.2	1.1	0.4
675	40.9	2.3	21.7	-0.4	0.7	0.6
676	40.9	2.0	20.3	-0.3	1.0	0.3
677	41.0	2.6	23.0	-0.3	1.0	1.0
678	41.1	2.2	21.0	-0.3	0.9	0.6
679	41.2	2.1	20.6	-0.2	1.1	0.6
680	41.3	2.0	20.3	-0.4	1.0	0.3
681	41.4	2.0	20.3	-0.4	1.1	0.3
682	41.5	2.2	21.1	-0.3	1.1	0.6
683	41.6	2.2	21.3	-0.4	1.0	0.6
684	41.7	2.0	20.4	-0.1	1.1	0.6
685	41.8	2.0	20.0	-0.3	1.0	0.4
686	41.9	2.0	20.3	-0.4	0.9	0.3
687	42.0	2.1	20.6	-0.3	1.0	0.4
688	42.1	2.0	20.2	-0.4	0.9	0.3
689	42.2	2.0	19.9	-0.5	1.0	0.1
690	42.3	2.1	20.8	-0.2	1.0	0.6
691	42.4	1.9	19.6	-0.1	0.9	0.4
692	42.5	2.0	20.0	-0.5	1.0	0.2
693	42.6	2.2	21.0	-0.3	1.0	0.6
695	42.8	2.3	21.6	-0.5	0.9	0.5
696	42.9	2.1	20.6	-0.3	1.0	0.4
697	42.9	2.1	20.9	-0.4	1.0	0.4
698	43.0	2.3	21.6	-0.2	1.0	0.8
699	43.1	1.9	19.7	-0.4	1.0	0.2
700	43.2	2.1	20.5	-0.2	1.0	0.6
701	43.3	2.1	20.6	-0.3	0.9	0.6

Depth (cm)	Age (GICC05 kyr BP)	Mg/Ca (mmol/mol)	T °C (Anand et al., 2003)	$\delta^{18}\text{O}$ (‰ PDB)	$\delta^{13}\text{C}$ (‰ PDB)	Thermocline $\delta^{18}\text{O}_{\text{sw}}$
702	43.4	2.0	19.9	-0.4	1.0	0.3
703	43.5	2.0	20.1	-0.4	1.0	0.3
704	43.6	1.9	19.6	-0.3	1.1	0.4
705	43.7	2.1	20.7	-0.3	1.0	0.5
706	43.8	2.1	20.5	-0.2	0.9	0.6
707	43.9	2.1	20.5	-0.2	1.0	0.5
708	44.0	2.0	20.0	-0.2	1.0	0.5
709	44.1	2.1	20.4	-0.3	1.0	0.4
710	44.2	2.1	20.9	-0.5	0.9	0.3
711	44.3	2.1	20.5	-0.1	1.0	0.7
712	44.4	2.2	21.3	-0.5	1.0	0.5
713	44.5	2.2	21.0	-0.3	1.0	0.5
714	44.6	2.2	21.3	-0.4	0.9	0.5
715	44.7	2.0	20.2	-0.5	0.9	0.2
716	44.8	2.1	20.5	-0.4	0.9	0.4
717	44.9	2.0	20.1	-0.3	1.0	0.4
718	45.0	2.1	20.8	-0.4	1.0	0.5
719	45.0	2.1	20.6	-0.5	1.0	0.3
720	45.1	2.2	21.0	-0.4	1.0	0.5
721	45.2	2.2	20.9	-0.2	0.8	0.7
722	45.3	2.0	20.0	-0.4	0.9	0.3
723	45.4	2.1	20.8	-0.3	0.9	0.5
724	45.5	2.0	20.2	-0.4	1.0	0.3
725	45.6	2.1	20.7	-0.4	0.9	0.5
726	45.7	2.1	20.4	-0.5	0.9	0.3
727	45.8	2.1	20.4	-0.5	0.9	0.3
728	45.9	2.1	20.9	-0.5	0.9	0.4
729	46.0	2.2	21.0	-0.5	1.0	0.5
730	46.1	2.0	20.2	-0.5	0.9	0.3
731	46.2	2.1	20.6	-0.2	0.7	0.7
732	46.3	2.2	21.0	-0.4	0.9	0.6
733	46.4	2.1	20.4	-0.3	0.9	0.5
734	46.5	2.0	20.3	-0.6	0.9	0.2
735	46.6	2.2	21.3	-0.4	1.0	0.7
736	46.7	2.1	20.5	-0.3	1.0	0.6
737	46.8	2.1	20.8	-0.3	1.0	0.7
738	46.9	2.1	20.5	-0.3	1.0	0.6

Depth (cm)	Age (GICC05 kyr BP)	Mg/Ca (mmol/mol)	T °C (Anand et al., 2003)	$\delta^{18}\text{O}$ (‰ PDB)	$\delta^{13}\text{C}$ (‰ PDB)	Thermocline $\delta^{18}\text{O}_{\text{sw}}$
739	47.0	2.0	20.2	-0.5	1.1	0.4
740	47.1	2.1	20.5	-0.5	0.7	0.5
741	47.2	2.4	22.2	0.3	0.6	
742	47.3	2.1	20.5	-0.2	1.0	0.8
743	47.3	2.2	21.2	-0.3	0.9	0.8
744	47.4	2.0	20.3	-0.2	1.0	0.6
745	47.5	1.8	18.9	-0.2	1.0	0.3
746	47.6	2.1	20.6	-0.4	1.0	0.5
747	47.7	2.0	20.1	-0.3	1.2	0.4
748	47.8	1.8	19.2	-0.3	1.0	0.2
749	47.9	2.0	20.0	-0.3	1.0	0.4
750	48.0	2.0	20.1	-0.4	1.0	0.3
751	48.1	2.0	20.2	-0.2	1.1	0.5
752	48.2	1.8	18.8	-0.3	1.0	0.1
753	48.3	2.0	20.2	-0.3	1.2	0.4
754	48.4	2.0	20.0	-0.3	1.0	0.4
755	48.5	1.9	19.5	-0.4	1.0	0.2
756	48.6	1.9	19.7	-0.5	1.0	0.1
757	48.7	2.2	20.9	-0.3	1.0	0.5
758	48.8	2.2	21.1	-0.5	0.9	0.3
759	48.9	1.9	19.7	-0.2	1.0	0.4
760	49.0	2.0	19.9	-0.4	1.1	0.3
761	49.1	2.2	21.0	-0.3	1.0	0.6
762	49.2	2.0	20.3	-0.5	0.9	0.3
763	49.3	2.0	20.2	-0.3	0.9	0.4
764	49.4	1.9	19.4	-0.3	1.1	0.2
765	49.5	2.2	21.0	-0.4	1.0	0.5
766	49.6	2.0	20.2	-0.4	1.0	0.4
767	49.7	2.0	20.0	-0.5	1.0	0.2
768	49.7	1.9	19.5	-0.3	1.1	0.2
769	49.8	2.2	21.0	-0.3	1.0	0.5
770	49.9	2.0	20.1	-0.4	1.0	0.3
771	50.0	2.1	20.8	-0.4	0.9	0.4
772	50.1	2.0	20.0	-0.3	1.0	0.3
773	50.2	2.0	20.1	-0.3	1.1	0.4
774	50.3	1.9	19.7	-0.4	1.1	0.2
775	50.4	2.4	22.2	-0.5	1.0	0.7

Depth (cm)	Age (GICC05 kyr BP)	Mg/Ca (mmol/mol)	T °C (Anand et al., 2003)	$\delta^{18}\text{O}$ (‰ PDB)	$\delta^{13}\text{C}$ (‰ PDB)	Thermocline $\delta^{18}\text{O}_{\text{sw}}$
776	50.5	2.0	20.0	-0.4	1.0	0.3
777	50.6	1.9	19.5	-0.3	0.9	0.3
778	50.7	2.1	20.6	-0.3	1.0	0.4
779	50.8	2.1	20.4	-0.3	0.9	0.5
780	50.9	1.8	19.2	-0.5	0.9	-0.1
781	51.0	2.0	20.0	-0.2	0.9	0.4
782	51.1	2.1	20.7	-0.7	1.0	0.1
783	51.2	2.0	20.1	-0.4	0.9	0.3
784	51.3	2.1	20.6	-0.5	0.9	0.3
785	51.4	1.9	19.7	-0.6	0.9	0.0
786	51.5	2.1	20.6	-0.5	0.9	0.2
787	51.6	2.2	21.0	-0.5	0.8	0.4
788	51.7	2.1	20.6	-0.4	0.9	0.4
789	51.8	1.9	19.5	-0.4	0.9	0.2
790	51.9	2.2	21.0	-0.5	1.0	0.4
791	52.0	2.1	20.5	-0.6	0.8	0.2
792	52.1	2.4	22.2	-0.5	0.9	0.6
793	52.2	2.4	22.2	-0.5	0.9	0.6
794	52.3	2.3	21.6	-0.4	0.9	0.6
795	52.4	2.1	20.6	-0.6	0.8	0.2
796	52.5	2.3	21.7	-0.7	0.9	0.4
797	52.5	2.3	21.5	-0.5	0.9	0.5
798	52.6	2.4	21.9	-0.6	0.9	0.5
799	52.7	2.0	20.3	-0.8	0.7	0.1
800	52.8	2.1	20.7	-0.6	0.7	0.3
801	52.9	2.0	20.0	-0.8	0.7	-0.1
802	53.0	2.0	19.9	-0.8	1.0	0.0
803	53.1	2.3	21.6	-0.6	0.7	0.5
804	53.2	2.1	20.8	-0.5	0.9	0.4
805	53.3	2.1	20.4	-0.7	0.7	0.2
806	53.4	2.2	21.2	-0.6	0.8	0.4
807	53.5	2.1	20.8	-0.6	0.8	0.3
808	53.6	2.0	20.1	-0.6	0.8	0.2
809	53.7	2.1	20.6	-0.5	0.8	0.4
810	53.8	2.6	22.8	-0.5	0.9	0.8
811	53.9	2.2	21.0	-0.7	0.7	0.4
812	54.0	2.0	19.9	-0.6	0.8	0.3

Depth (cm)	Age (GICC05 kyr BP)	Mg/Ca (mmol/mol)	T °C (Anand et al., 2003)	$\delta^{18}\text{O}$ (‰ PDB)	$\delta^{13}\text{C}$ (‰ PDB)	Thermocline $\delta^{18}\text{O}_{\text{sw}}$
813	54.1	2.3	21.6	-0.6	0.9	0.6
814	54.2	2.0	20.1	-0.6	0.9	0.3
815	54.3	2.0	20.2	-0.5	0.8	0.4
816	54.4	2.3	21.5	-0.6	0.7	0.6
817	54.5	2.1	20.9	-0.4	0.9	0.6
818	54.6	2.1	20.4	-0.5	0.9	0.4
819	54.7	2.2	21.2	-0.6	0.8	0.5
820	54.8	2.3	21.4	-0.6	0.8	0.6
821	54.9	2.1	20.6	-0.6	0.6	0.4
822	55.0	2.3	21.5	-0.5	0.7	0.6
823	55.1	2.0	20.2	-0.4	0.7	0.5
824	55.2	2.1	20.8	-0.3	0.9	0.6
825	55.3	2.3	21.6	-0.6	0.8	0.5
826	55.4	2.1	20.8	-0.5	0.8	0.4
827	55.5	2.1	20.8	-0.5	0.8	0.4
828	55.6	2.1	20.4	-0.5	0.8	0.4
829	55.6	2.0	20.3	-0.5	0.7	0.4
830	55.7	2.1	20.5	-0.3	0.8	0.6
831	55.8	2.3	21.7	-0.4	0.8	0.8
832	55.9	2.2	21.1	-0.6	0.7	0.3
833	56.0	2.1	20.6	-0.4	0.8	0.4
834	56.1	2.2	21.4	-0.3	0.9	0.6
835	56.2	2.1	20.8	-0.5	0.8	0.3
836	56.3	2.3	21.4	-0.4	0.8	0.6
837	56.4	2.1	20.7	-0.4	0.8	0.5
838	56.5	2.1	20.8	-0.4	0.7	0.5
839	56.6	2.1	20.6	-0.4	0.7	0.5
840	56.7	2.4	22.3	-0.6	0.8	0.6
841	56.8	2.3	21.7	-0.6	0.6	0.5
842	56.9	2.2	21.1	-0.6	0.6	0.3
843	57.0	2.1	20.8	-0.5	0.8	0.4
844	57.1	2.2	21.1	-0.4	0.8	0.5
845	57.2	2.1	20.9	-0.5	0.8	0.3
846	57.3	2.0	20.1	-0.6	0.7	0.1
847	57.4	2.2	21.0	-0.5	0.8	0.4
848	57.5	2.1	20.7	-0.5	0.8	0.4
849	57.6	2.0	20.0	-0.5	0.7	0.2

Depth (cm)	Age (GICC05 kyr BP)	Mg/Ca (mmol/mol)	T °C (Anand et al., 2003)	$\delta^{18}\text{O}$ (‰ PDB)	$\delta^{13}\text{C}$ (‰ PDB)	Thermocline $\delta^{18}\text{O}_{\text{sw}}$
850	57.7	2.2	21.1	-0.7	0.6	0.3
851	57.8	2.2	21.1	-0.5	0.6	0.5
852	57.9	2.1	20.5	-0.5	0.7	0.3
853	58.0	2.1	20.8	-0.5	0.8	0.5
854	58.1	2.2	21.1	-0.5	0.7	0.5
855	58.2	2.4	22.2	-0.4	0.8	0.9
856	58.3	2.4	22.2	-0.4	0.7	0.8
857	58.4	2.4	22.2	-0.6	0.7	0.7
858	58.4	2.4	21.9	-0.3	0.7	0.9
859	58.5	2.2	21.3	-0.4	0.7	0.7
860	58.6	2.4	22.3	-0.4	0.6	0.9
861	58.7	2.5	22.6	-0.4	0.6	1.0
862	58.8	2.3	21.9	-0.4	0.6	0.8
863	58.9	2.6	22.8	-0.6	0.7	0.9
864	59.0	2.4	22.2	-0.5	0.6	0.8
865	59.1	2.3	21.6	-0.4	0.6	0.8
866	59.2	2.4	22.3	-0.3	0.7	1.0
867	59.3	2.4	22.1	-0.4	0.7	0.9
868	59.4	2.3	21.4	-0.4	0.6	0.8
869	59.5	2.2	21.3	-0.5	0.6	0.7
870	59.6	2.4	22.2	-0.3	0.8	1.0
871	59.7	2.8	23.8	-0.3	0.6	1.4
872	59.8	2.3	21.8	-0.2	0.7	1.1
873	59.9	2.4	22.3	-0.3	0.7	1.0
874	60.0	2.3	21.5	-0.3	0.7	0.9
875	60.1	2.2	21.3	-0.2	0.7	0.9
876	60.2	2.2	21.1	-0.2	0.8	0.8
877	60.3	2.3	21.6	-0.4	0.7	0.8
878	60.4	2.5	22.4	-0.4	0.7	0.9
879	60.5	2.7	23.2	-0.2	0.8	1.2
880	60.6	2.4	22.0	-0.3	0.7	0.8
881	60.7	2.4	22.0	-0.4	0.8	0.7
882	60.8	2.3	21.7	-0.4	0.6	0.7
883	60.9	2.7	23.3	-0.3	0.8	1.2
884	61.0	2.3	21.8	-0.3	0.8	0.8
885	61.1	2.5	22.6	-0.3	0.7	1.0
886	61.2	2.2	21.3	-0.2	0.9	0.8

Depth (cm)	Age (GICC05 kyr BP)	Mg/Ca (mmol/mol)	T °C (Anand et al., 2003)	$\delta^{18}\text{O}$ (‰ PDB)	$\delta^{13}\text{C}$ (‰ PDB)	Thermocline $\delta^{18}\text{O}_{\text{sw}}$
887	61.2	2.3	21.4	-0.2	0.7	0.8
888	61.3	2.3	21.8	-0.5	0.8	0.6
889	61.4	2.3	21.4	-0.3	0.8	0.6
890	61.5	2.4	22.1	-0.3	0.7	0.8
891	61.6	2.4	22.2	-0.3	0.9	0.9
892	61.7	2.4	22.1	-0.2	0.8	0.9
893	61.8	2.4	22.2	-0.3	0.8	0.8
894	61.9	2.5	22.4	-0.2	0.7	
895	62.0	2.1	20.9	-0.3	0.8	

**Appendix D. SO185-18460 stable isotopes and Mg/Ca
of *Globigerinoides ruber* (white)**

Depth (cm)	Age (GICC05 kyr BP)	Mg/Ca (mmol/mol)	SST (°C) [Anand et al., 2003]	$\delta^{18}\text{O}$ (‰ PDB) [Dürkop, 2009]	$\delta^{13}\text{C}$ (‰ PDB) [Dürkop, 2009]	Surface $\delta^{18}\text{O}_{\text{sw}}$
356	23.5	4.2	26.7	-1.2	1.2	0.5
359	23.7	3.8	25.7	-1.2	1.1	0.3
363	24.0	3.7	25.2	-1.1	1.1	0.3
366	24.2	3.6	25.1	-1.1	1.2	0.4
369	24.4	3.6	24.9	-1.3	1.1	0.2
373	24.6	3.9	25.8	-1.3	1.2	0.2
376	24.8	3.8	25.7	-1.3	1.3	0.2
379	25.0	3.6	24.9	-1.2	1.3	0.1
383	25.3	3.8	25.5	-1.1	1.2	0.4
386	25.5	4.1	26.5	-1.3	1.4	0.4
389	25.7	3.6	24.8	-1.3	1.2	0.1
393	26.0	3.3	24.1	-1.3	1.3	-0.1
396	26.2	3.3	24.0	-1.1	1.3	0.0
399	26.4	3.5	24.7	-1.2	1.2	0.1
403	26.7	5.0	28.6	-1.3	1.2	0.8
406	26.9	3.4	24.3	-1.3	1.3	-0.1
409	27.1	3.3	23.9	-1.4	1.1	-0.2
413	27.4	3.4	24.3	-1.3	1.3	-0.1
416	27.6	3.4	24.3	-1.3	1.2	-0.1
419	27.8	3.5	24.7	-1.4	1.3	0.0
421	28.0	3.3	23.9	-1.4	1.1	-0.1
423	28.1	3.4	24.5	-1.4	1.2	0.0
425	28.2	3.7	25.2	-1.4	0.9	0.1
427	28.4	3.7	25.1	-1.5	1.2	0.1
429	28.5	3.8	25.5	-1.3	1.2	0.3
431	28.7	3.6	25.1	-1.5	1.2	0.1
433	28.8	3.5	24.5	-1.6	1.1	-0.2
435	29.0	3.5	24.7	-1.3	1.1	0.2
437	29.1	3.7	25.2	-1.4	1.2	0.2
439	29.3	3.5	24.8	-1.4	1.1	0.1
441	29.4	3.5	24.5	-1.3	1.2	0.1
443	29.6	3.5	24.8	-1.5	1.4	0.0

Depth (cm)	Age (GICC05 kyr BP)	Mg/Ca (mmol/mol)	SST (°C) [Anand et al., 2003]	$\delta^{18}\text{O}$ (% PDB) [Dürkop, 2009]	$\delta^{13}\text{C}$ (% PDB) [Dürkop, 2009]	Surface $\delta^{18}\text{O}_{\text{sw}}$
445	29.7	3.5	24.8	-1.3	1.3	0.2
447	29.9	3.8	25.5	-1.4	1.4	0.3
448	29.9	3.3	23.9	-1.5	1.4	-0.2
451	30.2	3.5	24.8	-1.4	1.4	0.2
453	30.3	3.6	24.9	-1.3	1.5	0.4
455	30.5	3.8	25.5	-1.4	1.3	0.3
456	30.5	3.4	24.3	-1.3	1.4	0.2
457	30.6	3.6	24.9	-1.2	1.3	0.2
459	30.8	3.3	24.0	-1.3	1.2	0.0
461	30.9	3.4	24.4	-1.4	1.5	0.0
463	31.1	3.4	24.5	-1.4	1.3	0.0
465	31.2	3.5	24.8	-1.5	1.5	-0.1
467	31.4	3.6	25.1	-1.4	1.3	0.1
469	31.5	3.6	24.9	-1.3	1.5	0.2
471	31.7	3.8	25.6	-1.4	1.2	0.3
473	31.8	3.5	24.6	-1.4	1.5	0.0
475	32.0	3.3	23.9	-1.2	1.5	0.1
477	32.2	3.5	24.5	-1.5	1.2	0.0
479	32.3	3.7	25.2	-1.5	1.5	0.2
481	32.5	3.7	25.3	-1.5	1.3	0.2
482	32.5	3.6	25.0	-1.4	1.4	0.1
483	32.6	3.9	25.8	-1.6	1.4	0.2
484	32.7	3.6	24.9	-1.5	1.4	0.0
485	32.8	3.9	25.8	-1.6	1.5	0.2
486	32.9	3.7	25.1	-1.6	1.4	0.0
487	32.9	3.4	24.4	-1.7	1.3	-0.2
488	33.0	3.7	25.2	-1.5	1.3	0.2
489	33.1	3.6	25.0	-1.6	1.4	0.1
491	33.3	3.5	24.7	-1.6	1.4	0.0
492	33.3	3.8	25.5	-1.4	1.5	0.3
493	33.4	3.6	24.9	-1.5	1.3	0.1
494	33.5	3.6	24.9	-1.6	1.4	0.0
495	33.6	3.4	24.4	-1.5	1.3	-0.1
496	33.6	3.6	25.0	-1.6	1.4	-0.1
497	33.7	3.5	24.7	-1.7	1.4	-0.2
498	33.8	3.6	25.0	-1.7	1.4	-0.1
501	34.0	3.6	25.1	-1.8	1.4	-0.2

Depth (cm)	Age (GICC05 kyr BP)	Mg/Ca (mmol/mol)	SST (°C) [Anand et al., 2003]	$\delta^{18}\text{O}$ (% PDB) [Dürkop, 2009]	$\delta^{13}\text{C}$ (% PDB) [Dürkop, 2009]	Surface $\delta^{18}\text{O}_{\text{sw}}$
502	34.1	3.5	24.7	-1.6	1.3	0.0
503	34.2	3.6	24.9	-1.5	1.3	0.1
504	34.3	3.6	24.8	-1.4	1.4	0.3
505	34.4	3.5	24.7	-1.5	1.4	0.2
506	34.4	3.6	24.9	-1.4	1.6	0.3
507	34.5	3.9	25.8	-1.5	1.5	0.4
508	34.6	3.5	24.6	-1.5	1.5	0.1
511	34.8	3.7	25.2	-1.6	1.3	0.1
512	34.9	3.7	25.4	-1.6	1.4	0.1
513	35.0	3.9	25.9	-1.6	1.4	0.2
514	35.1	4.2	26.8	-1.5	1.4	0.5
515	35.1	3.7	25.2	-1.6	1.5	0.1
516	35.2	3.8	25.6	-1.6	1.5	0.2
517	35.3	3.7	25.1	-1.6	1.5	0.1
518	35.4	3.8	25.6	-1.6	1.2	0.2
519	35.5	3.7	25.3	-1.5	1.2	0.3
521	35.6	4.1	26.4	-1.6	1.4	0.5
522	35.7	3.8	25.7	-1.6	1.4	0.4
523	35.8	3.9	25.7	-1.5	1.3	0.4
524	35.9	3.8	25.6	-1.5	1.5	0.4
525	35.9	3.8	25.7	-1.6	1.4	0.3
526	36.0	3.9	25.8	-1.6	1.3	0.3
527	36.1	3.5	24.5	-1.6	1.3	0.0
528	36.2	3.8	25.5	-1.6	1.3	0.2
529	36.3	3.6	25.1	-1.4	1.5	0.3
531	36.4	3.3	23.9	-1.4	1.4	0.0
532	36.5	3.4	24.4	-1.6	1.5	-0.1
533	36.6	3.5	24.7	-1.4	1.4	0.1
535	36.8	3.8	25.6	-1.5	1.4	0.2
536	36.8	3.7	25.3	-1.6	1.3	0.1
537	36.9	3.8	25.5	-1.5	1.4	0.2
538	37.0	3.9	25.7	-1.6	1.4	0.2
539	37.1	3.7	25.2	-1.7	1.3	0.0
541	37.2	3.7	25.2	-1.5	1.4	0.2
542	37.3	4.0	26.1	-1.5	1.2	0.4
544	37.5	3.6	24.8	-1.7	1.3	0.0
545	37.6	3.8	25.4	-1.7	1.4	0.2

Depth (cm)	Age (GICC05 kyr BP)	Mg/Ca (mmol/mol)	SST (°C) [Anand et al., 2003]	$\delta^{18}\text{O}$ (% PDB) [Dürkop, 2009]	$\delta^{13}\text{C}$ (% PDB) [Dürkop, 2009]	Surface $\delta^{18}\text{O}_{\text{sw}}$
546	37.6	3.8	25.6	-1.6	1.2	0.3
547	37.7	3.8	25.6	-1.6	1.2	0.2
548	37.8	3.6	25.0	-1.7	1.2	0.1
549	37.9	4.1	26.3	-1.8	1.3	0.3
550	38.0	3.7	25.4	-1.6	1.4	0.2
551	38.0	3.8	25.6	-1.6	1.5	0.3
552	38.1	3.6	24.9	-1.7	1.3	0.1
553	38.2	3.8	25.5	-1.7	1.4	0.3
554	38.3	3.6	25.1	-1.6	1.3	0.3
555	38.4	3.9	26.0	-1.6	1.3	0.5
556	38.5	3.6	25.1	-1.6	1.3	0.3
557	38.5	3.6	25.1	-1.6	1.2	0.4
558	38.6	3.8	25.5	-1.4	1.3	0.6
559	38.7	3.5	24.8	-1.6	1.2	0.2
561	38.9	3.7	25.2	-1.5	1.2	0.4
563	39.0	3.6	25.0	-1.7	1.2	0.2
564	39.1	3.6	25.0	-1.6	1.4	0.4
565	39.2	3.9	26.0	-1.3	1.2	0.8
567	39.4	3.5	24.8	-1.5	1.3	0.4
568	39.4	3.7	25.2	-1.6	1.2	0.4
569	39.5	4.1	26.3	-1.4	1.4	0.6
571	39.7	3.7	25.3	-1.4	1.4	0.3
572	39.8	3.7	25.3	-1.5	1.4	0.2
573	39.9	3.6	25.1	-1.5	1.4	0.2
574	39.9	3.9	25.8	-1.5	1.2	0.3
575	40.0	3.7	25.2	-1.5	1.4	0.2
576	40.1	3.8	25.6	-1.5	1.5	0.4
577	40.2	3.7	25.3	-1.4	1.5	0.3
581	40.5	3.8	25.7	-1.4	1.4	0.5
582	40.6	3.8	25.4	-1.5	1.3	0.3
583	40.7	3.6	25.0	-1.5	1.2	0.2
584	40.8	3.6	25.0	-1.6	1.3	0.1
585	40.8	3.6	25.1	-1.6	1.4	0.1
586	40.9	4.1	26.5	-1.5	1.3	0.4
587	41.0	3.9	25.9	-1.6	1.4	0.2
588	41.1	3.5	24.6	-1.6	1.4	0.0
589	41.2	4.2	26.6	-1.6	1.5	0.4

Depth (cm)	Age (GICC05 kyr BP)	Mg/Ca (mmol/mol)	SST (°C) [Anand et al., 2003]	$\delta^{18}\text{O}$ (% PDB) [Dürkop, 2009]	$\delta^{13}\text{C}$ (% PDB) [Dürkop, 2009]	Surface $\delta^{18}\text{O}_{\text{sw}}$
591	41.3	4.4	27.2	-1.6	1.4	0.5
592	41.4	3.8	25.7	-1.6	1.3	0.3
593	41.5	3.8	25.5	-1.6	1.3	0.2
594	41.6	3.8	25.5	-1.7	1.3	0.2
595	41.7	4.1	26.5	-1.6	1.3	0.4
596	41.8	4.1	26.3	-1.5	1.1	0.5
597	41.8	4.2	26.7	-1.4	1.1	0.7
598	41.9	4.5	27.5	-1.4	1.3	0.8
599	42.0	3.6	24.9	-1.6	1.2	0.1
603	42.3	3.8	25.6	-1.6	1.2	0.3
606	42.6	3.5	24.8	-1.7	1.3	0.0
609	42.8	3.9	25.8	-1.6	1.2	0.2
613	43.2	4.2	26.7	-1.5	1.3	0.6
616	43.4	4.4	27.3	-1.6	1.2	0.7
619	43.7	4.7	28.0	-1.5	1.3	0.9
623	44.0	4.0	26.1	-1.6	1.4	0.4
624	44.1	3.5	24.6	-1.4	1.3	0.3
625	44.2	3.6	25.1	-1.7	1.2	0.1
626	44.3	3.7	25.2	-1.6	1.4	0.2
627	44.4	3.6	25.1	-1.8	1.2	0.0
628	44.4	3.9	25.7	-1.6	1.2	0.4
629	44.5	3.6	24.9	-1.6	1.2	0.1
631	44.7	3.8	25.6	-1.8	1.2	0.1
632	44.8	4.0	26.0	-1.6	1.2	0.4
633	44.9	3.8	25.5	-1.7	1.2	0.1
635	45.0	3.9	25.8	-1.6	1.3	0.3
636	45.1	4.0	26.2	-1.6	1.4	0.4
637	45.2	3.8	25.7	-1.6	1.3	0.3
638	45.3	3.7	25.2	-1.7	1.3	0.1
639	45.4	3.6	25.1	-1.6	1.3	0.2
640	45.5	3.7	25.3	-1.6	1.2	0.2
641	45.5	3.8	25.5	-1.5	1.3	0.4
642	45.6	3.7	25.3	-1.6	1.1	0.2
643	45.7	3.9	25.9	-1.5	1.3	0.4
644	45.8	4.0	26.1	-1.7	1.2	0.3
645	45.9	3.9	26.0	-1.6	1.3	0.3
646	46.0	3.9	25.8	-1.6	1.3	0.3

Depth (cm)	Age (GICC05 kyr BP)	Mg/Ca (mmol/mol)	SST (°C) [Anand et al., 2003]	$\delta^{18}\text{O}$ (% PDB) [Dürkop, 2009]	$\delta^{13}\text{C}$ (% PDB) [Dürkop, 2009]	Surface $\delta^{18}\text{O}_{\text{sw}}$
647	46.1	3.8	25.5	-1.7	1.1	0.2
648	46.1	4.0	26.0	-1.6	1.1	0.3
649	46.2	3.9	25.9	-1.7	1.1	0.3
650	46.3	4.0	26.1	-1.7	1.2	0.3
651	46.4	3.9	26.0	-1.6	1.1	0.4
652	46.5	4.5	27.5	-1.6	1.1	0.7
653	46.6	3.5	24.5	-1.8	1.2	-0.1
654	46.7	3.6	25.0	-1.6	1.0	0.2
655	46.8	3.6	25.1	-1.6	1.2	0.3
656	46.8	3.9	25.8	-1.7	1.0	0.4
657	46.9	3.8	25.7	-1.6	1.2	0.5
658	47.0	3.8	25.5	-1.7	1.3	0.4
659	47.1	3.6	24.9	-1.5	1.1	0.4
660	47.2	3.4	24.4	-1.5	1.2	0.3
661	47.3	3.7	25.2	-1.6	1.1	0.4
662	47.4	3.3	24.2	-1.6	1.3	0.1
663	47.5	3.3	24.2	-1.5	1.1	0.2
664	47.6	3.7	25.4	-1.5	1.2	0.4
665	47.6	3.7	25.3	-1.5	1.2	0.5
666	47.7	3.8	25.5	-1.5	1.2	0.6
667	47.8	3.7	25.3	-1.5	1.2	0.4
668	47.9	3.6	25.1	-1.3	1.2	0.5
669	48.0	3.6	25.1	-1.5	1.1	0.3
670	48.1	3.9	25.7	-1.5	1.5	0.4
671	48.2	3.4	24.4	-1.7	1.1	-0.1
672	48.3	3.5	24.5	-1.4	1.1	0.2
673	48.4	3.6	24.9	-1.6	1.2	0.1
674	48.5	3.7	25.4	-1.6	1.1	0.2
675	48.6	3.6	24.9	-1.4	1.3	0.3
676	48.7	3.5	24.8	-1.5	1.3	0.1
677	48.8	3.4	24.2	-1.5	1.1	0.0
678	48.9	3.7	25.4	-1.5	1.4	0.2
679	48.9	3.5	24.8	-1.4	1.2	0.3
680	49.0	3.8	25.7	-1.6	1.4	0.2
681	49.1	3.6	24.9	-1.6	1.2	0.1
682	49.2	3.7	25.3	-1.7	1.2	0.1
683	49.3	3.4	24.4	-1.7	1.3	-0.1

Depth (cm)	Age (GICC05 kyr BP)	Mg/Ca (mmol/mol)	SST (°C) [Anand et al., 2003]	$\delta^{18}\text{O}$ (% PDB) [Dürkop, 2009]	$\delta^{13}\text{C}$ (% PDB) [Dürkop, 2009]	Surface $\delta^{18}\text{O}_{\text{sw}}$
684	49.4	3.0	23.1	-1.6	1.3	-0.2
685	49.5	3.5	24.7	-1.7	1.2	0.0
686	49.6	3.6	24.9	-1.5	1.3	0.2
687	49.7	3.5	24.6	-1.7	1.2	0.0
689	49.9	3.6	25.0	-1.6	1.2	0.1
690	50.0	3.6	24.9	-1.6	1.2	0.1
691	50.1	3.4	24.5	-1.5	1.3	0.1
692	50.2	3.7	25.3	-1.8	1.1	0.0
693	50.3	2.3	20.1	-1.4	1.2	-0.7
694	50.4	3.5	24.7	-1.7	1.2	-0.1
695	50.5	3.1	23.4	-1.6	1.0	-0.2
696	50.6	3.7	25.4	-1.6	1.2	0.3
697	50.7	3.6	25.1	-1.5	1.1	0.3
698	50.8	3.5	24.8	-1.6	1.3	0.2
699	50.9	3.0	23.1	-1.5	1.2	-0.1
700	51.0	4.0	26.1	-1.6	1.0	0.4
701	51.1	3.0	22.8	-1.6	1.2	-0.3
702	51.2	3.7	25.2	-1.7	1.4	0.0
703	51.3	3.8	25.5	-1.6	1.2	0.3
704	51.4	3.5	24.6	-1.7	1.3	0.0
705	51.5	3.5	24.6	-1.6	1.2	0.1
706	51.6	3.6	24.9	-1.7	0.9	0.1
707	51.7	3.9	25.9	-1.6	1.1	0.4
708	51.8	3.3	24.2	-1.6	1.1	0.0
709	52.0	3.3	24.2	-1.7	1.2	-0.1
710	52.1	3.6	25.0	-1.7	1.2	0.1
711	52.2	3.9	25.8	-1.7	1.1	0.2
712	52.3	3.3	24.0	-1.7	1.0	-0.1
713	52.4	3.7	25.2	-1.7	1.1	0.1
714	52.5	3.4	24.4	-1.8	1.1	-0.1
715	52.6	3.8	25.6	-1.6	0.9	0.3
716	52.7	3.7	25.2	-1.6	1.2	0.2
717	52.8	3.8	25.6	-1.7	1.2	0.2
718	52.9	3.9	25.9	-1.6	1.0	0.3
719	53.0	4.7	27.8	-1.9	1.0	0.5
720	53.1	3.7	25.2	-1.7	0.9	0.1
721	53.2	3.6	24.9	-1.9	1.1	-0.1

Depth (cm)	Age (GICC05 kyr BP)	Mg/Ca (mmol/mol)	SST (°C) [Anand et al., 2003]	$\delta^{18}\text{O}$ (% PDB) [Dürkop, 2009]	$\delta^{13}\text{C}$ (% PDB) [Dürkop, 2009]	Surface $\delta^{18}\text{O}_{\text{sw}}$
722	53.3	3.4	24.4	-1.8	1.2	-0.2
723	53.4	3.7	25.3	-1.7	1.3	0.1
724	53.5	3.8	25.5	-1.8	1.0	0.1
725	53.6	4.1	26.3	-2.0	1.2	0.1
726	53.7	3.7	25.3	-1.7	1.1	0.2
729	54.1	4.3	26.8	-1.8	1.1	0.5
730	54.2	4.4	27.2	-1.9	1.0	0.5
733	54.5	4.0	26.1	-1.5	1.2	0.7
736	54.8	4.7	28.0	-1.8	1.1	0.7
739	55.1	4.1	26.4	-1.6	1.2	0.5
740	55.2	3.9	25.9	-1.6	0.9	0.4
743	55.6	4.2	26.8	-1.8	1.0	0.4
746	55.9	4.3	26.9	-1.8	1.1	0.5
749	56.2	3.9	25.7	-1.5	1.1	0.5
750	56.3	3.7	25.3	-1.7	0.9	0.2
753	56.6	4.0	26.2	-1.7	1.0	0.3
756	57.0	4.0	26.2	-1.8	1.0	0.2
759	57.3	3.9	25.9	-1.6	1.1	0.3
760	57.4	4.1	26.4	-1.8	1.0	0.3
763	57.7	3.9	25.8	-1.7	0.9	0.2
766	58.0	4.2	26.7	-1.8	1.1	0.4
769	58.4	4.6	27.8	-1.8	0.9	0.7
770	58.5	4.2	26.8	-1.7	1.0	0.5
771	58.6	3.9	26.0	-1.9	1.1	0.1
773	58.8	4.1	26.3	-1.8	0.9	0.3
775	59.0	4.4	27.1	-1.7	0.8	0.6
777	59.2	4.1	26.3	-1.7	0.9	0.5
779	59.5	4.3	27.0	-1.6	0.8	0.7
781	59.7	4.2	26.6	-1.6	0.9	0.7
783	59.9	4.2	26.6	-1.7	0.8	0.6
785	60.1	4.2	26.7	-1.7	0.9	0.7
787	60.3	4.2	26.6	-1.6	0.8	0.6
789	60.5	4.2	26.7	-1.5	0.8	0.7
791	60.7	4.6	27.7	-1.6	0.9	0.8
793	61.0	5.2	29.0	-1.5	0.9	1.2
795	61.2	4.0	26.2	-1.4	1.0	0.6
797	61.4	4.1	26.4	-1.4	1.0	0.6

Depth (cm)	Age (GICC05 kyr BP)	Mg/Ca (mmol/mol)	SST (°C) [Anand et al., 2003]	$\delta^{18}\text{O}$ (% PDB) [Dürkop, 2009]	$\delta^{13}\text{C}$ (% PDB) [Dürkop, 2009]	Surface $\delta^{18}\text{O}_{\text{sw}}$
799	61.6	4.4	27.2	-1.3	1.0	0.8
801	61.8	4.4	27.3	-1.4	1.0	0.8
803	62.0	3.8	25.6	-1.4	1.1	0.4
805	62.3	4.0	26.1	-1.4	1.0	0.5
807	62.5	4.0	26.2	-1.5	1.0	0.4
809	62.7	5.9	30.5	-1.5	1.0	1.3
810	62.8	3.9	26.0	-1.4	1.1	0.4
813	63.1	3.7	25.3	-1.6	1.1	0.0
816	63.4	4.1	26.3	-1.6	0.9	0.3
819	63.8	3.9	26.0	-1.6	1.0	0.2
820	63.9	3.7	25.4	-1.6	1.0	0.0
826	64.5	3.9	26.0	-1.6	1.0	0.2
829	64.8	4.1	26.5	-1.7	1.0	0.3
830	65.0	3.6	24.9	-1.6	1.1	0.1
833	65.3	4.0	26.3	-1.6	1.0	0.4

**Appendix E. SO185-18460 stable isotopes and Mg/Ca
of *Pulleniatina obliquiloculata***

Depth (cm)	Age (GICC05 kyr BP)	Mg/Ca (mmol/mol)	T °C (Anand et al., 2003)	$\delta^{18}\text{O}$ (‰ PDB)	$\delta^{13}\text{C}$ (‰ PDB)	Thermocline $\delta^{18}\text{O}_{\text{sw}}$
356	23.5	1.9	19.4	0.1	0.9	0.3
359	23.7	1.9	19.7	0.3	0.9	0.6
360	23.8	1.8	19.2	0.4	1.0	0.6
363	24.0	1.8	19.2	0.2	0.9	0.4
366	24.2	1.9	19.5	0.3	1.0	0.6
369	24.4	2.0	20.2	0.2	0.9	0.6
370	24.4	2.0	20.0	0.3	0.9	0.7
373	24.6	2.0	19.9	0.3	1.0	0.6
376	24.8	1.9	19.5	0.3	1.1	0.5
379	25.0	1.7	18.5	0.2	1.0	0.2
380	25.1	1.9	19.4	0.3	1.0	0.5
383	25.3	1.7	18.6	0.3	1.1	0.3
386	25.5	1.9	19.7	0.2	1.0	0.5
389	25.7	2.0	19.9	0.1	1.0	0.4
390	25.8	2.0	20.1	0.3	1.1	0.7
393	26.0	1.8	18.8	0.3	1.0	0.4
396	26.2	1.9	19.8	0.2	1.0	0.5
399	26.4	2.0	19.9	0.0	1.0	0.3
400	26.5	2.1	20.5	0.1	1.0	0.5
403	26.7	1.9	19.8	0.1	1.1	0.4
406	26.9	1.8	19.1	0.2	1.0	0.3
409	27.1	2.0	19.8	0.2	1.1	0.6
410	27.2	2.1	20.7			
413	27.4	1.7	18.3	0.1	1.0	0.1
416	27.6	1.7	18.5	0.2	1.1	0.2
419	27.8	1.8	18.7	0.2	1.1	0.3
421	28.0	1.8	19.1	0.1	1.0	0.4
423	28.1	2.0	20.1	0.2	1.0	0.6
425	28.2	2.0	20.2	0.1	1.0	0.6

Depth (cm)	Age (GICC05 kyr BP)	Mg/Ca (mmol/mol)	T °C (Anand et al., 2003)	$\delta^{18}\text{O}$ (‰ PDB)	$\delta^{13}\text{C}$ (‰ PDB)	Thermocline $\delta^{18}\text{O}_{\text{sw}}$
427	28.4	2.0	19.9	0.3	1.2	0.7
429	28.5	2.0	19.8	0.2	1.0	0.6
431	28.7	1.9	19.7	0.1	1.1	0.5
433	28.8	1.9	19.6	0.3	1.0	0.7
435	29.0	2.1	20.8	0.1	1.1	0.8
437	29.1	2.0	20.0	0.1	1.1	0.5
439	29.3	2.1	20.5	0.2	1.0	0.7
441	29.4	1.9	19.4	0.2	1.1	0.5
443	29.6	1.7	18.5	0.1	1.1	0.2
445	29.7	1.7	18.6	0.3	1.2	0.5
447	29.9	1.7	18.1	0.4	1.2	0.4
449	30.0	1.8	18.6	0.3	1.1	0.5
451	30.2	1.8	18.9	0.4	1.1	0.7
453	30.3	1.7	18.4	0.4	1.1	0.7
455	30.5	1.8	18.7	0.2	1.1	0.5
456	30.5	1.7	18.5	0.3	1.1	0.5
457	30.6	1.9	19.6	0.2	1.2	0.6
459	30.8	1.8	19.2	0.3	1.1	0.5
461	30.9	1.8	18.9	0.3	1.2	0.5
463	31.1	2.1	20.6	0.2	1.2	0.8
465	31.2	2.0	20.2	0.2	1.2	0.7
467	31.4	1.9	19.5	0.2	1.2	0.5
469	31.5	1.5	17.1	0.1	1.2	0.0
471	31.7	2.0	19.9	0.1	1.2	0.6
473	31.8	1.9	19.3	0.2	1.2	0.6
475	32.0	2.0	20.2	0.1	1.1	0.7
477	32.2	1.8	18.8	0.2	1.2	0.5
479	32.3	1.8	18.9	0.2	1.1	0.5
481	32.5	1.7	18.4	-0.1	1.1	0.1
484	32.7	2.1	20.4			
487	32.9	1.8	18.6	0.0	1.1	0.3
489	33.1	2.2	21.0	0.2	1.1	1.0
493	33.4	2.3	21.5	0.1	1.1	1.0
496	33.6	2.1	20.5	-0.1	0.9	0.6
499	33.9	1.7	18.2	0.2	1.2	0.4
503	34.2	1.8	18.7	0.0	1.1	0.4
506	34.4	1.7	18.4	-0.1	1.1	0.3

Depth (cm)	Age (GICC05 kyr BP)	Mg/Ca (mmol/mol)	T °C (Anand et al., 2003)	$\delta^{18}\text{O}$ (‰ PDB)	$\delta^{13}\text{C}$ (‰ PDB)	Thermocline $\delta^{18}\text{O}_{\text{sw}}$
509	34.7	1.7	18.5	0.1	1.0	0.4
513	35.0	1.9	19.7	-0.1	1.0	0.4
516	35.2	2.1	20.5	-0.1	1.0	0.6
519	35.5	2.0	20.3	0.0	1.1	0.7
523	35.8	1.8	19.1	0.1	1.2	0.6
526	36.0	1.9	19.7	0.2	1.2	0.8
529	36.3	1.9	19.5	-0.2	1.0	0.3
533	36.6	1.8	19.2	0.1	1.2	0.5
536	36.8	1.9	19.4	-0.1	1.0	0.4
539	37.1	1.6	17.5	-0.7	0.7	-0.6
541	37.2	1.8	18.9	-0.5	0.9	-0.1
542	37.3	1.8	19.2	-0.1	1.0	0.3
543	37.4	1.9	19.4	-0.1	1.0	0.5
544	37.5	1.9	19.7	-0.1	1.0	0.5
545	37.6	2.1	20.8	-0.1	1.0	0.8
546	37.6	2.1	20.5	-0.1	1.0	0.7
547	37.7	1.9	19.7	-0.1	0.9	0.5
548	37.8	1.7	18.4	-0.1	0.9	0.3
549	37.9	1.9	19.4	0.0	1.0	0.6
550	38.0	2.0	20.3	0.0	1.0	0.8
551	38.0	2.2	21.1	-0.2	0.9	0.8
552	38.1	2.0	20.3	0.1	0.9	0.9
553	38.2	2.1	20.7	0.0	1.0	1.0
554	38.3	2.0	20.3	0.2	1.0	1.1
555	38.4	2.1	20.7	0.1	1.0	1.1
556	38.5	2.1	20.8	0.0	0.9	1.1
557	38.5	2.1	20.8	-0.1	0.9	1.0
558	38.6	2.2	20.9	0.0	0.9	1.0
559	38.7	2.0	20.2	0.0	1.0	0.9
560	38.8	1.9	19.4	0.0	1.0	0.7
561	38.9	1.7	18.5	0.1	0.9	0.6
562	38.9	2.1	20.6	0.0	1.0	1.0
563	39.0	1.9	19.7	0.0	1.0	0.8
564	39.1	2.1	20.5	0.1	1.0	1.2
565	39.2	1.9	19.5	0.0	1.0	0.8
567	39.4	1.6	17.8	0.1	1.2	0.5
568	39.4	1.7	18.3	-0.1	1.0	0.4

Depth (cm)	Age (GICC05 kyr BP)	Mg/Ca (mmol/mol)	T °C (Anand et al., 2003)	$\delta^{18}\text{O}$ (‰ PDB)	$\delta^{13}\text{C}$ (‰ PDB)	Thermocline $\delta^{18}\text{O}_{\text{sw}}$
569	39.5	1.8	18.7	0.1	1.1	0.5
570	39.6	2.1	20.5	0.1	1.2	0.8
571	39.7	2.0	20.0	0.2	1.1	0.8
572	39.8	2.1	20.4	0.0	1.1	0.7
573	39.9	1.8	18.8	0.0	1.0	0.3
574	39.9	1.7	18.0	0.1	1.2	0.3
575	40.0	1.8	19.0	0.1	1.1	0.5
576	40.1	2.0	20.0	0.1	1.0	0.8
577	40.2	2.0	20.1	0.1	1.2	0.8
578	40.3	2.4	22.3	0.0	1.0	1.2
579	40.3	1.7	18.2	0.0	1.0	0.3
580	40.4	1.7	18.3	0.0	1.1	0.4
581	40.5	1.7	18.6	0.0	1.0	0.4
582	40.6	2.3	21.4	0.1	1.0	1.1
583	40.7	1.9	19.4	0.1	1.0	0.6
584	40.8	2.0	20.0	-0.1	0.9	0.6
585	40.8	1.9	19.6	0.0	0.9	0.5
586	40.9	1.9	19.3	0.0	1.0	0.4
587	41.0	1.8	19.2	0.0	1.2	0.4
588	41.1	2.0	19.8	-0.1	1.0	0.4
589	41.2	1.8	19.2	0.0	1.0	0.4
590	41.3	1.8	18.8	0.0	1.0	0.3
591	41.3	1.8	18.8	-0.1	1.0	0.4
592	41.4	1.8	18.6	0.0	1.0	0.4
593	41.5	1.8	19.0	0.1	1.1	0.6
594	41.6	2.2	21.2	0.0	1.1	0.9
597	41.8	2.0	20.1	-0.1	1.1	0.7
598	41.9	1.9	19.3	0.0	1.1	0.5
599	42.0	2.1	20.5	-0.1	1.0	0.7
600	42.1	1.8	18.7	0.0	1.0	0.4
603	42.3	2.0	19.9	-0.1	1.0	0.5
606	42.6	2.0	19.9	-0.1	0.9	0.6
609	42.8	2.0	20.3	0.0	1.1	0.7
610	42.9	1.9	19.6	0.0	1.0	0.5
613	43.2	2.1	20.4	-0.1	1.0	0.7
616	43.4	1.8	19.0	-0.1	1.0	0.4
619	43.7	1.8	19.1	0.0	1.1	0.5

Depth (cm)	Age (GICC05 kyr BP)	Mg/Ca (mmol/mol)	T °C (Anand et al., 2003)	$\delta^{18}\text{O}$ (‰ PDB)	$\delta^{13}\text{C}$ (‰ PDB)	Thermocline $\delta^{18}\text{O}_{\text{sw}}$
620	43.8	1.8	19.0	-0.1	0.9	0.4
623	44.0	2.0	20.3	-0.2	0.9	0.6
626	44.3	1.9	19.4	0.0	1.0	0.6
629	44.5	1.7	18.4	-0.1	0.9	0.3
630	44.6	1.7	18.4	-0.1	1.0	0.3
633	44.9	2.1	20.6	-0.2	0.9	0.6
636	45.1	1.8	19.1	-0.2	1.0	0.3
639	45.4	2.1	20.4	-0.3	0.9	0.5
640	45.5	2.0	19.9	-0.1	0.9	0.6
643	45.7	1.8	18.8	-0.2	0.9	0.3
646	46.0	1.8	18.7	-0.3	0.8	0.1
649	46.2	1.6	17.4	-0.2	0.9	0.0
650	46.3	1.8	18.9	-0.2	0.8	0.3
651	46.4	1.8	18.7	-0.3	0.7	0.2
652	46.5	1.8	19.1	-0.3	0.8	0.3
653	46.6	1.7	18.3	-0.2	0.9	0.2
654	46.7	1.7	18.0	-0.2	0.8	0.2
655	46.8	1.9	19.5	-0.2	0.8	0.5
656	46.8	1.8	19.0	-0.2	0.9	0.4
657	46.9	1.7	18.0	-0.1	1.0	0.4
658	47.0	2.1	20.7	-0.2	0.9	0.8
659	47.1	1.9	19.5	-0.2	0.9	0.7
660	47.2	2.1	20.5	-0.2	1.0	0.8
661	47.3	1.9	19.7	-0.1	1.0	0.7
662	47.4	2.0	19.8	-0.1	1.0	0.8
663	47.5	1.9	19.4	-0.2	0.9	0.5
664	47.6	2.9	23.2	0.1	1.0	1.7
665	47.6	1.9	19.8	0.0	1.0	0.9
666	47.7	2.1	20.6	0.0	1.0	1.0
667	47.8	1.8	18.7	-0.1	0.9	0.5
668	47.9	1.6	17.7	0.0	0.9	0.3
669	48.0	1.8	19.1	-0.2	0.8	0.4
670	48.1	1.8	19.0	-0.1	1.0	0.4
671	48.2	1.7	18.5	0.1	1.0	0.5
672	48.3	1.9	19.3	-0.1	1.0	0.5
673	48.4	1.8	19.2	-0.1	1.0	0.4
674	48.5	1.8	18.8	0.9	0.9	1.3

Depth (cm)	Age (GICC05 kyr BP)	Mg/Ca (mmol/mol)	T °C (Anand et al., 2003)	$\delta^{18}\text{O}$ (‰ PDB)	$\delta^{13}\text{C}$ (‰ PDB)	Thermocline $\delta^{18}\text{O}_{\text{sw}}$
675	48.6	1.8	19.1	-0.1	1.0	0.4
676	48.7	2.0	20.0	-0.2	1.0	0.4
677	48.8	1.8	19.2	-0.4	0.7	0.1
678	48.9	2.1	20.4	-0.2	0.9	0.5
679	48.9	2.1	20.6	-0.1	1.0	0.7
680	49.0	1.9	19.6	-0.1	1.0	0.5
683	49.3	1.8	19.0	-0.1	1.0	0.4
686	49.6	1.8	19.0	-0.1	0.9	0.4
689	49.9	1.8	19.1	-0.1	0.9	0.4
690	50.0	2.0	20.3	-0.2	0.9	0.6
693	50.3	2.0	20.0			
696	50.6	2.0	19.9	-0.3	1.0	0.4
699	50.9	1.9	19.5	-0.3	1.0	0.4
700	51.0	1.9	19.6	-0.2	0.9	0.4
703	51.3	3.0	24.6	-0.3	1.0	1.4
706	51.6	1.6	17.6	-0.2	0.9	0.1
709	52.0	2.1	20.6	-0.3	0.8	0.5
710	52.1	2.0	20.2	-0.4	0.7	0.4
713	52.4	2.3	21.7	-0.3	0.8	0.8
716	52.7	2.0	20.4	-0.2	0.8	0.6
719	53.0	2.1	20.8	-0.4	0.8	0.5
720	53.1	2.1	20.9	-0.5	0.6	0.4
723	53.4	2.0	20.2	-0.4	0.8	0.4
726	53.7	2.1	20.8	-0.4	0.7	0.6
729	54.1	1.8	18.6	-0.4	0.8	0.2
730	54.2	1.9	19.6	-0.1	1.0	0.7
733	54.5	1.8	18.9	-0.2	0.8	0.6
736	54.8	1.7	18.1	0.0	0.9	0.5
739	55.1	1.8	18.7	-0.1	0.9	0.4
740	55.2	1.8	19.1	-0.1	0.9	0.5
743	55.6	2.0	20.0	-0.2	0.8	0.6
746	55.9	1.8	19.2	-0.2	0.9	0.4
749	56.2	2.0	20.3	-0.2	0.8	0.6
750	56.3	1.9	19.3	-0.2	0.8	0.5
753	56.6	1.9	19.6	-0.3	0.8	0.3
756	57.0	1.8	19.1	-0.3	0.8	0.2
759	57.3	1.9	19.7	-0.3	0.7	0.4

Depth (cm)	Age (GICC05 kyr BP)	Mg/Ca (mmol/mol)	T °C (Anand et al., 2003)	$\delta^{18}\text{O}$ (‰ PDB)	$\delta^{13}\text{C}$ (‰ PDB)	Thermocline $\delta^{18}\text{O}_{\text{sw}}$
760	57.4	2.0	20.1	-0.2	0.5	0.6
763	57.7	2.1	20.4	-0.3	0.7	0.6
766	58.0	2.5	22.4	-0.5	0.6	0.8
769	58.4	1.9	19.6	-0.5	0.7	0.2
770	58.5	2.1	20.4	0.0	0.9	0.8
771	58.6	2.1	20.8	-0.1	0.8	0.9
773	58.8	2.0	19.9	-0.1	0.6	0.7
775	59.0	2.1	20.6	-0.4	0.5	0.5
777	59.2	2.2	21.2	-0.3	0.6	0.9
779	59.5	2.0	20.3	-0.2	0.6	0.8
781	59.7	2.1	20.8	-0.2	0.6	0.8
783	59.9	2.2	21.2	-0.1	0.7	1.1
785	60.1	2.1	20.5			
787	60.3	2.2	20.9	-0.1	0.7	0.9
789	60.5	2.2	21.0	-0.1	0.6	0.9
791	60.7	2.0	20.1	-0.1	0.7	0.7
793	61.0	1.9	19.5	-0.1	0.7	0.7
795	61.2	1.9	19.6	-0.3	0.6	0.4
797	61.4	2.1	20.4	0.0	0.8	0.8
799	61.6	1.8	19.2	0.0	0.8	0.5
801	61.8	2.1	20.9	-0.1	0.8	0.8
803	62.0	2.1	20.7	-0.1	0.8	0.7
805	62.3	1.9	19.5	0.0	0.8	0.5
807	62.5	2.3	21.5	0.2	0.9	1.1
809	62.7	2.0	20.2	0.1	0.8	0.7
810	62.9	1.8	19.0	0.7	1.0	1.0
813	63.1	1.8	18.8	0.1	0.9	0.3
816	63.4	1.5	17.2	-0.1	0.8	-0.1
819	63.8	1.9	19.7	-0.3	0.8	0.2
820	63.9			-0.2	0.9	
823	64.2	1.8	19.0	-0.2	0.8	0.0
826	64.5	2.0	20.1	-0.3	0.8	0.3
829	64.8	2.0	19.9	-0.4	0.8	0.2
830	65.0			-0.1	0.9	
833	65.3	2.0	20.1	-0.2	0.8	0.4
835	65.5			0.0	0.9	

Appendix F. Temperature gradients of SO185-18460 and MD01-2378

Age (GICC05 age kyr)	MD01-2378 thermocline temp. (°C)	SO185- 18460 thermocline temp. (°C)	MD01-2378 SST (°C)	SO185- 18460 SST (°C)	ΔT MD01- 2378	ΔT SO185- 18460	Regional Δ SST	Regional Δ Thermo- cline
23.5	22.0	19.4	27.1	26.8	5.1	7.4	-0.3	-2.6
23.6	21.7	19.5	26.9	26.3	5.1	6.7	-0.6	-2.2
23.7	21.4	19.7	26.6	25.7	5.2	6.1	-0.9	-1.8
23.8	21.1	19.2	26.3	25.5	5.3	6.3	-0.8	-1.9
23.9	20.8	19.2	26.1	25.3	5.3	6.1	-0.8	-1.6
24.0	20.4	19.2	25.8	25.2	5.4	5.9	-0.6	-1.2
24.1	21.5	19.4	25.6	25.1	4.1	5.7	-0.5	-2.1
24.2	20.8	19.6	26.0	25.1	5.2	5.5	-0.9	-1.2
24.3	21.5	20.0	25.5	25.0	4.0	5.0	-0.5	-1.5
24.4	21.4	20.1	26.0	25.0	4.6	4.9	-1.0	-1.3
24.5	20.2	20.0	26.2	25.4	6.0	5.4	-0.8	-0.2
24.6	20.6	19.9	25.9	25.7	5.3	5.8	-0.2	-0.7
24.7	21.0	19.8	25.5	25.8	4.5	6.0	0.2	-1.2
24.8	21.4	19.6	26.2	25.7	4.8	6.1	-0.5	-1.8
24.9	20.1	19.2	25.7	25.5	5.6	6.2	-0.2	-0.9
25.0	20.2	18.7	25.7	25.1	5.5	6.3	-0.7	-1.5
25.1	21.4	19.3	25.2	25.0	3.9	5.7	-0.2	-2.0
25.2	21.7	19.0	25.8	25.2	4.1	6.2	-0.5	-2.7
25.3	21.9	18.6	25.8	25.5	3.9	6.9	-0.3	-3.3
25.4	20.6	19.1	25.5	26.0	4.9	6.8	0.5	-1.4
25.5	20.2	19.7	26.0	26.4	5.8	6.8	0.4	-0.6
25.6	20.4	19.8	25.6	25.8	5.2	6.0	0.2	-0.6
25.7	21.3	19.8	26.2	24.9	4.9	5.1	-1.3	-1.4
25.8	20.5	20.0	25.7	24.6	5.2	4.6	-1.1	-0.5
25.9	21.2	19.3	26.0	24.4	4.8	5.0	-1.6	-1.8
26.0	20.9	18.8	26.1	24.1	5.3	5.3	-2.0	-2.0
26.1	20.8	19.3	25.5	24.0	4.7	4.7	-1.4	-1.4
26.2	21.2	19.8	25.2	24.0	4.0	4.2	-1.2	-1.4
26.3	21.1	19.8	24.8	24.4	3.7	4.5	-0.5	-1.3
26.4	21.1	19.9	26.0	24.7	4.9	4.8	-1.3	-1.2
26.5	21.0	20.4	25.5	26.3	4.5	5.9	0.8	-0.6
26.6	21.0	20.1	25.5	27.6	4.4	7.6	2.2	-1.0
26.7	20.4	19.7	25.4	28.3	4.9	8.6	2.9	-0.7

Age (GICC05 age kyr)	MD01-2378 thermocline temp. (°C)	SO185- 18460 thermocline temp. (°C)	MD01-2378 SST (°C)	SO185- 18460 SST (°C)	DT MD01- 2378	DT SO185- 18460	D SST	D Thermo- cline
26.8	20.6	19.4	25.3	26.3	4.7	7.0	1.1	-1.2
26.9	20.6	19.1	24.6	24.2	4.0	5.1	-0.4	-1.5
27.0	21.4	19.5	24.7	24.1	3.3	4.6	-0.6	-1.9
27.1	21.2	19.9	25.5	23.9	4.3	4.0	-1.6	-1.3
27.2	20.5	20.4	25.4	24.1	4.8	3.7	-1.3	-0.1
27.3	20.6	19.3	25.9	24.2	5.3	4.9	-1.7	-1.3
27.4	21.4	18.3	25.3	24.3	3.9	6.0	-1.0	-3.1
27.5	20.8	18.4	25.4	24.3	4.6	5.9	-1.0	-2.4
27.6	22.0	18.5	25.5	24.3	3.5	5.8	-1.2	-3.4
27.7	21.2	18.6	25.3	24.5	4.1	5.9	-0.8	-2.6
27.8	21.4	18.7	25.3	24.7	3.9	6.0	-0.6	-2.7
27.9	21.5	18.9	25.5	24.2	4.0	5.3	-1.3	-2.6
28.0	20.9	19.4	25.4	24.1	4.5	4.7	-1.3	-1.5
28.1	21.0	20.1	25.9	24.5	5.0	4.5	-1.4	-0.9
28.2	21.7	20.1	25.4	25.0	3.7	4.9	-0.4	-1.5
28.3	21.3	20.1	25.5	25.2	4.2	5.1	-0.3	-1.3
28.4	21.6	19.9	26.2	25.2	4.6	5.3	-1.0	-1.7
28.5	21.8	19.8	25.5	25.4	3.7	5.5	-0.1	-1.9
28.6	22.2	19.8	26.1	25.3	3.9	5.5	-0.8	-2.4
28.7	21.6	19.7	25.6	25.0	4.0	5.3	-0.6	-2.0
28.8	21.0	19.6	26.0	24.6	5.0	5.0	-1.4	-1.3
28.9	21.7	20.2	26.0	24.6	4.3	4.4	-1.4	-1.4
29.0	20.3	20.6	25.8	24.8	5.5	4.2	-1.0	0.3
29.1	21.3	20.1	25.6	25.2	4.3	5.1	-0.4	-1.2
29.2	21.2	20.3	25.8	25.0	4.6	4.7	-0.8	-0.9
29.3	22.5	20.3	25.8	24.7	3.3	4.4	-1.0	-2.2
29.4	23.5	19.5	26.1	24.6	2.6	5.1	-1.6	-4.0
29.5	22.8	18.9	26.7	24.7	3.9	5.7	-2.1	-3.9
29.6	21.8	18.6	26.3	24.8	4.5	6.2	-1.5	-3.2
29.7	21.2	18.6	26.3	24.8	5.0	6.2	-1.5	-2.6
29.8	21.8	18.3	26.7	25.2	4.8	6.9	-1.5	-3.5
29.9	21.9	18.2	26.1	24.8	4.2	6.6	-1.3	-3.7
30.0	21.3	18.6	25.6	24.1	4.3	5.5	-1.5	-2.7
30.1	21.1	18.8	26.2	24.5	5.1	5.7	-1.7	-2.3
30.2	20.2	18.8	26.0	24.8	5.9	6.0	-1.2	-1.4
30.3	19.4	18.5	25.0	24.9	5.6	6.4	-0.1	-1.0
30.4	20.9	18.6	25.4	25.2	4.5	6.6	-0.2	-2.3
30.5	20.7	18.6	25.5	25.1	4.9	6.4	-0.5	-2.0
30.6	21.6	19.3	25.5	24.7	3.9	5.4	-0.8	-2.3

Age (GICC05 age kyr)	MD01-2378 thermocline temp. (°C)	SO185- 18460 thermocline temp. (°C)	MD01-2378 SST (°C)	SO185- 18460 SST (°C)	DT MD01- 2378	DT SO185- 18460	D SST	D Thermo- cline
30.7	21.0	19.4	25.7	24.4	4.7	5.1	-1.2	-1.6
30.8	20.2	19.1	25.6	24.1	5.4	5.0	-1.5	-1.1
30.9	20.6	19.0	26.1	24.3	5.5	5.4	-1.7	-1.6
31.0	20.9	19.8	25.3	24.4	4.5	4.7	-0.9	-1.1
31.1	20.9	20.6	25.8	24.5	4.9	3.9	-1.3	-0.4
31.2	20.8	20.3	26.1	24.7	5.4	4.5	-1.4	-0.5
31.3	21.1	19.9	25.5	24.9	4.4	5.1	-0.5	-1.2
31.4	20.7	19.3	26.0	25.1	5.3	5.8	-0.9	-1.4
31.5	21.5	17.8	25.4	25.0	3.9	7.2	-0.4	-3.7
31.6	20.6	18.3	26.1	25.2	5.4	7.0	-0.9	-2.4
31.7	20.9	19.9	26.0	25.6	5.0	5.7	-0.4	-1.1
31.8	21.2	19.5	26.0	24.9	4.8	5.4	-1.1	-1.7
31.9	20.5	19.6	25.9	24.4	5.4	4.7	-1.5	-0.9
32.0	20.9	20.2	25.7	23.9	4.8	3.7	-1.7	-0.6
32.1	21.6	19.4	25.8	24.3	4.2	4.9	-1.5	-2.3
32.2	20.4	18.8	26.0	24.7	5.6	5.9	-1.3	-1.6
32.3	21.2	18.8	25.5	25.2	4.4	6.3	-0.4	-2.3
32.4	21.7	18.6	25.9	25.3	4.2	6.7	-0.6	-3.1
32.5	21.5	18.7	25.7	25.2	4.1	6.5	-0.5	-2.8
32.6	21.1	19.6	25.6	25.5	4.5	6.0	-0.1	-1.5
32.7	21.7	20.4	26.1	24.9	4.3	4.5	-1.2	-1.3
32.8	20.5	19.7	26.1	25.6	5.7	5.9	-0.5	-0.8
32.9	21.2	18.9	26.0	24.8	4.9	5.9	-1.2	-2.3
33.0	20.2	19.6	26.4	25.0	6.2	5.4	-1.4	-0.5
33.1	20.4	21.0	25.2	25.0	4.8	4.0	-0.2	0.6
33.2	21.0	21.3	25.9	24.8	4.8	3.5	-1.1	0.2
33.3	21.5	21.5	25.2	25.2	3.7	3.7	0.0	0.0
33.4	21.1	21.7	25.8	25.0	4.7	3.2	-0.8	0.6
33.5	22.1	21.3	25.8	24.9	3.7	3.6	-0.9	-0.8
33.6	19.5	20.7	26.0	24.7	6.6	3.9	-1.4	1.3
33.7	21.3	20.0	26.4	24.8	5.1	4.8	-1.6	-1.3
33.8	20.5	19.0	25.6	25.0	5.2	6.0	-0.6	-1.4
33.9	21.1	18.2	25.7	25.0	4.7	6.8	-0.7	-2.8
34.0	20.8	18.4	25.9	25.1	5.1	6.7	-0.8	-2.4
34.1	20.9	18.5	26.0	24.8	5.1	6.2	-1.2	-2.3
34.2	20.1	18.7	25.7	24.9	5.6	6.2	-0.8	-1.5
34.3	20.1	18.5	26.2	24.8	6.1	6.2	-1.4	-1.6
34.4	20.7	18.4	25.3	24.8	4.6	6.4	-0.5	-2.2
34.5	20.8	18.4	26.1	25.7	5.3	7.3	-0.4	-2.4

Age (GICC05 age kyr)	MD01-2378 thermocline temp. (°C)	SO185- 18460 thermocline temp. (°C)	MD01-2378 SST (°C)	SO185- 18460 SST (°C)	DT MD01- 2378	DT SO185- 18460	D SST	D Thermo- cline
34.6	20.5	18.4	26.1	24.6	5.6	6.2	-1.5	-2.1
34.7	20.2	18.6	25.5	24.9	5.3	6.3	-0.6	-1.6
34.8	20.5	19.0	25.9	25.2	5.4	6.2	-0.7	-1.5
34.9	20.8	19.3	26.1	25.3	5.3	6.0	-0.7	-1.4
35.0	21.0	19.7	26.2	26.0	5.1	6.3	-0.1	-1.3
35.1	20.4	20.1	25.8	26.2	5.4	6.1	0.4	-0.4
35.2	20.3	20.4	25.9	25.5	5.5	5.1	-0.4	0.1
35.3	20.8	20.4	26.6	25.2	5.8	4.8	-1.4	-0.4
35.4	20.9	20.4	26.5	25.6	5.6	5.2	-1.0	-0.5
35.5	20.9	20.2	26.6	25.5	5.7	5.3	-1.2	-0.7
35.6	20.8	19.8	26.5	26.2	5.7	6.3	-0.3	-1.0
35.7	20.7	19.4	26.1	25.8	5.3	6.3	-0.3	-1.3
35.8	22.0	19.1	26.2	25.7	4.3	6.6	-0.5	-2.8
35.9	21.1	19.4	26.2	25.6	5.1	6.3	-0.6	-1.7
36.0	19.9	19.6	26.0	25.7	6.2	6.1	-0.3	-0.2
36.1	20.1	19.6	25.5	24.7	5.3	5.1	-0.8	-0.5
36.2	20.7	19.5	25.8	25.5	5.1	5.9	-0.3	-1.2
36.3	21.1	19.4	25.8	24.9	4.7	5.4	-0.9	-1.6
36.4	20.4	19.4	25.9	24.1	5.5	4.8	-1.7	-1.0
36.5	20.2	19.3	24.9	24.4	4.7	5.1	-0.5	-0.9
36.6	20.4	19.2	26.1	24.7	5.8	5.5	-1.4	-1.1
36.7	21.3	19.3	25.3	25.3	4.0	6.0	0.0	-2.0
36.8	21.5	19.4	25.4	25.4	3.9	6.0	0.0	-2.1
36.9	20.8	18.9	25.4	25.4	4.6	6.5	0.0	-1.9
37.0	20.5	18.1	26.1	25.7	5.6	7.6	-0.4	-2.4
37.1	20.6	17.7	25.3	25.2	4.7	7.5	-0.1	-2.9
37.2	21.8	18.6	25.8	25.2	4.0	6.6	-0.6	-3.2
37.3	20.6	19.2	26.8	25.9	6.1	6.8	-0.8	-1.5
37.4	20.9	19.4	26.5	25.5	5.6	6.1	-1.0	-1.5
37.5	21.0	20.0	26.4	25.0	5.3	5.0	-1.4	-1.0
37.6	20.6	20.6	25.7	25.5	5.1	4.9	-0.2	0.0
37.7	20.8	19.9	26.5	25.6	5.7	5.7	-0.9	-0.9
37.8	21.0	18.4	26.0	25.0	5.0	6.6	-1.0	-2.5
37.9	22.2	19.6	25.5	26.1	3.3	6.5	0.6	-2.5
38.0	22.1	20.7	26.1	25.5	3.9	4.8	-0.6	-1.4
38.1	22.1	20.6	25.9	25.2	3.8	4.5	-0.7	-1.4
38.2	22.2	20.7	26.0	25.4	3.9	4.7	-0.6	-1.5
38.3	22.3	20.3	26.2	25.2	3.9	4.9	-1.0	-1.9
38.4	21.1	20.8	26.1	25.6	5.0	4.9	-0.5	-0.3

Age (GICC05 age kyr)	MD01-2378 thermocline temp. (°C)	SO185- 18460 thermocline temp. (°C)	MD01-2378 SST (°C)	SO185- 18460 SST (°C)	DT MD01- 2378	DT SO185- 18460	D SST	D Thermo- cline
38.5	22.3	20.8	25.9	25.1	3.6	4.2	-0.8	-1.4
38.6	21.6	20.9	25.3	25.4	3.7	4.5	0.0	-0.8
38.7	21.0	20.1	25.6	24.8	4.6	4.7	-0.8	-0.8
38.8	21.3	19.2	25.9	25.0	4.6	5.8	-0.9	-2.1
38.9	20.8	19.5	25.4	25.1	4.6	5.6	-0.3	-1.2
39.0	21.4	20.0	25.7	25.0	4.4	5.0	-0.7	-1.4
39.1	20.8	20.5	26.0	25.0	5.1	4.5	-1.0	-0.4
39.2	21.0	19.4	26.1	25.9	5.1	6.5	-0.2	-1.6
39.3	22.1	18.4	25.3	25.2	3.3	6.8	-0.1	-3.7
39.4	21.8	18.0	25.4	25.0	3.7	7.0	-0.4	-3.7
39.5	20.3	18.6	25.5	26.1	5.3	7.5	0.5	-1.7
39.6	19.4	20.4	25.9	25.9	6.5	5.5	0.0	1.0
39.7	20.8	20.1	25.1	25.3	4.3	5.2	0.2	-0.7
39.8	21.3	19.8	25.3	25.2	4.0	5.4	-0.1	-1.5
39.9	20.2	18.3	25.3	25.6	5.1	7.2	0.3	-1.9
40.0	21.4	18.8	24.8	25.3	3.4	6.5	0.5	-2.5
40.1	20.1	20.0	25.2	25.6	5.0	5.6	0.4	-0.1
40.2	20.4	20.6	26.3	25.3	5.8	4.7	-1.0	0.2
40.3	20.0	20.7	24.6	25.4	4.6	4.8	0.9	0.7
40.4	20.2	18.3	25.0	25.6	4.8	7.3	0.5	-2.0
40.5	20.7	18.5	25.2	25.7	4.5	7.2	0.4	-2.2
40.6	20.6	21.4	24.9	25.4	4.4	4.0	0.5	0.9
40.7	20.6	19.5	25.1	25.0	4.5	5.4	-0.1	-1.0
40.8	20.8	19.8	25.1	25.1	4.3	5.3	0.0	-1.0
40.9	21.0	19.4	24.9	26.0	3.9	6.7	1.1	-1.6
41.0	21.9	19.2	25.2	26.0	3.2	6.8	0.8	-2.7
41.1	21.8	19.8	25.8	24.9	4.0	5.1	-1.0	-2.0
41.2	20.7	19.1	25.1	26.7	4.4	7.6	1.5	-1.6
41.3	20.4	18.8	24.8	27.0	4.4	8.2	2.2	-1.6
41.4	20.3	18.7	25.9	26.1	5.6	7.4	0.1	-1.6
41.5	21.0	18.9	25.5	25.5	4.5	6.6	0.1	-2.0
41.6	21.3	21.1	24.7	25.6	3.4	4.5	0.9	-0.2
41.7	20.4	20.7	24.9	26.5	4.5	5.7	1.6	0.3
41.8	20.0	20.3	24.8	26.5	4.8	6.2	1.8	0.3
41.9	20.3	19.5	24.5	27.3	4.2	7.8	2.8	-0.8
42.0	20.5	20.4	24.4	25.2	3.8	4.8	0.9	-0.1
42.1	20.2	18.7	25.1	25.1	4.9	6.4	0.0	-1.4
42.2	20.1	19.2	24.6	25.3	4.5	6.1	0.7	-0.8
42.3	20.5	19.7	25.1	25.6	4.6	5.9	0.5	-0.8

Age (GICC05 age kyr)	MD01-2378 thermocline temp. (°C)	SO185- 18460 thermocline temp. (°C)	MD01-2378 SST (°C)	SO185- 18460 SST (°C)	DT MD01- 2378	DT SO185- 18460	D SST	D Thermo- cline
42.4	19.7	19.9	25.8	25.4	6.1	5.6	-0.4	0.1
42.5	20.4	19.9	25.2	25.1	4.8	5.2	-0.1	-0.5
42.6	21.1	20.0	24.8	24.8	3.7	4.9	0.0	-1.2
42.7	21.4	20.1	24.6	25.2	3.1	5.2	0.7	-1.3
42.8	21.1	20.2	25.0	25.6	3.9	5.4	0.6	-0.9
42.9	20.7	19.8	25.7	26.0	5.0	6.1	0.3	-0.9
43.0	21.3	19.9	25.6	26.2	4.3	6.4	0.6	-1.4
43.1	20.5	20.2	25.6	26.5	5.1	6.3	0.9	-0.3
43.2	20.2	20.3	25.1	26.8	4.9	6.5	1.6	0.0
43.3	20.6	19.7	25.4	27.0	4.8	7.3	1.6	-0.9
43.4	20.1	19.1	25.7	27.2	5.6	8.1	1.5	-1.0
43.5	20.1	19.0	25.0	27.5	4.9	8.5	2.4	-1.1
43.6	19.7	19.1	25.2	27.7	5.5	8.7	2.6	-0.6
43.7	20.6	19.1	25.3	27.9	4.8	8.8	2.5	-1.5
43.8	20.5	19.2	25.3	27.3	4.8	8.1	2.0	-1.3
43.9	20.5	19.7	25.1	26.7	4.6	7.0	1.6	-0.8
44.0	20.0	20.2	24.6	26.1	4.6	5.9	1.5	0.2
44.1	20.4	20.0	25.2	24.6	4.8	4.6	-0.6	-0.4
44.2	20.8	19.7	25.1	25.1	4.3	5.5	0.0	-1.1
44.3	20.7	19.3	25.5	25.2	4.9	5.9	-0.4	-1.4
44.4	21.2	18.9	25.6	25.5	4.4	6.5	-0.1	-2.3
44.5	21.1	18.5	25.4	25.1	4.3	6.6	-0.2	-2.6
44.6	21.0	18.4	24.9	25.2	3.9	6.9	0.3	-2.6
44.7	20.3	19.3	24.9	25.6	4.6	6.4	0.7	-1.0
44.8	20.4	20.1	25.2	25.9	4.9	5.8	0.7	-0.2
44.9	20.4	20.4	25.3	25.5	4.9	5.1	0.2	0.0
45.0	20.7	19.8	24.9	25.7	4.2	5.9	0.8	-0.9
45.1	20.8	19.2	25.0	26.1	4.1	6.9	1.2	-1.6
45.2	20.9	19.5	24.8	25.7	3.9	6.2	0.9	-1.4
45.3	20.3	20.0	25.0	25.2	4.7	5.1	0.2	-0.3
45.4	20.5	20.2	24.7	25.2	4.2	5.0	0.5	-0.3
45.5	20.4	19.7	25.4	25.4	5.0	5.7	0.0	-0.7
45.6	20.6	19.3	25.5	25.4	4.9	6.1	-0.1	-1.3
45.7	20.5	18.8	25.0	25.8	4.5	7.0	0.9	-1.7
45.8	20.4	18.7	25.6	26.1	5.2	7.4	0.5	-1.7
45.9	20.8	18.7	25.6	26.0	4.7	7.3	0.4	-2.1
46.0	21.0	18.5	25.7	25.7	4.6	7.1	0.0	-2.5
46.1	20.2	18.1		25.7		7.7	25.7	-2.1
46.2	20.6	17.6	25.6	26.0	4.9	8.4	0.4	-3.0

Age (GICC05 age kyr)	MD01-2378 thermocline temp. (°C)	SO185- 18460 thermocline temp. (°C)	MD01-2378 SST (°C)	SO185- 18460 SST (°C)	DT MD01- 2378	DT SO185- 18460	D SST	D Thermo- cline
46.3	21.0	18.7	26.7	26.1	5.7	7.4	-0.6	-2.3
46.4	20.4	18.7	26.2	26.0	5.8	7.3	-0.2	-1.6
46.5	20.5	19.0	25.9	27.2	5.4	8.2	1.3	-1.5
46.6	21.2	18.2	26.3	24.6	5.1	6.4	-1.6	-2.9
46.7	20.6	18.6	26.3	25.0	5.7	6.4	-1.3	-1.9
46.8	20.7	19.2	25.7	25.5	5.0	6.3	-0.2	-1.5
46.9	20.4	18.3	25.6	25.7	5.3	7.4	0.1	-2.0
47.0	20.3	20.2	25.9	25.5	5.6	5.3	-0.4	-0.1
47.1	21.3	19.6	26.0	24.9	4.7	5.3	-1.0	-1.7
47.2	21.4	20.5	25.8	24.5	4.3	4.0	-1.2	-0.9
47.3	20.9	19.7	26.1	25.0	5.2	5.3	-1.1	-1.1
47.4	20.7	19.7	26.0	24.2	5.4	4.5	-1.9	-1.0
47.5	19.4	21.6	25.7	24.7	6.2	3.1	-1.0	2.2
47.6	20.0	22.0	25.8	25.3	5.8	3.3	-0.5	2.0
47.7	20.2	20.4	25.4	25.5	5.2	5.1	0.0	0.1
47.8	19.4	19.2	25.9	25.4	6.5	6.2	-0.5	-0.2
47.9	19.8	17.8	26.0	25.1	6.2	7.3	-0.9	-2.0
48.0	20.1	19.0	26.0	25.1	5.9	6.1	-0.9	-1.1
48.1	20.2	18.9	25.7	25.7	5.5	6.8	0.1	-1.2
48.2	18.9	18.6	25.8	24.4	6.9	5.8	-1.4	-0.3
48.3	20.1	19.3	25.3	24.6	5.2	5.3	-0.7	-0.8
48.4	20.0	19.1	26.0	25.0	6.0	5.9	-0.9	-0.9
48.5	19.5	18.9	25.8	25.2	6.2	6.3	-0.5	-0.6
48.6	19.8	19.5	25.0	24.8	5.1	5.3	-0.1	-0.3
48.7	20.9	19.6	25.3	24.5	4.4	4.9	-0.8	-1.3
48.8	20.9	19.8	25.6	24.8	4.6	5.0	-0.8	-1.2
48.9	19.7	20.5	25.0	25.1	5.3	4.6	0.0	0.7
49.0	20.2	20.0	25.7	25.2	5.5	5.2	-0.5	-0.1
49.1	20.8	19.5	25.5	25.2	4.7	5.8	-0.2	-1.3
49.2	20.3	19.3	25.2	25.1	4.9	5.9	-0.1	-1.0
49.3	19.9	19.0	25.3	24.7	5.4	5.7	-0.6	-0.9
49.4	20.1	19.0	25.6	23.6	5.6	4.6	-2.0	-1.1
49.5	20.7	19.0	25.7	24.2	5.1	5.2	-1.5	-1.7
49.6	20.1	19.0	25.3	24.9	5.2	5.8	-0.5	-1.1
49.7	19.8	19.0	25.1	24.7	5.3	5.7	-0.4	-0.7
49.8	20.4	19.1	25.4	24.7	5.0	5.7	-0.6	-1.3
49.9	20.5	19.1	25.8	24.9	5.3	5.8	-0.9	-1.4
50.0	20.6	20.0	25.6	24.9	5.1	4.9	-0.7	-0.6
50.1	20.3	20.2	25.4	24.6	5.1	4.3	-0.8	-0.1

Age (GICC05 age kyr)	MD01-2378 thermocline temp. (°C)	SO185- 18460 thermocline temp. (°C)	MD01-2378 SST (°C)	SO185- 18460 SST (°C)	DT MD01- 2378	DT SO185- 18460	D SST	D Thermo- cline
50.2	20.1	20.1	25.7	25.0	5.6	4.9	-0.6	0.0
50.3	19.8	20.0	25.5	21.9	5.7	1.9	-3.6	0.2
50.4	21.7	20.0	25.9	23.5	4.2	3.6	-2.4	-1.8
50.5	20.4	19.9	25.9	23.8	5.5	3.9	-2.1	-0.5
50.6	19.5	19.9	25.2	24.8	5.7	4.9	-0.4	0.3
50.7	20.4	19.8	25.5	25.2	5.1	5.4	-0.3	-0.7
50.8	20.5	19.7	25.4	24.9	4.9	5.2	-0.5	-0.8
50.9	19.2	19.6	25.0	23.6	5.8	4.1	-1.3	0.4
51.0	20.0	19.6	25.2	25.3	5.1	5.8	0.2	-0.5
51.1	20.7	21.0	26.2	23.9	5.5	3.0	-2.3	0.2
51.2	20.2	22.7	25.3	24.6	5.1	1.9	-0.7	2.5
51.3	20.5	24.2	25.8	25.4	5.3	1.3	-0.3	3.7
51.4	19.9	23.5	25.9	25.0	6.0	1.5	-0.9	3.6
51.5	20.6	21.4	24.9	24.6	4.3	3.2	-0.4	0.8
51.6	20.9	18.9	25.4	24.8	4.5	5.9	-0.6	-2.1
51.7	20.3	18.3	25.7	25.5	5.4	7.2	-0.2	-2.0
51.8	19.9	19.3	25.3	25.1	5.5	5.8	-0.3	-0.6
51.9	20.8	20.2	25.0	24.2	4.2	4.0	-0.9	-0.6
52.0	21.1	20.4	25.7	24.6	4.6	4.1	-1.1	-0.7
52.1	22.2	20.5	25.9	25.4	3.7	4.9	-0.5	-1.7
52.2	21.9	21.0	26.5	25.1	4.6	4.1	-1.5	-1.0
52.3	21.2	21.4	26.1	24.4	4.9	3.0	-1.6	0.3
52.4	21.1	21.6	25.5	24.9	4.4	3.3	-0.6	0.5
52.5	21.6	21.2	25.5	24.8	3.9	3.6	-0.7	-0.4
52.6	21.7	20.7	25.3	25.5	3.6	4.8	0.2	-1.0
52.7	21.0	20.4	25.6	25.3	4.6	4.9	-0.3	-0.6
52.8	20.6	20.5	25.7	25.7	5.1	5.2	0.0	0.0
52.9	20.3	20.6	25.9	26.1	5.6	5.5	0.2	0.4
53.0	19.9	20.8	26.1	27.6	6.2	6.8	1.5	0.9
53.1	21.1	20.9	25.6	25.2	4.4	4.3	-0.4	-0.3
53.2	21.1	20.7	25.6	24.9	4.5	4.2	-0.7	-0.4
53.3	20.5	20.4	25.0	24.4	4.5	4.0	-0.6	-0.1
53.4	21.0	20.2	25.4	25.1	4.4	4.9	-0.3	-0.8
53.5	20.9	20.3	25.3	25.4	4.5	5.1	0.1	-0.5
53.6	20.2	20.6	25.2	26.1	5.0	5.5	0.9	0.3
53.7	20.6	20.8	25.6	25.7	5.0	4.9	0.1	0.2
53.8	22.6	20.4	25.3	25.6	2.7	5.1	0.3	-2.2
53.9	21.1	19.8	26.2	26.1	5.0	6.3	-0.1	-1.3
54.0	19.9	19.1	25.3	26.6	5.4	7.5	1.2	-0.8

Age (GICC05 age kyr)	MD01-2378 thermocline temp. (°C)	SO185- 18460 thermocline temp. (°C)	MD01-2378 SST (°C)	SO185- 18460 SST (°C)	DT MD01- 2378	DT SO185- 18460	D SST	D Thermo- cline
54.1	21.6	19.0	26.3	27.0	4.7	7.9	0.7	-2.5
54.2	20.1	19.6	26.6	27.1	6.5	7.5	0.5	-0.5
54.3	20.3	19.3	25.5	26.7	5.2	7.4	1.3	-0.9
54.4	21.5	19.1	26.2	26.4	4.7	7.3	0.3	-2.4
54.5	20.8	18.9	25.3	26.2	4.5	7.3	0.8	-1.9
54.6	20.5	18.7	25.5	26.8	5.0	8.1	1.3	-1.9
54.7	21.2	18.4	25.7	27.4	4.4	9.0	1.7	-2.8
54.8	21.2	18.1	25.4	27.9	4.2	9.8	2.5	-3.1
54.9	20.8	18.3	26.0	27.6	5.2	9.3	1.6	-2.5
55.0	21.2	18.4	25.7	27.1	4.5	8.7	1.5	-2.8
55.1	20.4	18.6	25.3	26.6	4.9	8.0	1.4	-1.8
55.2	21.0	18.9	25.7	26.2	4.7	7.2	0.4	-2.1
55.3	21.3	19.3	25.5	26.1	4.2	6.8	0.6	-2.0
55.4	20.8	19.6	25.8	26.3	5.0	6.8	0.5	-1.3
55.5	20.7	19.8	25.6	26.6	5.0	6.7	0.9	-0.8
55.6	20.4	19.9	25.0	26.8	4.6	6.8	1.8	-0.4
55.7	20.4	19.7	24.8	26.8	4.4	7.1	2.0	-0.7
55.8	21.2	19.5	25.1	26.9	3.9	7.4	1.7	-1.8
55.9	21.3	19.2	25.9	26.9	4.6	7.6	0.9	-2.1
56.0	20.8	19.6	25.1	26.5	4.3	6.9	1.5	-1.2
56.1	21.1	19.9	24.4	26.2	3.3	6.3	1.7	-1.2
56.2	21.0	20.2	24.7	25.8	3.8	5.6	1.1	-0.7
56.3	21.2	19.5	25.6	25.4	4.4	5.9	-0.3	-1.8
56.4	20.8	19.3	25.8	25.5	4.9	6.2	-0.3	-1.5
56.5	20.7	19.4	26.1	25.8	5.3	6.3	-0.3	-1.3
56.6	20.7	19.5	25.5	26.0	4.9	6.5	0.5	-1.1
56.7	22.1	19.5	24.8	26.2	2.6	6.7	1.4	-2.6
56.8	21.8	19.3	26.3	26.2	4.5	6.9	-0.1	-2.4
56.9	21.2	19.2	25.4	26.2	4.2	7.0	0.8	-2.0
57.0	20.8	19.1	25.9	26.2	5.0	7.1	0.3	-1.7
57.1	21.1	19.3	25.7	26.1	4.6	6.8	0.4	-1.8
57.2	20.8	19.5	25.6	26.0	4.8	6.5	0.4	-1.3
57.3	20.2	19.7	25.7	26.0	5.5	6.3	0.3	-0.5
57.4	20.9	20.1	25.7	26.4	4.7	6.3	0.7	-0.8
57.5	20.6	20.2	26.4	26.2	5.8	6.0	-0.2	-0.4
57.6	20.3	20.3	25.8	26.1	5.6	5.7	0.2	0.0
57.7	21.1	20.4	26.4	25.9	5.3	5.5	-0.5	-0.7
57.8	20.9	20.9	26.1	26.0	5.2	5.1	-0.1	0.0
57.9	20.6	21.5	26.0	26.3	5.3	4.7	0.3	0.9

Age (GICC05 age kyr)	MD01-2378 thermocline temp. (°C)	SO185- 18460 thermocline temp. (°C)	MD01-2378 SST (°C)	SO185- 18460 SST (°C)	DT MD01- 2378	DT SO185- 18460	D SST	D Thermo- cline
58.0	20.9	22.1	25.5	26.5	4.5	4.4	1.1	1.2
58.1	21.5	22.0	25.7	26.8	4.2	4.8	1.1	0.5
58.2	22.2	21.2	25.8	27.2	3.6	6.0	1.4	-1.0
58.3	22.2	20.3	26.0	27.6	3.8	7.3	1.5	-1.9
58.4	22.1	19.8	26.0	27.5	3.9	7.7	1.5	-2.3
58.5	21.6	20.5	25.9	26.6	4.2	6.1	0.8	-1.1
58.6	21.9	20.8	26.1	26.0	4.2	5.2	-0.1	-1.1
58.7	22.5	20.4	26.7	26.1	4.2	5.8	-0.6	-2.1
58.8	22.1	19.9	25.7	26.3	3.6	6.4	0.6	-2.2
58.9	22.5	20.2	25.6	26.7	3.1	6.5	1.0	-2.3
59.0	22.4	20.6	25.9	27.0	3.6	6.5	1.1	-1.8
59.1	21.8	20.9	26.0	26.8	4.2	6.0	0.8	-0.9
59.2	22.2	21.1	25.8	26.5	3.6	5.3	0.7	-1.0
59.3	22.1	21.0	25.6	26.5	3.4	5.6	0.9	-1.2
59.4	21.5	20.5	25.9	26.8	4.4	6.3	0.9	-1.0
59.5	21.3	20.4	25.7	26.9	4.4	6.5	1.2	-0.9
59.6	22.2	20.6	25.7	26.7	3.5	6.1	1.0	-1.6
59.7	23.7	20.8	26.4	26.6	2.6	5.8	0.2	-2.9
59.8	21.8	21.1	26.4	26.6	4.5	5.5	0.2	-0.8
59.9	22.2	21.2	25.4	26.6	3.1	5.4	1.2	-1.1
60.0	21.5	20.9	26.0	26.6	4.5	5.8	0.6	-0.6
60.1	21.3	20.5	26.4	26.7	5.1	6.1	0.3	-0.7
60.2	21.2	20.7	25.8	26.7	4.6	6.0	0.8	-0.5
60.3	21.8	20.9	26.4	26.6	4.6	5.8	0.2	-0.9
60.4	22.6	21.0	26.3	26.7	3.8	5.7	0.3	-1.6
60.5	22.9	21.0	26.0	26.7	3.1	5.7	0.7	-1.9
60.6	22.0	20.7	26.2	27.0	4.2	6.3	0.8	-1.3
60.7	21.9	20.3	25.9	27.5	4.0	7.2	1.6	-1.6
60.8	22.3	19.9	25.9	28.0	3.6	8.1	2.1	-2.4
60.9	22.7	19.7	26.0	28.7	3.2	9.0	2.7	-3.1
61.0	22.2	19.5	25.5	28.5	3.4	9.0	3.0	-2.6
61.1	22.0	19.6	25.3	27.3	3.2	7.7	2.0	-2.4
61.2	21.4	19.7	25.2	26.2	3.8	6.5	1.0	-1.7
61.3	21.6	20.1	25.6	26.3	3.9	6.2	0.7	-1.5
61.4	21.6	20.4	25.4	26.4	3.9	6.0	1.0	-1.2
61.5	21.9	19.8	25.3	26.8	3.4	7.0	1.5	-2.0
61.6	22.2	19.2	25.6	27.2	3.4	8.0	1.6	-3.0
61.7	22.2	19.9	25.6	27.3	3.4	7.3	1.7	-2.2
61.8	22.2	20.7	25.4	27.3	3.1	6.6	2.0	-1.5

Age (GICC05 age kyr)	MD01-2378 thermocline temp. (°C)	SO185- 18460 thermocline temp. (°C)	MD01-2378 SST (°C)	SO185- 18460 SST (°C)	DT MD01- 2378	DT SO185- 18460	D SST	D Thermo- cline
61.9	22.3	20.8	25.3	26.7	2.9	5.9	1.5	-1.5
62.0	21.2	20.8	25.1	26.0	3.9	5.2	0.9	-0.4
62.1	19.5	20.4	24.9	25.8	5.4	5.3	0.9	0.9
62.2	17.5	19.9	24.7	26.0	7.2	6.1	1.3	2.4
62.3	15.0	20.0	24.5	26.1	9.5	6.1	1.6	5.0

Curriculum Vitae

Personal Data

Name : Rina Zuraida
Date and Place of Birth : Bandung, 9 December 1969
Status : Single

Work Experience

1997 - now Marine Geological Institute, Bandung, Indonesia
2006 - 2009 PhD student (until 15.08.2009) at Christian-Albrechts-Universität zu Kiel

Education

2000 - 2002 MSc student at University of Auckland, New Zealand
1999 - 2000 DipSci student at University of Auckland, New Zealand
1988 - 1994 BSc student at Institut Teknologi Bandung, Indonesia

Kiel, 23.11.2009